Uncertainty Quantification of Brake Squeal Instability via Surrogate Modelling

Amir Nobari

Submitted to University of Liverpool in fulfillment of the requirements for a Degree of

Doctor in Philosophy

in

Mechanical Engineering

November 2015

Abstract

Noise, vibration and Harshness (NVH) of automotive disc brakes have been an active research topic for several decades. The environmental concerns, on one hand, and the rising customer expectations of their car quality, on the other hand, have made NVH of brakes an important issue for car manufacturers. Of different types of noise and vibration that a brake system may generate, squeal is the main focus of the current study. Brake squeal is an irritating high-frequency noise causing a significant warranty cost to car manufacturers.

There are a number of reasons leading to squeal noise either at the end of production or during usage and services. Of these reasons, it is believed that manufacturing variability, several sources of uncertainty (such as friction and contact) and diverse loading cases have the most contribution in this problem. Car manufacturers are then recently encouraged to look into the uncertainty analysis of the brake systems in order to cover the influence of these variations on brake designs.

The biggest hurdle in the uncertainty analysis of brakes is the computational time, cost and data storage. In general, stochastic studies are done on the premise of deterministic analyses of a system. As the deterministic analyses of brake squeal instability essentially involve a great deal of computational workload, their stochastic (non-deterministic) analyses will be consequently very expensive. To overcome this issue, the method of surrogate modelling is proposed in this study. Briefly speaking, surrogate modelling replaces an expensive simulation code with a cheap-to-evaluate mathematical predictor. As a result, instead of using the actual finite element model of a brake for statistical analyses, its replacement model will be used alternatively.

There are three main advantages in surrogate modelling of brakes. First of all, it paves the way of structural modification of brakes, which are conventionally done for reducing squeal propensity. Secondly, structural uncertainties of a brake design can cost-effectively be propagated onto the results of the stability analysis. Thereafter, instead of making a single design point stable, a scatter of points should meet the stability criteria. Finally, the reliability and robustness of a brake design can be quantified efficiently. These two measures indicate the probability of unstable vibration leading to squeal noise for a brake design. Accordingly, car manufacturers will be able to estimate the cost of warranty claims which may be filed due to this particular issue. If the probability of failure which is calculated for squeal propensity is significant, surrogate modelling help come up with a solution during the design stage, before cars go into production.

In brief, two major steps must be taken toward constructing a surrogate model: making a uniform sampling plan and fitting a mathematical predictor to the observed data. Of different sampling techniques, Latin hypercube sampling (LHS) is used in this study in order to reduce the amount of computational workload. It is worth mentioning that the original LHS does not enforce the uniformity condition when making samples. However, some modifications can be applied to LHS in order to improve the uniformity of samples. Note that the uniformity of samples plays a crucial role in the accuracy of a surrogate model.

A surrogate model, in fact, is built on the premise of the observations which are made over a design space. Depending on the nonlinearity of the outputs versus the input variables and also depending on the dimensions of a design space, different mathematical functions may be used for a surrogate predictor. The results of this study show that Kriging function brings about a very accurate surrogate model for the brake squeal instability. In order to validate the accuracy of surrogate models, a number of methods are reviewed and implemented in the current study. Finally, the validated surrogate models are used in place of the actual FE model for uncertainty quantification of squeal instability.

Apart from surrogate modeling, a stochastic study is conducted on friction-induced vibration. Statistics of complex eigenvalues of a simplified brake models are studied under the influence of variability and uncertainty. For this purpose, the 2nd order perturbation method is extended to be applicable on an asymmetric system with non-proportional damping. The main advantage of this approach is that the statistics of complex eigenvalues can be calculated in just one run, which is massively more efficient than the conventional techniques of uncertainty propagation that use a large number of simulations to determine the results.

Acknowledgements

Table of Contents

Table of Figures

List of Tables

1. Introduction

This chapter outlines the contents of the current study. First of all, a brief introduction to the configuration of disc brakes is presented. There are a variety of noises and vibrations caused by friction in brake systems. The one which is the point of interest in this research is brake squeal. The reasons behind the importance of brake squeal to car manufacturers are explained. Then, a brief overview of the established determinist approaches toward the brake squeal problem is given in order to explain what the motivation behind the current research is. Moreover, the central aim and objectives of this research is reviewed in this chapter for clarifying the main contribution of the current work to the brake squeal problem. At the end, the layout of this thesis is presented for the convenience of readers.

1.1.   Disc brake configuration

A frictional brake system may be designed based on two configurations: disc brake and drum brake. In early days of development of brakes, drum brakes were commonly used in automotive industry; however, due to the reliable performance of disc brakes, they are extensively being used these days.

A disc brake is a very complex mechanical system consisting of several major components: disc, calliper, pads, pistons, shims, knuckle and axle hub. The disc is rigidly attached to the axle hub which is connected to the drive shaft. The pads, pistons and shims are housed in the calliper, which provide braking torque. Pad shims are used for reducing brake noises, whose effect will fully be explained later. The knuckle is, in fact, a part of suspension system on which the disc, calliper and axle hub are mounted.

Furthermore, there are a number of parts which are used in a brake assembly for assembling the major components. Pads' spring-clips, pads' guide-pins, knuckle bushes and calliper-to-knuckle bolted joints are typical examples of these parts. Figure 1.1 shows the configuration of a disc brake assembly plus the brake pad and shim.
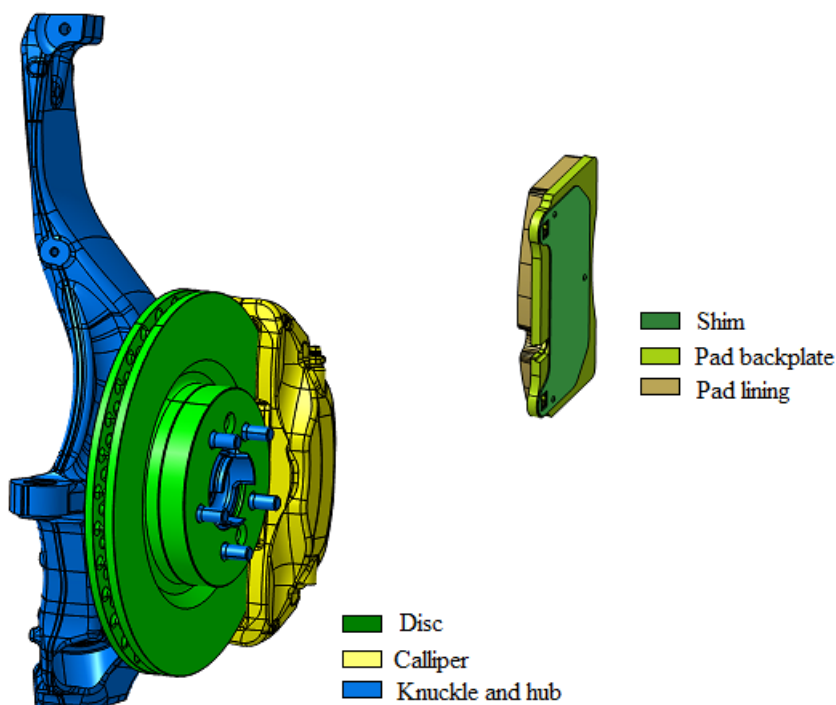
Figure 1.1. Configuration of a disc brake system

The design of disc brakes may be classified based on the design of callipers. There are two main layouts which are commonly used for the calliper design: fixed and floating. In a

fixed-calliper brake design, the brake pressure is applied on the brake pads by means of two sets of pistons located on both inner and outer sides of the disc. During a brake operation, the brake fluid is pressurised by the application of the brake pedal. Then, the fluid pressure moves the pistons which, in turn, force the brake pads to apply braking torque to the disc. Figure 1.2a displays the schematic of a fixed-calliper brake design.
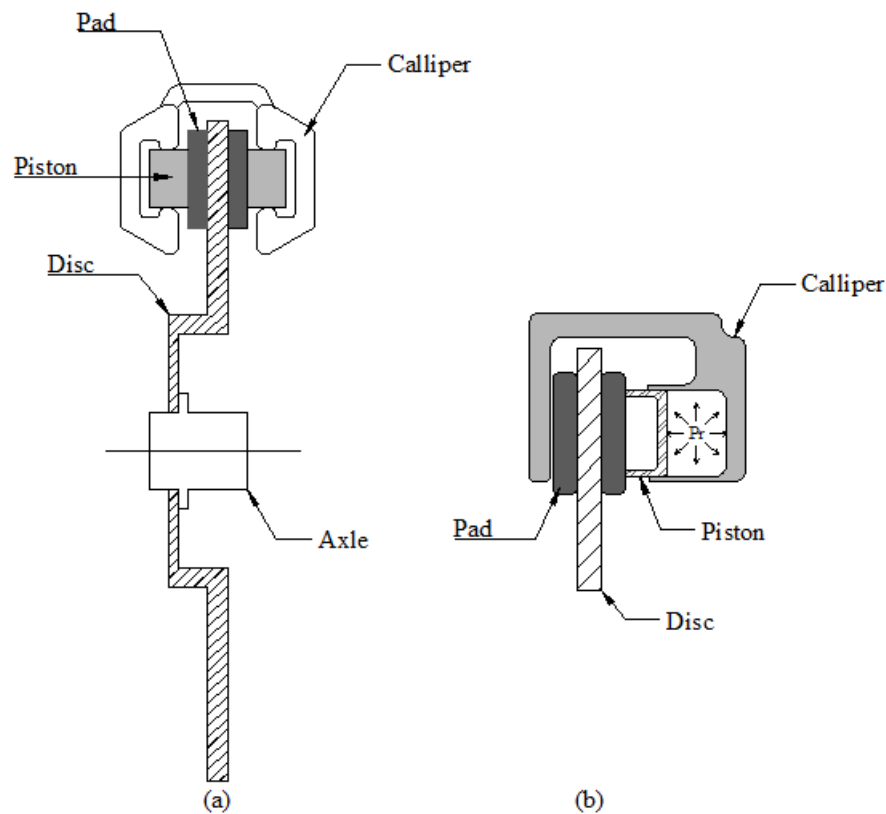
Figure 1.2. Schematic of disc brakes (a) fixed calliper (b) floating calliper

In a floating-calliper design, one piston is usually embedded inside the calliper on the inner side of the disc. When the brake fluid is pressurized, on one hand the pressure is applied on the piston and on other hand the reaction force slides the calliper along two guide pins in the opposite direction. As a result, the calliper moves the outer pad toward the disc. Figure 1.2b shows the schematic of a floating calliper brake design.

A brake engineer usually decides on the brake configuration based on the required safety and performance. Thereafter, the brake is analysed in terms of noise and vibration. Selecting a brake configuration is out of the scope of the current study. Instead, making more reliable predictions of noise and vibration generated by disc brakes, in particular squeal noise, is the point of interest in this study.

1.2. Friction noises

A variety of instabilities in the form of noise and vibration can occur in brake systems. These instabilities are classified into mechanical and dynamic instabilities. The frequency of a mechanical instability is proportional to wheel speed, while the resonant frequency of a dynamic instability is independent of rotor speed. Judder, creep-groan and squeal are the most important instabilities generated in a brake system. In fact, judder is a mechanical instability, groan is a semi-resonant vibration and squeal is a dynamic instability (Day et al., 2012).

From another perspective, these instabilities are classified according to their fundamental frequencies. As groan and judder usually occurs below 1 kHz, they are regarded as low-frequency instabilities. However, squeal which mostly occurs from 1 to 20 kHz is considered high-frequency instability. In order to get a better feeling of these instabilities, it is worth looking at their main features.

Brake judder appears in the form of low-frequency structural vibrations felt through the steering wheel, brake pedal and floor. The main feature of this instability is that the frequency of oscillations is dependent on wheel speed, so it can easily be identified. Its frequency often ranges from 10 to 20 Hz, mostly less than 100 Hz. However, the frequency of vibrations can sometimes become as high as 500 Hz (Jacobsson, 1999). In such cases, a noise can be heard by car passengers along with feeling the structural vibrations.

Brake Judder is, in fact, a combination of "cold judder" and "hot judder". The reason behind cold judder is mainly due to the geometrical irregularities caused by machining, non-uniform corrosion, off-brake wear and uneven surface film transfer (Fieldhouse et al., 2011). Uneven wear and corrosion can lead to Disc Thickness Variation (DTV) which is the main reason behind brake judder in many cases. The transfer film or friction film is a layer whose thickness is in the order of microns. It forms through transferring friction material to the disc and vice versa. This third-body layer determines the frictional behaviour of a brake (Jacobsson, 2003). An uneven surface film transfer can lead to Brake Torque Variation (BTV) and judder, indeed.

Hot judder, however, is formed by thermo-elastic instability. The heat generated at the frictional interface can deform the bodies in contact, which leads to non-uniform contact pressure and localized high-temperature regions known as "hot spots" (Jung et al., 2011). Hot spots are considered the root cause of thermo-elastic instability, hence hot judder. Hot judder mostly occurs during heavy braking. In such cases, energy absorption is significantly faster than energy dissipation. If the localized heating exceeds 726 ° C and a rapid cooling

occurs, it may lead to the formation of "blue spots". Blue spotting can generate a type of brake noise known as drone (Bryant et al., 2011).

Creep-groan is a semi-resonant brake instability whose frequency usually lies between 200 to 500 Hz. The stick-slip motion is assumed to be the reason behind this instability. This frictional mechanism will fully be explained in the next chapter. However, in brief, the difference between the static and kinetic friction coefficients leads to the formation of a repetitive motion known as stick-slip. Due to the fact that the friction-velocity gradient is steeper at lower speeds, groan often appears at low vehicle speeds (Day et al., 2012).

The third class of brake instabilities is squeal. Squeal is an irritating high-frequency noise which costs car manufacturers significantly. In terms of vibration characteristics, the fundamental frequency of brake squeal is within the range of 1 to 20 kHz, which is fairly independent of rotor speed. While out-of-plane modes of the disc are usually responsible for generating squeal, in-plane modes are often involved. Moreover, it is believed that the stick-slip motion is largely absent during squeal occurrence. In order to classify a brake noise as squeal, its sound pressure level is also important. If a single tone noise with such vibration characteristics is measured one meter away from a brake and its sound pressure level equals or become greater than 78 dB, it is named squeal (Bergman et al., 2000).

In the literature, sometimes brake squeal is categorised into two classes: low-frequency and high frequency squeal. Low-frequency squeal ranges from 2 to 4 kHz, while the frequency range of the latter one is from 4 to 15 kHz (Day et al., 2012). Dai and Lim (2008), in the chart shown in Figure 1.3, classified brake noises according to the fundamental frequency of oscillations, excitation source and annoyance level. In this figure, there are two other types of brake noise, i.e. howl and wire brush. The vibration characteristics of these two are not important for the purpose of this study.
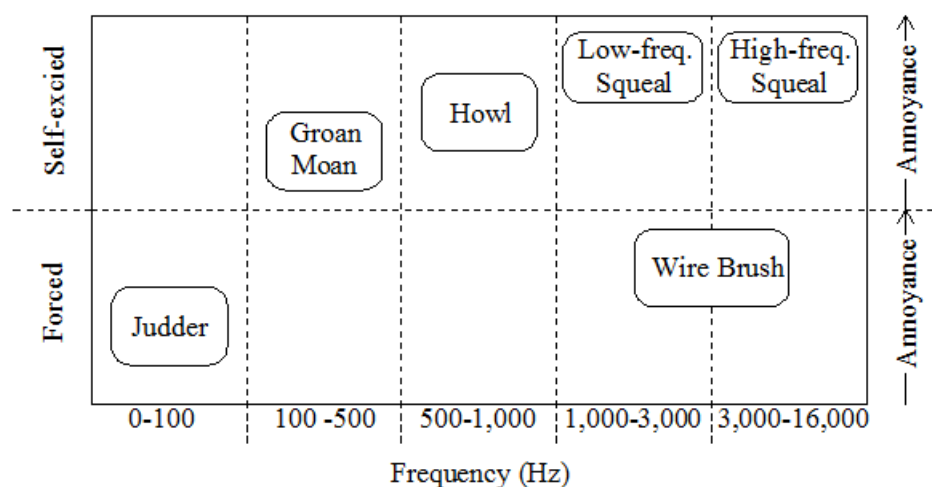
Figure 1.3. Classification of brake instabilities (Dai and Lim 2008)

As seen in Figure 1.3, the annoyance level of squeal noise is very high. Hence, it can urge customers to file warranty claims when hearing squeal from their car brakes. They may also assume that there is a fault in a noisy brake system. Indeed, the reason why squeal costs car manufacturers significantly is related to these warranty claims. This situation becomes more unfortunate to the manufactures being aware that the brakes mostly work faultlessly in terms of safety and performance while generating squeal.

Moreover, the undesired effects of squeal noise on the environment have become a major concern recently. Therefore, car manufacturers are leading a large number of investigations for addressing the brake squeal problem in order to deliver their customers' quality expectations and meet their commitments to environmental issues.

1.3. Conventional approaches

The conventional approaches toward the brake squeal problem are two deterministic ways: complex eigenvalues analysis and transient analysis. Regardless of how these analyses are performed, in brief, the system stability is determined through computing the system eigenvalues in the first approach, while time-domain simulations are used in the latter one. Needless to say, time-domain simulations always demand a significant amount of time and cost. Hence, complex eigenvalue analysis has a great advantage over transient analysis in this sense. Thus, complex eigenvalues analysis is widely used in car industry for the brake squeal problem. Note that there are some other advantages and disadvantages for each approach, which will be discussed in the following chapters.

Since these numerical approaches are deterministic, each run only produces the results of a single set of input variables. However, it is obvious that during brake operations, the trigging conditions such as temperature, pressure, humidity, friction and rotor speed vary from one case to another. Therefore, if a brake analyst aims to consider various trigging conditions, a large number of analyses must be performed.

In practice, however, it is not feasible to carry out such an amount of simulations. The reason, in fact, is due to the required time for a single analysis. For commercial brake models, a complex eigenvalue analysis approximately takes 24 to 36 hours. Unfortunately, the required time for a transient analysis is even longer: a few weeks, indeed. As a result, even via complex eigenvalue analysis, the effects of various loading cases and trigging conditions cannot fully be investigated.

This situation is exacerbated when the manufacturing variability is also considered for the brake squeal problem. A brake analyst usually conducts the deterministic approaches on the

nominal design of a brake system. Nevertheless, there is no doubt that material properties, component geometries and brake assemblies are not identical and vary from one brake to another. Incorporating the effects of these variations on the results is not possible unless an uncertainty propagation technique is implemented.

1.4. On the need of uncertainty analysis

The description given to the conventional deterministic approaches reveals a significant fact about the brake squeal problem: there are different sources of uncertainty and variability in a brake system. Indeed, many researchers believe that the major reason why the brake squeal problem has not fully been resolved so far is due to this fact.

There are two terminologies used for existing uncertainties in structures: variability and uncertainty. Variability, also called "irreducible uncertainty" or "aleatory uncertainty", is referred to those variations in structures, which mostly originate from manufacturing process (Möller and Beer, 2008). In the case of brake systems, the typical examples of variability are the variations of material properties, component geometries and assemblies from one brake to another. In the brake research community, everyone admits that the material properties of friction material are of high level of uncertainty. Moreover, the material properties of cast iron which is usually used for manufacturing of discs vary noticeably from one batch to another. Besides, there is no doubt that geometry of the components which are mass-produced by casting and/or machining is never identical. There is a similar experience with different brake assemblies.

The second class of uncertainties is called "epistemic uncertainty", "reducible uncertainty" or simply "uncertainty" (Möller and Beer, 2008). This group of uncertainty is mostly due to the lack of knowledge. In the case of brake squeal, friction and contact are the major sources of uncertainty. During brake operations, pressure-distribution (Fieldhouse, 200), thermal effects (Day et al. 1991), wear (Eriksson et al, 1999), humidity and friction coefficient (Chen et al. 2003) can be different from one case to another. Moreover, there are a number of uncertainties associated with nonlinearities. Incorporating all of these factors in the problem demands an extensive experimental study which can become very expensive. Even if it was affordable to do so, there are not enough knowledge and experimental facilities to totally realise the behaviour of these factors. As a result, commercial brake models are always associated with some inevitable simplifications. However, as future advances can reduce the present lack of the knowledge, they are classified as reducible uncertainty.

It is worth mentioning it is not always possible to make a distinction between variability and uncertainty.

The above discussion clarifies why car manufacturers have recently become interested in uncertainty analysis of the brake squeal problem. In fact, uncertainty analysis propagates the variations of input variables to the output space, and computes the results in a stochastic way. Therefore, the likelihood of unstable vibration for a brake design can be quantified by means of the output scatter. This likelihood determines how robust and reliable the design is in term of squeal instability. Depending on the parameters included in the uncertainty analysis, this instability may be caused by either the production variability or aging effects.

1.5.   Research motivation

Recently, car manufacturers have become aware that uncertainty analysis can play a significant role in reducing the likelihood of unstable vibrations leading to squeal noise. The simplest, yet most practical, technique of uncertainty analysis is Monte Carlo simulation. To get an idea of what uncertainty analysis means, a brief explanation of the simplest uncertainty technique, i.e. Monte Carlo simulation, is given here.

The conventional Monte Carlo simulation spreads a large number of samples over a design space. The corresponding output of each sampled point is computed by means of a mapping function. This process is repeated until the results of all sampled points are collected. Then, the statistics of the outputs are quantified by the use of output distributions.

Although there is no doubt that Monte Carlo simulation is the most practical way of uncertainty analysis, the above explanation reveals that this approach can become very expensive in term of computational cost and time. As stated earlier, a single run of complex eigenvalue analysis of commercial brake models takes 24 to 36 hours. This situation is even worse in the case of transient analysis. Thus, it is obvious that taking this approach toward the brake squeal problem requires several months or even years. Such an amount of time contravenes the tight deadlines of industrial jobs.

As a result, this study is seeking the most efficient way of uncertainty analysis applicable to commercial brake models. Even the computational workload of the deterministic analyses is a major issue for industry at the moment. Brake analysts are always looking for some ways for reducing computational time, cost and data storage of these analyses. Hence, it is not acceptable to suggest a statistical method adding a massive computational workload to their current jobs.

This study, therefore, suggest the method of "surrogate modelling" or "meta modelling" for uncertainty analysis of brake systems. In a nutshell, this approach replaces large-scale finite element models with a mathematical predictor. Then, the results of a single set of input variables are now produced in a few milliseconds, which is massively less than the required time by finite element models. Although there are many details and consideration for selecting and training a predictor, a well-trained predictor can produced the results quickly and accurately. Therefore, even the conventional Monte-Carlo simulation can be conducted on the replacement model for propagating the uncertainties.

1.6.   Aim and objectives

The central aim of this study is to establish a methodology for determining the likelihood of unstable vibrations leading to squeal noise. In order to do so, an efficient statistical approach should be taken toward the problem due to the large size of brake models. Indeed, one of the main concerns of this study is the applicability of the proposed method to commercial brake models.

The technique which is proposed in this study is called surrogate modelling. As mentioned earlier, a large-scale finite element model is replaced with a mathematical predictor. This predictor is, in fact, trained by means of a number of observations made over the design space. There are many details related to the construction of a replacement model, which will be discussed later. However, when a predictor is sufficiently accurate, it can be used instead of the finite element model in uncertainty analysis. The likelihood of unstable vibrations can also be determined as a result of uncertainty analysis.

The main specification of these predictors is that they are very cheap-to-evaluate. The output of a single sampled point is now computed in a few milliseconds, and the size of the predicted results is in the order of kilobytes. Hence, the issue of computational time, cost and data storage is fully addressed.

There are other great benefits gained from surrogate modelling of brake squeal instability. Surrogate modelling can facilitate structural modifications of brakes. These modifications are made to the nominal design in order to suppress or reduce the likelihood of squeal noise. At the moment, these modifications are done through trial-and-error approaches, and there is not any systematic way to do so. Surrogate modelling, instead, provides brake analysts with some mathematical functions which can easily be explored. Needless to say, finding an optimum design point can adequately be done by the use of these mathematical functions. When the optimum design point is obtained in this way, it can easily be validated by means

of the actual brake model. However, using the finite element model in the first place makes this procedure very time-consuming.

Furthermore, a surrogate model unveils which input variables are of high level of activity in different unstable modes. In other words, the sensitivity of unstable modes with respect to input variables is determined via surrogate modelling. The activity of each input variable is a useful piece of information, in particular for uncertainty quantification of squeal instability. For example, the general feeling about friction material is that it plays a significant role in squeal instability of a brake system. However, the results of this study show that it is not always the case. It is likely for a particular mode not to be sensitive to the properties of friction material. Then, including those properties in the uncertainty analysis causes a significant increase in the computational workloads, which suggests no more help.

1.7.   Originality of the current study

Uncertainty analysis of squeal instability has attracted the attention of researchers in recent years. There are a small number of studies investigating the application of uncertainty analysis on commercial brake models. Most studies were conducted on low-order models in order to establish a method. The remainders mostly used simplified brake models consisting of the disc and pads. However, the current study, in the first place, attempts to investigate the applicability of these techniques on full finite element brake models.

The outstanding novelty of this research is the use of surrogate modelling for predicting the likelihood of unstable vibrations. In particular, the mathematical predictor which is employed for this purpose is called "Kriging". The effectiveness of Kriging predictor has been proved for constructing a replacement model in multi-dimensional spaces. If a smooth function/model is replaced with Kriging function, the replacement model shows a high level of accuracy. The results of the current research show that although commercial brake models are very complex, their complex eigenvalues are smooth functions of input variables. As a result, Kriging predictor is proposed for constructing replacement models of brakes in this study.

Moreover, the second-order perturbation method is extended in this study for determining statistics of complex eigenvalues in friction-induced vibration. The perturbation method is an established way of uncertainty quantification in structural dynamics. However, some important modifications are made here in order to show the applicability of this method to friction-induced vibration. The great advantage of the second-order perturbation is that the statistics of outputs are produced in one-run which is considerably more efficient than other

techniques of uncertainty analysis. However, the major drawback of the proposed perturbation approach is that the distribution of input variables should be Gaussian. Although this assumption is not far from reality in many cases, this method is not as powerful as surrogate modelling being able to deal with any form of input distribution.

Finally, the reliability and robustness of brake systems in term of the likelihood of unstable vibrations can be determined via the proposed methods. At the moment, industry does not have any estimation of the percentage 'failure' caused by production variability or aging effects. This study provides industry with a design tool which is able to quantify the probability of 'failure'. Note that 'fail' and 'failure' are a terminology which is commonly used in engineering for an undesired state of a system. Throughout this study, these terms mean it is likely for a design to become unstable and 'fail' to satisfy a certain design function in a sense.

1.8.   Layout of the thesis

The contents of the current thesis are presented in the following order.

- *Literature review*

    It has been attempted to present a comprehensive state-of-the-art review in this chapter. Over 150 publications are reviewed, which mostly concern the causes and effects of brake squeal. There are a number of mechanisms which are considered for the root cause of brake squeal instability. These mechanisms are fully discussed, and then it is explained why many researchers believe mode-coupling is the main reason behind squeal noise. The remainder of the review focuses on different methods of uncertainty analyses. Note that an extensive discussion about the pros and cons of these methods is presented in chapter 6.

- *Finite element modelling*

    The finite element model of a commercial brake system is studied is this chapter. The first step in investigating brake squeal instability is to build a finite element model of the system under study. Then, normal mode analysis is conducted on each component in order to derive its natural frequencies and mode shapes. The results of the normal mode analysis are useful for "model updating" of brake systems.

- *Experimental results*

    In order to validate the finite element model of a brake system, "modal testing" should be conducted on both individual components and the full brake assembly. A

brief introduction to modal testing and model updating is given in this chapter. The results of modal testing on the disc, friction material, pad and calliper are reported. The experiments are done by means of the LMS test lab and also Polytec laser scanning vibrometer. Some conclusions are then drawn from the experimental results produced by these two measurement systems.

-   *Deterministic approaches toward the brake squeal problem*
    First of all, the pros and cons of complex eigenvalue analysis and transient analysis are discussed. The reason why complex eigenvalue analysis is chosen for the purpose of this study is explained. Then, a simple example is given in order to illustrate how complex eigenvalue analysis and transient analysis are performed. Then, complex eigenvalue analysis is conducted on the actual brake model. The experimental results collected from the brake under operational condition are also reported for the validation of full brake model. Moreover, an example of suppressing an unstable mode of brake through structural modification is given in this chapter.

-   *Non-deterministic approaches: Uncertainty Analysis*
    The concept of "uncertainty analysis" is fully explained in this chapter. Particular attention is given to different methods of uncertainty analysis. The pros and cons of each group of uncertainty technique are discussed, which clarify why surrogate modelling and perturbation method are selected for the purpose of this study. Various applications of uncertainty analysis in structural dynamics are reviewed. Moreover, a brief discussion is made about the assumptions and achievements of other studies in the uncertainty analysis of brake squeal instability.

-   *Statistics of complex eigenvalues in friction-induced vibration*
    In the literature, friction-induced vibration has mostly been studied by means of low-order models due to the fact that a deeper understanding can be gained in this way. Although the challenges associated with large-scale models still stand, the causes and effects of most phenomena are investigated via low-order models. As a result, a low-order model is selected to fully understand the meaning of stochastic eigenvalues and the applicability of the second-order perturbation method to friction-induced vibration.

-   *Surrogate Modelling*
    The concept of "surrogate modelling" and its implementing procedure are fully explained in this chapter. In general, a surrogate model is built on the basis of a

sampling plan made over the design space. Particular attention is given to the influence of different sampling plans on the results. Then, the theory behind Kriging predictor is explained. A few test functions are selected to show how a replacement model is built by means of Kriging predictor.

- *Brake surrogate models*

  Kriging predictor is used for constructing two brake surrogate models. In the first model, only two input variables are included in order to stay in a three-dimensional space. In this case, the response surface of the brake, i.e. Kriging predictor, can be plotted versus both input variables. Accordingly, some aspects of surrogate modelling can adequately be discussed by means of this model.

  Then, four input variables are considered for constructing another surrogate model. The efficacy of surrogate modelling in multi-dimensional spaces is tested. The required validation techniques in such spaces are discussed. Then, the model is used for propagating uncertainty and variability of input variables to the output space. At the end, the reliability and robustness of the brake under study in terms of the likelihood of unstable vibration is determined.

- *Discussions and conclusions*

  The established methodology, i.e. surrogate modelling of brake squeal instability, is summarized. Several concluding remarks are made. A number of ideas for future investigations are also suggested in this chapter.

2. Literature Review

This chapter is dedicated to the literature review of the studies which have previously been conducted on brake squeal instability. First of all, the main features of different frictional mechanisms that may be considered the root cause of squeal instability are discussed here. On the premise of these hypotheses, a number of studies have been carried out, which are reviewed next. The nonlinear behaviour of frictional systems and the effect of damping on these systems are two important features to which particular attention is given. Moreover, the effects of surface topography, roughness and wear plus thermal-effect and pressure distribution on squeal instability are fully discussed.

Most studies that are reviewed in this chapter have been conducted based on deterministic approaches. A brief introduction to non-deterministic approaches is also given here. However, a comprehensive review of non-deterministic approaches will be carried out in chapter 6.

The characteristics of brake squeal noise are fully reviewed in chapter 1. These characteristic can also be found in (Papinniemi et al. 2002). It is worth reminding that squeal is a type of self-excited vibration which is induced by friction. Secondly, the sound pressure level has a determining role in classifying a noise as squeal. Self-excited vibration causes instability in a system and sound pressure level is related to a nonlinear feature of an unstable system, which is known as "limit cycle". Therefore, in the preface of reviewing the literature for the brake squeal problem, it is worthwhile to explain the concepts of "instability", "self-excited vibration" and "limit cycle" due to the fact that these terms are frequently used in this study.

2.1.   Self-excited vibration and limit cycle

In structural dynamics, the ability of a system to recover an equilibrium state under small perturbations is termed "stability". On the other hand, "instability" is referred to a situation in which a system is unable to recover an equilibrium state and the amplitude of vibration grows without bound under small perturbations.

In many mechanical systems, the excitation force which leads to vibrations is external. However, sometimes a system can generate an excitation source internally. The internal excitation source means that a function of the system displacement, velocity or acceleration feeds energy into the system and causes the amplitude of vibration to grow. Therefore, this type of instability is termed "self-excited system". Due to the non-conservative nature of friction force, it can form a class of self-excited motion known as friction-induced vibration. Several mechanisms for friction-induced vibration are illustrated in this chapter, which may be considered the root cause of brake squeal.

The other term which is commonly seen in this subject is "limit cycle". According to the definition of instability, the amplitude of vibration should grow without bound in the linearsied system. However, what happens in reality is that nonlinear elements existing in any mechanical system impede this growth after a number of oscillations and the oscillations become steady. On the phase plan, the trajectories of this steady-state motion will be a closed-loop known as "limit cycle". In other words, the velocity-displacement trajectory of the system converges to a closed-loop over time (limit cycle).

In order to get a better understanding of these concepts, the Van der Pol equation (Rao, 2011) is briefly reviewed here. Although this equation is the mathematical representation of an electrical feedback circuit, it can be imagined as a second-order mechanical system. The Van der Pol equation may be written as:

$$\ddot{x} - \varsigma(1 - x^2)\dot{x} + x = 0 \qquad \varsigma > 0 \tag{2.1}$$

where ς is a constant. Depending on the displacement, 'damping' of the system can turn to either positive or negative. Similar to what is observed in many mechanical systems, the amplitude of vibration decays exponentially if the damping coefficient remains positive. Negative damping, nevertheless, causes the system response to grow in an exponential manner. Figure 2.1 shows the phase trajectories and time-domain response of the Van der Pol equation for $\varsigma = 0.3$, $x_0 = 0.1$ m and $\dot{x}_0 = 0$, in which the circle-covered closed loop represents the limit cycle of the system oscillations.
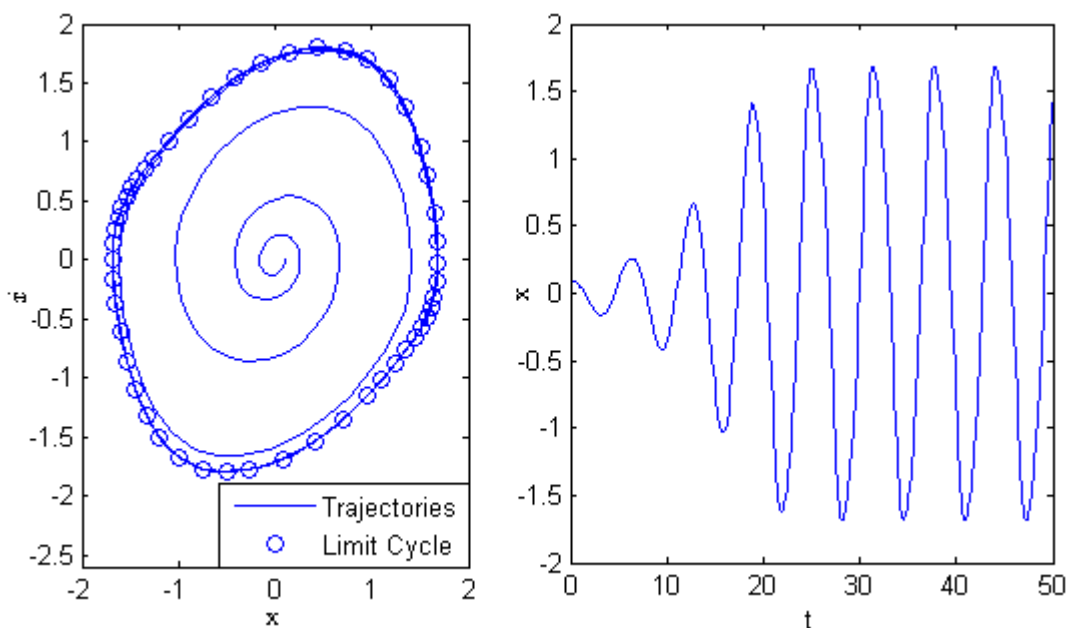
Figure 2.1. Limit cycle and time-domain response of the Van der Pol equation

The importance of the "limit cycle oscillation" (LCO) in this study would not be realised unless a second thought is given to the definition of squeal noise. According to this definition (chapter 1), in order to classify a noise as squeal, its sound pressure level should not be below 78 dB. Of course, the vibration characteristics of the noise should also meet the characteristics of squeal noise. Due to the fact that the sound pressure level of the noise is proportional to the amplitude of the steady-state response of the system, i.e. limit cycle, the size of the limit cycle then determines whether a noise is squeal or not. This aspect is fully discussed in this chapter.

2.2.   Numerical deterministic approaches

There are two numerical approaches which may be taken toward analysing the brake squeal problem: complex eigenvalue analysis and transient analysis. The implementations of these methods are fully explained in chapter 5. In brief, complex eigenvalue analysis determines the eigenvalues and eigenvectors/mode shapes of the linear or linearised system while transient analysis derives the time-domain response of the system. The detailed pros and cons of each method are discussed in chapter 5. Briefly speaking, due to the computational efficiency of complex eigenvalue analysis and also providing the mode shapes of the system in one run, this method has been widely used in industry. In this study, complex eigenvalue analysis is abbreviated as "CEA".

On the other hand, the nonlinear features of squeal instability such as limit cycle cannot be investigated via complex eigenvalue analysis. Unfortunately, the difficulties in doing a dynamic transient analysis have caused this approach to be used rarely for large-scale models. These difficulties will be also discussed in chapter 5.

2.3.   Brake squeal mechanisms

In the literature, there are a number of hypotheses about the root cause of brake squeal. Of these hypotheses, stick-slip, sprag-slip, negative friction-velocity slope and mode coupling are the four mechanisms which are frequently cited in the literature. Ibrahim (1994) and Kinkaid et al. (2003) comprehensively reviewed these mechanisms. In this section, their main features are discussed. As there is a general consensus among researchers that mode-coupling is the root cause of brake squeal noise, particular attention is given to this type of instability.

2.3.1.   Stick-slip and negative friction-velocity slope

In the literature, stick-slip motion and negative friction-velocity are mostly introduced as two separate frictional mechanisms. However, due to the common features of these two theories, here they are explained in one section. Stick-slip theory is developed based on two discrete friction values of friction coefficient (static and dynamic) while negative friction-velocity mechanism considers a continuous transition from static to dynamic friction force.

Stick-slip motion appears in many mechanical systems having two bodies in contact. In the literature, the motion of a bow on the violin string is usually cited as the typical example of stick-slip motion (Popp and Stelter, 1990). In fact, the sound that is heard from this

instrument is a type of self-excited oscillation consisting of repetitive slipping and sticking phases. In order to demonstrate the stick-slip mechanism, imagine that the motion of the bow on the string is maintained at a constant speed. Hence, it can be simply represented by a "mass-on-belt" system displayed in Figure 2.2.
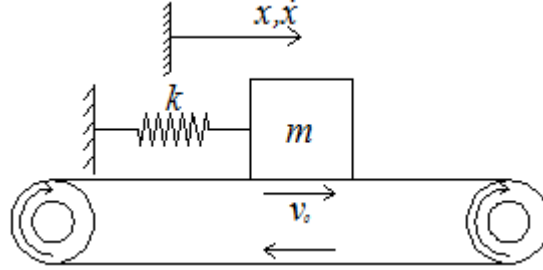
Figure 2.2. Single degree-of-freedom mass-on-belt system

When the force of the spring is smaller than the maximum static friction capacity, the mass sticks to the belt and moves in the direction of the moving belt. Once the spring force exceeds the maximum static friction capacity, the mass starts to slip. What feeds energy into the system and leads to a growth in the vibration amplitude is the negative gradient of friction-velocity relationship at low speeds (Figure 2.3).

To get better understanding of this type of instability, consider the equation of motion for the system shown in Figure 2.2:

$$m\ddot{x} + kx = -\mu(v_{\mathrm{r}})F_{\mathrm{N}}\mathrm{sgn}(v_r) \tag{2.2}$$

where μ and F_{N} represent the friction-coefficient and normal force, respectively. Moreover, v_{r} denotes the relative velocity between the mass and belt, i.e. $v_{\mathrm{r}} = \dot{x} - v_0$. The dependency of friction force on the relative velocity causes a negative velocity-dependent term to appear on the left hand side of the above equation. This negative term can play the role of negative damping which makes the system unstable.

A number of functions have been assigned to velocity-dependent friction coefficient in the literature. The one which is used in Figure 2.3 is:

$$\mu(v_r) = \frac{\mu_0 - \mu_1}{1 + \gamma|v_{\mathrm{r}}|} + \mu_1 + \beta v_{\mathrm{r}}{}^2 \tag{2.3}$$

where μ_0, μ_1, γ and β are constants. In the left plot of Figure 2.3, these values are taken as $\mu_0 = 0.4$, $\mu_1 = 0.1$, $\lambda = 1.42$ and $\alpha = 0.01$ (Oestreich et al., 1996). Due to the nonlinear terms in the friction force, the growth in the vibration amplitude stops after a few cycles and

the motion of the system tends to a limit cycle. The limit cycle of the stick-slip motion is shown in the right plot of Figure 2.3.
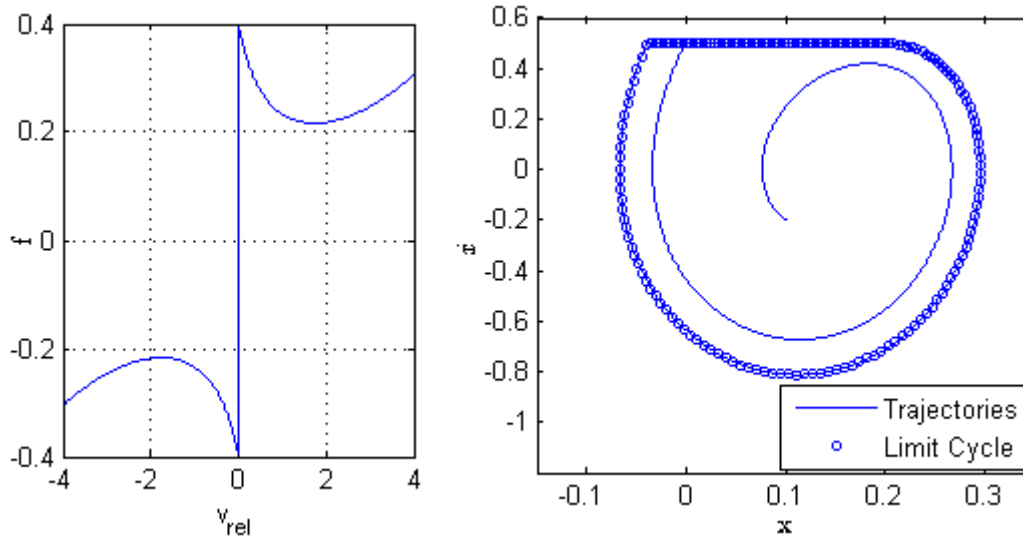
Figure 2.3. Velocity-dependent friction and corresponding limit cycle

Two distinct phases can be observed by looking at this limit cycle: stick and slip. During sticking phase, the relative velocity between mass and belt is zero ($v_r = 0$) and the static friction force is equivalent to $F_s = kx$. That part of the limit cycle which is in parallel with $x -$ axis represents sticking phase. The equation of motion in this state is:

$$\dot{x} = v_0 , \quad \ddot{x} = 0. \tag{2.4}$$

The circular part of the limit cycle represents the slipping phase. The equation of motion in the slipping follows equation (2.2). It is worthwhile to clarify that a discontinuous function for the friction force can still lead to stick-slip motion. In fact, in many studies, for the sake of simplicity, stick-slip mechanism has been presented by means of a discrete function (Figure 2.4). However, experimental studies on the behaviour of friction coefficient on microscopic scale have revealed that friction coefficient has a velocity-dependent feature.

As seen, the regimes of both limit cycles are almost the same. The major difference, nevertheless, is about the transition point from sticking phase to slipping phase. Stick-slip motion as brake squeal/squeak mechanism was first introduced by Mills (1938). He investigated the effect of velocity-dependent friction coefficient on squeal instability of drum brakes. However, later studies on squeal instability have revealed that stick-slip motion is largely absent during brake squeal. As mentioned in chapter 1, this mechanism is mostly considered the root cause of creep-groan.
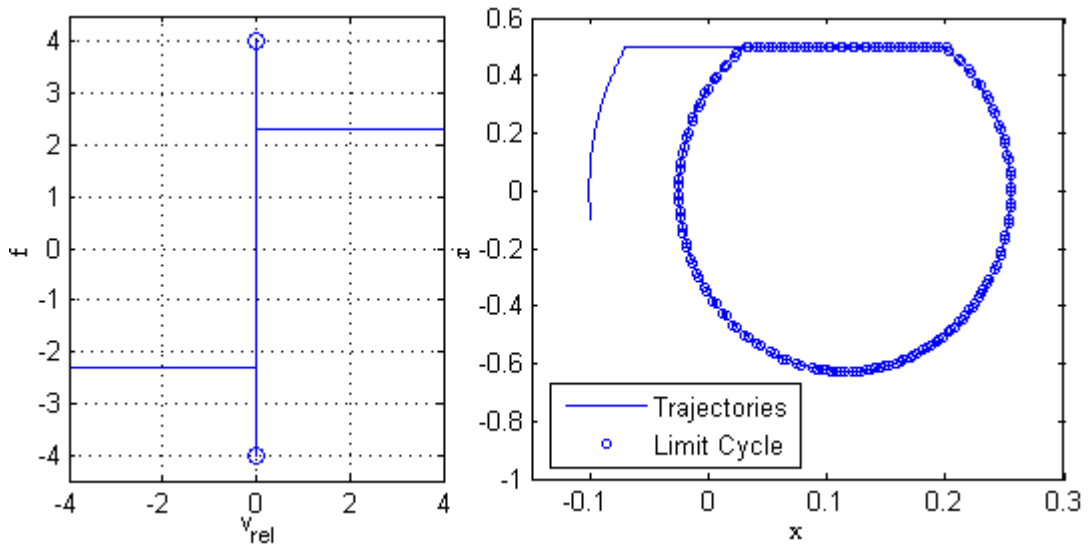
Figure 2.4. Discontinuous friction force and corresponding limit cycle

2.3.2. Sprag-slip

In 1961, Spurr developed a theory for brake squeal, which led to a school of thought about this phenomenon in later studies. Spurr believed that geometry of the components in a brake assembly is the root cause of brake squeal. In order to demonstrate his theory, Spurr used an experimental set-up shown in Figure 2.5. As seen, the brake pads were machined so that only a narrow strip of pad remained in contact with the disc on each side. The simplified model of Spurr's experimental set-up is also shown in Figure 2.5.
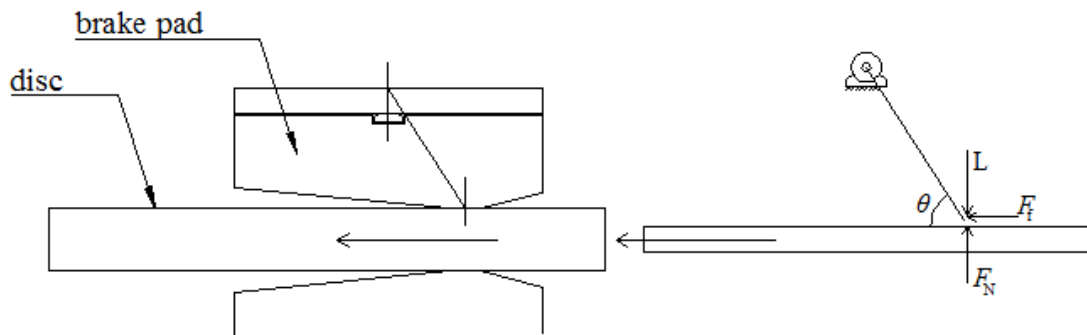
Figure 2.5. Spurr's experimental set-up

When the brake pressure is applied, the motion of the slider, i.e. disc, causes the resultant contact force to pass through pads' pivot points. The pivot points are, in fact, the location of pads' mounting points on the calliper. Consequently, the normal load and friction force become a function of the angle of inclination:

$$F_{\mathrm{N}} = \frac{L}{1 - \mu_{\mathrm{k}} \tan\theta}; \;\; F_{\mathrm{f}} = \frac{\mu_{\mathrm{k}} L}{1 - \mu_{\mathrm{k}} \tan\theta}. \tag{2.5}$$

21

In this case, If θ tends to $\tan^{-1}(1/\mu_k)$, it causes the contact force to become very large ($F_N \rightarrow \infty$).

What happens in this situation is that the slider locks to the sliding surface and moves toward the sliding direction. This situation was named "spragging" in Spurr's theory. The spragging situation continues to a point when the bodies in contact are sufficiently deformed. Thereafter, the flexibility of the components causes the slider to free itself from the spragging situation. If it is assumed that the slider moves with a constant velocity, a repetitive motion is formed, which is known as "sprag-slip". What is seen in Spurr's theory is that even a constant friction coefficient can cause instability, which is in contrast with stick-slip mechanism.

Jarvis and Mills (1963) extended Spurr's theory through an experimental study in which a cantilever was in contact with a rotating disc (Figure 2.6). They concluded that the cause of insatiability in this system was not the dependency of friction on the relative velocity, but rather the geometrical coupling between the two components seemed to be responsible for unstable vibrations.

Spurr's theory along with Jarvis and Mills' model were followed in a number of studies focusing on pin-on-disc friction induced vibrations. Although a pin-on-disc model should not necessarily be interpreted as a disc brake, such studies provide a phenomenological understanding of this type of instability. Besides, their approaches toward the existing nonlinearities and uncertainties of such systems can be extended to the disc brake squeal problem. As a case in point, particular attention will be given in this thesis to the nonlinear approach used in (D'Souza and Dweib, 1990) and the uncertainty analysis performed in (Butiln and Woodhouse, 2010).
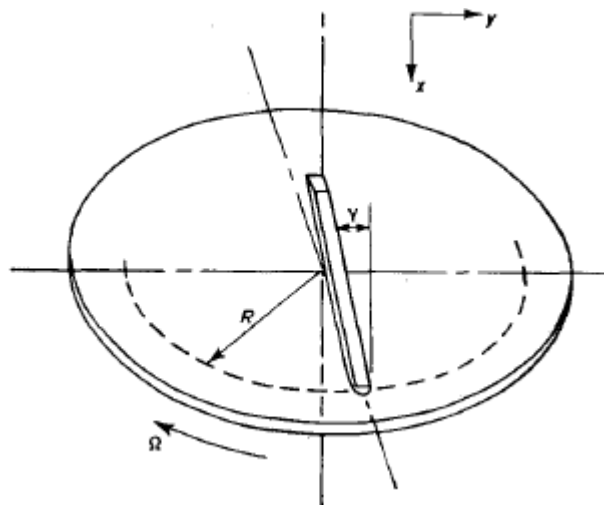
Figure 2.6. Jarvis and Mills' model (1963)

On the premise of Spurr's theory, a number of researchers believe that the location of dynamic centre of pressure is the main reason behind brake noise under light braking. In a series of experimental studies, Fieldhouse (2000) and Fieldhouse et al. (2008) showed when the dynamic centre of pressure moved toward the leading edge, the propensity of squeal noise increased. Moreover, the friction-coefficient at pads-to-disc contact interface, pad wear and brake mounting geometry are the factors affecting the leading offset. These effects will be discussed in detail later.

2.3.3.   Mode coupling

In 1972, North developed a theory of brake squeal, in which friction force was modelled as a follower force. In a lumped-mass model, North illustrated that friction force could break the symmetry of the stiffness matrix. In fact, he was the first person suggesting that the asymmetry of the stiffness matrix was responsible for the brake squeal problem.

The asymmetry of stiffness matrix attracted the attention of many researchers and, in fact, North's theory formed the basis of a type of instability which is known as mode-coupling, mode lock-in, or flutter instability these days. Recently, it is believed that mode-coupling is the root cause of unstable oscillations in many mechanical systems, in particular brake squeal (Akay, 2002). Hoffmann et al. (2002) demonstrated this type of instability in an undamped system with two-degrees-of-freedom (Figure 2.7). Due to the significance of mode-coupling instability to the current research, Hoffmann's model is fully reviewed here.
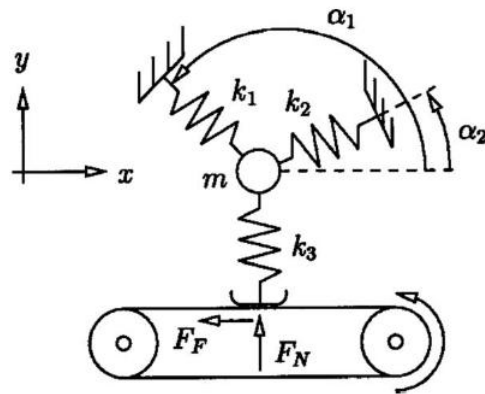
Figure 2.7. Hoffmann's two-degrees-of-freedom model (2002)

The equation of motion for the model shown in Figure 2.7 may be written as:

$$\begin{bmatrix} m & 0 \\ 0 & m \end{bmatrix} \begin{Bmatrix} \ddot{x} \\ \ddot{y} \end{Bmatrix} + \begin{bmatrix} k_1 \cos^2 \alpha_1 + k_2 \cos^2 \alpha_2 & k_{12} - \mu k_3 \\ k_{21} & k_1 \sin^2 \alpha_1 + k_2 \sin^2 \alpha_2 + k_3 \end{bmatrix} \begin{Bmatrix} x \\ y \end{Bmatrix} = \mathbf{0} \qquad (2.6)$$

where $k_{12} = k_{21} = k_1 \sin \alpha_1 \cos \alpha_1 + k_2 \sin \alpha_2 \cos \alpha_2$. Performing CEA of this system for the given example set of parameter in (Hoffmann et al., 2002) results in two pairs of eigenvalues: $\lambda_{1,2} = \pm \left[-2 \pm \sqrt{1 - 4\mu/3} \right]^{1/2}$. Depending on the values of μ, three scenarios may happen (Figure 2.8). For $\mu < 0.75$, there are two pairs of eigenvalues which are purely imaginary, but their values are different. If μ is set to 0.75, the eigenvalues will be purely imaginary and the same. When μ becomes larger than 0.75, the real parts of the eigenvalues will be no longer zero: one of them becomes positive while the other one turns into negative. Meanwhile, for $\mu > 0.75$, the imaginary parts of the two eigenvalues become equal. Since the positive real part causes the amplitude of vibration to grow exponentially, the coupling of these modes leads to an instability known as mode-coupling.

In Hoffmann's model, if friction coefficient is continuously increased from zero to 1.25, it is observed that the imaginary parts of the eigenvalues getting close to each other and at $\mu = 0.75$ they coalesce. Right after this point, the real parts of the eigenvalues bifurcate. This point is termed "bifurcation point" in the literature. The bifurcation behaviour of Hoffmann's model is shown in Figure 2.8.
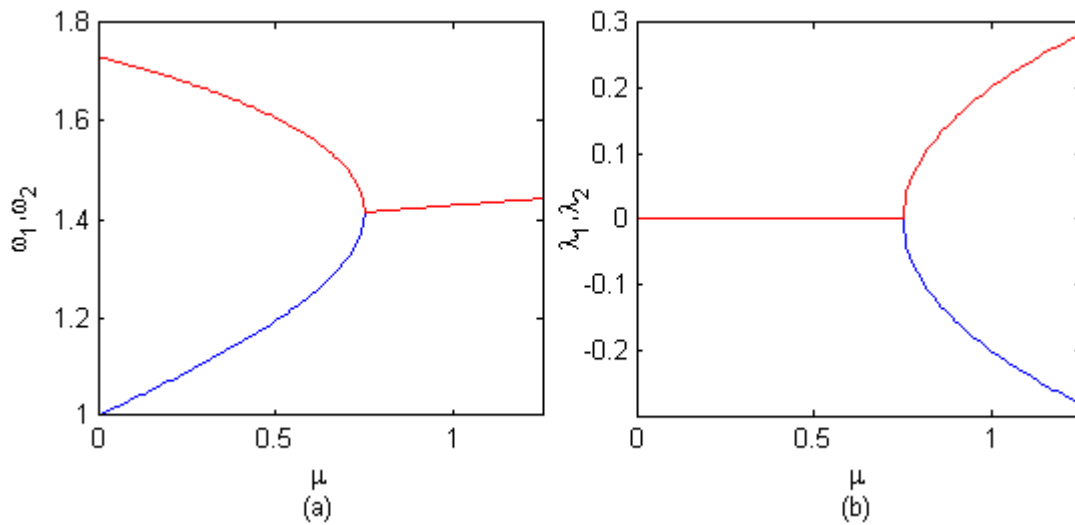
Figure 2.8. Bifurcation behaviour of Hoffmann's model (a) imaginary parts (b) real parts

As there was no nonlinear element in Hoffmann's model, it is not possible to predict the occurrence of squeal noise. However, "squeal propensity", i.e. the tendency of the system to unstable vibration, could be well-predicted. In order to understand the meaning of squeal propensity, the time response of Hoffman's model at $\mu = 1.25$ is displayed in Figure 2.9. As seen, due to the absence of nonlinear terms, the amplitude of vibration grows without bound.
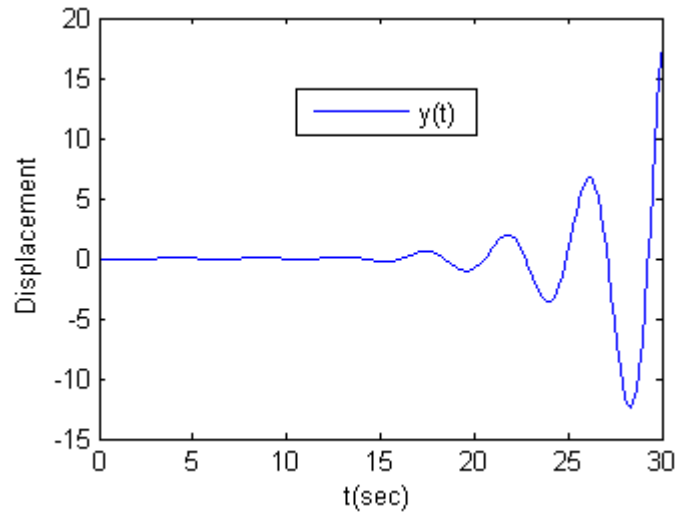
Figure 2.9. Time response of Hoffmann's model in y-direction ($\mu = 1.25$)

Many researchers believe that mode-coupling is the root cause of squeal noise although there is no general consensus on this matter. As a very simple friction model, i.e. Coulomb friction, is used in this approach, the soundness of predicted unstable modes has been debated in some recent studies (Woodhouse and Wang, 2011).

Chen et al. (2008) provided a further understanding of mode-coupling instability by looking into the contribution of time-delay between the varying normal force and the corresponding friction force. What they found was that changing the time delay between these two varying forces can affect the stable region without squeal and unstable region with squeal. Incidentally, it is not clear that the time-delay is either due to the effect of damping or friction force. This matter needs more investigation.

2.3.4.   Other squeal mechanisms

The mechanisms which have been discussed so far are considered the main hypotheses about squeal instability in the brake squeal research community. However, there are a few other hypotheses about the cause of this type of instability. As many researchers believe that a combination of different mechanisms may lead to squeal instability, it is worth reviewing all hypotheses about this phenomenon.

In 1989, Rhee et al. proposed a mechanism for the brake noise of disc brakes, known as "hammering". They considered the fact that the excitation source of modal testing is mostly provided by a hammer. Similarly, brake components may get hammered into their resonant frequencies during braking. The first question that might come into mind was how brake components get hammered. Based on some experimental works, Rhee et al. explained that

some waviness, hills and valleys would appear on the rotor surface after a certain number of braking stops. Moreover, frictional heat during braking could result in hot spotting. When the brake pads slide over the rotor surface, they rock up and down over the uneven surface of the rotor and could excite the other brake components into vibration. As a consequence of this vibration, the brake might generate noise.

Nishiwaki in 1993 presented a generalised theory of brake noise. Three different types of brake noise, i.e. drum brake squeal, disc brake squeal and disc brake groan, were theoretically studied. Then, it was concluded that the root cause of these problems were mathematically the same: dynamic instability of the brake system caused by variations of friction force. It was stated that if the results of stability analysis produced eigenvalues with positive real parts, the system would become dynamically unstable and might generate noise. This noise could appear in the form of squeal or groan depending on its frequency.

More recently, moving loads were also suggested as a brake squeal mechanism. In section 2.3.3, it is mentioned that North (1972) investigated the contribution of friction force in the stiffness matrix by modelling it as a follower force. This contribution can also be observed when friction is modelled as a moving load. Briefly speaking, if the direction of a force follows the deformation of the surface/body on which it acts, it is called "follower force". For example, when the friction force is considered to always act in the instantaneous tangential plane that would rotate during deformation, it is treated as a follower force, as was done by Chan et al. (1993) for the vibration of a friction-loaded disc. In the case of "moving load", the location of force on the surface changes over time. Either a follower force or a moving load can lead to instability and to be considered a squeal mechanism. Ouyang et al. (2000, 2003) considered friction to be both a follower force and moving load. As the truthfulness of a follower force is debated, in 2004 Ouyang et al. investigated a dynamic instability of disc brakes by taking friction only as a moving load in the circumferential direction. Hochlenert et al. (2007) also studied the moving load nature of friction in both radial and circumferential directions in order to provide a better understanding of this brake squeal mechanism.

In a comprehensive review paper, Kinkaid et al. (2003) surveyed the brake squeal mechanisms which had been proposed by that time. In 2005, the same research group came up with a new idea for the brake squeal mechanism based on the results of transient analysis of friction-induced vibration. They explained their findings in this way: "During a braking event, we may consider two braking directions, longitudinal and transverse. In an automotive disc brake, the longitudinal direction is the circumferential direction of the brake rotor while the transverse direction is the radial direction of the brake rotor. As the braking event proceeds, the slip velocity in the longitudinal direction eventually approaches the same order

of magnitude as the slip velocity in the transverse direction. As the slip velocity passes through zero, the direction of the friction force experiences a sharp change. This change is experienced by modes in the transverse direction as a rapidly varying force which induces vibrations in this direction. It is probable (owing to asymmetries in the rotor geometry, contact conditions and the Poisson effect) that the vibration in the radial direction will lead to out-of-plane vibrations of the rotor. If any of these vibrations are in the audible range, they will contribute to disc brake squeal. The frequencies of vibration do not necessarily correspond to natural frequencies of the stationary, frictionless brake system".

2.4.   Application of brake squeal mechanisms

The application of brake squeal mechanisms in literature may be divided into three sets of studies: low-order models, finite element models and experimental studies. While low-order models are mostly focused on phenomenological aspects of squeal instability, large-scale FE models investigate the cause and effect of this phenomenon for real brakes. On a different approach, experimental studies attempt to test physical frictional brakes and draw conclusions based on the observed data.

2.4.1.   Low order models

Flint and Hultén (2002) took an analytical approach to prove which frictional mechanism was the root cause of squeal instability. By the use of a low-order model and Galerkin method, it was shown that no sensible interrelationship existed between squeal instability and stick-slip motion. The effect of follower force was marginal. However, lining-deformation-induced coupling was considered very important in the generation of squeal instability.

A two degree-of-freedom model was used in (Shin et al. 2002) for better understanding of the basic frictional mechanisms leading to squeal, including stick-slip. It was found that one of the essential conditions leading to disc brake noise was the close proximity of natural frequencies of the disc and pad. Moreover, it was stated that damping played a major role in the system instability. While damping could bring about a more stable system, it could also cause instability. The same two degree-of-freedom system was also used in (Paliwal et al., 2005) for analyzing the nonlinear behavior of stick-slip motion through a parametric study. A number of scenarios about the design parameters which could cause instability were discussed. It was also explained what would be the effect of these scenarios on the limit cycle of nonlinear oscillations.

Sinou et al. (2003) studied the sprag-slip theory for a different type of brake noise (judder). The nonlinear behavior of sprag-slip about the bifurcation point was the point of interest in Sinou's study. A simplified model was used to evaluate the efficacy of "center manifold approach" for analyzing the nonlinear behavior of the system. The advantage of using this approach was that the contribution of nonlinear elements could be kept in the reduced-order model while its behavior was comparable with the original model.

In 2007, Hetzler et al. investigated the bifurcation behaviour of stick-slip motion in a "mass-on-belt" oscillator. The friction-coefficient was velocity dependent and the results showed that negative friction-velocity slope could be a convincing reason for low-frequency brake noise (groan). However, no correlation between velocity-dependent friction and brake squeal was reported.

Von Wagner et al. (2007) reviewed the minimal models in the literature for the brake squeal problem and concluded that the vibration of the disc was an important piece of information which was missed in these studies. Needless to say, the disc had a dominant role in the instability of disc brakes and ignoring the disc vibrations through modelling it as a rigid slider with constant velocity could not well represent squeal instability. Von Wagner et al. therefore came up with a new minimal brake model containing a wobbling disc in point contact with two pads.

An analytical approach was taken in (Kang et al. 2009) in order to study different types of modal interaction in mode-coupling instability. This study introduced a new index (modal stability index) through which the necessary condition for this type of instability could be determined. A number of reduced-order models were analytically studied and it was shown that the main features of the reduced-order models could also be seen in full scale finite element models. It was then concluded that using reduced-order model along with an analytical approach had an advantage over the conventional complex eigenvalue analysis since modal interactions of components could be better examined in this way.

Ryzhik (2009) first took an analytical approach to demonstrate that the sliding friction force would result in a transverse contraction in the disc material. As a consequence, it could establish a feedback between orthogonal eigen-modes of the disc, which could result in instability. Ryzhik confirmed his findings through finite element analysis.

Hochlenert et al. (2010) considered another issue which might be caused by the brake squeal problem. In a minimal brake model, it was demonstrated that brake squeal is not always a comfort problem. In light-weight brake design, squeal instability could cause safety issues leading to failure as well. It was also suggested that this effect of squeal noise should be investigated in more detail via finite element analysis or multi-body dynamics codes.

2.4.2.   *Finite element models*

The application of stability analysis for the finite element brake models, in the first place, was seen in Liles' paper (1989). He used CEA to determine the squeal propensity of a brake model consisting of disc, pads and caliper. He conducted a sensitivity analysis for an example set of design parameters in order to measure the degree of instability of the brake versus the design parameters. The degree of instability in his study was defined as the standard deviation of the damping ratios of all unstable modes. Although his approach has been debated by many researchers since he did not consider the time-domain response for predicting the squeal occurrence and the analysis only relied on CEA, industry still takes this approach toward the brake squeal problem due to the computational cost of transient analysis of large FE models.

In 2004, Bajer et al. showed that including friction-induced damping in CEA of brakes can improve the over/under prediction of stability analysis. The over/under prediction of CEA is commonly observed in industry as there is no extensive study on the damping model of friction material. It is worth noting that the friction coefficient must be dependent on slip velocity if the effect of friction-induced damping is going to be considered in CEA.

Júnior et al. (2008) emphasized the importance of contact stiffness at pads-to-disc contact interface and used a few methods for measuring the contact stiffness. Thereafter, the power balance method was introduced as a powerful technique for this purpose. Moreover, the effect of operational parameters, i.e. friction coefficient, wear, brake pressure and temperature, on the results of stability analysis was studied in (Júnior et al., 2008). As these parameters could affect the contact area and contact stiffness, they could make a considerable influence on the stiffness matrix, and consequently the stability. At last, it was stated that careful consideration was needed when using noise insulators (shims) since they could cause instability although their general application was suppressing brake squeal.

In contract with most studies in the literature that ignore gyroscopic effects, the gyroscopic effect of a rotating disc with two stationary pads was investigated in (Kang, 2009). Among different frictional mechanisms, they found that mode-coupling and negative slope friction-velocity had major roles in the instability of the system under their study. A number of parameters such as the gyroscopic effect of disc rotation, the radial component of friction force, the negative slope of friction force and the variation of friction force were introduced as the most important factors to the system instability, especially for non-mode-coupling modes.

Oberst et al. (2013) provided some guidelines for finite element modelling of brakes, which are shown to bring about reliable predictions of squeal propensity.

2.4.3.   *Experimental studies*

Fieldhouse and Newcomb (1996) extended the application of holographic interferometry to the brake squeal problem. What the classical holographic interferometry method could provide was the information about the amplitude of oscillations. Fieldhouse and Newcomb demonstrated an experimental method by which more information such as phase relationship between vibrating components could be gained. Bryant et al. (2012) completed the application of holographic interferometry by using several piezoelectric beams on the pad corners. As the displacement of the pad could not be seen by the laser beam, the vibration of pad had remained as missing information from holographic interferometry. The combination of these two methods could provide a full image of the vibrating components.

To do a modal test on a rotating disc, a technique was developed in (Stanbridge and Ewins, 1999) by means of a scanning laser Doppler vibrometer (LDV). The operational deflection shapes of a rotating disc are an important piece of information in rotating machinery and this technique helped to measure out-of-plane modes of the disc, determining the location of its nodal diameters and identify where a mode is travelling or stationary.

Chen et al. (2003) experimentally studied squeal events of a reciprocating slider. Three main conclusions were drawn in their study. First of all, the dominant squeal frequency was very close to natural frequencies of the friction system. Secondly, the dominant squeal frequency remained unchanged during the squeal event. Lastly, there was no direct correlation was found between the negative friction-velocity slope and the squeal occurrence.

In 2006, Giannini and his colleagues presented two journal papers for investigating the dynamic behaviour of squeal instability through an experimental approach. The good point about their approach was the squeal occurrence could be repeatedly tested via their simple test rig, and therefore the characteristics of squeal instability could be identified. Based on their experimental results, Giannini and Sestieri (2006) concluded that the linear stability analysis was sufficient for predicting the onset of instability. Moreover, it was observed that the nonlinear behavior of materials, contacts and friction could not cause squeal instability. However, these factors played a major role in stabilizing the squeal vibration on a limit cycle.

In 2008, Giannini and Massi used the same test rig and deepened their knowledge about the characteristics of squeal instability. This time, they emphasized on the importance of the length of the brake pad in comparison with the wavelength of the disc modes. It was then concluded that depending on the pad length three different forms of squeal instability might occur: the sine-mode squeal, the cosine-mode squeal and the rotating squeal. Akay et al. (2009) reviewed the observations which had been made from this simple test rig.

One of the major difficulties of the brake squeal problem is modelling and measuring the dynamic friction force at the sliding interface. Wang and Woodhouse (2011) conducted an experimental study in which the difficulties of measuring the dynamic friction force were illustrated. Thereafter, in a companion paper (Woodhouse and Wang, 2011), a systematic comparison of the simple friction models reported in the literature was made by using the experimental data published in the first paper. The main conclusion of this study was that using very simple friction models such as Coulomb friction could lead to inaccurate prediction of unstable modes.

2.5.   The effect of doublet modes

In structural dynamics, especially in plate theory, the term "doublet modes" is frequently seen. A doublet mode refers to two modes of a structure whose frequencies are exactly the same, but their phases are different by 90 degree. For example, if a brake disc is modelled with an annular plate, the second nodal-diameter mode of the disc can appear in two ways as shown in Figure 2.10. The positive sign indicate the upward deformation of the plate along the out-of-plane direction while the negative sign indicates a downward deformation. Doublet modes appear when a structure is geometrically symmetric.
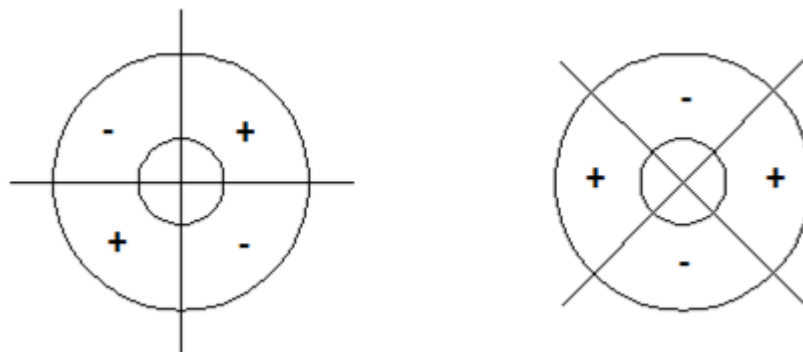
Figure 2.10. Doublet modes

The reason behind the importance of doublet modes in this study is that doublet modes can increase the risk of mode-coupling instability. In a brake assembly, the frequencies of doublet modes can be shifted slightly from the natural frequencies of the disc and will be no longer identical. Then, two close frequencies will exist in the system, which may be coupled in brake applications. As a result, in the design stage, it is always attempted to break the symmetry of the disc as much as possible. One possible solution is using a prime number of

the disc pillars. However, this approach is not always successful as the disc geometry will remain nearly symmetric.

2.6.   The effect of nonlinearities

One of the earliest studies on nonlinear dynamics of brake squeal was done by Chargin et al. (1997). A very simplified finite element model was used in their study for predicting the characteristics of squeal noise numerically. Some techniques for optimising the integration time and improving the convergence of analysis were also suggested in (Chargin et al., 1997). Many experimental observations of brakes under squealing condition could be simulated by these numerical results. The transient analysis of the brake model was carried out in MSC/NASTRAN. In those days, Abaqus had not yet developed CEA for systems with frictional contact.

The difficulties of conducting a dynamic transient analysis are fully explained in chapter 5. In brief, the computational cost of this approach has led to a limited usage of this method in practice. As a result, some researchers used different simplification and linearisation techniques in order to include the contributions of nonlinearities in the linearised system. In 1990, Dweib and D'Souza conducted a comprehensive study on a pin-on-disc system. In the first part (D'Souza and Dweib, 1990), the experimental setup of their study was described. More interestingly, in the second part (Dweib and D'Souza, 1990), they presented the results of the linear stability analysis along with limit cycles of nonlinear oscillations. For predicting the limit cycle motion of the system, they employed the method of "describing functions" (DFs). The friction force was defined by a polynomial of order three. This polynomial could represent the regime of the friction force in the static and dynamic states. Employing the method of describing functions could overcome the difficulties of doing the transient analysis.

It is worth mentioning that depending on the form of nonlinearities, the method of describing function can become mathematically arduous. It is fairly straightforward to deal with cubic nonlinearities via DFs. The "harmonic balance method" (HBM) can also be used for this purpose. On the other hand, if a non-smooth nonlinear function is used by these methods several harmonic terms must be included in the analysis, which makes the derivation of the required terms very difficult. As the friction force has a non-smooth behaviour, the implementation of these methods is still not very straightforward. Moreover, the application of these methods for large scale finite element models has only been done for cubic nonlinearities and a simplified brake model (Coudeyras et al. 2009a; 2009b).

In 2007, Massi et al. employed both complex eigenvalue analysis and dynamic transient analysis for investigating the squeal occurrence of a simple model consisting of a disc, a small friction pad and a supporting beam. The main conclusion was that the onset of instability could cost-effectively be predicted with CEA. CEA overestimated the number of unstable mode, as expected due to the absence of damping. Then, the nonlinear time-domain analysis was carried out in their study to demonstrate the significant role of the contact in stabilising the nonlinear oscillations on a limit cycle. Both CEA and transient analysis were therefore considered essential for predicting the squeal occurrence.

Theoretically if a bifurcating periodic solution (limit cycle) is stable, the bifurcation is called "supercritical", while an unstable bifurcating periodic solution is called "subcritical". In 2009, Hochlenert published a paper in which the existence of a subcritical Hopf bifurcation was investigated for the brake squeal problem. Hochlenert conducted this study to justify some observations from physical test rigs, which had not been covered by the existing theories. For example, according to the experimental observations, the frequency of squeal was independent of the rotational speed of the disc. However, squeal could only occur when the disc speed was below a certain level.

It was believed in Hochlenert's study that the reason for the afore-mentioned phenomenon is the existence of a subcritical bifurcation. In his study, the centre manifold theory was used for nonlinear stability analysis of a simplified brake model consisting of 12-degrees-of-freedom. The centre manifold theory with the application for friction-induced instability was fully explained in (Sinou et al. 2003; Sinou et al. 2004). The same brake model as the one in Hochlenert's study was used in (Von Wagner and Hochlenert, 2011) for making this point that nonlinearities could affect the stability boundary of a system, and therefore the linear stability analysis might be insufficient for predicting unstable modes.

Grange et al. (2009) proposed a method in which the nonlinear dynamic response of a pad-beam squealing contact was replaced with an equivalent linear system. The equivalent response was found by a spectral linearization of the nonlinear system with unilateral contact and friction conditions.

In 2012, Kruse et al. applied the harmonic balance method (HBM) to determine the limit cycle of nonlinear oscillations of a minimal brake model. In their study, the characteristics of joints and connectors in brakes were taken as the major source of nonlinearity. The application of HBM helped identify the critical unstable modes leading to squeal. In the authors' view, the focus of brake engineers on uncritical unstable modes would be time-wasting if they were not supposed to generate squeal. Therefore, it was better to identify the squealing via HBM and target them for squeal suppression.

Vermot des Roches et al. (2013) introduced a model reduction method in order to make transient analysis practical for industrial applications. This method which was called "component mode tuning" was applied on a train brake. Vermot des Roches et al. stated that as the only adjustable parameter for brakes in railway industry was pad, the pad must remain unreduced and the other components could be reduced. In this way, nonlinear simulations could be integrated cost-effectively during the design process.

2.7. The effect of damping

The bifurcation behavior which is shown in Figure 2.8 reveals that if there is no damping in the system, before the bifurcation point the real parts of the unstable mode are exactly the same and equal to zero. However, including damping makes the bifurcation behavior very complicated. Hoffmann et al. (2003) used a two-degree-of-freedom system in order to demonstrate how the bifurcation behavior would be affected if damping existed in a system. The first finding was that the imaginary parts of the eigenvalues did not coalesce in the presence of damping. Instead, there was a region in which the imaginary parts got close markedly and simultaneously the real parts diverged from each other. The second point was the real parts of the unstable mode were not the same before bifurcation. The eigenvalues of the system possess two negative-valued real parts whose values were dependent on the damping coefficients before bifurcation.

The last and the most important observation was that damping could cause "destabilization paradox" (Kirillov, 2004; Sinou and Jézéquel, 2007) in friction-induced vibration. Another example of friction-induced vibration in which the destabilization paradox occurs is squeal instability of clutches (Hervé et al. 2008). This paradox means that although the general function of damping is to shift the real part of eigenvalues toward the stable region ("lowering effect"), the non-uniform distribution of damping can make a system more unstable ("smoothing effect"). Chapter 5 extensively discusses the effect of damping on the bifurcation behavior of mode-coupling instability.

The effect of modal damping on the squeal occurrence was also investigated in (Massi et al. 2006a; Massi et al. 2006b). By means of an experimental setup consisting of the disc and pad, Massi et al. concluded that a large modal damping could help prevent squeal since damping generally could reduce the dynamic response of a particular model. On the other hand, a highly damped mode could be coupled with the other modes due to the effect of damping on its resonant frequency. Consequently, this study once again emphasized on the complexity of damping function in mode-coupling instability. Moreover, they stated that a simplified brake assembly could not fully represent the effect of different components on the

squeal occurrence and only the effect of a subset of squeal instabilities could be investigated by means of such experimental setups.

Cantone and Massi (2011) conducted an experimental study and confirmed the theoretical results of (Duffour and Woodhouse, 2004a) and (Sinou, J.-J. and Jézéquel, 2007). The main conclusion of this study was that homogenous distribution of damping reduced the probability of squeal instability while non-homogenous damping distribution could increase the risk of mode coupling instability.

2.8.   The effects of surface topography, roughness and wear

Bergman et al. investigated the influence of surface topography on the squeal occurrence in 1999. To make their point, a shot-blasted disc was tested in an experimental study. The shot-blasted disc reduced the contact areas which consequently resulted in a reduction in the microscopic friction coefficient. Then, it was shown that as far as the friction coefficient remained lower than 0.4, squeal noise would not occur. It was also found that the pattern of grit blasting had an important effect of the success of this method for reducing squeal occurrence. In 2006, Hammerström and Jacobson came up with a new pattern for grit-blasting of the brake disc. It was shown if the grit blasting was done in a spiral shape, it could significantly reduce the squeal occurrence. However, due to the effect of wear on the disc, this modification could last only for a limited number of braking.

The same research group also presented a paper (Eriksson et al. 1999) in which the surface topography of the pad was studied under silent and squealing condition. The results showed a relation between the size of contact plateaus and the probability of squeal noise generation. According to their observations, many small contact plateaus on the pad surface would increase the tendency of squeal noise while a few large plateaus were less likely to generate noise. Moreover, it was shown that the size of contact plateaus affected the silent pressure intervals. However, the variation of disc temperature from 100ºC to 200ºC had a minor effect on the size of the plateaus.

Chen et al. (2002) investigated the correlation between the different states of the squeal occurrence and surface topography of wear scars under reciprocating sliding. Four states for the squeal occurrence were considered: 1) no squeal occurred for 3800 cycles or more reciprocating sliding; 2) when the friction coefficient was smaller than a critical value in the beginning stage of sliding, no squeal occurred; 3) after a certain value of friction coefficient (critical value), squeal occurred 4) after a few cycles, sometimes squeal disappeared. A noticeable correlation was observed between these four states and surface topography of the

war scars. The results showed that for the flat-flat contact area of a wear scar under squealing condition, an uneven pit-like detachment of material could be observed. Moreover, adhesively joined asperities could be seen on microscopic scales for flat-ball contact area of a wear scar (again related to squeal).

A new index for considering the effect of surface topography on establishing or vanishing squeal was introduced by Sherif in 2004. This index was defined according to two topographic features: "the mean radius of asperities and the standard deviation of the height distribution of asperities of the sliding surfaces". Then, it was found that there was a threshold for this index above which squeal noise could not be triggered regardless of the sliding velocity. On the other hand, the triggering of the squeal could happen for the values lower than this threshold. Moreover, the establishment of severe squeal noise could only occur when this index was far less than this threshold.

Through an analytical approach, Slavič et al. (2007) looked into the roughness-induced vibration of a slider. In contrast with the other studies in which variations of friction law had been considered for this purpose, Slavič et al. used Poisson's impact law and Coulomb's friction law in their study. The effect of roughness was incorporated through a detailed modelling of the surfaces in contact. Interestingly, they found that distinct vibrations could be induced by modelling the roughness in a 'geometric' way and there was no need for incorporating the variations of friction force to see distinct vibrations. A closed-form solution for the frequency of induced vibration was also reported in their study, which was also validated experimentally. According to this closed form solution, the influence of different parameters such as the slider mass, wear etc. on the frequency of distinct vibrations could be identified.

AbuBakar and Ouyang (2008) and AbuBakar et al. (2008) included the effect of wear and surface topography in the stability analysis of a brake model. They showed that under prolonged brake application due to the effect of wear the pads surface became smoother and the contact area grew. As the contact analysis had a considerable contribution to the system stiffness, and consequently complex eigenvalue analysis), including the effect of wear could bring about more reliable squeal propensity predictions. For the experimental validation of the wear effect, pressure indicating films were used in this study.

The surface topography of the contact in a simple brake model was studied by Massi et al. (2008). What they observed was that the surface of the friction material contained several cracks after squeal events while quiet brake applications came along with a smooth and compact pad surface. The reason behind appearance of these cracks was considered due to

the fatigue of the friction material. In the authors' view, the fatigue was caused by the localized oscillations of the pad under squealing conditions.

Mortelette et al. (2009) focused on the impact of mineral fibres on squeal events. Recent advances in the design of brake pad led to the invention of "non-asbestos organic" (NAO) pads. In the authors' view, the composition of friction material could have a noticeable impact on squeal generation. They also observed that after squeal events the pad-rubbing surface had a highly structured morphology while it was flat and compacted after silent braking.

In 2012, Hetzler and Willner studied the influence of contact tribology on the results of stability analysis of brake systems. First, a statistical contact model was introduced in their study and two constitutive contact laws were derived according to this statistical model. The constitution contact laws defined the contact stiffness as a function of the local contact pressure. Then, a minimal brake model was used to investigate the effect of the contact model on the results of stability analysis. Interestingly, they found that at low and medium contact pressure, the contact stiffness/microscopic contact properties could have a significant influence on the results of stability analysis.

Magnier et al. (2012) investigated the correlation between the contact heterogeneities and squeal occurrence. They found that if the contact surface contained a heterogeneous distribution, the probability of the squeal occurrence would be increased in comparison with a homogenous pad material. A reasonable size for the contact heterogeneities for avoiding the squeal problem was also reported in their study.

The influence of wear on thermoelastic instabilities of disc brakes was investigated in (Ostermeyer and Graf, 2013). Wear was included as a boundary condition in the nonlinear analysis in terms of time-dependent contact topography and load-distribution. As a result, a periodic movement of hot bands which influence the effective braking radius could be observed in these results.

2.9.   Thermal effects, humidity and pressure distribution

Day et al. (1991) divided the thermal effects in brakes into two categories: bulk and localized effects. In disc brakes, the typical example of bulk thermal effects is disc coning. In brief, coning is a form of thermal problems causing distortion in the disc and consequently the disc surface will be no longer parallel to the wheel mounting surface. The localized thermal effects can cause hot spotting (which leads to thermo-elastic instabilities), damage on the rotor surface and wear. Day et al. explained that brake manufacturers should minimize the

variation of the pressure distribution at the contact interface in order to avoid localized thermal effects.

For including thermal effects in the result of squeal propensity predictions, Hassan et al. (2009) presented a paper in which the process of a fully coupled thermo-mechanical transient analysis was explained. Incorporating the thermal effects could update the heat that was generated underneath the pad in contact with disc, and consequently modified the contact pressure distribution. As a result, more reliable prediction of squeal propensity could be achieved.

Ouyang et al. (2009) conducted a transient analysis which included heat conduction, contact pressure and vibration analyses. First, the thermal analysis determined the temperature distribution at pads-to-disc contact interface. Then, the contact analysis was carried out to calculate the pressure distribution under the influence thermal deformation. At last, the dynamic transient analysis was done in order to determine the vibration level of the components. The results illustrated that the vibration level of the model with thermal effects were lower than the same analysis of the model without thermal effects.

Ishii-Dodson et al. (2012) investigated the dependency of squealing modes on temperature. It was observed that some unstable modes were largely temperature dependent while the others showed a weak dependency. Ishii-Dodson et al. then concluded that in-plane modes were noticeably temperature-dependent due to the dependency of the shear moduli of friction material and shim on temperature. Moreover, temperature had a considerable effect on the hat torsional stiffness. On the other hand, it was stated that out-of-plane mode were largely under the influence pressure distribution rather than temperature.

2.10.   Suppression of squeal noise

Structural modification of brakes is the most common method for suppressing squeal events. In order to identify which modal properties of which substructure plays a significant role in the generation of an unstable mode leading to squeal, a "design sensitivity analysis" (DSA) must be carried out. Guan et al. (2006) demonstrated how the conventional sensitivity analysis must be conducted for a brake under squealing condition and also how the results of DSA could help the process of structural modification.

Cunefare and Graf introduced an interesting technique of squeal suppression in 2002. A stack of piezoelectric elements were installed inside calliper's piston of a brake. The purpose of using piezoelectric elements was to generate a high-frequency harmonic force to suppress the squeal. Therefore, via an active control method, squeal noise could be eliminated. The

idea of using active control method for supressing squeal noise was followed in (Hochlenert and Hagedorn, 2009). The concept of 'smart pads' was introduced, which meant that the pads contained piezoceramic staple actuators. Two different control laws (optimal control with Kalman-Bucy filter and maximising the dissipated energy generated by friction force) were used in this study. Interestingly, both methods were able to suppress brake squeal. The advantage and disadvantages of using each method were also discussed in (Hochlenert and Hagedorn, 2009).

Due to the expensive implementation of active control techniques, Spelsberg-Korspeter (2010) investigated the capability of passive technique for squeal suppression. From the theoretical viewpoint, it was known that breaking the symmetry of a structure could help to avoid friction-induced vibration. Accordingly, he aimed to establish a systematic way of optimisation for the rotor design by breaking disc symmetries. The feasibility of taking such an approach has been always debated in industry. Some discussion regarding this matter was also presented in (Spelsberg-Korspeter, 2010). Spelsberg-Korspeter (2012) emphasized the potential of the rotor design for avoiding friction-induced vibration through an experimental study. In Spelsberg-Korspeter's view, splitting the doublet modes of the disc could significantly decrease the probability of unstable vibration and this goal could be achieved by structural optimisation of the disc.

More recently, a number of commercial software packages have been developed, which are able to optimise the geometry of a structure based on a desired objective function. Park et al. (2012) used Altair/Optistruct to carry out a shape optimisation on the brake components for reducing brake squeal propensity. In order to identify which components have the most contribution to mode-coupling instability, "modal participation factor to system" (MPFS) and "modal participation factor to component" (MPFC) were calculated. Then, the shape optimisation was conducted on the components with the most contributions. It is worthwhile to clarify that a target unstable mode can be treated in this way. However, this approach is always risky since new unstable modes may be generated, as a side effect.

The effectiveness of multilayer viscoelastic insulators (shims) for reducing the occurrence of squeal noise was studied in Fetjens et al. (2012). These insulators are commonly used by car manufacturers as it is believed that they are globally beneficial for stability of disc brakes. However, as mentioned earlier, these insulators can cause instability as well, which is in contrast with what is expected from their function. The difficulty of predicting the effect of these insulators on the stability of brakes is related to insufficient modelling of damping and stiffness of these viscoelastic materials. Fetjens et al. (2012) showed how the viscoelastic properties of shims could be integrated in finite element models and how the effect of these insulators on the system stability could be investigated.

Allert and Müller (2014) discussed the pros and cons of the common practices in industry for reducing squeal propensity such as structural modification of brakes based on the component contribution factor (CCF) and component mode contribution factor (CMCF). Thereafter, they presented a method to identify the sensitivities of brake systems to geometrical changes. As the direct implementation of sensitivity and optimization approach was expensive for large-scale FE brake models, they proposed a reduction method to efficiently define the countermeasures against the brake problem.

2.11. Chaotic behaviour of squeal

In 2011, Oberst and Lai presented a paper in which the chaotic behaviour of brake squeal was investigated in an experimental study. On the premise of some analytical studies in the literature on low-order models, in which the chaotic behaviour of friction-induced instability were investigated, Oberst and Lai treated brake squeal noise as chaos. Their experimental evidence showed that it was likely for brake squeal noise to become chaotic, but it was also stated that chaos was not the only brake squeal mechanism. Further analytical and experimental investigations are required to get a better insight into this aspect of brake squeal noise.

2.12. Stochastic/non-deterministic approaches

Each of the factors which are reviewed in this chapter can make a contribution to the generation of squeal noise. The variations in the values (numerical representation) of these factors can lead to a high level of uncertainty about the results of deterministic approaches of the brake squeal problem. This situation is exacerbated if the effect of manufacturing variability is also taken into consideration. In order to incorporate the effect of variability and uncertainty in the prediction of squeal propensity, a statistical technique must be used for the analysis of brake models. Chapter 6 comprehensively reviews the stochastic studies conducted on the brake squeal problem in the literature. As chapter 3 to chapter 5 are mostly dedicated to the conventional techniques (deterministic approaches) of the brake squeal problem, it is decided to review the statistical studies in chapter 6. Chapter 6 may be taken as transition from deterministic methods to statistical/non-deterministic methods of analysing the brake squeal problem.

3. Finite Element Modelling

As one of the main purposes of this study is to consider the effect of variability of brake components on squeal instability, the variations of material properties and also manufacturing tolerances must be considered in the 'brake surrogate models'. In this study, Young's moduli of the components are chosen to represent these variations regardless of being due to material properties or manufacturing tolerances.

Therefore, the normal mode analysis of the major brake components is done in this chapter. These results will be followed by measured frequencies and mode shapes of the components in the next chapter. Then, the material properties of the FE models are updated such that a high correlation between the simulated and measured frequencies and modes is achieved.

Finally, in chapter 9, it is assumed that the updated Young's moduli are the mean values of the input distributions representing the variability of components. Then, for each component, a deviation from the mean value will be considered to represent the expected range of variation caused by manufacturing processes.

3.1. CAD model of the brake

Finite element modelling of a mechanical system starts at the point that its CAD model is handed over to a FE analyst. Generally, there are many features in the CAD, which are merely for manufacturing and assembling purposes, and there is no need to mesh them in the finite element model. The most typical examples are edge fillets, bolts, nuts, plastic parts etc. Although some elements should be considered in the FE model to represent the joint and connectors precisely, it is not necessary to have meshes on the bolt/nut threads and so on. Figure 3.1 shows the CAD model of the brake under study.
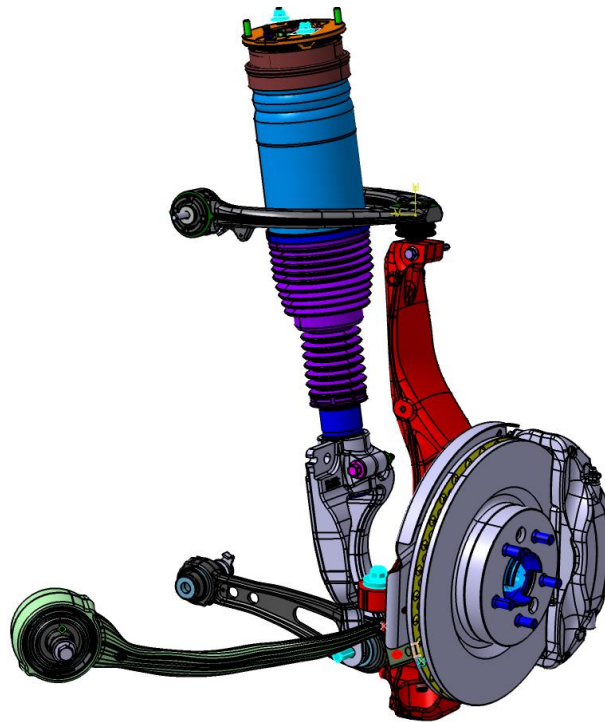
Figure 3.1. CAD model of the brake under study

3.2. Full FE model of the brake

Depending on the unstable mode which is the point of interest in a study, those components playing a minor role in the results of CEA can be excluded from the FE model. Including several components in the FE analyses increases the job running time significantly, yet not much useful information can be gained from them. On the other hand, this study attempts to deal with the complexity of industrial FE models, so it is aimed no to end up with a very simplified model in which industry shows little interest. Figure 3.2 shows the FE model of the brake used for the purpose of this study. As seen, in contrast with most previously studied brakes in the literature, this model consists of several components and is of high level of complexity.

The major components in this model are disc, calliper, knuckle, hub, pads, shims and pistons. Apart from these components, some connectors such as bushes, joints and guide-pins are also included in the model. Four bushes are embedded in the knuckle holes, which are used to apply the right boundary condition. The small conical shape on the top of the knuckle is one of these bushes. The points of the bushes along with the disc holes are clamped. If the other components (see Figure 3.1) were needed to be modelled, these bushes could be used to attach the knuckle to the lateral links. The total number of degrees-of-freedom in this model is over 2.3 million.
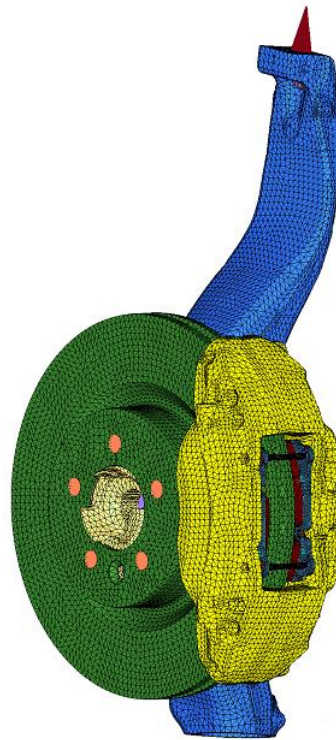
Figure 3.2. Finite element model of the brake

In the FE model, a number of contact interfaces also exist. In Abaqus, there are several contact formulations depending on the surface role, contact discretisation and tracking approach. A surface role can be a choice of "master" or "slave". The main constraint regarding the surface role is that a slave node should not penetrate into the master surface during the analysis. The contact discretisation can be either "node-to-surface" or "surface-to-surface". In the first approach, a slave node interacts with a group of nodes on the master surface, which are located close to the slave node. A slave node never penetrates into the master surface in this way.

However, in the surface-to-surface contact discretisation, the interaction occurs over some regions which are determined by averaging the positions of salve nodes. As a result, a small number of the master nodes may penetrate into the slave surface, but it does not happen

largely during analysis. Since in a surface-to-surface contact, the interactions occur in an average sense, it brings about more accurate stresses (smoother stress contours) in comparison with a node-to-surface contact. Note that there are a number of contact interfaces in a brake model such as pads-to-disc, pads-to-pistons and pads-to-calliper (abutment) interfaces which are modelled as surface-to-surface contact. These interfaces increase job running time significantly. However, it is vital to include them in the FE model since contact analysis is an essential step for CEA.

There are two options for tracking approach in Abaqus/Standard: small-sliding and finite-sliding. The major difference is that two bodies in contact may largely be deformed in the small-sliding approach while the relative sliding motion is small. Therefore, this approach can deal with many geometrically nonlinear problems. However, a relatively large sliding motion and even separation may occur in the finite-sliding tracking approach (Abaqus documentation). For the brake, small-sliding with friction has been chosen for the contact interfaces. Figure 3.3 displays pads-to-disc contact interfaces.
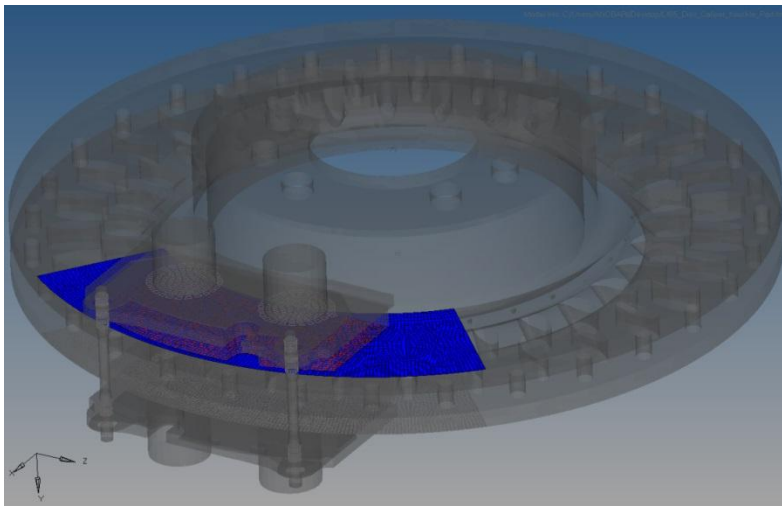
Figure 3.3. Pads-to-disc contact interfaces

In this study, friction at the contact interfaces is assumed to be Coulomb friction. It is worth mentioning that in the basic Coulomb model, friction coefficient is considered the same for all directions. However, an extended version of this model is also available in Abaqus for contact analysis. This version allows the friction coefficient to be different in various directions. Moreover, depending on the friction coefficient and contact pressure, a sticking phase may also exist during an analysis. However, no sticking phase is investigated in the current study.

The contact pressure is defined in Abaqus based on a choice of hard or softened contact. In the first option, the contact pressure and the overclosure of the surfaces are monitored in order to find out whether the contact is open or closed. When the contact pressure is zero and

also the overclosure of the surfaces is smaller than zero, the contact is open. On the other hand, the contact is closed when the pressure is greater than zero and the overclosure of the surfaces is zero. This constraint applies with a Lagrange multiplier during an analysis. In the case of the softened contacts, a user-defined relationship between the contact pressure and overclosure of the surfaces is required in the analysis (Abaqus documentation). The contacts of the brake model follow the principle of the hard contacts.

In the literature, it is very common to pressurize the pistons of a brake model with uniform loads. However, three-dimensional, 3-node hydrostatic fluid elements are employed here to model the brake fluid. It is believed that the pressure at the piston-pad interfaces generated by brake pressure is better represented in this way. Brake pressure has a significant influence on the static equilibrium point, which consequently affects the results of CEA and squeal propensity. Therefore, modelling in a more realistic way brings about more reliable results.

The fluid elements are provided in Abaqus for defining fluid cavities. In order to use these elements, the pressure and temperature of the fluid must be uniform at any point in time although the pressure and temperature can vary during the analysis (Abaqus documentation). In the finite element model of the brake, these elements fill the gaps between the calliper and pistons. Figure 3.4 displays a cross-section of the calliper in which the red elements show a part of the fluid elements and the blue elements represent one of the pistons. For the fluid elements, a reference node with a single degree-of-freedom must also be defined. This node is associated with the fluid pressure, whose location is specified by the geometry of the fluid cavity. Moreover, in order to define the fluid properties, there is an option in Abaqus specifying the fluid "TYPE". For the brake fluid, it is set to "HYDRAULIC", which means that the fluid is incompressible or approximately incompressible (Abaqus documentation).
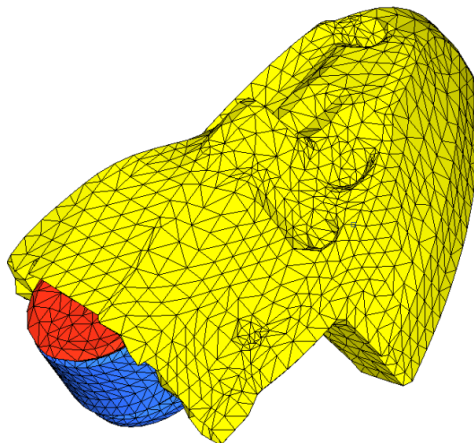
Figure 3.4. The fluid elements representing the brake fluid

3.3. Normal mode analysis

Normal mode analysis is usually executed to extract the natural frequencies and mode shapes of the individual components. Since there is no damping in the FE model of the components, the eigenvalue problem may be expressed as

$$(-\omega^2 \mathbf{M} + \mathbf{K})\boldsymbol{\phi} = \mathbf{0} \tag{3.1}$$

where $\mathbf{M}$ and $\mathbf{K}$ are the mass and stiffness matrices, ω represents the natural frequency and $\boldsymbol{\phi}$ indicates the eigenvector of the system. Generally, the results of the normal mode analysis are used for model updating of individual components. For individual components, the material properties such as Young's modulus, Poisson's ratio and density will typically be obtained through model updating. For the assembly structure, on the other hand, the properties of the interactions such as bolted joints, welds and bushes are identified in an updating process.

As mentioned earlier, model updating of the brake is not the main focus of this study. However, the results of normal mode analysis are presented here to get an idea about frequencies, mode shapes and material properties of the individual components. Randomising material properties can affect the modal properties of the components significantly, so it is useful to understand how they behave at the baseline design point.

3.3.1. Normal mode analysis of the disc

In disc brakes, rotor plays a significant role in generating noise, in particular squeal. According to the definition of squeal, out-of-plane and/or in-plane modes of the disc are often involved in squeal noise. As a result, modal analysis of the disc is of the highest significance in the brake squeal problem. Moreover, the results of this research show that the unstable mode which is the point of interest to the car mar manufacturer is highly sensitive to disc's Young's modulus. Therefore, it is worth looking into the modal analysis of the disc in the first place.

Figure 3.5 displays the generated mesh on the disc. Note that HyperMesh has been used as the meshing tool for all components and also for the full brake assembly. In this figure, a plot of the disc is also presented in order to illustrate the geometry of disc is of high level of complexity due to the shapes of the pillars and cooling vanes. Therefore, it is very time-consuming to mesh the disc if someone uses HEX elements. In industry, due to the tight deadlines of the projects, tetrahedral elements are mostly used for generating meshes. Since the car manufacturer sponsoring this study wants to assess the applicability of the proposed method on its daily jobs, it is attempted to follow their convention, i.e. using tetrahedral elements, to mesh the components.
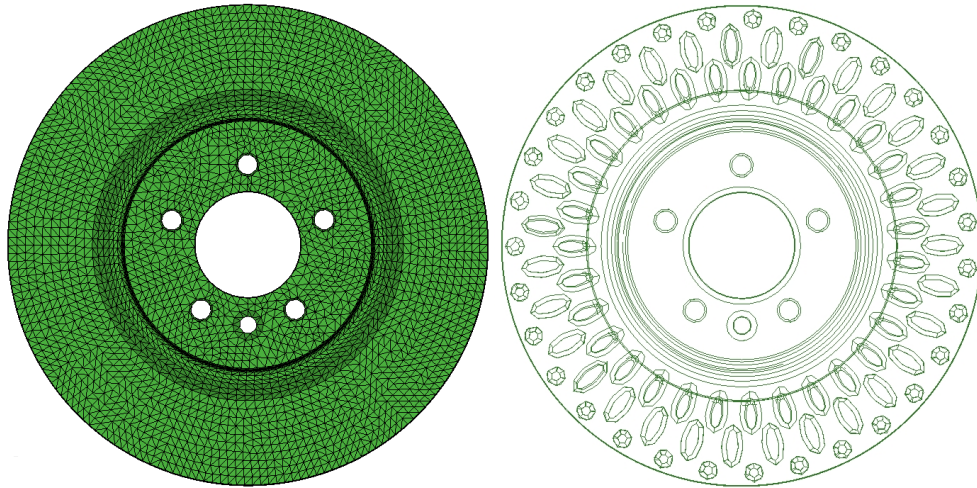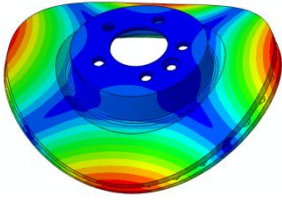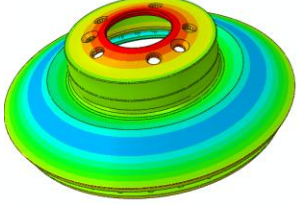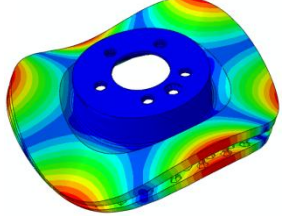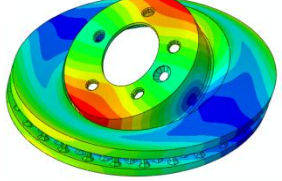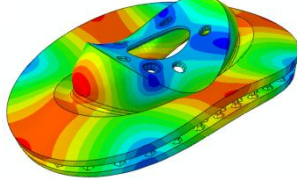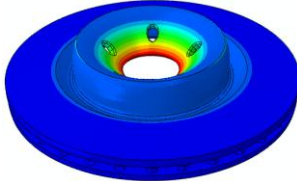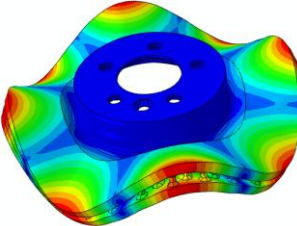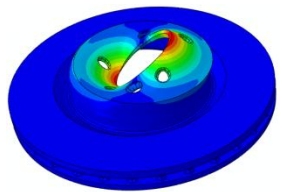
Figure 3.5. Mesh on the disc and the geometry of cooling vanes
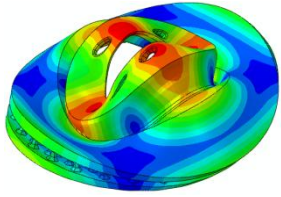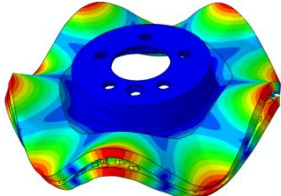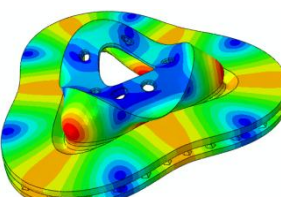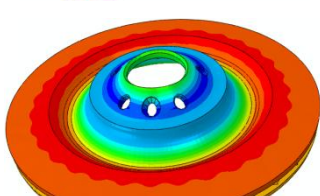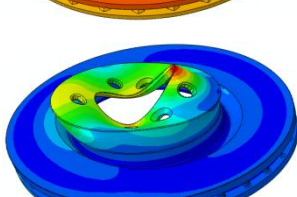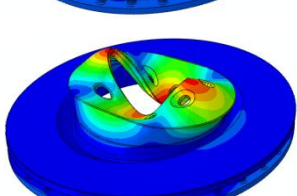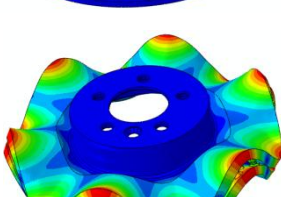
In this place, it is also useful to consider an important point in regard to the disc design. The plot of the disc shows that the number of pillars and cooling vanes are 31 at each circumference, which is a prime number, indeed. The reason behind choosing a prime number for the pillars and vanes is due to the fact that it is always advantageous to break the axis-symmetry of the disc geometry. The axis-symmetry of the disc leads to the formation of doublet modes. As discussed in chapter 2, the frequencies and mode shapes of doublet modes are exactly the same and only their phases are different by 90 degrees. The formation of doublets modes increases the risk of mod-coupling instability, and therefore choosing a prime number for the pillar and vanes helps to reduce this risk to some level. It is worth clarifying that this consideration cannot completely eliminate the formation of doublets modes.

In regard to the material properties of the disc, first of all, it is important to know brake discs are usually made from cast iron due to its thermal performance, resistance to cracking and distortion. Knowing this information helps get an idea about the limits within which material properties vary. Then, through an updating/optimisation process the disc's Young's modulus and density are determined so that a strong correlation between the measured and predicted modes is achieved. Note that the normal mode analysis of the individual components is carried out in Abaqus. The predicted frequencies and mode shapes of the disc are listed in Table 3.1.

For the predicted results, Young's modulus and density of the cast iron are set to 109.9 GPa and 7172 kg/m^3, respectively. Its Poisson's ratio is taken as 0.26. Please note that in the simulation results, out-of-plane modes appear in pairs, i.e. doublet modes, while only one of each pair is reported here.

Table 3.1. Predicted natural frequencies and mode shapes of the disc

Mode No.	Predicted frequency (Hz)	Mode shape
1	676.6	
2	1269.7	
3	1575.2	
4	1619.9	
5	1898.4	
6	2483.8	
7	2643.1	
8	3062.1	

9	3569.2	
10	3791.7	
11	3969.9	
12	4229.9	
13	4335.1	
14	4335.8	
15	4980.4	

Note that model updating of the disc is done by comparing the measured and predicted out-of-plane modes of the disc since it is more convenient to measure the out-of-plane modes in comparison with in-plane modes. The measured frequency and mode shapes of the disc are reported in the following chapter.

3.3.2. Normal mode analysis of the friction material

There are many challenges associated with the measurement of friction material properties. Despite a large number of investigations that have been conducted so far, still there is a great deal of uncertainty about the friction material properties. The measurement of these properties is out of the scope of the current work. What is important here is how to include the friction material uncertainties in the results of CEA. For this purpose, it is worthwhile to review the stress-strain law of the friction material.

Several experimental studies have confirmed that friction material is transversely (or planar) isotropic. In such materials, there are five independent parameters $E_p, E_t, \nu_p, \nu_{pt}$ and G_t where p and t represent "in-plane" and "transverse", respectively. E represents Young's modulus, G indicates the shear modulus and ν denotes Poisson's ratio. The stress-strain law of the friction material can be written as:

$$
\begin{Bmatrix} \varepsilon_{11} \\ \varepsilon_{22} \\ \varepsilon_{33} \\ \gamma_{12} \\ \gamma_{13} \\ \gamma_{23} \end{Bmatrix} = \begin{bmatrix} 1/E_p & -\nu_p/E_p & -\nu_{tp}/E_t & 0 & 0 & 0 \\ -\nu_p/E_p & 1/E_p & -\nu_{tp}/E_t & 0 & 0 & 0 \\ -\nu_{pt}/E_p & -\nu_{pt}/E_p & 1/E_t & 0 & 0 & 0 \\ 0 & 0 & 0 & 1/G_p & 0 & 0 \\ 0 & 0 & 0 & 0 & 1/G_t & 0 \\ 0 & 0 & 0 & 0 & 0 & 1/G_t \end{bmatrix} \begin{Bmatrix} \sigma_{11} \\ \sigma_{22} \\ \sigma_{33} \\ \sigma_{12} \\ \sigma_{13} \\ \sigma_{23} \end{Bmatrix} \tag{3.2}
$$
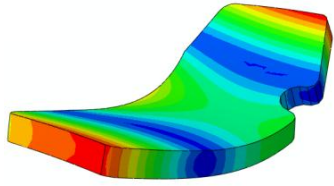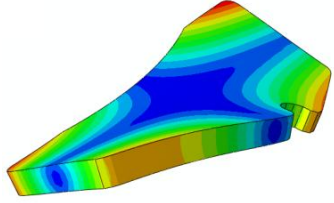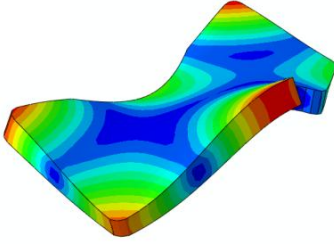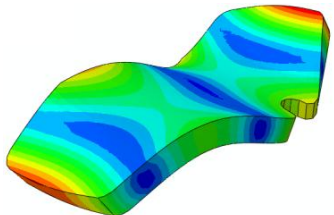
where $G_p = E_p/2(1 + \nu_p)$ and $\nu_{tp} = E_t \nu_{pt}/E_p$.

To derive friction material properties, first of all, what is common in industry is to carry out a few compressibility tests on the pad along the transverse direction (thickness), and also a few compressibility tests on a cubic cut of friction material along different directions. Although compressibility test provides pad's force-displacement data and there is not any information about pad's frequencies and mode shapes, it helps to have some estimates for pad's elastic moduli and Poisson's ratios.

Thereafter, a few modal tests are done on the pads and friction material in order to derive frequencies and mode shapes of the pad and friction material. Finally, during a model updating process, the experimental data from compressibility test are used as the initial guesses of the unknowns (elastic and shear moduli plus Poisson's ratios) and their values are updated so that a good agreement between the test and numerical results are achieved.

In Abaqus, the friction material is modelled as a composite material. Then, normal mode analysis is conducted to extract its frequencies and mode shapes. Table 3.2 lists the results of modal analysis on the friction material. For the predicted results, $E_p = 3487$ MPa, $E_t = 607$ MPa, $G_t = 800$ MPa, $\nu_p = 0.4529$ and $\nu_{pt} = 0.6154$. Moreover, the density of the friction material is set to 2670 kg/m^3.

Table 3.2. Predicted frequencies and mode shapes of the friction material

Mode No.	Predicted Frequency (Hz)	Mode shapes
1	701.7	
2	815.9	
3	1689.7	
4	1789.1	

Please note that the reported elastic and shear moduli plus the Poisson's ratios are the updated values which have been determined through minimising the differences between numerical and experimental data. The experimental data, i.e. the results of the modal tests, are fully discussed in the next chapter.
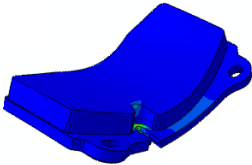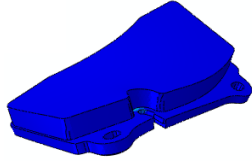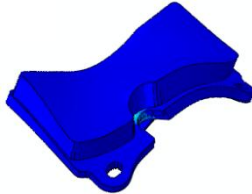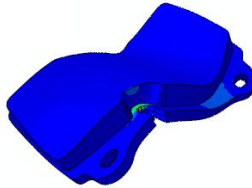
3.3.3.   Normal mode analysis of the pad

Brake pads consist of two parts: backplate and friction material. Although the friction material properties affect the modal properties of brake pads considerably, backplate makes the major contribution to the stiffness/elastic properties of the pads. The pad's backplate in the brake under study are made from steel. The positive point about steel is that there is not much uncertainty about the measurement of its material properties, and also it does not largely deviate from its nominal values. These values can accurately be determined through modal testing.

As conducting normal mode analysis on pad's backplate individually is not very informative, the analysis is done on the full pad.

Table 3.3 lists the predicted frequencies and mode shapes of the pad. For the predicted results, backplate's Young's modulus is 206.8 GPa and Poisson's ratio is 0.29. The material properties of the friction material are the same as those reported in the previous section.

Table 3.3. Predicted frequencies and mode shapes of the pad

Mode No.	Predicted Frequency (Hz)	Mode shapes
1	1884.2	
2	2059.9	
3	4468.6	
4	4788.3	

It is worth mentioning in the range of low frequency squeal (from 1 to 6 kHz), only four modes of the pad turn up in the results of normal mode analysis: the first and second bending modes, the first and second torsional modes. According to brake engineers' experience in industry, disc's out-of-plane modes and pad's 1st and 2nd bending and torsional modes play a significant role in the instability of brakes in the low frequency squeal. Hence, it is important to identify the first four modes of the pad accurately. In the next chapter, the experimental results on the pad reveal that a high correlation between the predicted and measured modes of the pad is obtained by the use of the updated material properties in the FE model.

3.3.4. Normal mode analysis of the calliper

In a brake system, calliper has the most complex geometry. Figure 3.6 shows the geometry and mesh on the calliper. As seen, there are many geometrical features on the calliper, which

cause a great deal of difficulties for FE analysts to mesh this component. Even cleaning-up the geometry does not help very much, and also the geometry cleaning-up is a formidable task by itself. Thus, tetrahedral elements are the only option for meshing of the calliper.
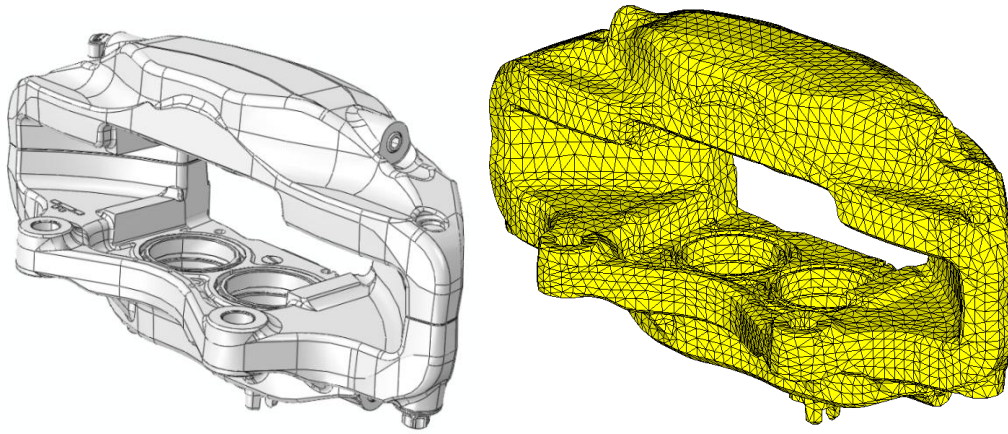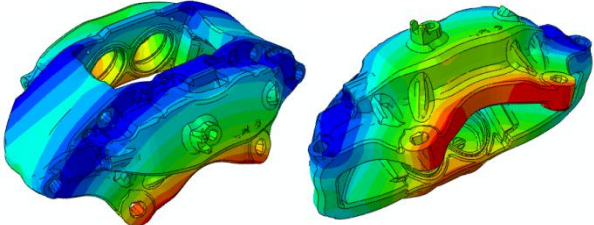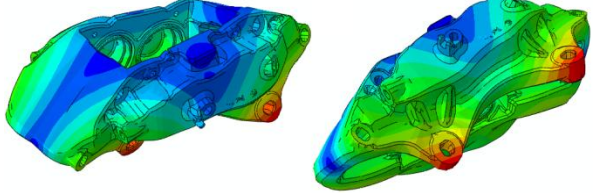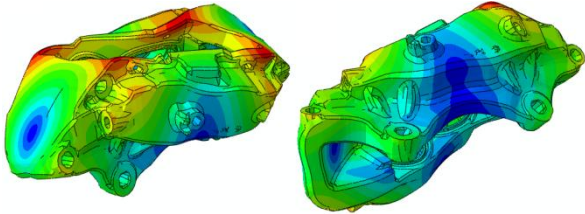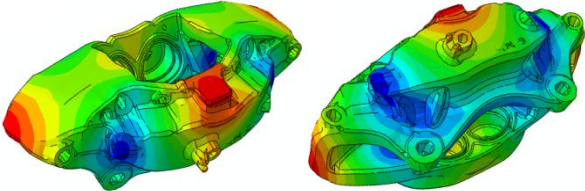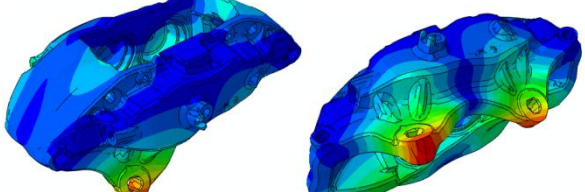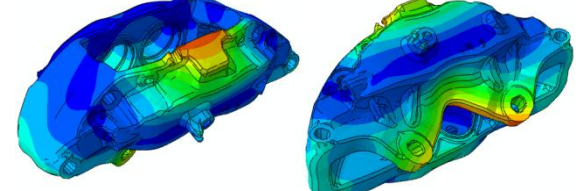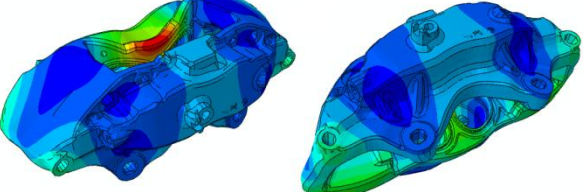
Figure 3.6. Calliper geometry and mesh

In regard to the material properties, the calliper is made from aluminium. Similar to steel, the positive point about the aluminium is that there is not much uncertainty about the measurement of its properties. Young's modulus, density and Poisson's ratios usually are close to the nominal values, yet some slight variations may be observed.

Table 3.4 lists the predicted frequencies and mode shapes of the calliper. For these results, Calliper's Young's modulus and Poisson's ratio are set to 70.0 GPa and 0.33. Moreover, the density of aluminium is taken as 2750 kg/m^3.

Table 3.4. Predicted frequencies and mode shapes of the calliper

Mode No.	Predicted Frequency (Hz)	Mode shapes
1	1830.4	
2	2037.1	

3	2800.4	
4	3355.6	
5	3702.6	
6	3948.0	
7	4470.8	

Since one side of the calliper is not enough to recognise a mode shape, the deformation of the top and side views of the calliper in the same phase have been listed in the above table. The same convention will be used for the experimental results in chapter 4.

3.3.5. Normal mode analysis of the knuckle

Depending on the frequency of the unstable mode which is explored in a study, knuckle may or may not be included in the FE model. In the literature, when the unstable frequency is lower than 2 kHz, it is recommended to consider the contribution of the suspension system. Otherwise, suspension links can be discarded from the FE model. Later on, it will be seen that the squeal noise under this study is at about 2.5 kHz. As this mode is quite close to the range within which the knuckle can contribute, the car manufacturer prefers to keep the knuckle up in the FE model. Figure 3.7 shows the mesh on the knuckle.
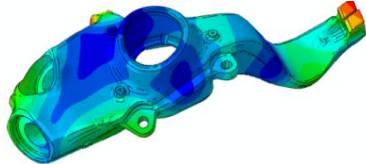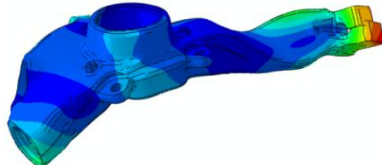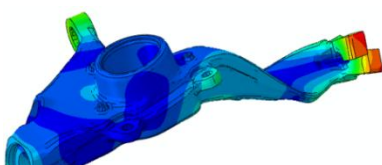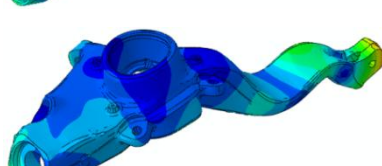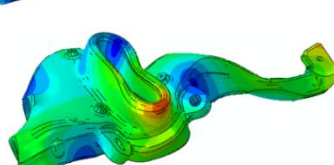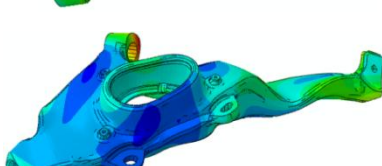
Figure 3.7. Meshes on the knuckle

Similar to the calliper, the knuckle is made from aluminium. The material properties of these two components are the same. In other words, Knuckle's Young's modulus is 70.0 GPa, Poisson's ratio equals 0.33 and its density is 2750 kg/m^3. Table 3.5 lists the predicted frequencies and mode shapes of the first ten modes of the knuckle.

Table 3.5. Predicted frequencies and mode shapes of the knuckle

Mode No.	Predicted Frequency (Hz)	Mode shapes
1	480.6	
2	840.6	
3	1025.1	
4	1494.1	

55

5	1832.1	
6	2139.7	
7	2632.4	
8	2964.2	
9	3245.7	
10	3310.3	

As the knuckle was delivered as a part of the full brake assembly and assembling of the brake needed a special expertise and measuring devices which were not accessible in Liverpool University, it was decided not to disassemble the brake assembly. Fortunately, there is not a great deal of uncertainty about the material properties of knuckle since it is made from aluminium. Therefore, it is assumed that the knuckle does not largely deviate from the nominal properties. This assumption will be supported when the full brake assembly is tested for the validation of the full brake assembly.

3.3.6. *Normal mode analysis of the hub*

The generated mesh on the hub is shown in Figure 3.8. The hub is a very stiff component made from steel. Its Young's modulus is 206.8 GPa and Poisson's ratio is 0.29.
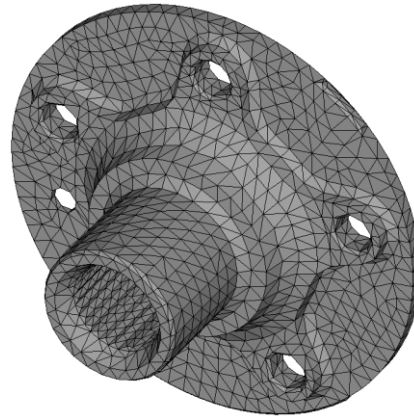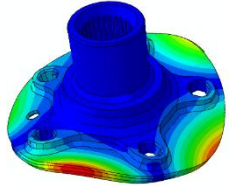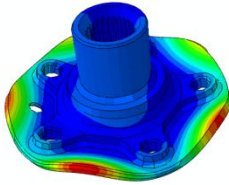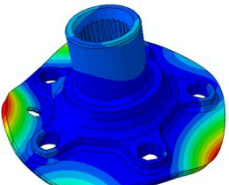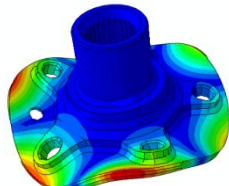
Figure 3.8. Meshes on the hub

Table 3.6 lists the results of normal mode analysis of the hub under free-free boundary condition from 100 Hz to 6.0 kHz. As seen, the first natural frequency of the hub is at about 4.0 kHz which supports how stiff this component is. Moreover, due to the axis-symmetry of the hub geometry, the out-of-plane modes turn up in pairs (doublet modes) in the results of the normal mode analysis.

Table 3.6. Predicted frequencies and mode shapes of the hub

Mode No.	Predicted Frequency (Hz)	Mode shapes
1	3956.8	
2	5076.6	
3	5361.1	
4	5562.3	

Similar to the knuckle, the hub was delivered as a part of the full brake assembly, so it was decided not to detach the hub from the assembly for modal testing. Incidentally, as the unstable mode under this study is at about 2.5 kHz, the modal properties of the hub may have the least contribution to this mode in comparison with the other components. However, it is important to apply the right boundary condition to the FE model of the brake assembly.

3.4. Conclusions

Finite element modelling of the brake is an essential part of squeal propensity predictions. In fact, surrogate model is built on the premise of the FE brake model. More accurate FE model leads to more realistic squeal predictions. In order to validate a full FE model of a brake assembly, normal mode analysis should be conducted on the brake components. Although model updating of brake models is out of the scope of the current study, the results of normal mode analyses have been presented to get an idea about the material properties, natural frequencies and mode shapes of the components. Since the effect of variability of these properties will be investigated in the following chapters, these properties have been reported in detail here.

4. Experimental Results

Following the results of normal mode analysis of the brake components in chapter 3, the measured modal test data of the same components are presented in this chapter. Then, the material properties in the FE model are updated such that a high correlation between the simulated and measured frequencies and mode shapes is obtained.

In chapter 9, it is assumed that the updated values of material properties are the mean values of the input distributions representing components' variability. Thereof, a deviation is assigned to each Young's modulus to represent the expected ranges of variation. These variations may be considered due to the deviation of material properties from their nominal values or due to manufacturing tolerances.

4.1.   Modal testing and analysis

Modal analysis provides useful pieces of information about the dynamic behaviour of a structure in terms of frequencies, modal damping and mode shapes. This information is obtained by the analysis of a set of experimental data which are collected via modal testing. In order to do a modal test, an excitation source like an instrumented hammer or electromagnetic shaker feeds energy into the structure. Then, the structure responds to the source according to the excitation amplitude and frequency range. The response of the structure may be collected by means of accelerometers, laser vibrometers, etc. Thereafter, the acceleration, velocity or displacement of measured nodes is determined through integration or differentiation of the recorded signal.

In order to purify the measured data from the influences of the external force given by the hammer or shaker, the amplitude of the output response are divided by the amplitude of input force through signal processing techniques. The result is known as "frequency response function" which is a function of driving frequency and abbreviated as FRF in the literature. For a lightly damped structure, a number of sharp peaks are usually observed in the output spectrum. These peaks indicate the locations of natural frequencies of the structure within the excitation frequency range. Damping of a particular mode is measured by the 'strength' of the peak. The higher level of damping leads to a flatter peak and vice versa.

Moreover, if only one excitation point and one measuring node exist in a test, it is not possible to map the mode shapes of a structure. A number of nodes are usually excited or measured in a test in order to capture the mode shapes of the structure. The required number of excited/measured nodes is dependent on the complexity of geometry of a structure. Obviously, more nodes results in more accurate mode shapes. Note that the explanation given to modal analysis and testing is related to the linear dynamic behaviour of structures. Nonlinear modal behaviour of structures is not investigated here.

In this study, the LMS test lab is used for conducting modal test and analysis on the disc, friction material and pad. For post-processing of the data, LMS uses a very well-known algorithm: Polymax. This algorithm fits a mathematical function on the collected data and produces the frequency response function (FRF) of the test data. The FRF provides useful pieces of information about frequencies, mode shapes and damping of the tested structure. In fact, Polymax indicates the location of stable poles of the fitted mathematical function, which are the frequencies of the structure.

Moreover, Polytec laser scanning vibrometer and its software are used for measuring the natural frequencies and deflection shapes of the friction material, pad and calliper. Thereafter, a number of conclusions have been drawn based on the experimental results

produced by LMS and Polytec. These conclusions are useful for the future experimental studies of friction materials and also modal analysis of a structure with complex geometry.

It is worth to clarify that Polytec laser scanning vibrometer provides users with the average output spectrum of measured nodes and also the deflection shapes of a structure. It means that the velocity, displacement or acceleration of the measured nodes in response to the excitation source are processed and reported at the end. Incidentally, the deflection shapes produced by Polytec software is so good that the mode shapes can qualitatively be compared with the predicted mode shapes by FE models. However, if someone aims to update a FE model via the Polytec experimental results, it is necessary to determine the FRFs of the structure via signal processing techniques. Thereafter, the predicted and measured mode shapes can be compared quantitatively as well.

4.2.   Modal test on the disc

In order to identify the material properties of a structure, a modal test is done under free-free boundary condition. The reason is that the properties of boundaries like joints, welds, etc., can somewhat affect the stiffness matrix of the structure and lead to inaccurate material properties. Furthermore, depending on the structure, the test can be done by roving hammer technique, roving accelerometer technique or under operational condition. In the case of disc, roving hammer is the most suitable and convenient approach.

In this technique, an instrumented hammer excites the structure from different places. The input force is measured by means of a force transducer connected to the hammer head and the response of the structure is measured via one or two accelerometers. Ewins (2000) recommended using two or more accelerometers since using only one accelerometer increases the risk of measuring the response from a node of one or more modes of the structure. A node is a point where the displacement of the structure is zero in a particular mode, so the response of the system cannot be measured at these places.

The measurement set up for the disc is shown in Figure 4.1. As seen, the disc rim is divided into 24 segments and it is excited at the two ends of each segmenting line (48 measuring points). The response is measured by means of two accelerometer located on the outer circumference of the disc. The measured FRF from 500 Hz to 2200 Hz and from 2200 Hz to 5000 Hz are plotted in Figure 4.2 and Figure 4.3, respectively. Moreover, the measured frequencies, modal damping and mode shapes of the disc are listed in Table 4.1.

Figure 4.1. Measurement setup for the disc — LMS

Please note that these experimental results have been produced by means of the LMS test lab. As the mode shapes can be clearly identified and compared with the numerical results, there is no point to do another modal test with the Polytec laser vibrometer. The out-of-plane mode shapes of the disc with 2,3,4,5 and 6 nodal diameters are usually used for the purpose of model updating. These mode shapes are displayed in red for the convenience of readers. Comparing the predicted mode shapes (chapter 3) with the measured ones reveals that the material properties of the disc are well defined in the model. These values are reported in section 3.3.1.

Figure 4.2. The sum FRF of the disc from 500 Hz to 2200 Hz — LMS
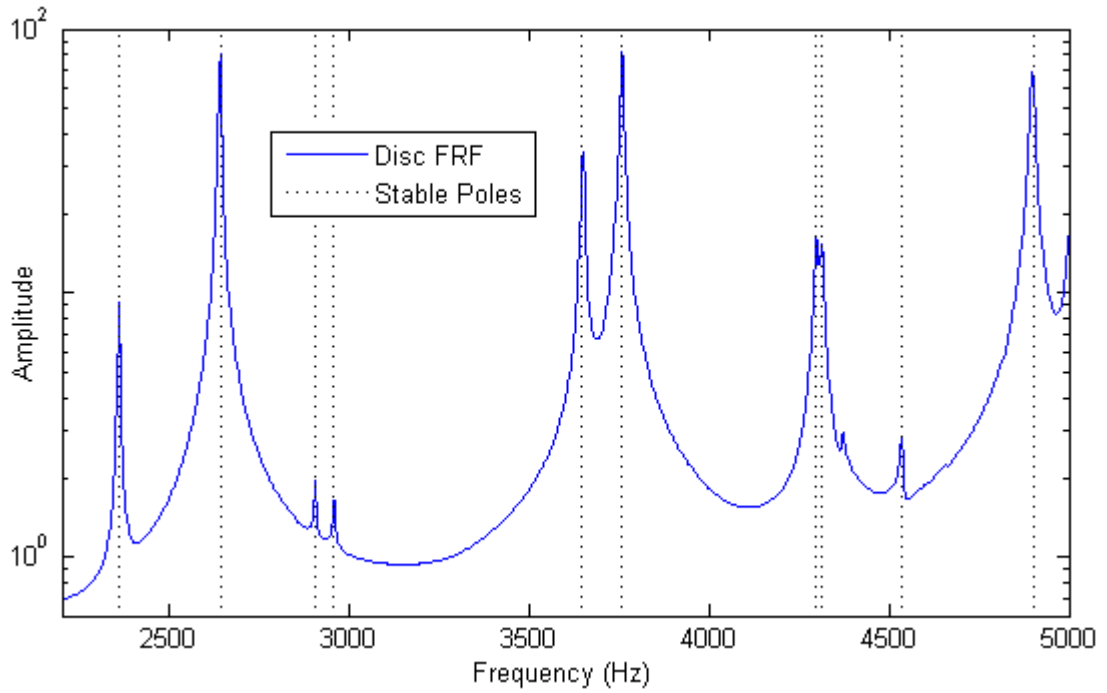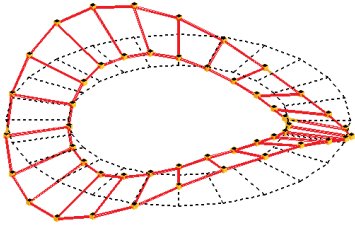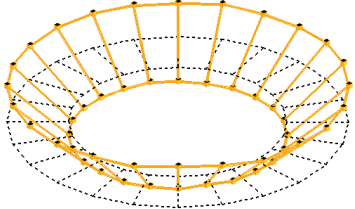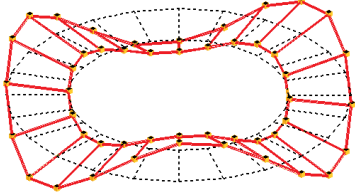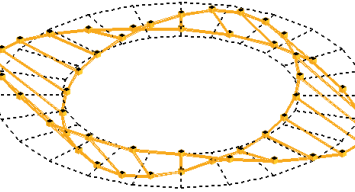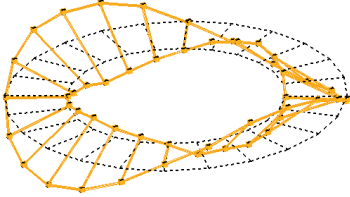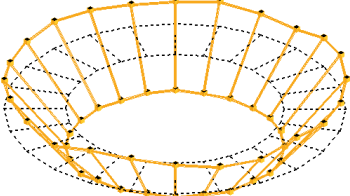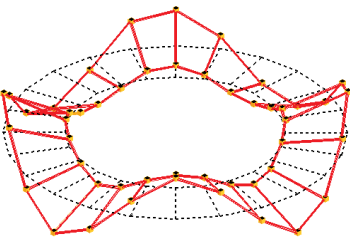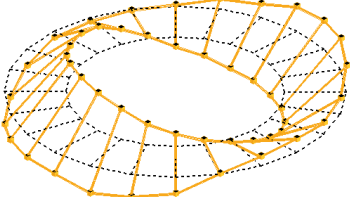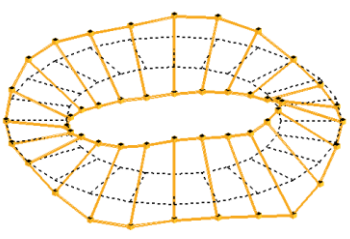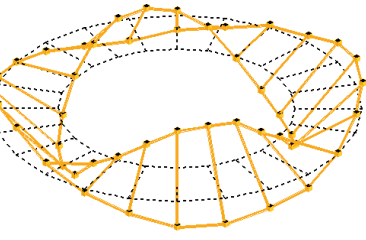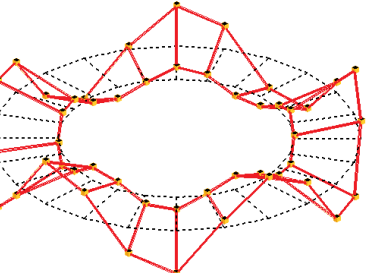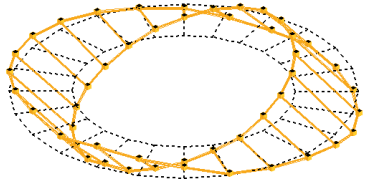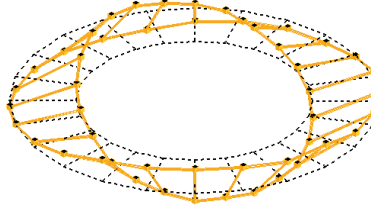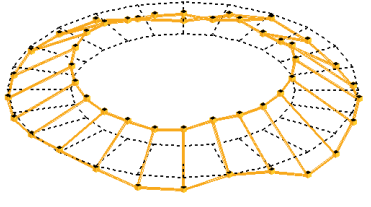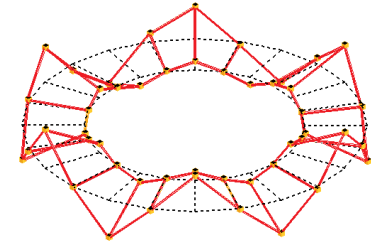
Figure 4.3. The sum FRF of the disc from 2200 Hz to 5000 Hz — LMS

Table 4.1. Measured frequencies, damping and mode shapes of the disc — LMS

Mode No.	Measured frequency (Hz)	Modal damping (%)	Mode shape
1	676.1	0.10	
2	1341.3	0.09	
3	1583.8	0.19	
4	1599.4	0.19	

5	1986.7	0.08	
6	2357.0	0.11	
7	2641.8	0.12	
8	2902.6	0.11	
9	2956.9	0.14	
10	3645.1	0.10	
11	3757.5	0.11	

12	4295.5	0.12	
13	4310.8	0.14	
14	4533.9	0.09	
15	4900.6	0.12	

4.3.   Modal test on the friction material

There are many challenges associated with the measurement of friction material properties. Due to the nature of this material which is a combination of glue with a variety of chemicals, a large variation in its properties occurs. This variation is not only observed from one brake pad to another, it is also seen when the loading case on a particular specimen changes. The identification of the friction material properties needs an extensive investigation which is not the aim of this study. However, it is useful to see how close its predicted and measured modes are. Incidentally, although there is a great deal of uncertainty about the properties of the friction material, the backplate mostly provides the elasticity of a brake pad and it will be seen that the measured modes of the brake pad closely match the numerical results. Thus, there is not much concern about the validation of the full brake assembly. This statement will be supported when the results of the modal test on the brake assembly is presented in the next chapter.

Figure 4.4 shows the measurement setup for the friction material. The test is done under free-free boundary condition, and the roving hammer technique is used for measuring the response of 19 points of the specimen. It is worth mentioning the nature of the friction material causes many difficulties in doing the hammer test. First of all, the surface of the friction material always remains uneven even though a proper finishing process is carried out on the surface. Consequently, it makes the impact test arduous. The roughness of the surface leads to experience many double impacts, so the specimen must be impacted many times until a few acceptable impulses are fed into the structure. Secondly, the recorded signal is very noisy due to the nature of this material. As a result, Polymax is not able to fit the mathematical function properly and find the stable poles. This issue will be fully discussed in section 4.4. The damping of this material is another issue. Damping always results in having flat peaks instead of sharp ones and can cause difficulty for Polymax in identifying the stable poles, in particular for close modes.
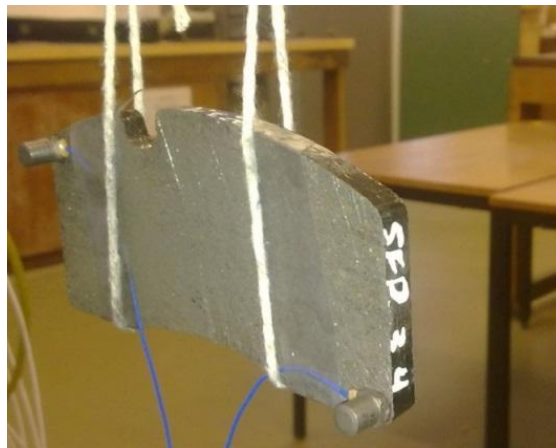
Figure 4.4. Measurement setup for the friction material — LMS

After all, the aspect ratio of the specimen is so that the structure is not sufficiently deformed in the hammer test, so it is very difficult to match the measured high-frequency mode shapes with the predicted ones. The FRF of the friction material measured by LMS test lab along with its stable poles are shown in Figure 4.5. It is worth mentioning that this test has been done several times and the best result is shown here. Moreover, the measured frequencies, damping and mode shapes of the friction material are listed in Table 4.2. The first three mode shapes are shown in red since they can be recognised with complete confidence and compared with the results of the finite element model. Respectively, these modes are the first bending, first torsional and second bending mode of the friction material. However, there is a little uncertainty about matching the fourth mode with the predicted one.
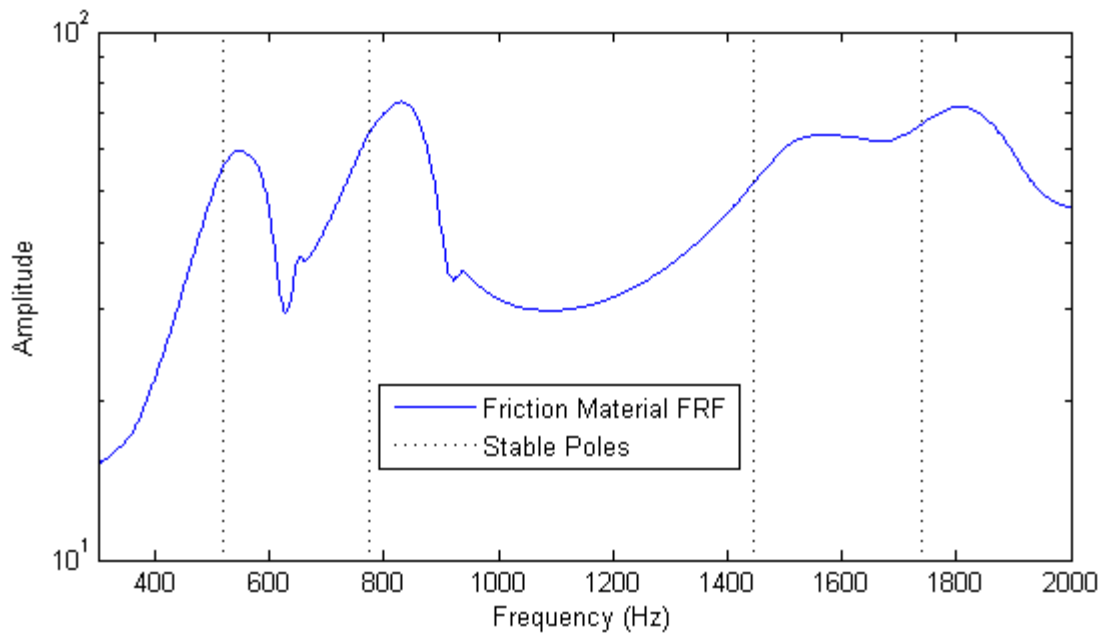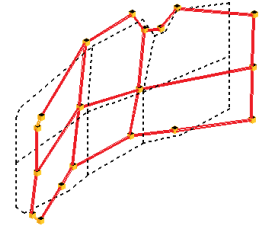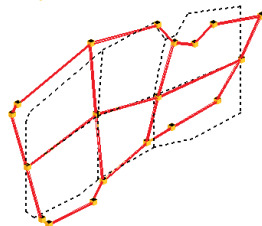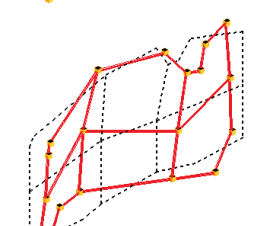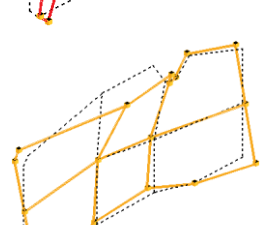
Figure 4.5. The sum FRF of the friction material from 300 Hz to 2000 Hz — LMS

Table 4.2. Measured frequencies, damping and mode shapes of the friction material — LMS

Mode No.	Measured frequency (Hz)	Modal damping (%)	Mode shape
1	520.23	6.70	
2	773.04	7.58	
3	1443.9	9.97	
4	1738.7	8.18	

Due to the difficulties of the impact test on the friction material and also the noisy response recorded by the accelerometers, another test is carried out by means of the Polytec laser scanning vibrometer. Unfortunately, there was a two-year gap between these two tests and the specimen used in the LMS test was no longer available for the Polytec test. Note that the dimensions of the new specimen are used for the finite element model. As a result, readers are recommended comparing the results of the Polytec test with those of the finite element model.

There are a number of positive points about doing the test via the Polytec laser vibrometer. First of all, the number of measuring points is so many that the results are presented very well and the mode shapes can be recognised with complete confidence. Secondly, the non-contact sensor, i.e. laser vibrometer, helps improving signal-to-noise ratio. Lastly, the frequency range within that a laser vibrometer works is much wider than accelerometers.

Figure 4.6 displays the test setup and measuring nodes of the new specimen. The boundary condition is again free-free but this time an electromagnetic shaker with a sine-sweep signal feeds energy into the structure instead of the instrumented hammer in the previous test. The average spectrum of the output is plotted from 500 Hz to 2000 Hz in Figure 4.7. Moreover, the measured frequencies and mode shapes are listed in Table 4.3. There is no doubt that the mode shapes produced by Polytec is much more recognisable than the mode shapes measured by LMS.
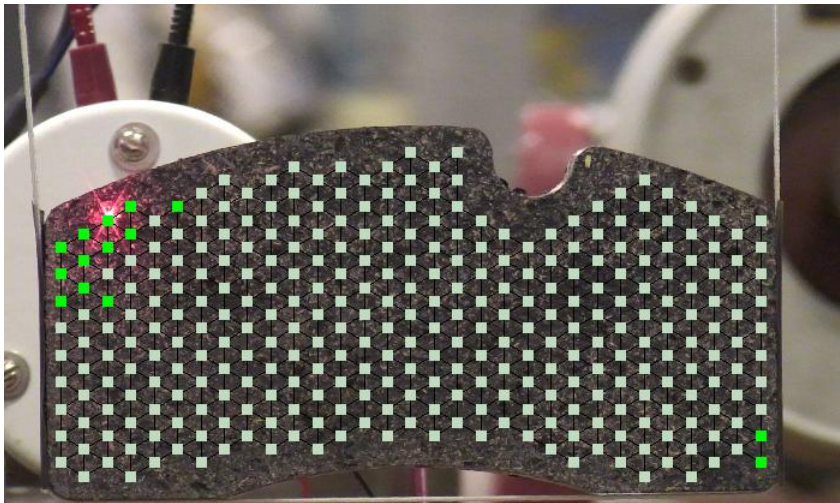
Figure 4.6. Measurement set-up for the friction material — Polytec
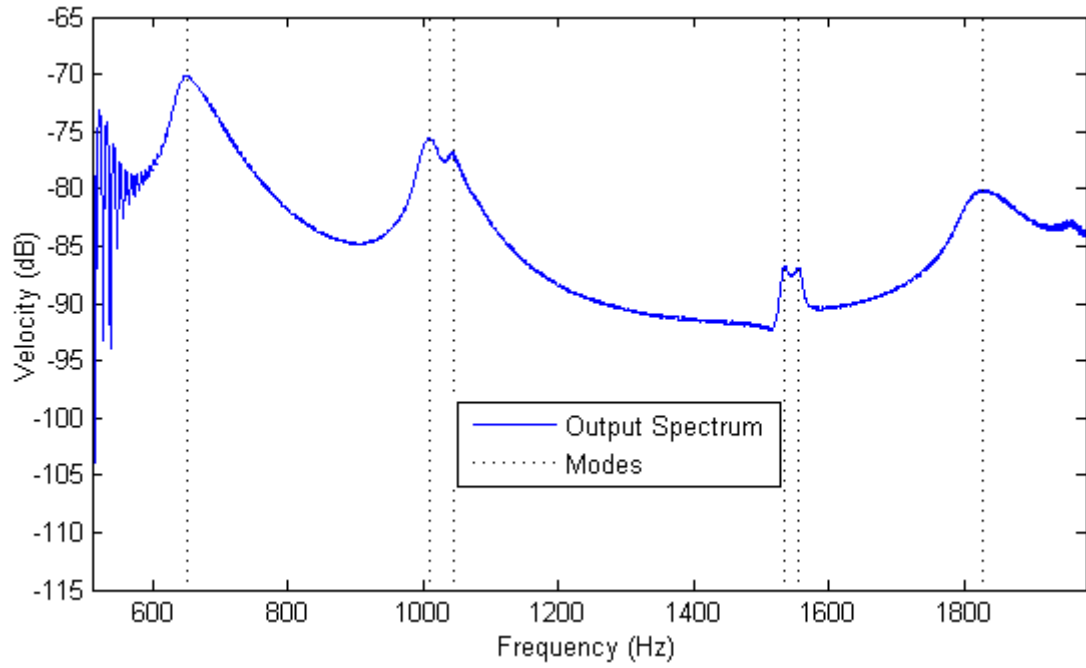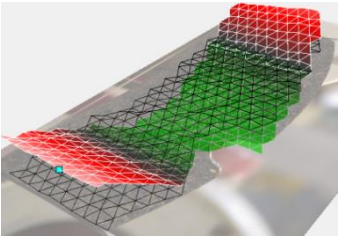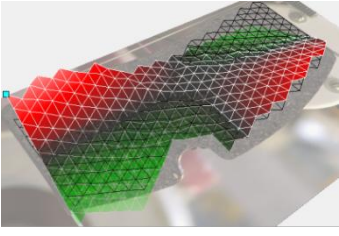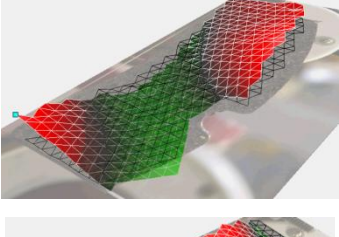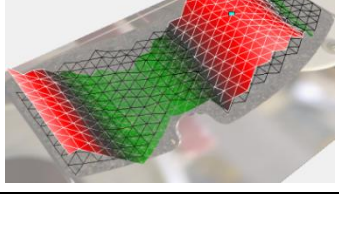
Figure 4.7. Output spectrum of the friction material from 500 Hz to 2000 Hz — Polytec

Table 4.3. Measured frequencies and mode shapes of the friction material — Polytec

Mode No.	Measured frequency (Hz)	Mode shape
1	650.15	
2	1010.2	
3	1533.2	
4	1828.6	

69

Please note that at about 1 kHz and 1.5 kHz, two peaks are produced by the software, while their corresponding mode shape shapes are exactly the same, at least from the out-of-plane angle. Hence, in Table 4.3, the first frequency and mode shape of each pair is displayed to avoid confusion. The reason behind this occurrence is fully discussed in section 4.4 since the same occurrence is observed in the results of the test on the pad by means of LMS.

4.4.   Modal test on the pad

Similar experimental approach is taken toward the brake pad. In other words, the brake pad is also tested under free-free boundary condition in order to find out how accurate its finite element model is. Figure 4.8 shows the measurement setup for the pad. The pad is hanged, and two accelerometers record the response of the impact test. In this test, the backplate is used for giving the impacts to the pad due to its proper surface finishing which avoids having double impacts.

The average FRF of the pad is plotted in Figure 4.9. As seen, two stable poles are found by Polymax for the first Bending, first and second torsional modes of the pad. Polymax produces two apparently close mode shapes for each, which in fact contravenes the orthogonally of modes. As a result, it is believed that Polymax misinterprets the measured data, and only one of each pair must be considered as the measured frequency and mode shape of the pad. Similar misinterpretation is also made by Polytec while the modes of the friction material are measured.
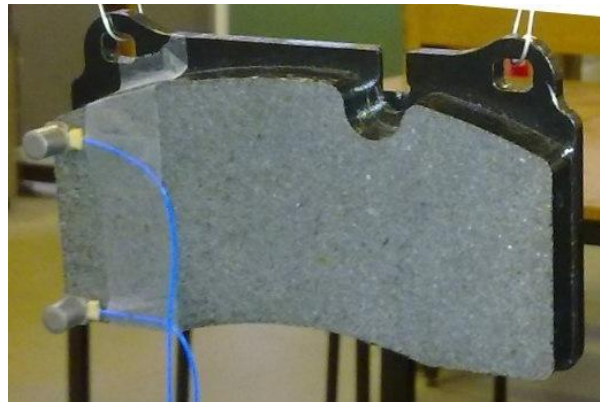
Figure 4.8. Measurement setup for the pad — LMS

According to the discussion made with the experts working at Brembo, it is recommended to take the first stable pole of each pair as the actual mode of the pad and ignore the second one. As a result, only the frequencies, damping and mode shapes of those modes are listed in Table 4.4.
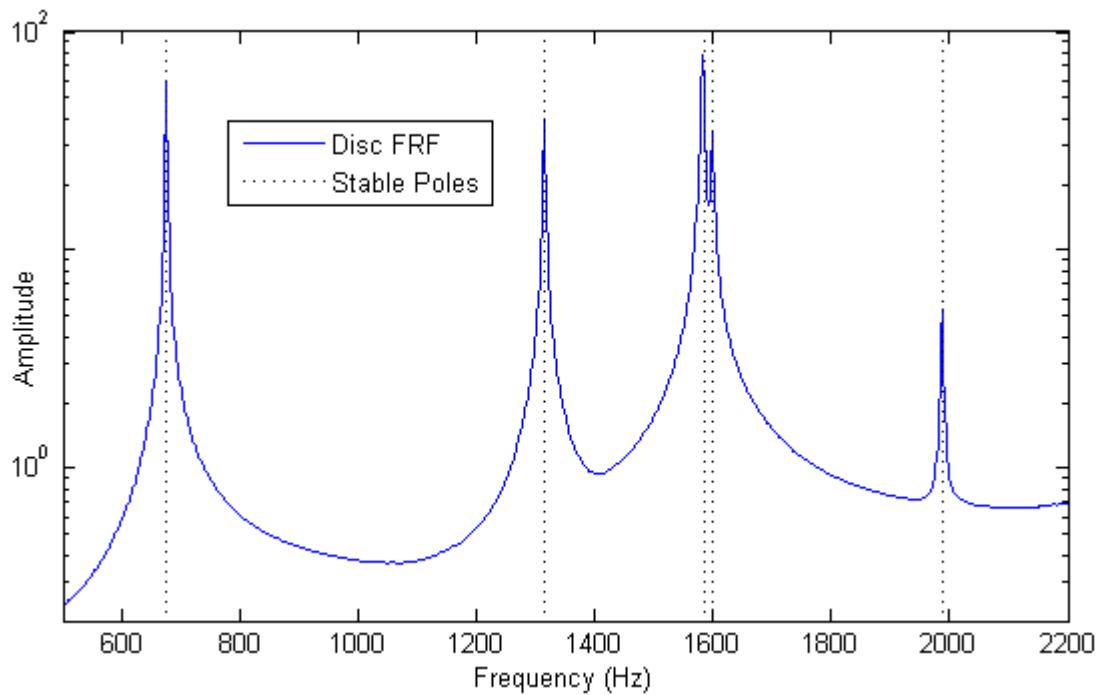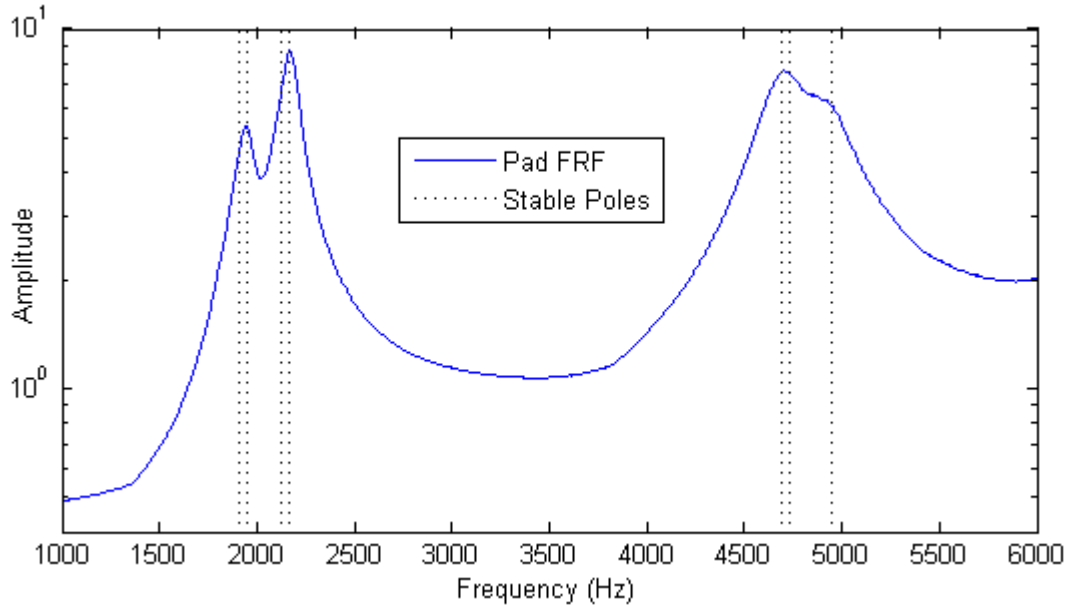
Figure 4.9. The sum FRF of the pad from 1000 Hz to 5500 Hz — LMS

Table 4.4. Measured frequencies, damping and mode shapes of the pad — LMS

Mode No.	Measured frequency (Hz)	Modal damping (%)	Mode shape
1	1912.1	5.96	
2	2120.3	4.06	
3	4691.3	3.78	
4	4944.2	4.15	

Similar to the friction material, the modal behaviour of the pad is also explored by the Polytec laser vibrometer. Figure 4.10 displays the measuring points on the pad. This test is carried out in two runs in order to better feed the structure with the input force. In the first run, an electromagnetic shaker feeds a sine-sweep force from 0 to 3 kHz into the pad. In the second run, the pad is excited from 3 to 6 kHz with the same form of the input signal. The output spectrums along with the locations of the natural frequencies are shown in Figure 4.11 and Figure 4.12.

Moreover, Table 4.5 lists the measured frequencies and mode shapes produced by Polytec. The positive point about these results is that no misinterpretation happened during the post-processing of the recorded data and also the mode shapes are very well presented.
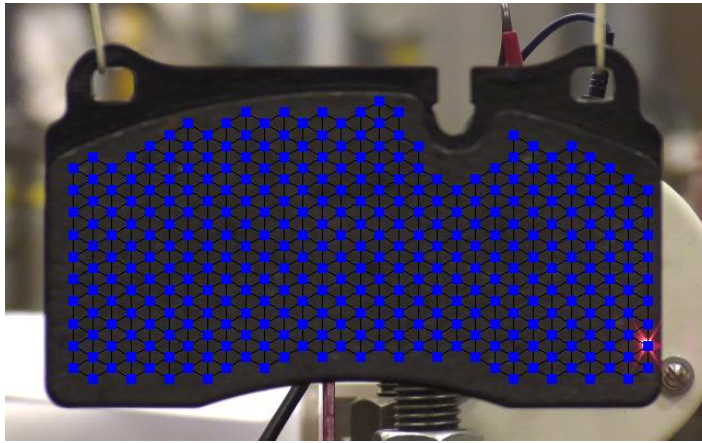
Figure 4.10. Measurement set-up for the pad — Polytec
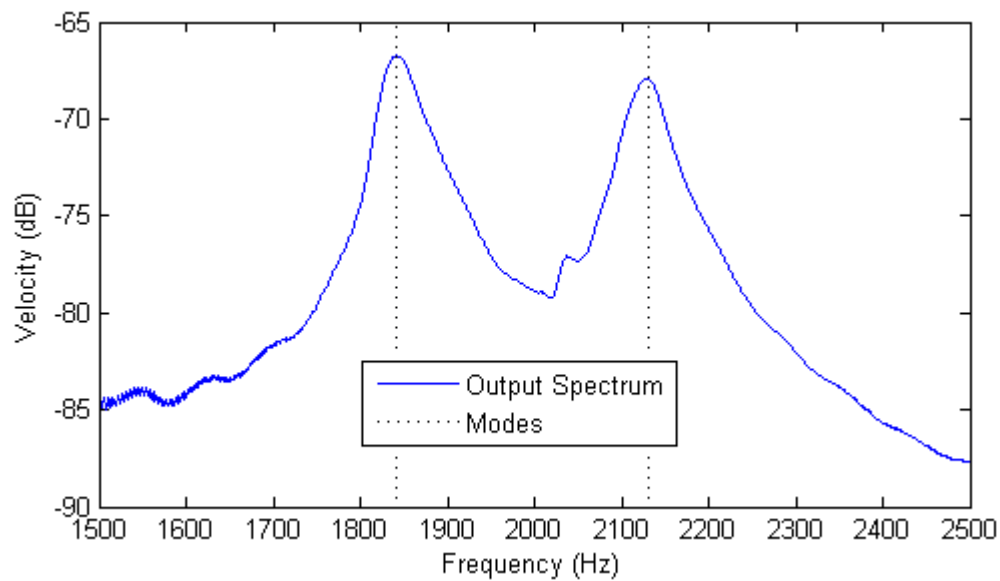
Figure 4.11. Output spectrum of the pad from 1500 Hz to 2500 Hz — Polytec

72
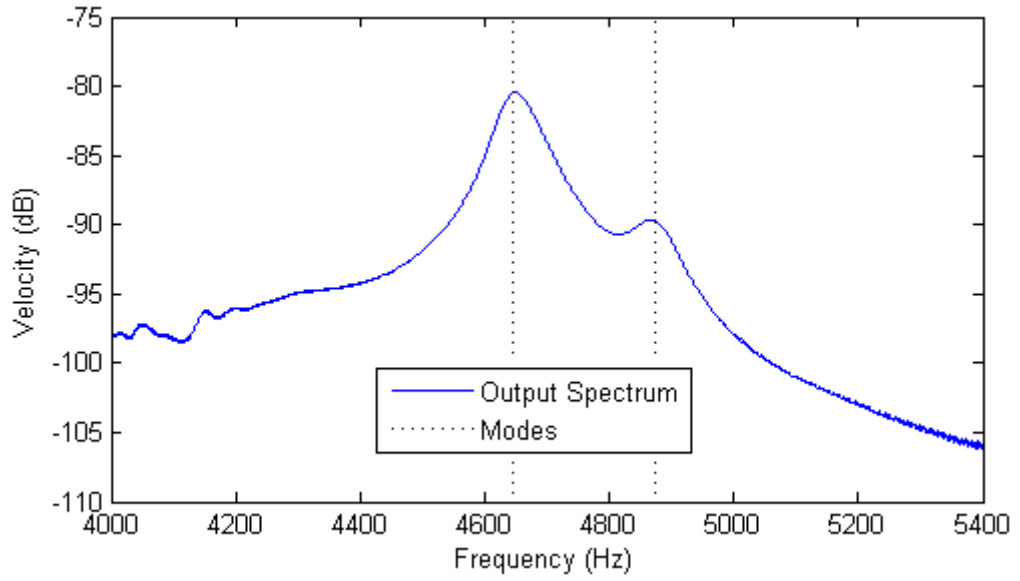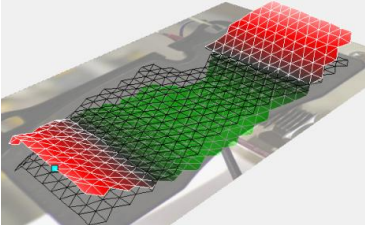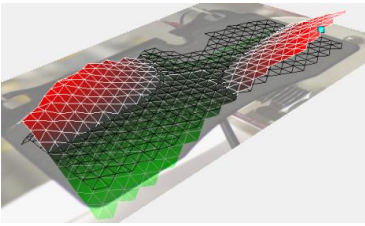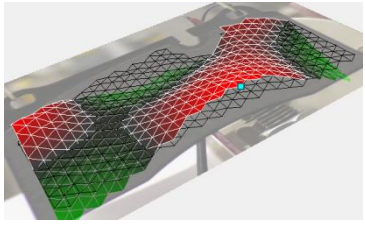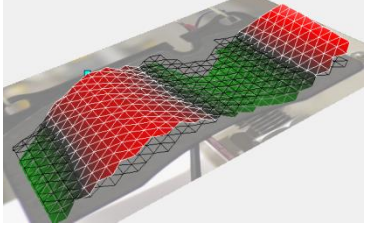
Figure 4.12. Output spectrum of the pad from 4000 Hz to 5400 Hz — Polytec

Table 4.5. Measured frequencies and mode shapes of the pad – Polytec

Mode No.	Measured frequency (Hz)	Mode shape
1	1841.5	
2	2130.1	
3	4644.5	
4	4873.5	

Once again, it is worth to clarify that the specimens used in the Polytec tests are different from those of LMS. Since there was a two-year gap between these two tests, the specimens used in the LMS tests were no longer available. Due to the better quality of the results produce by the lase vibrometer, it has been attempted to match the material properties of the finite element model with the ones measured by Polytec.

However, a number of pads have been tested by LMS to get an idea of how the friction material properties should be randomised for the purpose of uncertainty analysis. These results will be presented later. For now, it has been attempted to match the numerical and experimental results for a particular pad, not the mass-produced one.

4.5.   Modal test on the calliper

The calliper is only tested via the Polytec laser vibrometer. The number of measuring points, the convenience and speed of doing test and also the accuracy of results produced by the laser scanning vibrometer convince any modal analyst to use it for complex geometries like the calliper. If someone intends to use the LMS test lab for the calliper, a large number accelerometers must be used for recognising the mode shapes. Even the roving hammer technique brings no benefit in this case. Many places of the calliper body must be impacted while the response cannot be as detailed as those of Polytec.

Similar to the FE results, two sides of the calliper are tested since the deflection shape of one side is not enough for recognising the mode shapes. Figure 4.13 shows the measuring nodes on the calliper top. The output spectrums of the tests on the calliper top and side along with the locations of natural frequencies are shown in Figure 4.14 and Figure 4.15.
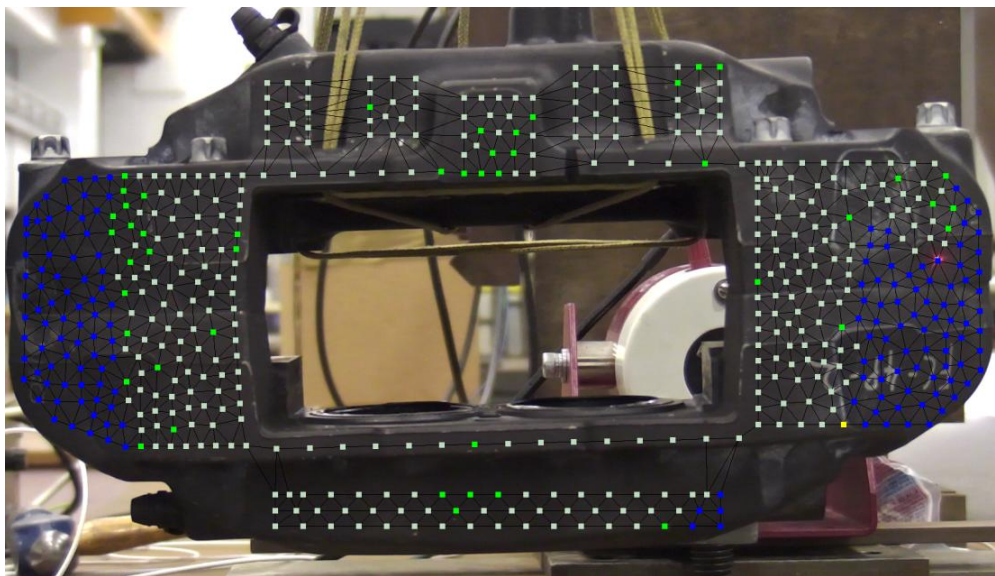
Figure 4.13. Measurement set-up for the topside of the calliper — Polytec
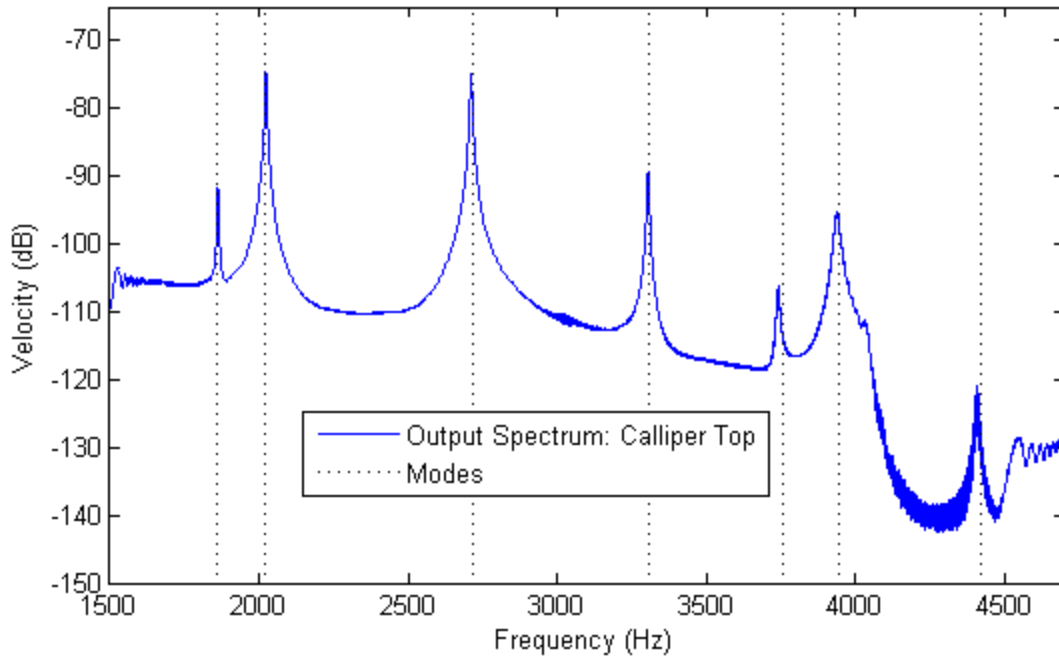
Figure 4.14. Output spectrum of the calliper top from 1500 Hz to 5000 Hz — Polytec
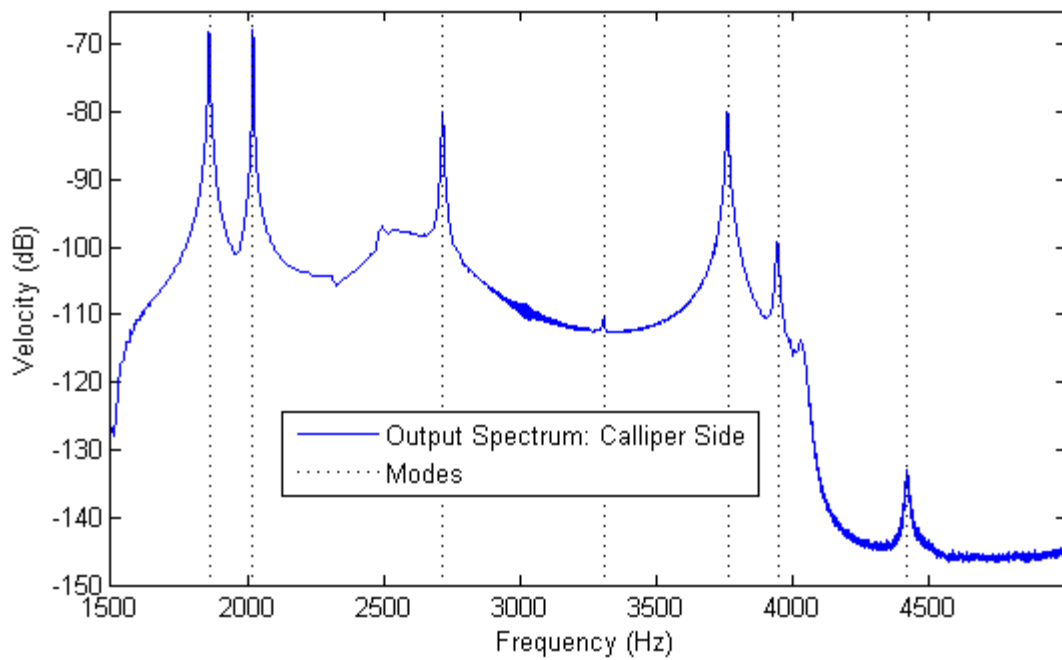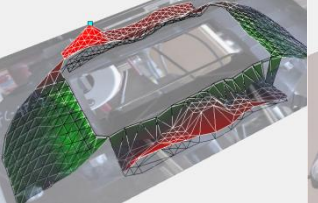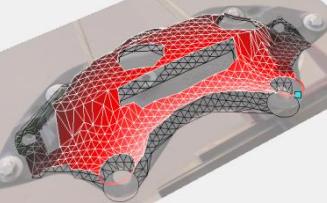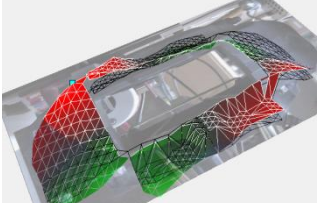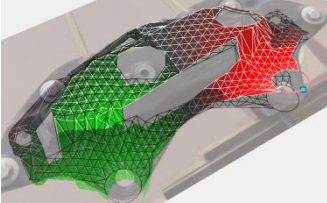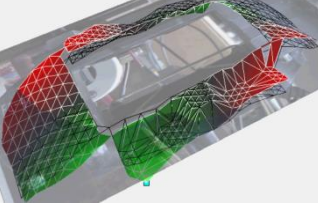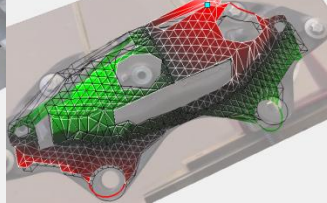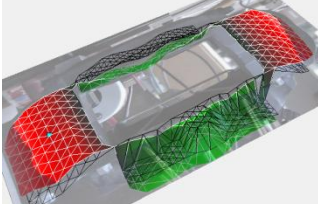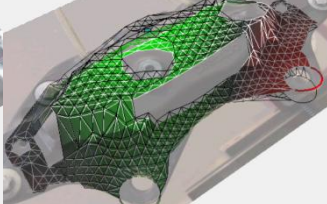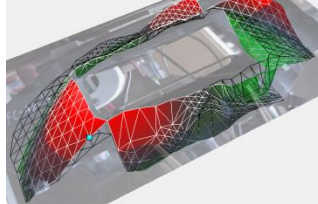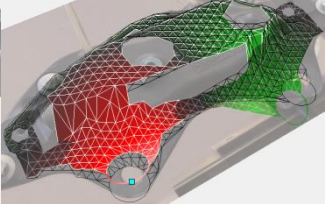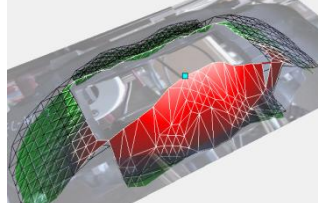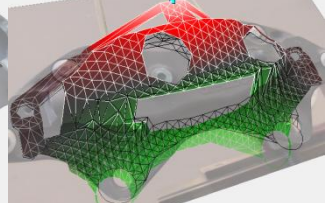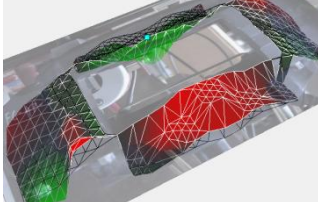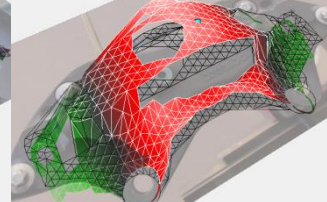
Figure 4.15. Output spectrum of the calliper side from 1500 Hz to 5000 Hz — Polytec

Table 4.6 lists the measured frequencies and mode shapes of calliper. As seen, the presentation of the mode shapes by Polytec is impressive. Even better judgment can be made when the animation of the mode shapes is considered. Moreover, it can be seen that there is a very good agreement between these experimental results and the predicted ones by the FE model (chapter 3).

Table 4.6. Measured frequencies and mode shapes of the calliper – Polytec

Mode No.	Frequency (Hz)	Mode shape
1	1859.77	
2	2020.3	
3	2716.0	
4	3306.4	
5	3760.5	
6	3943.4	
7	4420.3	

4.6.   Conclusions

The results of the modal tests and analysis on the major components of the brake are presented to become familiar with the dynamic behaviour of the individual components. Moreover, the accuracy of material properties which are used in their finite element models can be assessed by the results of this chapter.

For the purpose of modal testing and analysis, the LMS test lab and Polytec laser vibrometer have been used. Since Polytec laser scanning vibrometer measures the response of a large number of points by means of a very accurate non-contact sensor, it may be preferred to the LMS test lab for structures with complex geometries or sophisticated material properties.

5. Deterministic Approaches

In general, there are two deterministic numerical approaches toward the brake squeal problem: complex eigenvalues analysis (CEA) and the transient analysis. The pros and cons of each method along with a simple example illustrating the implementation of both methods are presented in this chapter. It is also explained why the complex eigenvalue analysis has been chosen for the purpose of the current study.

CEA is applied on an asymmetric system with non-proportional damping. This system will be used in the following chapters for extending the perturbation method to be applicable on friction induced vibration. Then, the results of CEA on the full brake assembly are presented. The experimental results on the physical brake are also reported for the validation of the FE model. Thereafter, an example of a structural modification on the brake under this study is given here in order to illustrate the common approach in industry for suppressing unstable modes of brakes, which may lead to squeal noise.

The difficulties of conducting a dynamic transient analysis on a full brake assembly are briefly discussed at the end.

5.1. Numerical approaches toward the brake squeal problem

In general, there are two numerical approaches toward friction-induced problems: complex eigenvalue analysis and transient analysis. As complex eigenvalue analysis deals with the linearised system, it can only predict the onset of instability. In fact, this approach finds eigenvalues of a system in a complex form like $\lambda_j = \alpha_j + i\,\omega_j$ where α_j and ω_j are the real and imaginary parts of the jth eigenvalue, and then assesses the system stability by the sign of the real part. The real part of an eigenvalue indicates the growth/decay rate of the system oscillations, while the imaginary part shows the oscillation frequency. One or more positive real parts of the system eigenvalues indicate instability. A positive real part enlarges the amplitude of oscillations without bound in the linearised system.

On a different approach, transient analysis finds the time-domain response of a system with respect to an initial disturbance (free vibration) or an excitation source (forced vibration). The time domain response contains useful pieces of information including the amplitude of nonlinear oscillations, the frequency of oscillations, the limit cycle of oscillations, the time-delay between the input force and system response, etc. Ideally, it is more informative to use both approaches for a single problem. What happens in reality though is that complex eigenvalue analysis is being used much more widely than transient analysis, especially in industry. The reason will be discussed in the next section.

5.2. CEA versus transient analysis

In 2005, Ouyang et al. comprehensively reviewed the pros and cons of doing CEA and transient analysis for the brake squeal problem. In general, if the solution close to the static equilibrium point is being sought, CEA can provide a very good approximation of the system stability. However, if the solution far from the static equilibrium point is needed or if the effects of time-dependent loads, time dependent material and also nonlinearities are being investigated, transient analysis is the right choice. To be more precise, the following aspects should be considered when deciding which approach must be taken toward this problem.

- *Time efficiency*

    CEA produces the unstable modes of a system in one run. Not only can the real and imaginary parts of the eigenvalues, but also the mode-shapes of the unstable frequencies be determined in one run. In this sense, CEA has a great advantage over transient analysis. Although "Fast Fourier Transform" (FFT) of the time-response of a particular DOF can provide unstable frequencies and amplitudes, it is impractical to determine the mode shapes of large-scale FE models via transient analysis.

The very useful piece of information which can be found via transient analysis and is missed in CEA is the limit cycle of nonlinear oscillations. This information cannot be determined via CEA since nonlinear elements cause the response to tend to a limit cycle. However, note that all runs of transient analysis do not necessarily converge to a limit cycle. Many attempts must be made until one of the runs produces the limit cycle. Moreover, the time of each analysis does matter. While one CEA of the brake under this study takes 12 to 36 hours, a transient analysis may take one week or so. Of course, these estimations are totally dependent on the computational facilities and how many seconds of the time-response are needed. As a result, there is no doubt that CEA is much more cost-effective than transient analysis and this is the main reason behind the extensive use of CEA in industry.

- *Nonlinearities and non-stationary features*

One of the main drawbacks of CEA is that the effects of nonlinearities and non-stationary features such as time-dependent material properties cannot be incorporated in the analysis. CEA linearises the equation of motion about a nonlinear static equilibrium point, so the effects of nonlinearities are accurate close to steady sliding point (Ouyang et al., 2005). If the solution far from the equilibrium point is needed or if time-dependent loads or material properties exist in a problem, transient analysis can provide more accurate results.

- *Squeal propensity*

As discussed earlier, CEA produces the real and imaginary parts of the eigenvalues and also the eigenvectors of a system. Although in this way the unstable frequencies and mode shapes of the system are identified quickly, it cannot be determined which unstable modes leads to squeal at the end. A positive real part only shows the growth rate of oscillations, i.e. squeal propensity or the tendency of divergence in the solution, but in reality the solution does not grow unboundedly and nonlinear elements of the system impede this growth. After a limited number of oscillations, what is observed in reality is that the solution of the system tends to a limit cycle motion. The limit cycle motion can be only determined via transient analysis. However, bear in mind that selecting a node of the geometry which has the largest amplitude in the time-domain approach is also tricky.

- *Structural modifications of brakes*

Another main reason that CEA has gained a very good reputation among brake engineers is the format of its results. Since mode shapes of unstable frequencies can

pave the way of structural modification, CEA is preferred to transient analysis by far in industry. What is common in car industry for reducing the likelihood of squeal noise is to make some structural modification on brakes in order to reduce the number of unstable modes. For this purpose, it is vital to know which degrees-of-freedom have the largest deformation or zero displacement in a particular mode. This information helps to find out at where the stiffness or mass of the system can be changed for suppressing an unstable mode with the least side effect on the others. In fact, brake engineers choose a more conservative option in this way since they attempt to reduce the number of unstable modes regardless whether they lead to squeal or not.

It is worth mentioning that some researchers used different simplification and linearisation techniques in order to include the contributions of nonlinearities in the linearised system. A number of methods such as Describing Functions (D'Souza and Dweib, 1990), Centre Manifold (Sinou et al., 2003; Sinou et al. 2004) and Constrained Harmonic Balance (Hervé et al., 2009) have been employed in the literature for this purpose. Interestingly, Coudeyras et al. (2009a; 2009b) determined the limit cycle of nonlinear oscillations via Constrained Harmonic Balance Method for a simplified brake system. However, the main shortcoming of these approaches is that there are a variety of nonlinearities that cannot be studied in this way. For example, the limit cycle of a system with a cubic nonlinearity can adequately be determined through these techniques, while it is arduous to take the same approaches for a system with a non-smooth nonlinearity.

Sinou et al. emphasized the significance of both complex eigenvalue analysis and transient analysis in (Sinou, 2010; Sinou et al. 2013). For simplified finite element brake models, transient analysis was carried out along with complex eigenvalue analysis in (Sinou, 2010; Soobbarayen et al. 2013). However, for large-scale finite element models, transient analysis can sometimes become very expensive. In such cases, industry only relies on the results of complex eigenvalue analysis and attempts to design a system so that it remains stable under various circumstances. In other words, they prefer to take a cost-effective conservative approach rather than a very expensive accurate method.

For the same reasons, CEA is also used for the purpose of the current study.

5.3.   Complex eigenvalue analysis (CEA)

Consider the generalized form of the equation of motion for a system with N degrees-of-freedom:

$$\mathbf{M}\ddot{\mathbf{u}}(t) + \mathbf{C}\dot{\mathbf{u}} + \mathbf{K}\mathbf{u}(t) = \mathbf{f_{ext}} \tag{5.1}$$

where $\mathbf{M}$, $\mathbf{C}$ and $\mathbf{K}$ represent the mass, damping and stiffness matrices. Moreover, as the problem under study is a self-excited system, there is no external force: $\mathbf{f_{ext}} = \mathbf{0}$.

In order to perform a complex eigenvalue analysis, it is assumed that the solution can be expressed as $\mathbf{u}^{\mathrm{T}} = \mathbf{U}\exp\lambda t$ where λ and $\mathbf{U}$ represent the complex eigenvalues and eigenvectors of the system. Substituting the solution into equation (5.1) results in

$$[\lambda^2\mathbf{M} + \lambda\mathbf{C} + \mathbf{K}]\mathbf{U} = \mathbf{0}. \tag{5.2}$$

The non-trivial solution of equation (5.2) is obtained when $\det(\lambda^2\mathbf{M} + \lambda\mathbf{C} + \mathbf{K})$ is set to zero. The result consists of N complex eigenvalues which may be written as: $\lambda_j = \alpha_j + i\omega_j$. The terms α_j and ω_j represent the real and imaginary parts of the jth eigenvalue of the system. The real part of an eigenvalue α_j indicates the growth/decay rate of oscillations and the imaginary part ω_j shows the oscillation frequency. $\mathbf{U}_j$ denotes the eigenvector/mode shape of the jth mode.

5.4.   Transient analysis

A dynamic transient analysis is usually carried out to find the numerical solutions of time-dependent differential equations. This analysis can be done by means of explicit or implicit approaches. Briefly speaking, explicit methods use the current status of a system $\mathbf{u}(t)$ to derive the later status of the system $\mathbf{u}(t + \Delta t)$, while implicit approaches use both $\mathbf{u}(t)$ and $\mathbf{u}(t + \Delta t)$ to calculate the status of the system at a later time. According to this explanation, it seems that explicit solutions are computationally more efficient than implicit methods. In practice though, it turns out implicit approaches are faster due to the fact that the equations of motion of many systems are classified as "stiff equations". In such problems, in order to bring the numerical errors within the acceptable levels, a very small steps (Δt) must be chosen for explicit methods, which leads to a large computational time. On the other hand, implicit methods can converge to a solution faster with larger steps.

Of different numerical approaches which may be taken to solve an ordinary or partial-differential equation of motion, Runge-Kutta is a family of implicit and explicit methods, which is commonly used in the literature. The details of its algorithm are available in many

references and are not reviewed here. However, in order to gain a better understanding of the results which are produced by CEA and transient analysis, they are implemented on the same simple example in the next section.

5.5.   Implementation of CEA and transient analysis

A two-degree-of freedom system with a hardening spring is used for the purpose of this section (Figure 5.1). The equation of motion for this system may be written as ($\alpha = 45°$):

$$\begin{bmatrix} m & 0 \\ 0 & m \end{bmatrix} \begin{Bmatrix} \ddot{u}_1 \\ \ddot{u}_2 \end{Bmatrix} + \begin{bmatrix} c_1 & 0 \\ 0 & c_2 \end{bmatrix} \begin{Bmatrix} \dot{u}_1 \\ \dot{u}_2 \end{Bmatrix} + \begin{bmatrix} k_1 + 0.5k_3 & \mu k_2 - 0.5k_3 \\ -0.5k_3 & k_2 + 0.5k_3 \end{bmatrix} \begin{Bmatrix} u_1 \\ u_2 \end{Bmatrix} + \begin{bmatrix} k_1^{NL} & 0 \\ 0 & 0 \end{bmatrix} \begin{Bmatrix} u_1^3 \\ u_2^3 \end{Bmatrix} = 0 \quad (5.3)$$

where m represents massc_1, and c_2 denote damping along u_1 and u_2 directions, k_1, k_2 and k_3 are the linear stiffness terms, k_1^{NL} is the nonlinear stiffness term and μ is the friction coefficient. An example set of parameters are considered for demonstrating the results: $m = 1$ kg, $c_1 = c_2 = 0.2$ Ns/m $k_1 = k_2 = k_3 = 1000$ N/m and $k_1^{NL} = 2000$ N/m^2. For this set of parameters, when $\mu > 0.5$, the system becomes unstable. Therefore, μ is set to 0.52 in order to study an unstable state of the system.
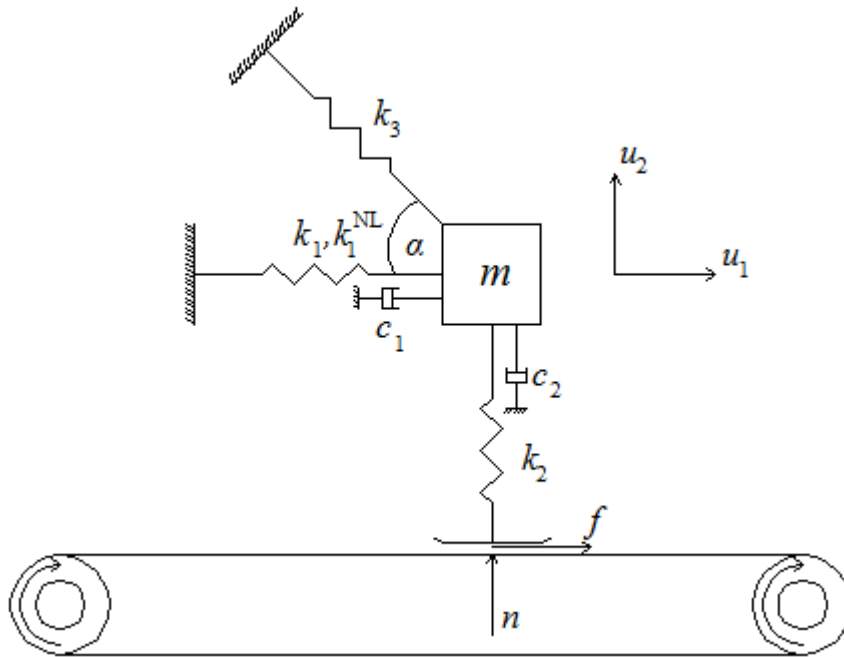
Figure 5.1. A two-degree-of-freedom system

To perform CEA, it is assumed the solution of the system is $\{u_1, u_2\}^T = \mathbf{U} \exp \lambda t$ and the nonlinear term is neglected. The eigenvalues of the system are then calculated by finding the roots of $\det(\lambda^2 \mathbf{M} + \lambda \mathbf{C} + \mathbf{K})$:

$\lambda_1 = -1.3903 + 38.7512$ i and $\lambda_2 = 1.1903 + 38.7512$ i.

The eigenvectors of the system can also be determined accordingly $U_1 = \{1, 5i\}^T$ and $U_2 = \{1, -5i\}^T$. As seen, at the unstable state, the magnitude of the mode shapes is the same while their phases are different.

To perform a dynamic transient analysis, the 4th-order Runge-Kutta is used to simulate the time response of the system from 0 to 200 seconds. The results are displayed in the top left plot of Figure 5.2. As seen, from 0 to about 50 seconds a combination of transient and steady-state solutions are observed in the response, while from 50 seconds onward, the response tends to a limit cycle motion. The last second of the time response [199, 200] is displayed in the top right plot to better display the amplitude and frequency of the limit cycle.
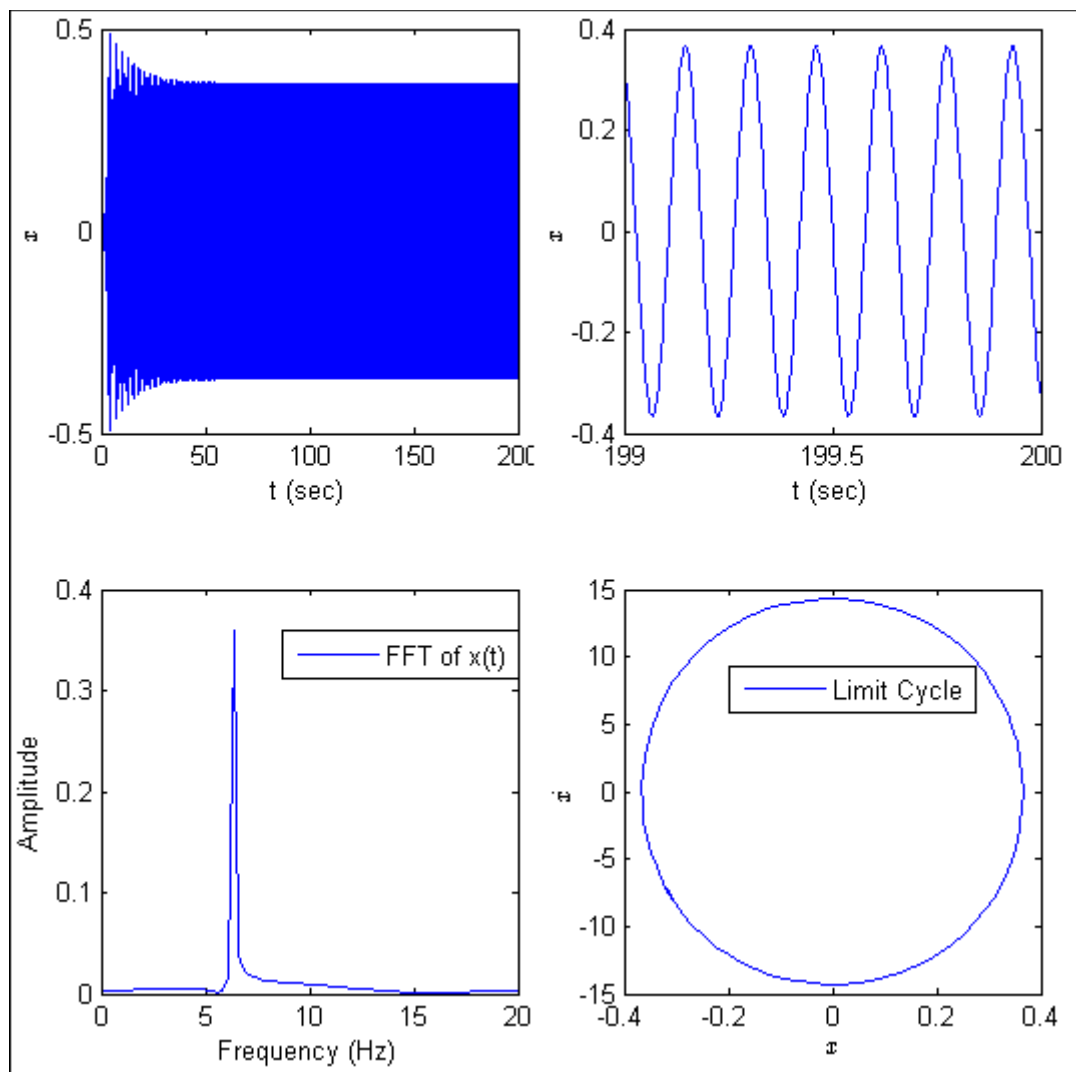
Figure 5.2. Transient analysis of the two-degree-of-freedom model

Then, Discrete Fourier Transform of the response is calculated and shown in the bottom left plot. Probably, this plot provides the most valuable piece of information that can be achieved via a dynamic transient analysis. As seen, the unstable frequency (at about 6.3 Hz) and also

the amplitude of the limit cycle motion (about 0.36 m) can be determined in this way. The limit cycle of the oscillations is also displayed in the bottom right plot.

It is useful to remind that the imaginary part of the complex eigenvalues is $\omega = 38.75\,\text{rad}/s$ which is equal to $f = 6.2\,\text{Hz}$. Therefore, both approaches can provide the unstable frequencies accurately, but CEA can provide them much faster. As discussed earlier, CEA cannot report the amplitude of nonlinear oscillations since it is implemented in the linearised system.

It is also important to know the nonlinear stiffness term plays a significant role in the amplitude of the limit cycle motion. For example, if k_1^{NL} is increased to $5000\,\text{N/m}^2$, the amplitude of the limit cycle will be 0.23 m. Therefore, there is no doubt that in order to make an accurate prediction of squeal noise via transient analysis, modelling of nonlinear elements should be done very carefully. This issue will be discussed in section 5.10.

5.6.   CEA of an asymmetric system with non-proportional damping

Friction-induced vibration with non-proportional damping occurs in many mechanical systems. In chapter 2, different frictional mechanisms leading to instability are explained and also it is stated that mode-coupling is believed to be the root cause of unstable oscillations in many mechanical systems with friction. Akay (2002) cited a number of examples in which mode lock-in could generate self-exited vibrations. Perhaps the most challenging example is automotive brake squeal due to its significant warranty cost to the manufacturers. Before applying the complex eigenvalue analysis to the full brake assembly, a low-order model is studied here to understand how to deal with an asymmetric system with non-proportional damping. Later on, this system will be used for extending the perturbation method to be applicable on friction-induced vibration.

Once again consider the generalised equation of motion (5.1). In order to carry out complex eigenvalue analysis for an asymmetric system with non-proportional damping, two aspects of equation (5.1) should be considered. First, as the stiffness matrix is not symmetric, the left and right eigenvectors are not the same. Secondly, damping of the system is non-proportional. As a result, the state-space equations of motion should be used in place of the second-order equations. It is worth mentioning that one may employ the second-order equations of motion directly (Adhikari and Friswell, 2001). However, it is mathematically more convenient to use the state-space form:

$$\mathbf{A}\dot{\mathbf{z}}(t) + \mathbf{B}\mathbf{z}(t) = \mathbf{0} \tag{5.4}$$

where $\mathbf{z} = \{\mathbf{u}, \dot{\mathbf{u}}\}^T$, $\mathbf{A} = \begin{bmatrix} \mathbf{C} & \mathbf{M} \\ \mathbf{M} & \mathbf{0} \end{bmatrix}$ and $\mathbf{B} = \begin{bmatrix} \mathbf{K} & \mathbf{0} \\ \mathbf{0} & -\mathbf{M} \end{bmatrix}$.

To derive the eigenvalues and eigenvectors of equation (5.4), the complex eigenvalue analysis is performed as $\mathbf{z} = \mathbf{Z}\, e^{\lambda t}$. The solution consists of N pairs of eigenvalues which are complex conjugates. Since the stiffness matrix is not symmetric, the associated eigenvectors are derived in the following way:

$$(\lambda_j \mathbf{A} + \mathbf{B})\mathbf{u}_j = \mathbf{0} \; ; \; \mathbf{v}_j^T(\lambda_j \mathbf{A} + \mathbf{B}) = \mathbf{0} \tag{5.5}$$

where $\mathbf{u}_j$ and $\mathbf{v}_j$ are the right and left eigenvectors, respectively. Later on, the normalized eigenvectors will be used in the equations. The normalization means (Murthy and Haftka, 1988):

$$\mathbf{v}_j^T \mathbf{A} \mathbf{u}_j = 1. \tag{5.6}$$

In the literature, friction-induced vibration is often investigated in systems with a limited number of degrees-of-freedom. However, Butlin and Woodhouse (2009) discovered that very low-order models reduced from the large original model may not represent the original problem well. Here a model with four degrees-of-freedom is studied with the aim to include the effect of a sufficient number of modes in the results of stability analysis.
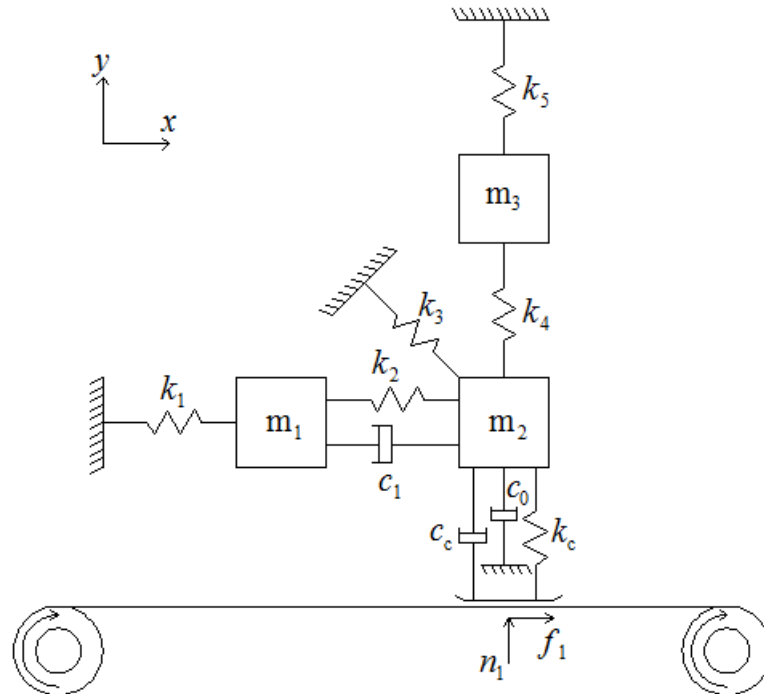
Figure 5.3. An asymmetric system with non-proportional damping

Ouyang (2010) employed this model in order to demonstrate the technique of pole-assignment for stabilizing friction-induced vibrations. This model is shown in Figure 5.3. Here, the only difference is that there is contact damping at the slider-belt interface in addition to the grounded damping in (Ouyang, 2010).

This lumped mass model may be imagined as a simplified brake system in which the slider serves as the disc and m_2 acts as the brake pad with the stiffness of k_2, k_3 and k_4 along different directions. The angle of inclination for k_3 is 45°. The contact stiffness and damping at the slider-belt interface are k_c and c_c, respectively. Masses m_1 and m_3 may be considered as representing the abutment and pad backplate. The stiffness of the abutment is k_1 and the backplate is k_5.

Mass m_1 has one degree-of-freedom along $x-$ direction, m_2 is free to move in both $x-$ and $y-$ directions and m_3 can only oscillate in y-direction. The normal force is n_1 and the friction force is f_1. It is assumed that the belt velocity is constant and no stick-slip motion is experienced. The matrices of mass, damping and stiffness corresponding to the vector $\mathbf{u} = \{x_1, y_3, x_2, y_2\}^{\mathrm{T}}$ are:

$$\mathbf{M} = \begin{bmatrix} m_1 & 0 & 0 & 0 \\ 0 & m_3 & 0 & 0 \\ 0 & 0 & m_2 & 0 \\ 0 & 0 & 0 & m_2 \end{bmatrix}; \quad \mathbf{C} = \begin{bmatrix} c_1 & 0 & -c_1 & 0 \\ 0 & 0 & 0 & 0 \\ -c_1 & 0 & c_1 & \mu c_c \\ 0 & 0 & 0 & c_0 + c_c \end{bmatrix};$$

$$\mathbf{K} = \begin{bmatrix} k_1 + k_2 & 0 & -k_2 & 0 \\ 0 & k_4 + k_5 & 0 & -k_4 \\ -k_2 & 0 & k_2 + 0.5k_3 & \mu k_c - 0.5k_3 \\ 0 & -k_4 & -0.5k_3 & k_4 + 0.5k_3 + k_c \end{bmatrix}$$

(5.7)

where $m_i = 1$ kg ($i = 1, 2, 3$), $k_i = 100$ N/m ($i = 1, 2, \cdots 5$), $k_c = 2k_1$, $c_1 = c_0 = 0.5$ Ns/m and $c_c = 0.1$ Ns/m. These values are the same as those of in (Ouyang, 2010). However, adding the contact damping to the model causes the value of the critical friction coefficient to become different from the one in (Ouyang, 2010). The matrices given in equation (5.7) reveal how the friction force breaks the symmetry of stiffness and damping matrices by relating the normal force to the tangential one.

In order to evaluate the system stability with respect to different system parameters, the complex eigenvalue analysis is conducted. For the example set of input parameters, the complex eigenvalue analysis is performed with four different friction coefficients. The results are shown in Table 5.2. Although each input parameter makes a contribution to the system stability, the friction coefficient usually plays the most significant role in low order models. This fact will be proved for this system via the sensitivity analysis presented in chapter 7. As seen in Table 5.1, the real part of the first pair of eigenvalues becomes positive when μ is larger than 0.4205. The same behaviour is observed for the fourth eigenvalue

if $\mu > 1.2165$. In order to understand the bifurcation behaviour of the system versus the friction coefficient, the real and imaginary parts of all eigenvalues are shown in Figure 5.4.

Table 5.1. Eigenvalues of the system with four different friction coefficients ($\boldsymbol{\mu}$)

	First pair	Second pair	Third pair	Fourth pair
$\mu = 0.4000$	$-0.0012 \pm 8.7580i$	$-0.0626 \pm 12.1832i$	$-0.5125 \pm 16.7569i$	$-0.2236 \pm 19.8421i$
$\mu = 0.4205$	$0.0000 \pm 8.7963i$	$-0.0632 \pm 12.1736i$	$-0.5154 \pm 16.7700i$	$-0.2215 \pm 19.8201i$
$\mu = 1.2165$	$0.1027 \pm 10.3224i$	$-0.1395 \pm 11.5937i$	$-0.7632 \pm 17.4289i$	$0.0000 \pm 18.8467i$
$\mu = 1.3000$	$0.4097 \pm 10.8802i$	$-0.4388 \pm 11.2679i$	$-1.0005 \pm 17.6370i$	$0.2295 \pm 18.5560i$

Comparing the bifurcation behaviour of this system with the Hoffmann's model (Hoffmann et al., 2002) presented in chapter 2 reveals the existence of damping prevents the imaginary parts of eigenvalues from coalescing, yet they get markedly close. The effects of input parameters including damping on the bifurcation behaviour of mode-coupling instability has extensively been discussed in (Hoffman and Gaul, 2003; Sinou and Jézéquel, 2007). It is worth mentioning that damping can cause the destabilisation paradox (Kirillov, 2004; Kirillov and Seyranian, 2005) in friction-induced vibration— having either "lowering effect" or "smoothing effect" on mode-coupling instability. In brief, the configuration and values of damping in a system can results in instability known as "smoothing effect". This fact is in contrast with the general expectation of damping which usually shifts the eigenvalues towards the stable region ("lowering effect").

This phenomenon was fully investigated in (Hoffman and Gaul, 2003; Sinou and Jézéquel, 2007) for low-order models. Fritz et al. (2007a, 2007b) investigated the impact of the destabilization paradox on mode-coupling instability of a finite element brake model. It is out of the scope of this study to investigate these relationships for the system shown in Figure 5.3. What is important here is to find out in what manner the variability and uncertainty of input parameters can be propagated to the output space cost-effectively. Uncertainty analysis of this low-order model (Figure 5.3) will be presented in chapter 7.
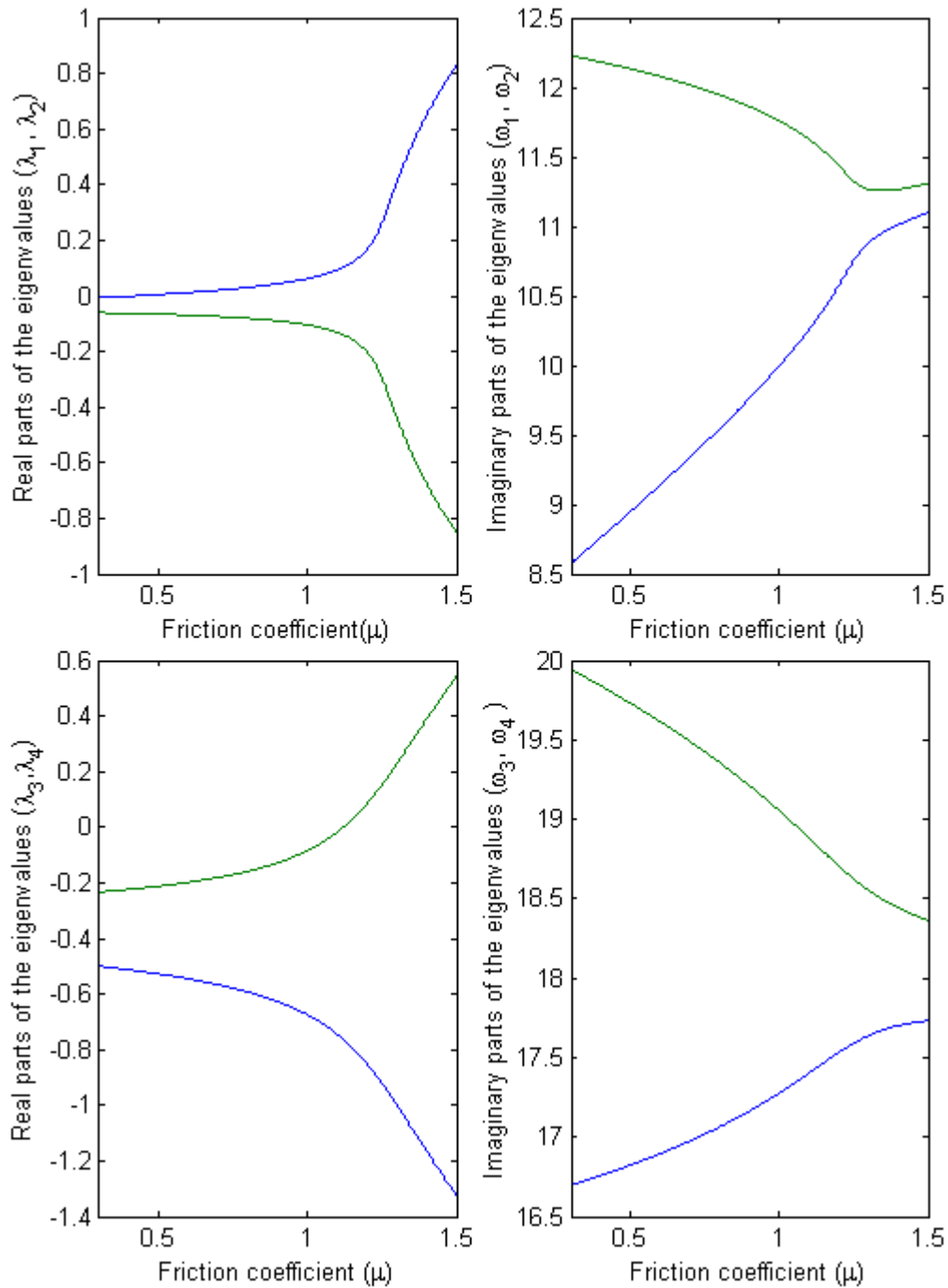
Figure 5.4. The bifurcation behaviour of the low-order model

5.7.   CEA of the full brake assembly in Abaqus

In order to carry out CEA on a FE brake model, Abaqus/Standard is widely used in industry. The reason is this software provides an option to define frictional contact interfaces and incorporates the contribution of friction to the stiffness matrix. To do CEA in Abaqus, a few steps must be followed (Kung et al., 2003):

- Nonlinear static analysis for applying brake pressure
- Nonlinear static analysis for spinning the disc
- Normal mode analysis of the full brake assembly
- Complex eigenvalue analysis of the full brake assembly.

As there are a number of contact interfaces in the full brake assembly in addition to pads-to-disc contact interface, before pressurising the pistons, a few pre-loading steps are usually taken for establishing these contacts. Then, through pressurising the pistons, the pads-to-disc contact interface is established and the effect of nonlinear geometry is incorporated in the analysis. According to chapter 3, three-dimensional, 3-node hydrostatic fluid elements are employed in this study to model the brake fluid. For the brake squeal problem, various brake pressures are usually considered in order to include different loading cases in the results. The brake pressure is commonly selected as 2,5,10 or 20 bar. Figure 5.5 shows the results of the nonlinear static analysis for 10-bar brake pressure on the backplate and friction material.
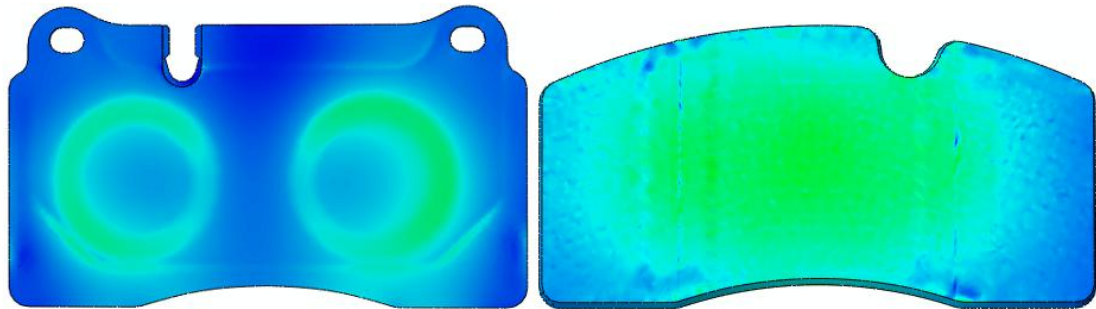
Figure 5.5. Pressure distribution on the pad and backplate

The second step is to spin the disc virtually. For this step all nodes of the disc are assigned to a node set (*NSET) and spun around the disc centre. The friction coefficient at the pads-to-disc contact interface is also set in this step. This coefficient is usually selected as 0.3, 0.4, 0.5, 0.6 or sometimes 0.7. Although the nominal value of the friction coefficient is mostly about 0.4 to 0.44, a variety of reasons such as humidity, thermal effects, ambient temperature, etc., can increase or decrease the friction coefficient. Imposing the rotational speed in this way leads to the formation of shear forces at pads-to-disc contact interface. Moreover, if someone wants to include a velocity-dependent friction coefficient, its definition can be tabulated in this step. However, such a friction regime is not considered in the current investigation.

The third step is normal mode analysis of the full brake assembly. This analysis was done in chapter 3 for the individual brake components. This time the full brake assembly must be analysed. In Abaqus, the effects of damping and also the contribution of friction into the stiffness matrix are neglected during normal mode analysis. Therefore, there is no real part

for the eigenvalues of the system and they become purely imaginary. The symmetrised eigenvalue problem then may be written as (AbuBakar and Ouyang, 2006):

$$(-\omega^2 \mathbf{M} + \mathbf{K}_s)\boldsymbol{\phi} = \mathbf{0} \tag{5.8}$$

where $\mathbf{K}_s$ represents the symmetrised stiffness matrix. One of Abaqus eigensolvers, mostly Lanczos, is used to derive the eigenvalues and eigenvectors of the assembly.

The last step is to calculate the complex eigenvalues and eigenvectors of the system. For this purpose, the original mass, damping and stiffness matrices are projected onto a subspace determined by the eigenvectors of the symmetrised system (Abaqus documentation):

$$\begin{aligned}
\mathbf{M}^* &= [\boldsymbol{\phi}_1, \boldsymbol{\phi}_2, \dots, \boldsymbol{\phi}_n]^{\mathrm{T}} \mathbf{M} \, [\boldsymbol{\phi}_1, \boldsymbol{\phi}_2, \dots, \boldsymbol{\phi}_n] \\
\mathbf{C}^* &= [\boldsymbol{\phi}_1, \boldsymbol{\phi}_2, \dots, \boldsymbol{\phi}_n]^{\mathrm{T}} \mathbf{C} \, [\boldsymbol{\phi}_1, \boldsymbol{\phi}_2, \dots, \boldsymbol{\phi}_n] \\
\mathbf{K}^* &= [\boldsymbol{\phi}_1, \boldsymbol{\phi}_2, \dots, \boldsymbol{\phi}_n]^{\mathrm{T}} \mathbf{K} \, [\boldsymbol{\phi}_1, \boldsymbol{\phi}_2, \dots, \boldsymbol{\phi}_n]
\end{aligned} \tag{5.9}$$

As there is no damping in the FE model of the brake under this study, $\mathbf{C} = \mathbf{0}$. The reduced eigenvalue problem is then solved via the standard QZ method:

$$[\lambda^2 \mathbf{M}^* + \mathbf{K}^*]\mathbf{U}^* = \mathbf{0}. \tag{5.10}$$

Briefly speaking, the QZ method is a well-known algorithm in linear algebra for matrix decomposition and determining its eigenvalues and eigenvectors. Eventually, the original eigenvectors of the system must be recovered:

$$\mathbf{U}_k = [\boldsymbol{\phi}_1, \boldsymbol{\phi}_2, \dots, \boldsymbol{\phi}_n]\mathbf{U}_k^*. \tag{5.11}$$

Note that Abaqus reports the approximation of the right eigenvector due to the fact that the left and right eigenvectors are different for a system with asymmetric stiffness matrix.

Running CEA produces complex eigenvalues ($\lambda_j = \alpha_j + \mathrm{i}\omega_j$) and eigenvectors of the system. As long as all real parts of the system are negative or zero, the steady-state solution is stable. However, a positive real part causes instability and may result in squeal noise. Many studies in the brake squeal research community take the damping ratio $\zeta_j = -2\alpha_j/\omega_j$ as an index to evaluate the quality of a brake in terms of noise. Each car manufacturer accordingly sets a target value for the 'squeal index'. If the absolute values of this index remain smaller than the target level from different CEA runs, this brake design will be considered acceptable. Otherwise, some structural modifications must be made to avoid squeal. Although it is not guaranteed that smaller real parts lead to a quieter brake and larger ones causes squeal, this index is taken as a criterion to evaluate squeal propensity in this study.

What is common in industry for the brake squeal problem is to run a number of analyses with different friction coefficients at the pads-to-disc contact interface and also different

brake pressures. In spite of the fact that this study aims to propose a method for covering the effects of variability and uncertainty including the friction coefficient and brake pressure, for now the common approach in industry is followed here. Figure 5.6 shows the results of CEA on the brake under this study for different friction coefficients from 0.3 to 0.6 and brake pressure form 2 to 20 bar. An example target level is shown in Figure 5.6. This threshold is set by brake engineers based on their industrial experience.
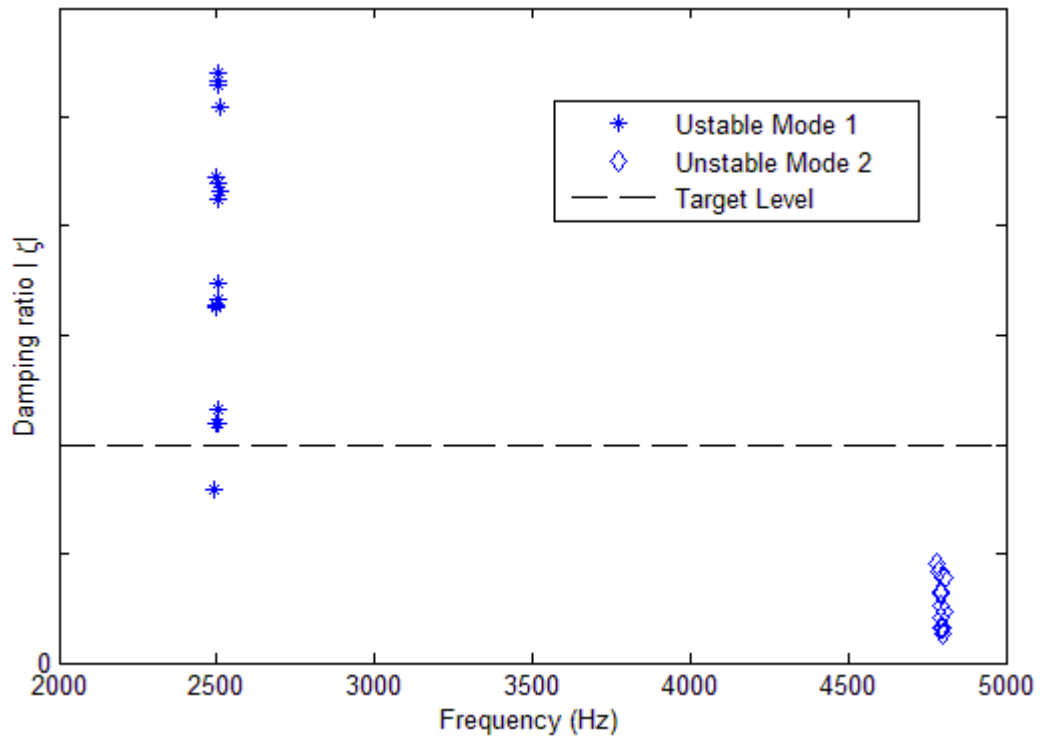
Figure 5.6. CEA of the brake model with different friction coefficients and brake pressures

In the range of 2.0 to 5.0 kHz (low-frequency squeal range), there are two unstable modes for the brake under this study. The mode shapes of the first and second unstable mode are displayed in Figure 5.7. This study is focused on the first unstable mode, which was considered a priority for the car manufacturer. This mode occurs in the form of calliper's shear mode and disc's 4-ND out-of-plane mode (ND represents "nodal diameter"). In the second unstable mode, only pads' ears and guide-pins are deformed (effectively there is no deformation elsewhere). Therefore, the calliper has been removed from Figure 5.7b in order to better display the second unstable mode.

In industry, brake engineers usually identify the critical mode and the components that have a significant amount of strain energy within that mode. Structural modifications will be proposed and if they bring the 'squeal index' within acceptable levels, the recommendations are discussed for feasibility with the suppliers. If they are practical, they will be incorporated

into the design ready for validation on a test rig. An example of structural modification on this brake will be presented later in section 5.9.
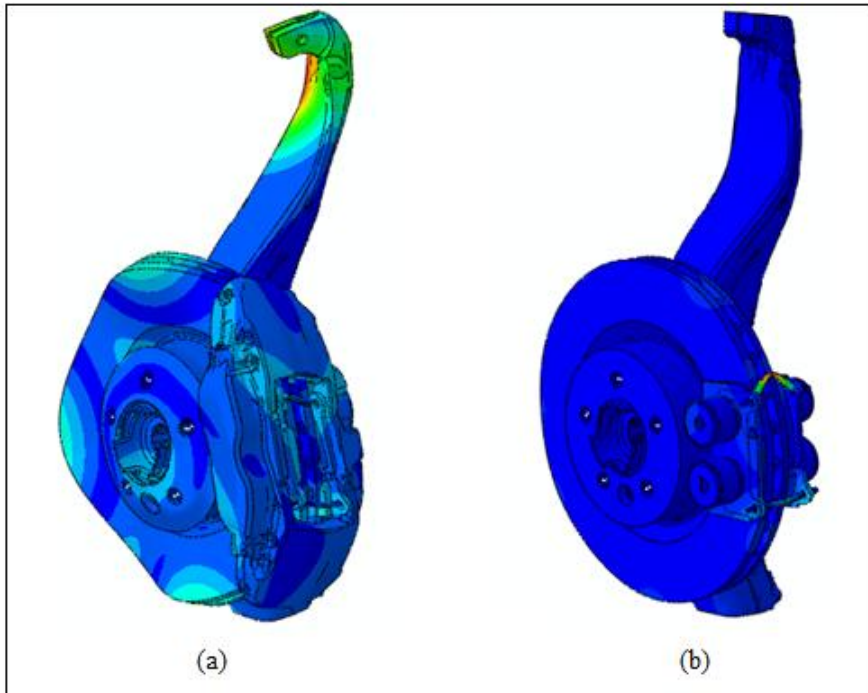
Figure 5.7. The unstable modes of the brake: a) the 1st unstable mode at about 2.5 kHz; b) the 2nd unstable mode at about 4.8 kHz

As in CEA the nonlinear terms leading to a limit is neglected, some Dyno tests must be carried out in parallel with the numerical simulations in order to identify which one of the predicted unstable mode causes squeal. This matter will be discussed in the next section.

5.8.   Validation of CEA results via dynamometer test data

In order to validate the results of the complex eigenvalue analysis, the physical brake assembly is tested. The measurement setup for the brake squeal test is shown in Figure 5.8. Polytec laser scanning vibrometer is used for measuring the deflection shapes of the nodes displayed in Figure 5.9. The test is done under operational condition. In order words, the disc is rotated by means of a Dyno, the hydraulic pressure is applied and when the disc is heated up to some degrees, the friction causes instability and the brake starts squealing. The initial condition leading to squeal is disc temperature of 95ºC and the brake line pressure of 6 bar. However, it is worth mentioning that this initial condition is not unique and a number of initial conditions can lead to squeal noise.
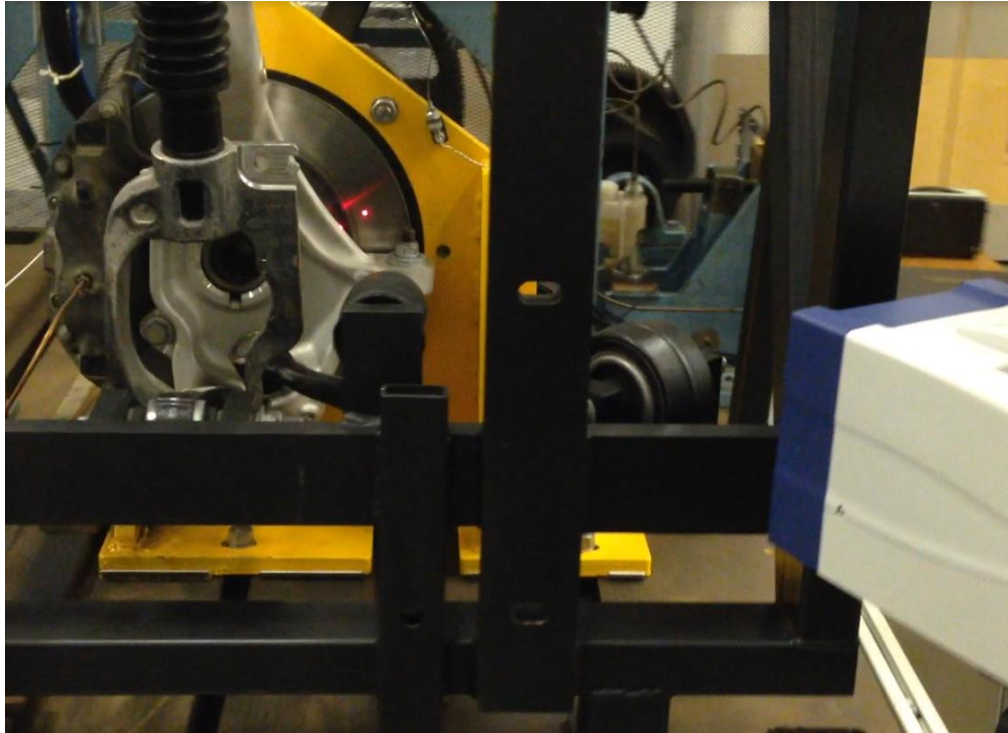
Figure 5.8. Measurement set-up for the brake squeal test
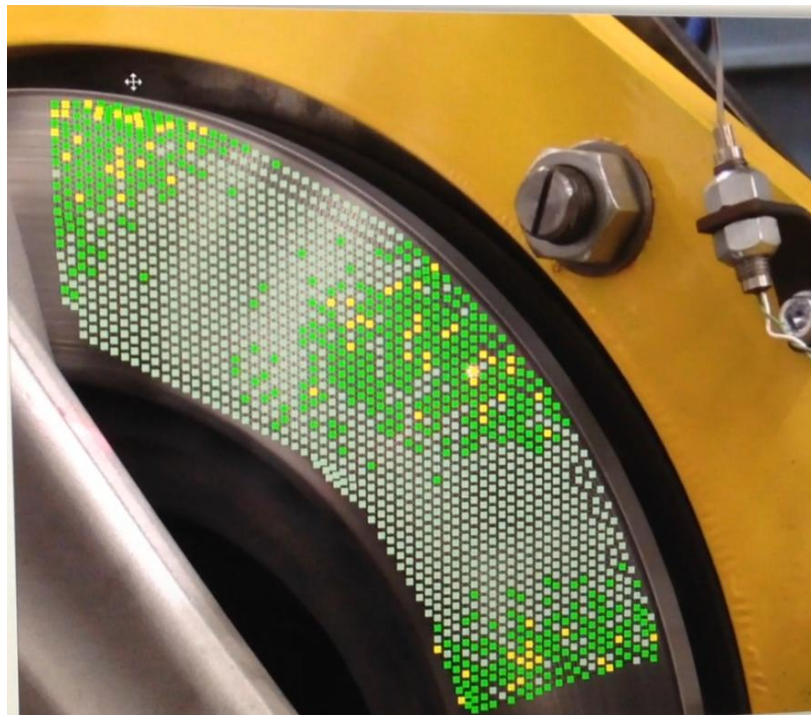
Figure 5.9. Scanned points/nodes of the full brake assembly

One of the important settings for doing any modal test is the trigger setting. For example, in the roving hammer technique, before starting the measurement, a number of impacts are given to a structure continuously in order to set a range for the input force and also a range

for the sensitivity of the accelerometers. Thereafter, during the measurement, when the input force and response are within the ranges, the measured data is recorded. Otherwise, another impact within the ranges must be given to the structure.

The same approach must also be taken for the brake squeal test under operational condition. The reason is that the noise may go on and off during the test and recording the response of a quiet brake is not useful. Therefore, Polytec provides users with external hardware and a microphone to set the trigger setting for this type of tests. The hardware is shown in Figure 5.10. When the brake starts squealing, the dominant unstable mode will appear on a computer screen. Then, the dominant frequency of the noise can be used for the trigger setting. For example, in this run, the dominant squeal frequency occurs at about 2.45 to 2.50 kHz. Therefore, the centre frequency is set to 2.45 kHz with a bandwidth of ± 30 percent. When the indicator is on, it means the brake is squealing and the measuring nodes are being scanned. Otherwise, the vibrometer stops scanning and wait for the signal from the trigger to continue scanning. Moreover, in order to coordinate the phase of all measured nodes, a non-contact capacitive sensor is also used during test. This coordination is essential for mapping the deflection shape of the measured nodes at the end of the test.

Figure 5.10. Trigger setting for the squeal test

The average output spectrum of the measured nodes from 1.0 kHz to 5.0 kHz is shown in Figure 5.11. As seen, there is one dominant squeal frequency at about 2.44 kHz. The deflection shape of a part of the disc corresponding to this frequency is displayed in Figure 5.12. There is no doubt that the deflection shape is in the form of the disc's 4-ND out-of-plane mode. Therefore, comparing the experimental and numerical results shows no doubt that the FE model of the brake assembly is sufficiently accurate for the purpose of the current study.
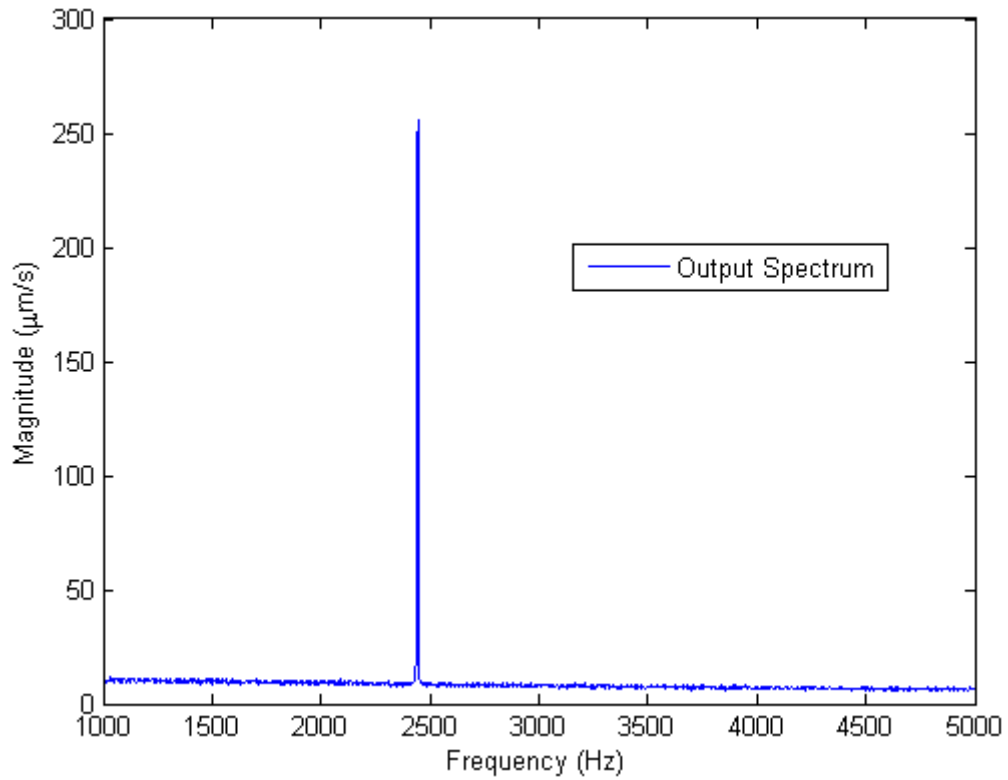
Figure 5.11. The average vibration velocity of scanned points/nodes
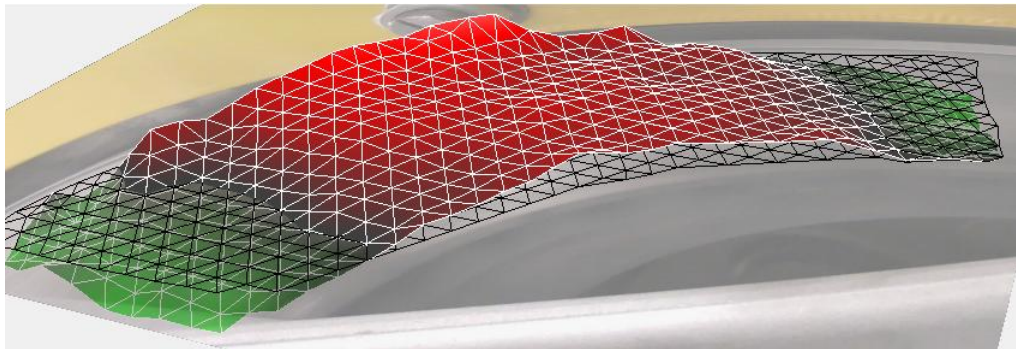
Figure 5.12. The deflection shape of the disc under squealing condition

There are a few points that seem important to be discussed here. First of all, looking at Figure 5.8 may bring this question to mind why the laser head is not vertically pointed to the disc. The reason is that from the vertical angle only a smaller area of the disc could be scanned, so there was a little concern whether the deflection shape resembled disc's 4-ND out-of-plane mode or not. To support this statement, the deflection shape of the disc from the vertical angle is shown Figure 5.13. As a result, it was decided to take a wider scan to better present the deflection shape.
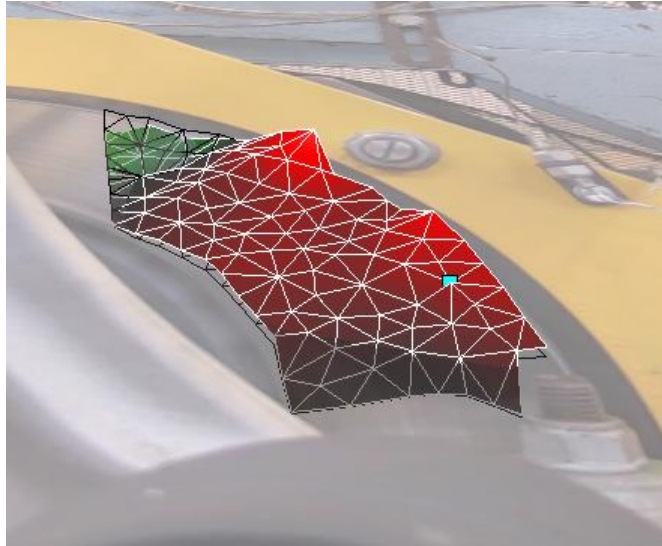
Figure 5.13. The deflection shape of the disc from vertical angle

Moreover, although the average displacement of the nodes showing the disc's 4-ND mode, there are a few local valleys and hills in the deflection shape. Two reasons may be attributed for this effect. Firstly, when the number of nodes for measuring the shape is not enough like Figure 5.13, the gaps between the measured nodes are filled via a straight line. Therefore, a smoother shape will be achieved when the nodes are increased sufficiently (Figure 5.12). Secondly, the roughness of the disc surface results in an uneven deflection shape. Since before doing the test, the geometry of the disc is scanned via the laser vibrometer, the roughness of the surface will be also mapped in the results. In fact, the geometry scanning is a very useful feature when a curve or a surface with different surface levels is needed to be scanned. However, as a side effect the roughness of the surface will also be seen in the results. For this particular test scanning the geometry is done since the laser head is not vertical to the disc surface.

The last point is that the dominant squeal frequency can be slightly different from one test to another. As mentioned earlier, a number of initial conditions including brake pressure and friction can lead to squeal noise. Therefore, the stiffness matrix is slightly different when the brake pressure varies. Hence, it is not unexpected to observe a variation of 100 Hz in the dominant squeal frequency. The same manner is also observed in the numerical results when the loading case and friction coefficient differ from one analysis to another. Note that a number of squeal tests were run and the range of the dominant squeal frequency was from 2.44 to 2.52 kHz.

5.9. Structural modification of the brake via CEA

In industry, the typical approach to the brake squeal problem is to carry out CEA for different brake pressures and friction coefficients (Figure 5.6). If all unstable modes meet the target level, the brake design is signed off for manufacturing. Otherwise, some local or global modifications are made on the design to bring the damping ratios of all unstable modes within the acceptable levels. Although structural modification of a brake design is not the central aim of this study, it will be seen later that one of the main advantages of building a brake surrogate model is to make the process of structural modification more convenient and systematic. Therefore, it is useful to review the conventional way of structural modification.

As discussed earlier, the unstable mode at about 2.5 kHz has been the main concern of the sponsor of this project. Figure 5.6 illustrates that the squeal index of this particular mode exceeds the target level significantly. Then, the conventional approach is identifying the components having the most contribution to this particular mode. Typically, in a trial and error approach, it is attempted to change the mass and stiffness of those components so that the squeal index of this particular unstable mode decreases while not much increase in the squeal indices of the other modes occur. There is no doubt that changing the mass and stiffness of a component always comes along with the change in all frequencies and mode shapes. However, if for example the modification is wisely made on the node of a particular mode with zero displacement, it is expected to see the least effect on that mode while adding mass to a place with maximum deformation brings about the most influence.

Figure 5.14 displays the modified calliper of the brake under this study. Two solid blocks which are made from forged steel are attached to the calliper body in order to shift its natural frequencies slightly and avoid mode coupling instability. Table 5.2 compares predicted frequencies and mode shapes of the calliper with and without the blocks.
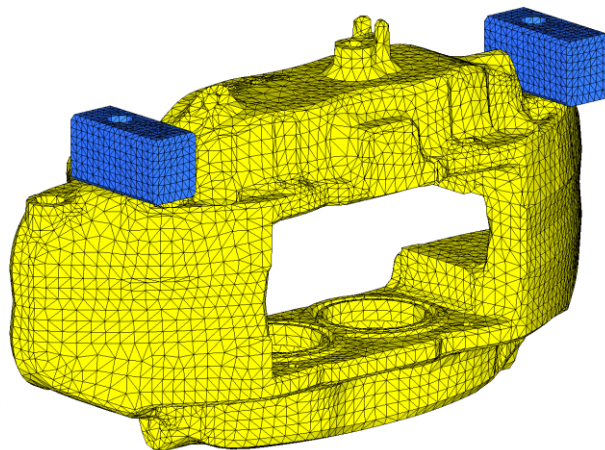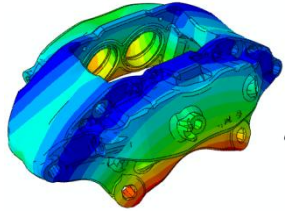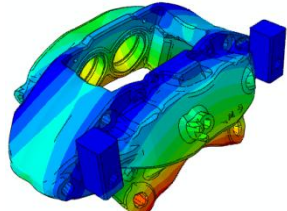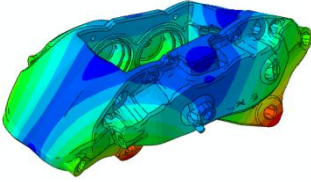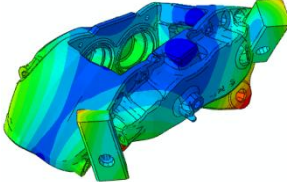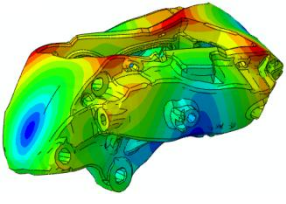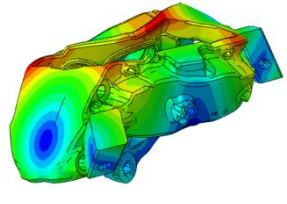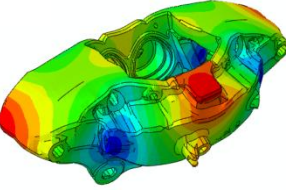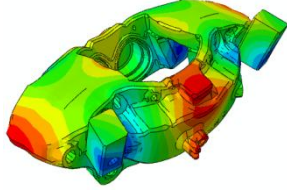
Figure 5.14. The calliper with solid blocks

Table 5.2. Predicted frequencies and mode shapes of the calliper with and without solid blocks

Mode No.	Freq. (Hz)	Mode shapes	Freq. (Hz)	Mode shapes
1	1830.4		1833.2	
2	2037.1		1986.1	
3	2800.4		2692.1	
4	3355.6		3256.0	

The results illustrate that the effect of additional solid blocks on the first mode of the calliper is almost negligible as they are located on a nodal line. However, the influence of the lump masses on the third mode whose frequency is fairly close to the unstable mode of the brake at about 2.5 kHz is considerable. Now, the complex eigenvalue analysis is carried out again to see the effects of added blocks on the unstable modes of the full brake assembly.

Table 5.3 and Table 5.3 show the results of the CEA before and after structural modification. As seen, the additional solid blocks could cancel out the unstable mode at about 2.5 kHz. However, two new unstable modes appear at 1994 Hz and 3110 Hz. As the squeal indices of these modes are not as large as the one before modification, the brake with the modified calliper meets the target level of the car manufacturer. The experimental results also confirmed that the brake with the additional blocks bring about a quieter design, since it will no longer generate squeal with the dominant frequency of 2.5 kHz.

Table 5.3. The results of CEA of the brake assembly before structural modification

Mode No.	Real part of the eigenvalue	Frequency (Hz)	Damping ratio
24	0.000	1604.0	0.00000
25	0.000	1707.9	0.00000
26	0.000	1731.4	0.00000
27	0.000	1776.6	0.00000
28	0.000	1832.4	0.00000
29	0.000	1962.3	0.00000
30	0.000	1993.3	0.00000
31	0.000	1998.9	0.00000
32	0.000	2171.2	0.00000
33	0.000	2245.0	0.00000
34	0.000	2348.2	0.00000
35	0.000	2430.7	0.00000
36	0.000	2466.4	0.00000
37	0.000	2491.4	0.00000
38	-174.80	2500.6	0.02225
39	174.80	2500.6	-0.02225
40	0.000	2654.3	0.00000
41	0.000	2721.6	0.00000
42	0.000	2901.7	0.00000
43	0.000	2947.4	0.00000
44	0.000	3131.1	0.00000
45	0.000	3288.7	0.00000

Until now, the common deterministic approach toward the brake squeal problem has been studied. As seen, CEA is only carried out for a small number of brake pressures and friction coefficients, and there is no guarantee that the brake design remains quiet under the influence of manufacturing variability and uncertainties.

As a result, the sponsor of this project is keen to find an efficient statistical method for incorporating these effects in the results of CEA and evaluate how robust and reliable their designs are with respect to manufacturing tolerances, aging and environmental effects etc. The procedure which has been followed until now is an essential part of the non-deterministic approaches due to the fact that those methods are built on the premise of deterministic approaches. The implementation of non-deterministic approach on the brake squeal problem will be explained in the following chapters.

Table 5.4. The results of CEA of the brake assembly after structural modification

Mode No.	Real part of the eigenvalue	Frequency (Hz)	Damping ratio
22	-6.5466	1399.9	0.00149
23	6.5466	1399.9	-0.00149
24	0.000	1435.4	0.00000
25	0.000	1467.9	0.00000
26	0.000	1473.5	0.00000
27	0.000	1590.7	0.00000
28	0.000	1652.2	0.00000
29	0.000	1698.5	0.00000
30	0.000	1727.4	0.00000
31	0.000	1783.5	0.00000
32	0.000	1821.1	0.00000
33	0.000	1915.2	0.00000
34	-12.336	1994.2	0.00197
35	12.336	1994.2	-0.00197
36	0.000	2052.4	0.00000
37	0.000	2146.1	0.00000
38	0.000	2186.9	0.00000
39	0.000	2276.8	0.00000
40	0.000	2348.2	0.00000
41	0.000	2415.6	0.00000
42	0.000	2434.6	0.00000
43	0.000	2492.7	0.00000
44	0.000	2506.4	0.00000
45	0.000	2540.7	0.00000
46	0.000	2644.9	0.00000
47	0.000	2692.7	0.00000
48	0.000	2899.2	0.00000
49	0.000	2948.1	0.00000
50	-96.286	3110.4	0.00985
51	96.286	3110.4	-0.00985

5.10. Transient analysis of brakes in Abaqus

There are a number of issues associated with transient analysis of FE brake models in Abaqus. These issues are briefly discussed here. First of all, there is no extensive study on the damping of friction material in the literature. In a brake system, friction material contributes mostly to damping. Hence, the available options for modelling damping such as Rayleigh damping, is not sufficiently accurate for friction materials. Secondly, as illustrated in section 5.5, the nonlinear terms play a significant role in the amplitude of a limit cycle motion. What mostly behaves nonlinearly in the brake squeal problem is friction material. Unfortunately, in Abaqus it is only possible to define nonlinear isotropic material and there

is no option to define nonlinear behaviour in different directions of a single material. As a result, modelling a nonlinear friction material is not yet feasible. Future advances may resolve this issue.

Finally, as discussed earlier, the computational workload of a dynamic transient analysis is the biggest hurdle. Abaqus/Standard uses implicit methods to find the numerical solutions of differential equations. However, for highly nonlinear problems or problems containing many contact interfaces, users have been provided with Abaqus/Explicit. To get an idea about how small the step size must be for the brake squeal problem, it is useful to review the stability limit of Abaqus/Explicit. This limit is defined based on the highest frequency of the system (Abaqus documentation). The stability limit is $\Delta t \leq 2/\omega_{max}$ when there is no damping in the system. Therefore, it can be seen that in order to keep the contribution of high frequencies in the solution, the step size must be very small which lead to a very long simulation.

Moreover, the interval of integration (time span) is another significant issue. A transient analysis can be done in a few days if a few seconds of the response is needed. However, if the response does not tend to a limit cycle quickly, it will massively increase the computational workload. This situation is exacerbated when it is known that many attempts must be made until a limit cycle motion is found. In other words, all runs of transient analysis do not necessarily converge to a limit cycle motion.

Taking these factors into consideration, no doubt will remain that CEA is the right choice for the purpose of this study.

5.11. Conclusions

The implementation of CEA and transient analysis are illustrated in this chapter. The pros and cons of each method are fully discussed and it is unveiled why CEA has been selected for the purpose of this study. The results of CEA on the full brake assembly are presented and validated with dynamometer test data. An example of structural modification on brakes for reducing the squeal index is also given here.

Moreover, the results of CEA of an asymmetric low-order system with non-proportional damping are presented in this chapter. This model will be used later for extending the perturbation method to be applicable on friction-induced vibration.

6. Non-deterministic Approaches

Recently particular attention has been given to uncertainty analysis of brake systems by car manufacturers. The deterministic approach of either CEA or transient analysis is only carried out for a set of design parameters and there is no information about the effect of variations of these parameters on the outputs. Although a brake design may remain stable at the baseline design point, the reliability and robustness of the design in terms of the likelihood of unstable vibration leading to squeal noise is still unclear. It is believed that variability and uncertainty are responsible for squeal noise in many cases and cause a significant warranty cost to car manufactures.

In this chapter, a brief review of different methods of uncertainty analysis is presented and then it is explained why surrogate modelling has been selected for the purpose of this study. This chapter may be taken as the transition from deterministic approaches to statistical approaches toward the brake squeal problem.

6.1.   Variability and uncertainty

There are two terms which are frequently used in this study: variability and uncertainty. In the literature, structural uncertainties are classified into two groups: aleatory and epistemic (Möller and Beer, 2008). Yet it is not always possible to make a distinction between them. Aleatory uncertainty, also called irreducible uncertainty or variability, refers to the random nature in the system properties, which originates from manufacturing processes. Variations of material properties, component geometries and assemblies are the most typical examples of this type of uncertainty. Epistemic uncertainty, known as reducible uncertainty, is mainly due to the lack of information. This type of uncertainty is called reducible since future advances and/or investigations can provide new insights into the problems which are not fully understood yet.

In spite of the extensive investigations that have been conducted so far, predicting the behaviour of friction, contact and wear remains very complicated. In addition to the tribological interactions, the degree of uncertainty in a friction-induced vibration problem is increased by the thermal effects, humidity, diverse loading cases, etc. Variability also imposes a considerable level of uncertainty to the problem. The growing importance of variability in brake noise is well explained in (Day, 2014):

"One of the most interesting (and frustrating) features of brake noise is its fugitive nature; it is well known that even across different vehicles of the same make and model with the same brake installation, some exhibit brake noise, while others do not. Given the complexity of the underlying physical principles of brake noise generation that have been outlined above and the emphasis on instability, it appears that relatively small changes in one or more of the many design and operational parameters associated with friction brakes can tip a brake installation from quiet to noisy. Operational parameters such as temperature, speed, actuation pressure and humidity have all been mentioned, and many vehicle and brake manufacturers have studied the possible influence of variation arising from manufacturing tolerances. The role of the pad assembly in disc brake noise is becoming increasingly well understood, and the nature of the abutment contact is influenced by the dimensional tolerances between the pad back-plate and the calliper abutments, which may change over time as a result of wear, plastic deformation, and the build-up of debris and corrosion. Brake pads are generally closely toleranced in terms of thermo-physical properties during and immediately after manufacture, but once they enter the customer domain, variability increases. The manufacture of brake discs and drums is closely controlled but achieving and maintaining close tolerances on the internal geometry of ventilated brake discs, for example, is costly. Examination by the author of samples of ventilated brake discs within the same batch and

across different batches has indicated a 3σ variation of $\pm 5\%$ in resonant frequencies up to 6 kHz, with pair (doublet) modes separated by amounts ranging from 10 to 60 Hz. The close examination of components from examples of brakes that exhibit noise, and comparison with nominal dimensions and values, is thus a useful exercise."

Ignoring the effect of variability and uncertainty in CEA causes underestimation or overestimation of the number of unstable modes. Therefore, in order to make more reliable predictions of unstable modes, it is necessary to perform an uncertainty analysis.

6.2. Uncertainty analysis

An uncertainty analysis may be carried out via probabilistic, non-probabilistic or mixed uncertainty techniques. The most fundamental, yet practical, probabilistic method of uncertainty analysis is Monte Carlo simulation (Schenk and Schuëller, 2005). The conventional Monte Carlo simulation spreads a large number of samples over the design space and collects the results of the sampled points by means of a mapping function. In fact, the mapping function is the relation between the outputs and input variables. Then, the statistics of the outputs are quantified by the use of the output scatter. Figure 6.1 displays a schematic of the conventional Monte Carlo simulation.

The conventional Monte Carlo simulation is mentioned here in order to explain the concept of uncertainty analysis. However, this method can become very expensive in practice, especially when the mapping function itself is an expensive simulation code or experiment. As a result, a great effort has been made by researchers to establish cost-effective methods of uncertainty analysis. These methods are reviewed in this chapter.
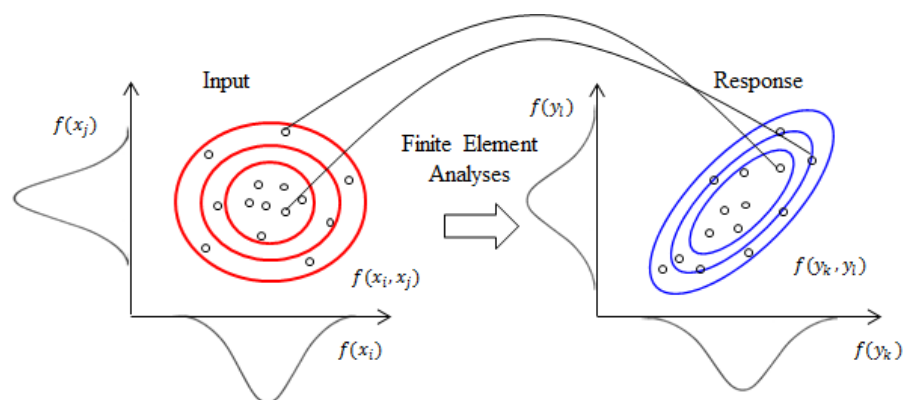
Figure 6.1. A schematic of Monte Carlo simulation (Schenk and Schuëller, 2005)

Note that for the brake squeal problem, the mapping function is the complex eigenvalue analysis. As there is no explicit expression for the relation between the real or imaginary parts of eigenvalues and the input variables (unless a system consists of a very limited number of degrees-of-freedom), the complex eigenvalues and eigenvectors of the brake

assembly must be calculated numerically. Now the question is which uncertainty method can provide the statistical description of the output scatter by considering the fact that one CEA run of the full brake assembly takes 12 to 36 hours to be completed.

6.3. Probabilistic approaches

Once again, the features of Monte Carlo simulation are reviewed here to explain what a probabilistic method of uncertainty analysis means. Looking at the left plot of Figure 6.1 shows if the input space is projected onto the horizontal and vertical axes, there is a probability distribution for each input parameter. In this schematic, the probability distributions are Gaussian, yet a number of probability distributions such as Log-normal, Gamma, Beta, uniform, etc. are available in the literature.

Regardless of the form of a probability distribution, all of them have one feature in common. This feature is that the probability of having a particular value/number in the distribution can be quantified by using their "probability density functions" (PDF) or a scatter of a large number of samples. This feature can become very important when a reliability analysis needs to be carried out. Briefly speaking, a reliability analysis is performed for evaluating the robustness of a design. In other words, the reliability analysis quantifies the failure probability of a design. The term "failure" is widely used in engineering for various undesired states of a system. In this study, 'failure' means that one of the system eigenvalues becomes unstable, i.e. the sign of the associated real part turns positive, or the squeal index exceeds the target level of the car manufacturer sponsoring this project.

As mention in section 6.2, Monte Carlo simulation is the most fundamental probabilistic method of uncertainty analysis. There are two advantages for this approach in comparison with the other techniques. First, the idea behind this method is very simple. The samples are mapped one-by-one to the output space until the statistical description of the output scatter is achieved. In industry, sometimes engineers are not willing to take an approach which is mathematically very complicated, and in this sense Monte Carlo simulation is preferred to other techniques. Secondly, when the output or mapping function is a nonlinear function of input variables, the most reliable way of uncertainty propagation is Monte Carlo simulation (Schenk and Schuëller, 2005).

On the other hand, the major drawback of Monte Carlo simulation is its computational inefficiency. This method employs a random generator to produce a considerable amount of samples over the design domain. Then, the corresponding output distributions are achieved by the use of the mapping function. Therefore, if the mapping function is very expensive to evaluate like the FE model of the full brake assembly, running Monte Carlo simulation is not

doable. Collecting the results of thousands of observations from the actual FE model may take several months or even one year depending on the accessible computational facilities.

As a result, a number of methods have been established in the literate for doing stochastic finite element analyses efficiently. Of these approaches, perturbation method and Polynomial Chaos expansions have been widely used in the literature. In fact, the perturbation method in the first place was developed for the analysis of nonlinear dynamic systems (Nayfeh, 1973). Then its application was extended to stochastic analyses. In Brief, the stochastic behaviour of a system is approximated about its mean value using Taylor expansion. This method is used in this study for investigating the statistics of complex eigenvalues in friction-induced vibration. A detailed explanation of this method will be given in the next chapter.

Polynomial Chaos is indeed a particular form of Karhunen-Loeve expansions. It is mostly applied to represent a stochastic process in terms of several orthogonal (orthonormal) functions. Ghanem and Spanos (2003) fully derived the Polynomial Chaos expansions of different orders and showed how the orthogonality condition must be satisfied between different polynomial terms. Although Polynomial Chaos is a non-sampling-based method and does not have the issue of computational workloads, the derivation of the polynomial terms and meeting the orthogonally condition is a difficult task, especially when the dimension of space exceeds three or four. Incidentally, Ghanem and Spanos (2003) reported Polynomial Chaos expansions of order zero to order four for 1D to 4D spaces.

6.4.   Non-probabilistic approaches

Another class of methods of uncertainty analysis is non-probabilistic approaches. In contrast with the probabilistic techniques, there is no distribution for the definition of parameters. Instead, an interval specifies the range within which the parameters vary. As a result, non-probabilistic approaches are not as informative as probabilistic ones from the statistical point of view. Defining a range for a parameter means the probability having the bounds of the interval is as same as the mean value of the interval. However, in practice, it is known that many physical parameters like material properties have Gaussian distributions. It is then very conservative to take an interval approach toward such properties. On the other hand, probabilistic methods are usually associated with some difficulties in terms of computation or mathematical derivation. Therefore, in many cases, a simple conservative approach may be preferred to a complicated accurate one.

Figure 6.2 shows a schematic of the interval analysis. There are two issues associated with this approach. Firstly, the mapping function should technically follow the rules of "interval

arithmetic". In many practical examples though, there is no explicit expression on which this arithmetic is implemented. Secondly, as explained above, the probability distribution of the outputs cannot be determined and this approach is somewhat conservative.
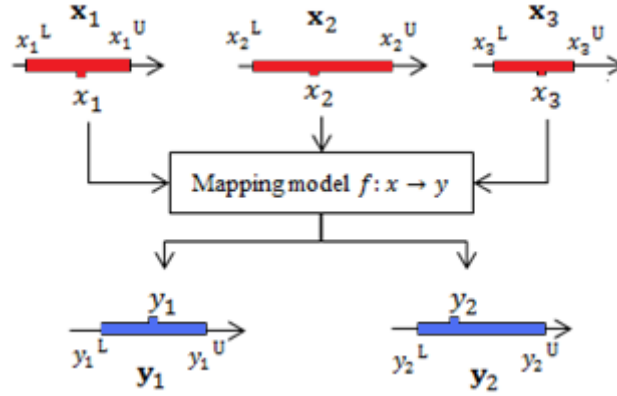
Figure 6.2. A schematic of interval analysis (Möller and Beer, 2008)

To tackle these issues, the application of fuzzy random variables (Puri and Ralesco, 1986) has been introduced to the subject by researchers. Instead of making predictions of the output ranges with crisp intervals, their fuzzy membership functions are evaluated in this way (Möller and Beer, 2008; Adhikari and Haddad-Khodaparast, 2014). Figure 6.3 shows a schematic of fuzzy analysis. As seen, the membership functions of the input variables are divided into different levels by a few "alpha-level-cuts". Then, at each alpha-level, there is an interval for each input parameter which must be mapped to the output space along with the intervals of the other inputs. Following this approach for all alpha-levels brings about the membership function of the output variable. Therefore, the role of membership functions in non-probabilistic methods may be interpreted as the role of probability distributions in the probabilistic approaches. Incidentally, this role is sometimes debated by statisticians.
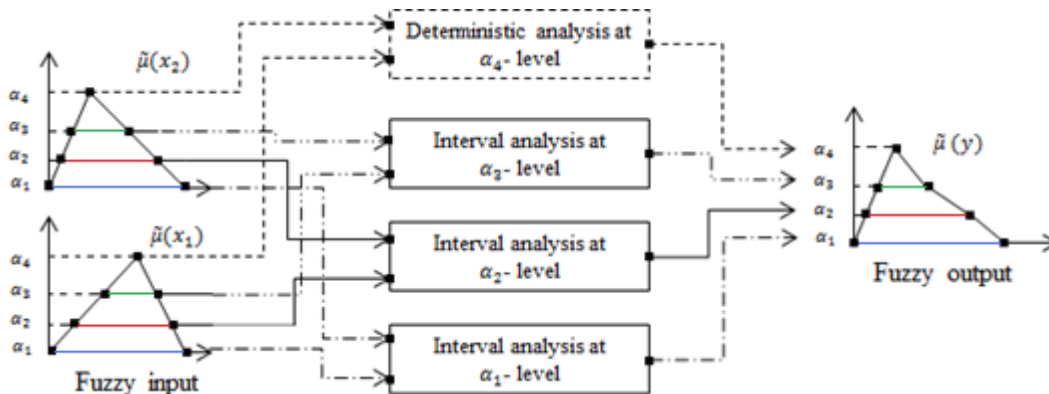
Figure 6.3. A schematic of fuzzy analysis (Moens and Vandepitte, 2006)

Moreover, the issue of interval arithmetic has been also resolved. As explained above, at each alpha-level, there is an interval for each input parameter. Then, instead of using the

interval arithmetic to map the ranges onto the output space, an optimisation algorithm is used to minimise and maximise the output variable within the input ranges. In this way, even when there is no explicit expression for the relation between the outputs and inputs, by means of numerical methods the bounds of output variables can be determined.

6.5.   Uncertainty analysis of friction-induced instabilities

In the brake squeal research community, uncertainty analysis has received much attention in the recent decade. These studies may be classified according to their approaches (probabilistic vs. non-probabilistic) or the order of the system (low-order/simplified vs. large scale/industrial models). Investigating simplified models is useful for phenomenological understanding of a problem. On the other hand, dealing with the issue of computational cost and time of large-scale FE models needs particular consideration as well. It has been attempted to highlight all of these factors for the studies in the literature.

First, the lumped models and then the industrial models are reviewed in a chronological order. In 2010, Butlin and Woodhouse investigated the effects of uncertainties on the instability of a pin-on-disc model. The transfer functions between the disc and 'brake' (pin) were studied analytically and validated experimentally. The analytical derivation of these transfer functions were fully explained in (Duffour and Woodhouse, 2004a; 2004b). Then, the first order perturbation method was employed in (Butlin and Woodhouse, 2010) for incorporating the variations of the system parameters in the results of stability analysis. Therefore, a probabilistic approach of uncertainty analysis was taken in this study. Later on, the same system and experimental set-up were used in (Butlin and Woodhouse, 2011) for measuring a large volume of 'squeal' data/occurrences. These data were post-processed in order to characterise the dynamical properties of the system under the influence of uncertainties. Then, the roles of symmetry, pre-load, speed and structural perturbations in squeal initiations were identified. The important conclusion of Butlin and Woodhouse's study was that it was experimentally proved Coulomb friction is not enough for predicting squeal initiations.

Nechak et al. (2013) applied the non-instructive generalised polynomial chaos method and Lyapunov indirect method to predict the stable and unstable regions of a mass-with-double-rubbers system under the influence of uncertainty. The only uncertain parameter in this study was friction coefficient. This study proposed an efficient method of uncertainty analysis in comparison with the classic Monte Carlo simulation. Sarrouy et al. (2013a) used the same system in order to determine both uncertain eigenvalues and stochastic limit cycles of nonlinear oscillations. For improving the efficiency of uncertainty analysis, Polynomial

Chaos expansions were used in this study. Moreover, in order to predict the limit cycles of nonlinear oscillations, a constrained harmonic balance method was employed. In other words, the time-response of the system was not directly used for the stochastic limit cycles. Finally, the predicted results were validated via Monte Carlo simulation.

For continuous systems, Gauger et al. (2006) took a non-probabilistic approach toward CEA of a simplified brake model consisting of the rotor, pads and calliper. The effects of two uncertain parameters were investigated in this study: friction coefficient and 'contact parameter'. Instead of the 'hard contact' (based on Abaqus terminology), an exponential function was assigned to define the relation between the brake line pressure, contact pressure and contact over-closure. This relation contained a parameter which was termed as 'contact parameter' and could be determined experimentally. However, the level of uncertainty about the measurement of this parameter was high. As a result, fuzzy arithmetic was used to quantify the uncertainty of complex eigenvalues under the influence of variations of these two parameters.

Culla and Maasi (2009) carried out an uncertainty analysis of contact instability which may lead to squeal noise. Their model which may be interpreted as a very simplified brake consisted of a disc, a small pad and a support. Monte Carlo simulation was used in this study to propagate the uncertainties of friction coefficient, pad's Young's modulus and stiffness of the springs holding the support. The uncertainty propagation was done on the results of stability analysis in order to determine the stochastic eigenvalues of the reduced model. As the authors used Monte Carlo simulation for this purpose, their approach was probabilistic.

In contrast with the many numerical studies in the literature, Oberst and Lai (2011b) took a statistical experimental approach toward the squeal problem. In a "design of experiment" study (DOE), they evaluated the effects of various geometrical features (pad's slots) on a noise index. It is worthwhile to remind that different configurations of slots are usually made on pads by brake manufacturers with the aim of designing a quieter brake. The experimental results were then ranked based on the noise index, warm and cold stops. For the statistical interpretation of the results, a correlation analysis was done between the time-averaged friction coefficient and the peak of the sound pressure level due to the fact that the measured data were time-dependent. Their results showed that the higher level of nonlinearity for the relation between these two factors leads to the worse squeal noise. The term "worse" could make sense here since they ranked the results according to the noise index.

Sarrouy et al. (2013b) implemented the method of polynomial chaos expansions on a simplified brake model consisting of a disc and two pads. The uncertainty of two parameters, friction coefficient and contact stiffness, were propagated onto the results of stability

analysis. The distributions of random parameters were assumed to be either uniform or Gaussian. Incidentally, no experimental data was reported to prove how valid these assumptions are. In fact, it is a very expensive and arduous task to portray the random nature of such parameters, experimentally. Hence, so far most studies make some assumptions for the distributions of the random parameters without experimental validation. The proposed method in (Sarrouy et al., 2013b) introduced an efficient statistical tool (polynomial chaos expansions) to the brake squeal problem. However, bear in mind that only two uncertain parameters were included in this study. If it was aimed to include several input parameters, the mathematical derivation of the required terms would be tricky.

In 2014, Tison et al. published an interesting journal paper on uncertainty and robustness of squeal simulations. In their investigation, an industrial brake model consisting of the disc, pads, calliper, knuckle, suspension links, etc. was studied. Instead of uncertainty and variability of material properties, contact stiffness and friction coefficient (the common uncertain parameters in the literature), they mainly focused on the surface topography at the pads-disc contact interface. The form, waviness and roughness of the pad surface were modelled via random fields in the problem. The effects of this random nature were then mapped onto the results of the complex eigenvalue analysis. For the interpretation of the results, "modal assurance criteria" (MAC) were employed to classify the stochastic eigenvalues. After this classification, the number of unstable modes was reduced to those occurring frequently in the random field. In this way, predictions of CEA were improved as well. For example, an unstable mode which was missed in the deterministic results but had been observed in the Dyno test data could be retrieved in the stochastic analysis. Secondly, a robustness analysis could be done based on the sensitivity of the unstable eigenvalues in each class with respect to the random variables. Note that reliability and robustness have different interpretations in different applications and studies. The robustness and reliability analysis in Tison's was done so that the frequency of occurrence of each class of unstable mode was determined. However, it is aimed in the current study to determine the percentage of 'failure' (likelihood of unstable vibrations leading to squeal noise) caused by variations of different parameters.

6.6. Surrogate/Meta Modelling

Reviewing the previous studies and considering the needs of the sponsor of this project remain no doubt that "surrogate modelling" is the best option for the purpose of this study. An efficient statistical approach, informative from statistical viewpoint, applicable in practice (within the daily jobs and tight deadlines of industry) and also understandable to a

large audience of engineers (not very complicated mathematical approach) is being sought for the purpose of this project.

On one hand, Monte Carlo simulation is very practical, informative yet simple which exactly meets what is needed for this project. On the other hand, it is computationally very expensive and cannot directly be applied to an industrial brake model with millions of degrees-of-freedom. Monte Carlo simulation can provide the full statistical description of the output scatter. The first moments of the output random variables such as their mean value, standard deviation, skewness, etc. can be calculated, and moreover the reliability analysis of a brake design can be carried out. Until now, there is no information about the percentage of 'failure' of a brake design in terms of likelihood of unstable vibrations leading to squeal noise, and therefore there is no estimation for the warranty costs of a new brake design due to noise issues.

What can tackle the issue of computational workload and keep the advantages of using Monte Carlo simulation is constructing a surrogate model in place of the actual FE model. In brief, surrogate modelling replaces the expensive finite element code with a cheap-to-evaluate mathematical function. Then, instead of using the actual FE model in the Monte Carlo simulation, the replacement model can be used cost-effectively. It is important to consider that surrogate modelling is not a method of uncertainty analysis. All methods of uncertainty analysis techniques either probabilistic or non-probabilistic can be applied to this model. In fact, the surrogate model can be taken as the mapping function of all methods. However, when it is affordable to run a Monte Carlo simulation for producing the output scatter, why brake engineers should be bothered with other complicated and less informative approaches? The implementation of this approach will be fully explained in chapter 8 and 9.

6.7.   Conclusions

The differences between the probabilistic and non-probabilistic approaches of uncertainty analysis are discussed in this chapter. The pros and cons of each approach are explained and it is clarified why the probabilistic approaches are generally more informative than non-probabilistic ones and why they are interesting for the purpose of this study.

As uncertainty analysis has been recently introduced to this subject, there are not many studies in the literature conducting a stochastic analysis on the friction-induced problem or the brake squeal problem. Incidentally, it is attempted to highlight the main features and the limitations of all existing studies. Then, it is briefly explained why surrogate modelling is used in the current study. An extensive discussion on the idea behind surrogate modelling and its implementation will be presented in the following chapters.

7. Statistics of Complex Eigenvalues in Friction Induced Vibration

Variability and uncertainty of input variables play a significant role in the results of stability analysis of friction-induced problems. In order to incorporate their effects, a second-order perturbation method is extended and employed in this chapter. The moments of the output distribution along with its joint moment generating function are used for quantifying the statistics of the complex eigenvalues. Moreover, the eigen-derivatives required for the perturbation method are presented in a way that they can deal with the asymmetry of the stiffness matrix and non-proportional damping. Since the eigen-derivatives of such systems are complex-valued numbers, it is mathematically more informative and convenient to derive the statistics of the eigenvalues in a complex form, without decomposing them into two real-valued real and imaginary parts. Then, the variance and pseudo-variance of the complex eigenvalues are used for determining the statistics of the real and imaginary parts. The reliability and robustness of the system in terms of stability can also be quantified by the approximated output distribution.

7.1.   Uncertainty analysis via perturbation method

As discussed in chapter 6, the main drawback of the classic Monte Carlo simulation is the computational costs and time. Therefore, researchers have been encouraged to use more efficient uncertainty techniques such as the perturbation methods and polynomial chaos expansions, etc. The technique to be employed in this paper is the 2nd order perturbation method. Adhikari and Friswell (2007) applied this method for random matrix eigenvalue problems. As there was no sliding contact with friction in their examples, the stiffness matrix remained symmetric. Moreover, the effect of non-proportional damping was not discussed in (Adhikari and Friswell, 2007). Consequently, the distributions of the imaginary parts of eigenvalues, i.e. frequencies, were the point of interest in their work.

However, this chapter focuses on friction-induced vibration with non-proportional damping. Friction makes the stiffness matrix asymmetric and introducing non-proportional damping means that the problem should be solved in the state-space. What is important here is to obtain the probabilistic distributions of the real parts of eigenvalues for evaluating the system stability. For this purpose, a few mathematical expressions are derived for the statistics of the complex eigenvalues. The first moment of the output distribution is the mean value and the joint moment generating function is employed for the calculation of the variance of the scatter of the complex eigenvalues. The statistics of the real and imaginary parts is then calculated by the use of the derived expressions.

The implementation of the complex eigenvalue analysis on a system with asymmetric stiffness matrix and non-proportional damping is given in section 5.6. Once again, consider the eigenvalue problem in the state-space:

$$(\mathbf{B} + \lambda_j \mathbf{A})\mathbf{u}_j = \mathbf{0} \; ; \; \mathbf{v}_j^T(\mathbf{B} + \lambda_j \mathbf{A}) = \mathbf{0} \tag{7.1}$$

where

$$\mathbf{A} = \begin{bmatrix} \mathbf{C} & \mathbf{M} \\ \mathbf{M} & \mathbf{0} \end{bmatrix}, \mathbf{B} = \begin{bmatrix} \mathbf{K} & \mathbf{0} \\ \mathbf{0} & -\mathbf{M} \end{bmatrix}, \tag{7.2}$$

and $\lambda_j = \alpha_j + i\omega_j$ is the jth eigenvalues of the system with the real part α_j and imaginary part ω_j. Vectors $\mathbf{u}_j$ and $\mathbf{v}_j$ are the normalised right and left eigenvectors, respectively. The normalisation is done so that $\mathbf{v}_j^T \mathbf{A} \mathbf{u}_j = 1$ (Murthy and Haftka, 1988).

Obviously, the eigenvalues of the system λ_j are functions of the system parameters θ_k. If the joint probability distribution of the input variables is Gaussian, the complex eigenvalues can be approximated by Taylor series about the mean value of the system parameters ξ_k. This approximation may be written in a quadratic form as (Adhikari and Friswell, 2007):

$$\lambda_j(\boldsymbol{\theta}) \approx \lambda_j(\boldsymbol{\xi}) + \mathbf{d}_{\lambda_j}^{\mathrm{T}}(\boldsymbol{\xi}) (\boldsymbol{\theta} - \boldsymbol{\xi}) + \frac{1}{2}(\boldsymbol{\theta} - \boldsymbol{\xi})^{\mathrm{T}} \mathbf{D}_{\lambda_j}(\boldsymbol{\xi}) (\boldsymbol{\theta} - \boldsymbol{\xi}) \tag{7.3}$$

where θ_k represents kth random input variable, $\mathbf{d}_{\lambda_j}$ is the gradient vector and $\mathbf{D}_{\lambda_j}$ denotes the Hessian matrix. Therefore,

$$\left\{ \mathbf{d}_{\lambda_j}(\boldsymbol{\xi}) \right\}_k = \left. \frac{\partial \lambda_j(\boldsymbol{\theta})}{\partial \theta_k} \right|_{\boldsymbol{\theta}=\boldsymbol{\xi}} \text{ and } \left\{ \mathbf{D}_{\lambda_j}(\boldsymbol{\xi}) \right\}_{kl} = \left. \frac{\partial^2 \lambda_j(\boldsymbol{\theta})}{\partial \theta_k \partial \theta_l} \right|_{\boldsymbol{\theta}=\boldsymbol{\xi}}. \tag{7.4}$$

The eigen-derivatives which were reported in (Adhikari and Friswell, 2007) are not directly applicable to the problem under the current study due to the asymmetry of the stiffness matrix and the presence of non-proportional damping. Plaut and Huseyin (1973) derived the derivatives of the eigenvalue and eigenvector of a non-self-adjoint system. The derivation is reviewed here for the convenience of readers.

Pre-multiplying the eigenvalue problem given in equation (7.1) by $\mathbf{v}_j^{\mathrm{T}}$ results in a scalar equation:

$$\mathbf{v}_j^{\mathrm{T}}(\boldsymbol{\theta}) \left(\mathbf{B}(\boldsymbol{\theta}) + \lambda_j(\boldsymbol{\theta})\mathbf{A}(\boldsymbol{\theta}) \right) \mathbf{u}_j(\boldsymbol{\theta}) = 0 \tag{7.5}$$

For the sake of simplicity, in some of the equations below, it is not shown that the eigenvalues, eigenvectors, matrix $\mathbf{A}$ and $\mathbf{B}$ are functions of $\boldsymbol{\theta}$. Differentiating equation (7.5) leads to

$$\mathbf{v}_{j,k}^{\mathrm{T}}\left(\mathbf{B} + \lambda_j\mathbf{A} \right)\mathbf{u}_j + \mathbf{v}_j^{\mathrm{T}}\left(\mathbf{B}_{,k} + \lambda_{j,k}\mathbf{A} + \lambda_j\mathbf{A}_{,k} \right)\mathbf{u}_j + \mathbf{v}_j^{\mathrm{T}}\left(\mathbf{B} + \lambda_j\mathbf{A} \right)\mathbf{u}_{j,k} = 0 \tag{7.6}$$

where $\mathbf{u}_{j,k}$ denotes $\partial \mathbf{u}_j(\boldsymbol{\theta})/\partial \theta_k$, for example.

As $\left(\mathbf{B} + \lambda_j\mathbf{A} \right)\mathbf{u}_j = \mathbf{0}$, $\mathbf{v}_j^{\mathrm{T}}\left(\mathbf{B} + \lambda_j\mathbf{A} \right) = \mathbf{0}$ and $\mathbf{v}_j^{\mathrm{T}}\left(\mathbf{B} + \lambda_j\mathbf{A} \right)\mathbf{u}_j = \mathbf{0}$, equation (7.6) becomes:

$$\mathbf{v}_j^{\mathrm{T}}\left(\mathbf{B}_{,k} + \lambda_{j,k}\mathbf{A} + \lambda_j\mathbf{A}_{,k} \right)\mathbf{u}_j = 0 \tag{7.7}$$

Therefore, rearranging (7.7) and considering the normalisation condition ($\mathbf{v}_j^{\mathrm{T}}\mathbf{A}\mathbf{u}_j = 1$) yields:

$$\boxed{\frac{\partial \lambda_j(\boldsymbol{\theta})}{\partial \theta_k} = -\left(\mathbf{v}_j^{\mathrm{T}}(\boldsymbol{\theta})\mathbf{G}_{jk}(\boldsymbol{\theta})\mathbf{u}_j(\boldsymbol{\theta}) \right)} \tag{7.8}$$

where $\mathbf{G}_{jk}(\boldsymbol{\theta}) = \left(\frac{\partial \mathbf{B}(\boldsymbol{\theta})}{\partial \theta_k} + \lambda_j(\boldsymbol{\theta}) \frac{\partial \mathbf{A}(\boldsymbol{\theta})}{\partial \theta_k} \right)$.

The derivation of the elements of Hessian matrix is a little more complicated:

$$\lambda_{j,kl} = -\mathbf{v}_{j,l}^{\mathrm{T}}\mathbf{G}_{jk}\mathbf{u}_j - \mathbf{v}_j^{\mathrm{T}}\mathbf{G}_{jk}\mathbf{u}_{j,l} - \mathbf{v}_j^{\mathrm{T}}\left(\mathbf{B}_{,kl} + \lambda_j\mathbf{A}_{,kl} + \lambda_{j,l}\mathbf{A}_{,k} \right)\mathbf{u}_j. \tag{7.9}$$

Assume the right and left eigenvectors can be expressed as $\mathbf{u}_{j,l} = \sum_{r=1}^{N}(c_{jlr}\mathbf{u}_r)$ and $\mathbf{v}_{j,l} = \sum_{r=1}^{N}(d_{jlr}\mathbf{v}_r)$. Then,

$$\lambda_{j,kl} = -\sum_{r=1}^{N}d_{jlr}\mathbf{v}_r^{\mathrm{T}}\mathbf{G}_{jk}\mathbf{u}_j - \sum_{r=1}^{N}c_{jlr}\mathbf{v}_j^{\mathrm{T}}\mathbf{G}_{jk}\mathbf{u}_r - \mathbf{v}_j^{\mathrm{T}}(\mathbf{B}_{,kl} + \lambda_j\mathbf{A}_{,kl})\mathbf{u}_j + (\mathbf{v}_j^{\mathrm{T}}\mathbf{A}_{,k}\mathbf{u}_j)(\mathbf{v}_j^{\mathrm{T}}\mathbf{G}_{jl}\mathbf{u}_j) \tag{7.10}$$

Rearranging equation (7.11) yields:

$$\lambda_{j,kl} = -\mathbf{v}_j^{\mathrm{T}}(\mathbf{B}_{,kl} + \lambda_j\mathbf{A}_{,kl})\mathbf{u}_j + (\mathbf{v}_j^{\mathrm{T}}\mathbf{A}_{,k}\mathbf{u}_j)(\mathbf{v}_j^{\mathrm{T}}\mathbf{G}_{jl}\mathbf{u}_j) - (d_{jlj} + c_{jlj})\,\mathbf{v}_j^{\mathrm{T}}\mathbf{G}_{jk}\mathbf{u}_j - \sum_{\substack{r=1\\r\neq j}}^{N}(c_{jlr}\mathbf{v}_j^{\mathrm{T}}\mathbf{G}_{jk}\mathbf{u}_r + d_{jlr}\mathbf{v}_r^{\mathrm{T}}\mathbf{G}_{jk}\mathbf{u}_j) \tag{7.11}$$

Note that the differentiation of $\mathbf{v}_j^{\mathrm{T}}\mathbf{A}\,\mathbf{u}_j = 1$ with respect θ_l results in:

$$\mathbf{v}_{j,l}^{\mathrm{T}}\mathbf{A}\,\mathbf{u}_j + \mathbf{v}_j^{\mathrm{T}}\mathbf{A}_{,l}\,\mathbf{u}_j + \mathbf{v}_j^{\mathrm{T}}\mathbf{A}\,\mathbf{u}_{j,l} = 0 \tag{7.12}$$

Then,

$$\sum_{r=1}^{N}(c_{jlr}\mathbf{v}_j^{\mathrm{T}}\mathbf{A}\,\mathbf{u}_r + d_{jlr}\mathbf{v}_r^{\mathrm{T}}\mathbf{A}\,\mathbf{u}_j) = -(\mathbf{v}_j^{\mathrm{T}}\mathbf{A}_{,l}\,\mathbf{u}_j) \tag{7.13}$$

Therefore, the orthogonality of the eigenvectors leads to:

$$(c_{jlj} + d_{jlj}) = -(\mathbf{v}_j^{\mathrm{T}}\mathbf{A}_{,l}\,\mathbf{u}_j)\ \text{ for } r = j \tag{7.14}$$

Moreover, the differentiation of $\mathbf{v}_r^{\mathrm{T}}(\mathbf{B} + \lambda_j\mathbf{A})\mathbf{u}_j = 0$ with respect θ_l results in:

$$\mathbf{v}_{r,l}^{\mathrm{T}}(\mathbf{B} + \lambda_j\mathbf{A})\,\mathbf{u}_j + \mathbf{v}_r^{\mathrm{T}}(\mathbf{B}_{,l} + \lambda_j\mathbf{A}_{,l} + \lambda_{j,l}\mathbf{A})\,\mathbf{u}_j + \mathbf{v}_r^{\mathrm{T}}(\mathbf{B} + \lambda_j\mathbf{A})\,\mathbf{u}_{j,l} = 0 \tag{7.15}$$

As $\mathbf{v}_r^{\mathrm{T}}\mathbf{A}\mathbf{u}_j = 0$,

$$\sum_{p=1}^{N}(c_{jlp}\mathbf{v}_p^{\mathrm{T}}(\mathbf{B} + \lambda_j\mathbf{A})\mathbf{u}_r) + \mathbf{v}_r^{\mathrm{T}}\mathbf{G}_{jl}\mathbf{u}_j = 0. \tag{7.16}$$

Also $\mathbf{v}_r^{\mathrm{T}}\mathbf{B}\mathbf{u}_r = -\lambda_r$, therefore

$$c_{jlr} = -\frac{\mathbf{v}_r^{\mathrm{T}}\mathbf{G}_{jl}\mathbf{u}_j}{(\lambda_j - \lambda_r)}\ \text{ if } r \neq j \tag{7.17}$$

Similarly,

$$d_{jlr} = -\frac{\mathbf{v}_j^{\mathrm{T}}\mathbf{G}_{jl}\mathbf{u}_r}{(\lambda_j - \lambda_r)}\ \text{ if } r \neq j \tag{7.18}$$

Finally,

$$
\frac{\partial^2 \lambda_j(\boldsymbol{\theta})}{\partial \theta_k \partial \theta_l} = -\mathbf{v}_j^{\mathrm{T}}(\boldsymbol{\theta}) \left[\frac{\partial^2 \mathbf{B}(\boldsymbol{\theta})}{\partial \theta_k \partial \theta_l} + \lambda_j(\boldsymbol{\theta}) \frac{\partial^2 \mathbf{A}(\boldsymbol{\theta})}{\partial \theta_k \partial \theta_l} \right] \mathbf{u}_j(\boldsymbol{\theta}) \ + \cdots
$$

$$
\left(\mathbf{v}_j^{\mathrm{T}}(\boldsymbol{\theta}) \frac{\partial \mathbf{A}(\boldsymbol{\theta})}{\partial \theta_k} \mathbf{u}_j(\boldsymbol{\theta}) \right) \left(\mathbf{v}_j^{\mathrm{T}}(\boldsymbol{\theta}) \mathbf{G}_{jl}(\boldsymbol{\theta}) \mathbf{u}_j(\boldsymbol{\theta}) \right) + \left(\mathbf{v}_j^{\mathrm{T}}(\boldsymbol{\theta}) \frac{\partial \mathbf{A}(\boldsymbol{\theta})}{\partial \theta_l} \mathbf{u}_j(\boldsymbol{\theta}) \right) \left(\mathbf{v}_j^{\mathrm{T}}(\boldsymbol{\theta}) \mathbf{G}_{jk}(\boldsymbol{\theta}) \mathbf{u}_j(\boldsymbol{\theta}) \right) + \cdots
$$

$$
\sum_{\substack{r=1 \\ r \neq j}}^{N} \frac{\left(\mathbf{v}_j^{\mathrm{T}}(\boldsymbol{\theta}) \mathbf{G}_{jk}(\boldsymbol{\theta}) \mathbf{u}_r(\boldsymbol{\theta}) \right) \left(\mathbf{v}_r^{\mathrm{T}}(\boldsymbol{\theta}) \mathbf{G}_{jl}(\boldsymbol{\theta}) \mathbf{u}_j(\boldsymbol{\theta}) \right) + \left(\mathbf{v}_j^{\mathrm{T}}(\boldsymbol{\theta}) \mathbf{G}_{jl}(\boldsymbol{\theta}) \mathbf{u}_r(\boldsymbol{\theta}) \right) \left(\mathbf{v}_r^{\mathrm{T}}(\boldsymbol{\theta}) \mathbf{G}_{jk}(\boldsymbol{\theta}) \mathbf{u}_j(\boldsymbol{\theta}) \right)}{(\lambda_j(\boldsymbol{\theta}) - \lambda_r(\boldsymbol{\theta}))}.
$$

(7.19)

The quadratic form of the complex eigenvalues which is expressed in equation (7.3) cannot directly be used since θ_k is a random variable. In other words, this equation is not deterministic. However, the statistics of the complex eigenvalues can be obtained by the use of this quadratic form. For the convenience of readers, the theoretical background of this approach is briefly discussed in the following section.

7.2.   Statistics of complex eigenvalues

The main objective of this section is to predict the statistics of the complex eigenvalues without decomposing them into the real and imaginary parts. As the eigen-derivatives expressed in (7.8) and (7.19) produce complex-valued numbers, the moments and cumulants of the output distributions are also derived in the complex form.

7.2.1.   Derivation of the mean value

In the theory of statistics, the mean value of a random variable is its first moment about the origin. Considering the fact that the input variables are real-valued while $\lambda_j(\boldsymbol{\theta})$ is a complex function of the input variable, the mean value or the first moment of the jth eigenvalue may be calculated by:

$$
\hat{\lambda}_j = E[\lambda_j(\boldsymbol{\theta})] = \int_{-\infty}^{+\infty} \cdots \int_{-\infty}^{+\infty} \lambda_j(\boldsymbol{\theta}) \, p_{\boldsymbol{\theta}}(\boldsymbol{\theta}) \mathrm{d}\theta_1 \cdots \mathrm{d}\theta_m \tag{7.20}
$$

where $E[\lambda_j(\boldsymbol{\theta})]$ represents the expected value of λ_j and $p_{\boldsymbol{\theta}}(\boldsymbol{\theta})$ denotes the joint probability density function of $\boldsymbol{\theta}$. Vector $\boldsymbol{\theta}$ consists of m real-valued random input variables. Any joint probability density function can be substituted in place of $p_{\boldsymbol{\theta}}$. However, in many cases but the multivariate Gaussian distribution, it is not feasible to derive a closed-form expression

for $\hat{\lambda}_j$. In Johnson and Kotz (1972), the joint probability density function of an m-dimensional Gaussian distribution is given in a quadratic form:

$$p_{\theta}(\theta) = (2\pi)^{-\frac{m}{2}} |V|^{-\frac{1}{2}} \exp[-\frac{1}{2}(\theta - \xi)^T V^{-1}(\theta - \xi)] \tag{7.21}$$

where ξ is the vector of mean values and V is the covariance matrix of the input variable vector θ. In this study, $|A|$ denotes the determinant of matrix A.

It is more convenient to transform the variable of integration (7.20) to $y = \theta - \xi$. Therefore,

$$\hat{\lambda}_j = (2\pi)^{-\frac{m}{2}} |V|^{-\frac{1}{2}} \int_{-\infty}^{+\infty} \cdots \int_{-\infty}^{+\infty} \left[\lambda_j(\xi) + d_{\lambda_j}^T(\xi)y + \frac{1}{2}y^T D_{\lambda_j}(\xi)\, y \right] \exp\left[-\frac{1}{2}y^T V^{-1}y\right] dy_1 \cdots dy_m. \tag{7.22}$$

Due to the fact that the covariance matrix is positive definite, it can be decomposed as $V = LL^T$, where L is a non-singular lower triangle matrix (Johnson and Kotz, 1972). By the use of the Jacobian matrix, the variable of integration in (7.22) is transformed to $z = L^{-1}y$:

$$\hat{\lambda}_j = (2\pi)^{-\frac{m}{2}} \int_{-\infty}^{+\infty} \cdots \int_{-\infty}^{+\infty} \left[\lambda_j(\xi) + d_{\lambda_j}^T(\xi)Lz + \frac{1}{2}z^T L^T D_{\lambda_j}(\xi)\, Lz \right] \exp\left[-\frac{1}{2}z^T z\right] dz_1 \cdots dz_m. \tag{7.23}$$

Since $z^T z = \sum_{j=1}^m z_j^2$, the multiple integral given in (7.23) turns into the product of m single variable integrals. Indeed, that is one of the advantages of using the theory of quadratic forms. Considering $\int_{-\infty}^{+\infty} \exp\left[-\frac{x^2}{2}\right] dx = \sqrt{2\pi}$ and $\int_{-\infty}^{+\infty} x \exp\left[-\frac{x^2}{2}\right] dx = 0$, equation (7.23) becomes:

$$\hat{\lambda}_j = \lambda_j(\xi) + (2\pi)^{-\frac{m}{2}} \int_{-\infty}^{+\infty} \cdots \int_{-\infty}^{+\infty} \left[\frac{1}{2}z^T L^T D_{\lambda_j}(\xi)\, Lz\right] \exp\left[-\frac{1}{2}z^T z\right] dz_1 \cdots dz_m \tag{7.24}$$

The symmetry of the matrix $L^T D_{\lambda_j}(\xi)\, L$ brings about the same left and right eigenvectors. If Δ and Ψ respectively represent the diagonal matrix of the eigenvalues and the matrix of the normalized eigenvectors of $L^T D_{\lambda_j}(\xi)\, L$, pre- and post-multiplying this matrix by Ψ^T and Ψ results in:

$$\hat{\lambda}_j = \lambda_j(j\xi) + (2\pi)^{-\frac{m}{2}} \int_{-\infty}^{+\infty} \cdots \int_{-\infty}^{+\infty} \left(\frac{1}{2}w^T \Delta w\right) \exp\left[-\frac{1}{2}w^T w\right] dw_1 \cdots dw_m \tag{7.25}$$

where $w = \Psi^T z$. As matrix Δ is diagonal, $w^T \Delta\, w = \sum_{i=1}^m \Delta_i w_i^2$. Therefore, the mean value of the jth complex eigenvalues can explicitly be determined as:

$$\hat{\lambda}_j = \lambda_j(\boldsymbol{\xi}) + \frac{1}{2}\sum_{i=1}^{m} \Delta_i \,. \tag{7.26}$$

The eigenvalues of $\mathbf{L}^\mathrm{T}\mathbf{D}_{\lambda_j}(\boldsymbol{\xi})\,\mathbf{L}$ are equivalent to those of $\mathbf{V}\mathbf{D}_{\lambda_j}(\boldsymbol{\xi})$ (Johnson and Kotz, 1972). Furthermore, the summation of eigenvalues of any matrix is evidently equal to the trace of that matrix. Therefore, equation (7.26) can be re-written as

$$\hat{\lambda}_j = \lambda_j(\boldsymbol{\xi}) + \frac{1}{2}\mathrm{Trace}\left(\mathbf{V}\mathbf{D}_{\lambda_j}(\boldsymbol{\xi})\right). \tag{7.27}$$

It is worth mentioning that the expression derived for the mean value of the complex eigenvalues has the same form as the one reported in (Adhikari and Friswell, 2007) for a symmetric system without damping. However, equation (7.27) produces a complex number whose real part is the mean value of the real parts of the jth complex eigenvalues and whose imaginary part is the mean value of the imaginary parts.

7.2.2. *Derivation of the variance*

The variance of a complex random variable is usually defined as a real-valued number which is calculated by

$$\mathrm{Var}\left(\lambda_j(\boldsymbol{\theta})\right) = E[(\lambda_j(\boldsymbol{\theta}) - \hat{\lambda}_j)(\lambda_j(\boldsymbol{\theta}) - \hat{\lambda}_j)^*] \tag{7.28}$$

where "*" denotes conjugate of a complex number. Before starting to derive the expression of the variance, it is important to re-consider the central aim of this study, which is the evaluation of the system stability under the influence of structural uncertainties. In other words, the distribution of the real parts of the complex eigenvalues is the main point of interest in this study.

If Σ_{α_j} and Σ_{ω_j} represent the variance of the real and imaginary parts, and also $\Sigma_{\alpha_j\omega_j}$ and $\Sigma_{\omega_j\alpha_j}$ stand for the covariance between the real and imaginary parts, equation (7.28) can be expressed with these terms as:

$$\mathrm{Var}\left(\lambda_j(\boldsymbol{\theta})\right) = \left(\Sigma_{\alpha_j} + \Sigma_{\omega_j}\right) \tag{7.29}$$

due to the fact that $\Sigma_{\alpha_j\omega_j} = \Sigma_{\omega_j\alpha_j}$.

Obviously, equation (7.29) is not sufficient to calculate the variance of the real and imaginary parts. However, what can resolve this issue is the use of pseudo-variance:

$$\widetilde{\mathrm{Var}}\left(\lambda_j(\boldsymbol{\theta})\right) = E\left[\left(\lambda_j(\boldsymbol{\theta}) - \hat{\lambda}_j\right)^2\right]. \tag{7.30}$$

Similar to the variance, the pseudo-variance can expressed in terms of the variances and covariance of the real and imaginary parts:

$$\widetilde{\mathrm{Var}}\left(\lambda_j(\boldsymbol{\theta})\right) = \left(\Sigma_{\alpha_j} - \Sigma_{\omega_j}\right) + \mathrm{i}\left(2\,\Sigma_{\omega_j\alpha_j}\right). \tag{7.31}$$

As seen, in contrast with the variance, $\widetilde{\mathrm{Var}}\left(\lambda_j(\boldsymbol{\theta})\right)$ is a complex-valued number and it provides a way to determine the variance of the real and imaginary parts along with equation (7.29).

Now in order to derive an expression for the variance of the complex eigenvalues, the joint moment generating function is used. In fact, the moment generating function is an alternative way of calculating the moments of a random variable (Johnson and Kotz, 1969). The joint moment generating function of $\lambda_j(\boldsymbol{\theta})$ and $\lambda_j^*(\boldsymbol{\theta})$ can be written as

$$M_{\lambda_j,\lambda_j^*}(s_1, s_2) = E\left[\exp(s_1\lambda_j(\boldsymbol{\theta}) + s_2\lambda_j^*(\boldsymbol{\theta})\right] \tag{7.32}$$

Using the definition of the expected value results in:

$$M_{\lambda_j,\lambda_j^*}(s_1, s_2) = (2\pi)^{-\frac{m}{2}}|\mathbf{V}|^{-\frac{1}{2}} \int_{-\infty}^{+\infty} \exp\left\{s_1\lambda_j(\boldsymbol{\xi}) + s_2\lambda_j^*(\boldsymbol{\xi}) + \left[s_1\mathbf{d}_{\lambda_j}^{\mathrm{T}}(\boldsymbol{\xi}) + s_2\mathbf{d}_{\lambda_j^*}^{\mathrm{T}}(\boldsymbol{\xi})\right]\mathbf{y}\cdots \right.$$
$$\left. -\frac{1}{2}\mathbf{y}^{\mathrm{T}}\left[\mathbf{V}^{-1} - s_1\mathbf{D}_{\lambda_j}(\boldsymbol{\xi}) - s_2\mathbf{D}_{\lambda_j^*}(\boldsymbol{\xi})\right]\mathbf{y}\right\}\mathrm{d}\boldsymbol{y} \tag{7.33}$$

This integral is, in fact, the generalized version of Gaussian integral in an m-dimensional domain. Like the procedure for the mean value, the solution of this integral can also be found:

$$\int_{-\infty}^{+\infty} \exp\left[-\frac{1}{2}\mathbf{x}^{\mathrm{T}}\mathbf{A}\mathbf{x} + \mathbf{B}\mathbf{x}\right]\mathrm{d}\mathbf{x} = (2\pi)^{\frac{m}{2}}|\mathbf{A}|^{-\frac{1}{2}}(\frac{1}{2}\mathbf{B}\mathbf{A}^{-1}\mathbf{B}) \tag{7.34}$$

where $\mathbf{A}$ is a symmetric matrix.

According to (7.34), the joint moment generating function can explicitly be determined:

$$M_{\lambda_j,\lambda_j^*}(s_1, s_2) = \frac{\exp\left(s_1\lambda_j(\boldsymbol{\xi}) + s_2\lambda_j^*(\boldsymbol{\xi})\right)}{\left|\mathbf{I} - s_1\mathbf{D}_{\lambda_j}(\boldsymbol{\xi}) - s_2\mathbf{D}_{\lambda_j^*}(\boldsymbol{\xi})\right|} \times \cdots$$
$$\exp\left\{\left[s_1\mathbf{d}_{\lambda_j}^{\mathrm{T}}(\boldsymbol{\xi}) + s_2\mathbf{d}_{\lambda_j^*}^{\mathrm{T}}(\boldsymbol{\xi})\right]\mathbf{V}\left[\mathbf{I} - s_1\mathbf{D}_{\lambda_j}(\boldsymbol{\xi}) - s_2\mathbf{D}_{\lambda_j^*}(\boldsymbol{\xi})\right]^{-1}\left[s_1\mathbf{d}_{\lambda_j}(\boldsymbol{\xi}) + s_2\mathbf{d}_{\lambda_j^*}(\boldsymbol{\xi})\right]\right\}. \tag{7.35}$$

In the theory of statistics, it is quite common to use the cumulant generating function rather than the moment generating function. The cumulant generating function is the natural

logarithm of the moment generating function and the second cumulant of a distribution is the variance. Hence, the variance of the complex eigenvalues is obtained via $\mathrm{Var}\left(\lambda_j(\boldsymbol{\theta})\right) = \frac{\partial^2}{\partial s_1\, \partial s_2} \ln M_{\lambda_j,\lambda_j^*}(s_1,s_2)\Big|_{s_1=s_2=0}$.

After differentiating $\ln M_{\lambda_j,\lambda_j^*}(s_1,s_2)$ and equating s_1 and s_2 to zero, the variance of the complex eigenvalues can be expressed as

$$\mathrm{Var}\left(\lambda_j(\boldsymbol{\theta})\right) = \mathbf{d}_{\lambda_j}^{\mathrm{T}}(\boldsymbol{\xi})\mathbf{V}\mathbf{d}_{\lambda_j^*}(\boldsymbol{\xi}) + \frac{1}{2}\mathrm{Trace}\left(\mathbf{V}\mathbf{D}_{\lambda_j}(\boldsymbol{\xi})\,\mathbf{V}\mathbf{D}_{\lambda_j^*}(\boldsymbol{\xi})\right). \tag{7.36}$$

Similarly, the pseudo-variance is obtained by

$$\widetilde{\mathrm{Var}}\left(\lambda_j(\boldsymbol{\theta})\right) = \mathbf{d}_{\lambda_j}^{\mathrm{T}}(\boldsymbol{\xi})\mathbf{V}\mathbf{d}_{\lambda_j}(\boldsymbol{\xi}) + \frac{1}{2}\mathrm{Trace}\left([\mathbf{V}\mathbf{D}_{\lambda_j}(\boldsymbol{\xi})]^2\right). \tag{7.37}$$

The pseudo-variance has the same mathematical expression as the variance of eigenvalues given in (Adhikari and Friswell, 2007), yet the difference here is that it produces complex-valued numbers. As discussed earlier, expressions (7.36) and (7.37) will be employed together for the calculation of Σ_{α_j} and Σ_{ω_j}.

7.3.   A lumped mass model

Figure 7.1 shows the lumped mass model which is used here for the demonstration of the extended 2nd order perturbation method. In chapter 5, the deterministic analysis of this model is presented. Now what is being investigated in chapter 7 is how uncertainty and variability of system parameters affects the results of stability analysis.

Once again, imagine the system shown in Figure 7.1 represents a very simplified brake model. Many experimental studies have shown that the level of variability and uncertainty of friction material is very high. Not only the variability of material properties (k_2, k_3 and k_4), but also the friction coefficient (μ), contact stiffness (k_c) and contact damping (c_c) are major sources of uncertainties in this problem. When the friction coefficient is 0.4, according to the results of CEA in chapter 5 (Table 5.1), all eigenvalues of the system are stable. It would be very useful to find out whether the system would remain stable or not when subjected to uncertainty.
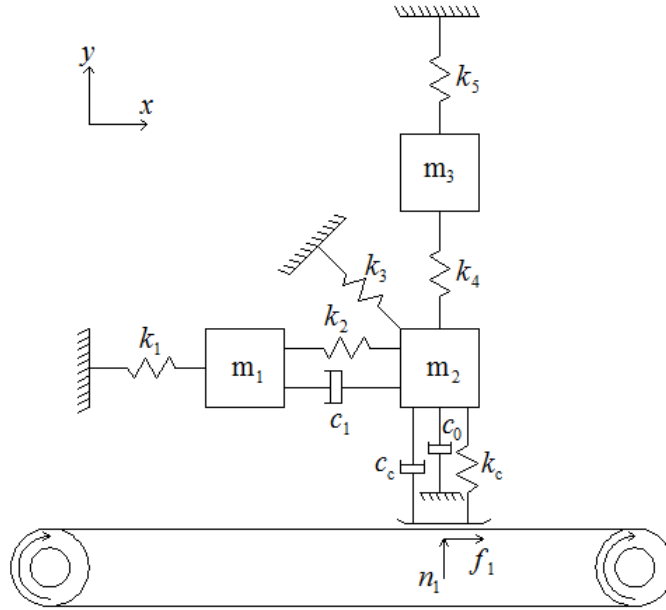
Figure 7.1. A lumped mass model

7.4.   Sensitivity analysis

When a very complicated model with a number of uncertain parameters is under study, one of the key steps in selecting the parameters for the uncertainty analysis is "sensitivity analysis". For example, although the level of uncertainty in the material properties of friction material is high, it does not necessarily mean that they have the most contribution in the results of stability analysis. In particular, for a large-scale FE models, including several variables can lead to a significant amount of computational workload. Thus, only those parameters to which the unstable modes are highly sensitive should be included in the uncertainty analysis.

To find out how sensitive the real parts of the eigenvalues are with respect to the selected input variables, a sensitivity analysis is done by means of equation (7.8). Meanwhile, one consideration bringing about more reliable results is to normalize the sensitivities in order to avoid scaling issues. The mean values of the input variables and corresponding real parts are used for this purpose, i.e. $\frac{\partial \lambda_j(\theta)/\lambda_j(\xi)}{\partial \theta_k/\xi_k}$. Table 7.1 lists the normalised sensitivities of the real parts of the eigenvalues versus the selected system parameters.

As seen, the real part of the first eigenvalue which is in the vicinity of instability shows high sensitivity to the friction coefficient. This supports the statement in chapter 5 why friction coefficient is taken as the most active parameter in low-order models. Moreover, the contact stiffness and k_2 take the second and third places. Now, it is aimed to evaluate the efficacy of the extended 2nd-order perturbation method for quantifying the statistics of the eigenvalues

124

under the uncertainty and variability of all selected variables. Thereafter, a further study is carried out by randomising only the two most active variables, i.e. μ and k_c.

Table 7.1. Normalised sensitivities of the real parts of the eigenvalues

Variable	First pair	Second pair	Third pair	Fourth pair
k_c	−9.7175	−1.2743	0.0263	0.3497
k_2	−8.5165	0.0854	0.1006	−0.2079
k_3	−1.6676	−0.4114	0.0018	0.1203
k_4	0.2253	0.9047	−0.0812	−0.0686
c_c	1.6344	0.1566	0.0026	0.1648
μ	−19.3073	0.1628	0.1077	−0.1872

7.5.   Uncertainty quantification of all selected variables

To perform an uncertainty analysis, it is assumed that the deviation of k_2, k_3 and k_4 from their nominal values is 5 percent and the deviation of k_c and c_c is 10 percent. As μ can change significantly in a brake application, 15 percent variation is allocated to the friction coefficient. In order to validate the proposed approach, the conventional Monte Carlo simulation is run for the verification of the results. One-million samples are made via a multivariate Gaussian random generator. The mean value and variance of the real and imaginary parts are calculated separately and compared with the outcomes of the expressions given in section 7.2. Table 7.2 to

Table 7.4 list the results of the perturbation method and Monte Carlo simulation. In these tables, the term "Perturb." abbreviates the 2nd order perturbation method and "MSC" means Monte Carlo Simulation.

Table 7.2. Mean values of the real parts of the complex eigenvalues

	Real part of the 1st pair	Real part of the 2nd pair	Real part of the 3rd pair	Real part of the 4th pair
Perturb.	-1.4447×10^{-3}	-63.0119×10^{-3}	-512.8562×10^{-3}	-222.6897×10^{-3}
MCS	-1.4564×10^{-3}	-62.9989×10^{-3}	-512.9682×10^{-3}	-222.5765×10^{-3}

Table 7.3. Mean values of the imaginary parts of the complex eigenvalues

	Imaginary part of the 1st pair	Imaginary part of the 2nd pair	Imaginary part of the 3rd pair	Imaginary part of the 4th pair
Perturb.	8.7516	12.1715	16.7552	19.8448
MCS	8.7515	12.1716	16.7553	19.8450

Table 7.4. Variances of the real parts of the complex eigenvalues

	Real part of the 1st pair	Real part of the 2nd pair	Real part of the 3rd pair	Real part of the 4th pair
Perturb.	14.4840×10^{-6}	77.3989×10^{-6}	85.3810×10^{-6}	126.1762×10^{-6}
MCS	14.9092×10^{-6}	76.3613×10^{-6}	101.5279×10^{-6}	139.0542×10^{-6}

Table 7.5. Variances of the imaginary parts of the complex eigenvalues

	Imaginary part of the 1st pair	Imaginary part of the 2nd pair	Imaginary part of the 3rd pair	Imaginary part of the 4th pair
Perturb.	20.6140×10^{-3}	29.1216×10^{-3}	97.0271×10^{-3}	202.2144×10^{-3}
MCS	20.6556×10^{-3}	29.4715×10^{-3}	97.5162×10^{-3}	201.9559×10^{-3}

According to these results, the error in the predictions of the mean values is practically zero. The error in the predicted variance of the real part of the third unstable mode is the largest amongst all predicted variances. This error is about 15 percent and is large only because of the smallness of the values of the variances.

The distinct advantage of the 2nd-order perturbation method is that it produces the results in just one run while a significant number of simulations should be used for determining the same results via a Monte Carlo simulation. In actual applications, running Monte Carlo simulation for large models is almost impossible due to the required workload for the computation of the results. Instead, the 2nd-order perturbation method suggests an efficient way of uncertainty analysis with remarkable accuracy in the prediction of results.

Generally speaking, when the mapping function is nonlinear, the projection of a multivariate Gaussian variable to the output space is no longer Gaussian. Depending on how nonlinear a function is, the output distribution can be skewed or its kurtosis may be different from the normal distribution. In the theory of statistics, the skewness and kurtosis are the shape descriptors for real-valued random variables. Although it is possible to quantify the higher moments of a complex-valued random variable, the interpretation and relation of these moments to its real and imaginary parts are not straightforward.

Therefore, the approximation of output distributions with Gaussian probability density function does not perfectly represent the results. However, it is useful to portray the output profile via Gaussian probability density function in order to have a better understanding of the distributions of the results. In the literature, it is also common to use the normal/Gaussian probability density function for this purpose (Adhikari and Friswell, 2007). A bivariate Gaussian distribution is considered for the real and imaginary parts of each eigenvalue. This assumption helps to plot the elliptical contours of the scatter of the results. The ellipse equation is (Johnson and Kotz, 1972):

$$\left(\frac{x_{\alpha_j} - \xi_{\alpha_j}}{\sigma_{\alpha_j}}\right)^2 - 2\rho\left(\frac{x_{\alpha_j} - \xi_{\alpha_j}}{\sigma_{\alpha_j}}\right)\left(\frac{x_{\omega_j} - \xi_{\omega_j}}{\sigma_{\omega_j}}\right) + \left(\frac{x_{\omega_j} - \xi_{\omega_j}}{\sigma_{\omega_j}}\right)^2 = \text{Constant} \qquad (7.38)$$

where ξ_{α_j} and ξ_{ω_j} are the mean value of the real and imaginary parts of the jth eigenvalue. σ_{α_j} and σ_{ω_j} are the associated standard deviations. Parameter ρ is the correlation between the real and imaginary parts, i.e. $\rho = \Sigma_{\alpha_j\omega_j}/\sigma_{\alpha_j}\sigma_{\omega_j}$, which is calculated by (7.29) and (7.31).

Figure 7.2 compares the results of Monte Carlo simulation (the scatters of the points) with the elliptical contours determined by the perturbation method. As seen, the perturbation method well estimates the statistics of the scatter of the real and imaginary parts of the complex eigenvalues.
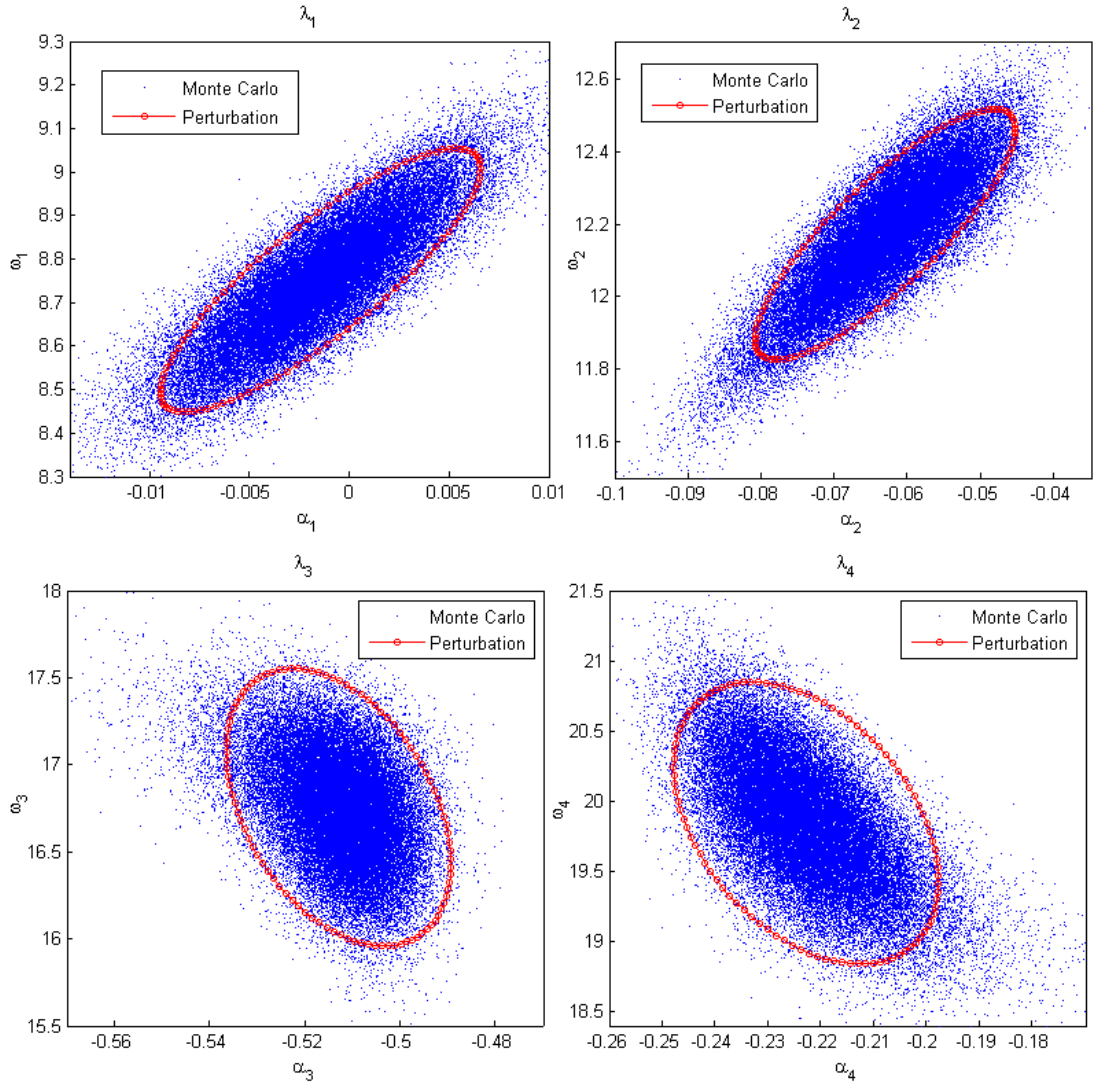
Figure 7.2. Contours of the real and imaginary part of the eigenvalues

When fairly large variations are considered for the input variables (like the example set of parameters in this study), the nonlinearity of the mapping function causes the skewness and kurtosis of the outputs to deviate from those of the normal/Gaussian distribution. To support this statement, the distributions of the real parts of the eigenvalues are plotted in Figure 7.3. The histograms show the results of the Monte Carlo simulation, while the red circle-dashed lines indicate the approximated distributions via Gaussian probability density function. Likewise, the distributions of the imaginary parts are shown in Figure 7.4.
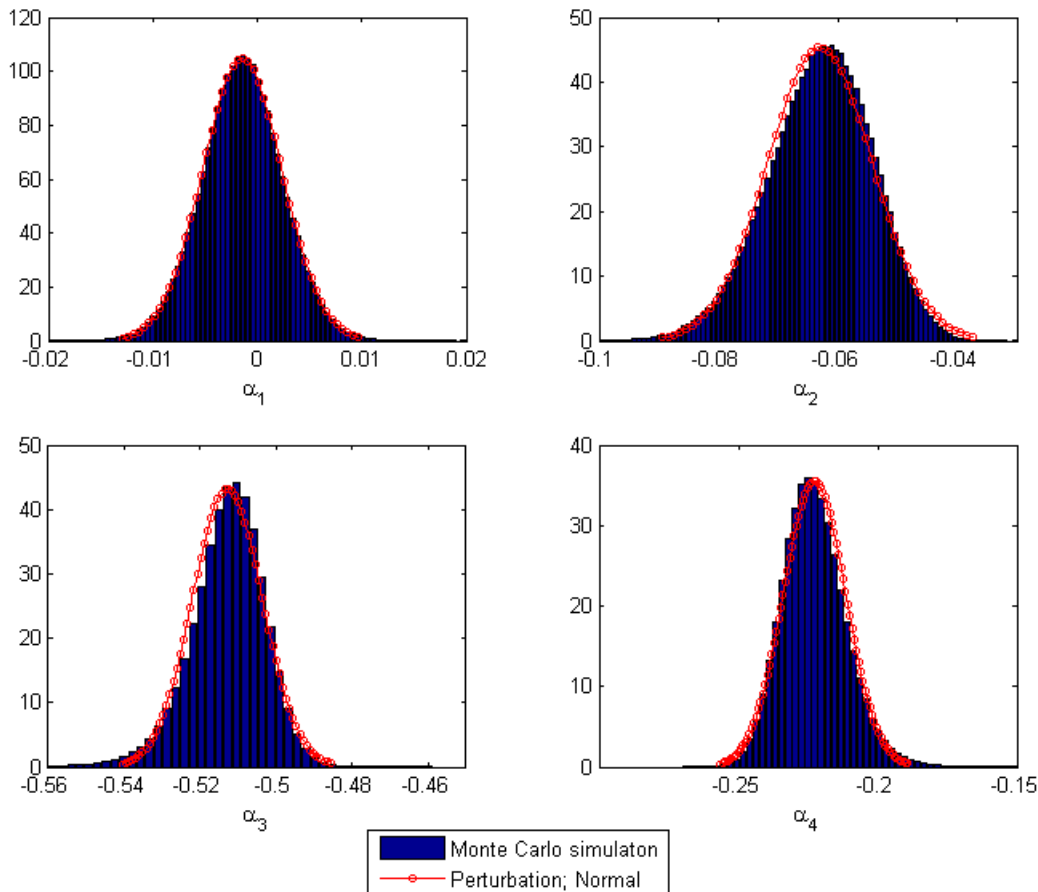
Figure 7.3. Distributions of real parts of the eigenvalues

As seen in Figure 7.3, the distributions of the real parts of the first and second eigenvalue are nearly Gaussian. However, the real parts of the third and fourth eigenvalues are negatively and positively skewed, respectively. It can also be seen in Figure 7.4 that all imaginary parts of the eigenvalues are almost Gaussian. The reason is mainly due to the fact that the imaginary parts are not much influenced by the friction coefficient.

Table 7.6 and Table 7.7 list the skewness and kurtosis of the real and imaginary parts of all eigenvalues. It is worth mentioning that the kurtosis of the normal distribution is equal to three, but in the theory of statistics, it is also common to use the excess kurtosis, which is defined as kurtosis minus three. However, in this study, the excess kurtosis is not used.
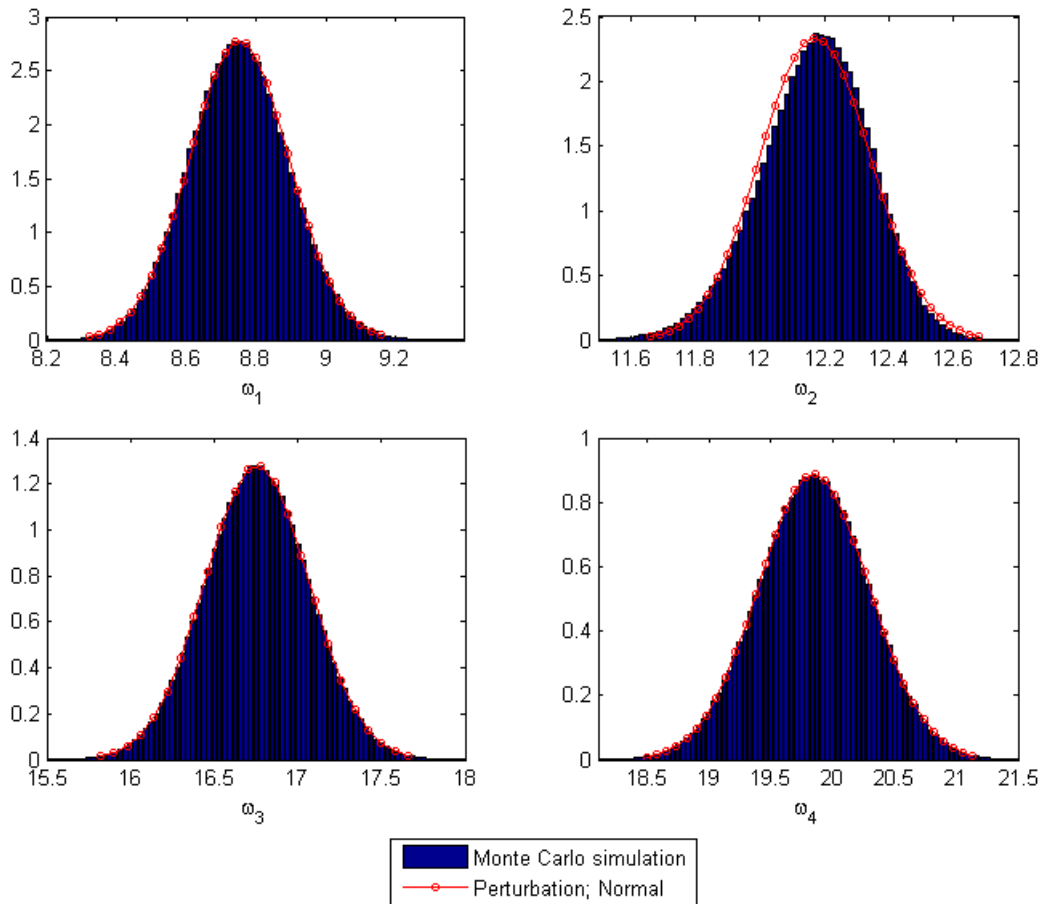
Figure 7.4. Distributions of the imaginary parts of the eigenvalues

Table 7.6. Skewness of the real and imaginary parts

Eigenvalue	The 1st pair	The 2nd pair	The 3rd pair	The 4th pair
Real parts	-0.030	-0.278	-0.965	0.706
Imaginary parts	0.049	-0.290	-0.014	-0.017

Table 7.7. Kurtosis of the real and imaginary parts

Eigenvalue	The 1st pair	The 2nd pair	The 3rd pair	The 4th pair
Real parts	3.208	3.055	8.391	6.119
Imaginary parts	3.005	3.200	3.024	2.989

The second important conclusion is that although all of the eigenvalues of the system were stable before the uncertainty analysis, the variation of the input parameters causes the first eigenvalue of the system to exceed the stable region and become positive for some samples. Once again, if it is imagined that the system represents a simplified brake model, there will no doubt that at the end of the production, well designed and manufactured brakes are still likely to experience friction-induced instability during services because of inherent uncertainty and variability in them. The probability distributions of outputs then help to evaluate how robust and reliable a design is in terms of noise and vibration. Due to this fact,

uncertainty analysis of brake systems has received intensive attention of car manufacturers recently.

7.6. Randomising the most effective parameters (μ and k_c)

As discussed earlier, the major problem in the uncertainty analysis of industrial-scale finite element models is the issue of computational workload. Although the perturbation method can sufficiently overcome this issue, reducing the number of uncertain variables can help further. If a sensitivity analysis reveals that some of the selected input variables are of low activity in a particular model, excluding them from the uncertainty analysis will be a right decision. Even if there is a high level of uncertainty about one variable, it can be excluded when its influence on a particular unstable mode is negligible. Both the levels of sensitivity and uncertainty should be considered when right uncertain input parameters are selected.

To illustrate this point, it is worthwhile to re-consider the results of the sensitivity analysis. Table 7.1 shows that the real part of the first eigenvalue which is in the vicinity of instability is highly sensitive to the friction coefficient (μ). Its sensitivity to the contact stiffness (k_c) is also considerable. However, for example, the contact damping has a minor effect on this particular mode. Although contact damping is sometimes considered one of the major sources of uncertainty, here it is not necessary to include this variable in the uncertainty analysis.

In order to get a better understanding of what is being discussed, the uncertainty analysis is re-performed in this section. However, only the variations of μ and k_c are considered this time. Since the first eigenvalue is at high risk to become unstable, only the probability distribution of its real part is shown here. Figure 7.5 displays the distribution of the real part of the first eigenvalue.

Two interesting points may be concluded based on these results. First, when the parameters of low activity are set aside from the analysis, the results are almost the same with less computational workload. The mean value and variance of the output distribution for the real part of the first eigenvalue is -1.3743×10^{-3} and 13.8163×10^{-6} in Figure 7.5, while they were -1.4564×10^{-3} and 14.9092×10^{-6} in Figure 7.3. Secondly, the number of samples in the conventional Monte Carlo simulation is 10,000 this time. Consequently, the output histogram is not as smooth as the one presented in the first example. In fact, this is another drawback of the conventional Monte Carlo simulation. Although the convergence in the values of the mean and variance may occur when enough number of samples is collected, a smoother distribution will be achieved when the number of samples is significantly

increased. Incidentally, even collecting 10,000 samples is not feasible in many practical applications.
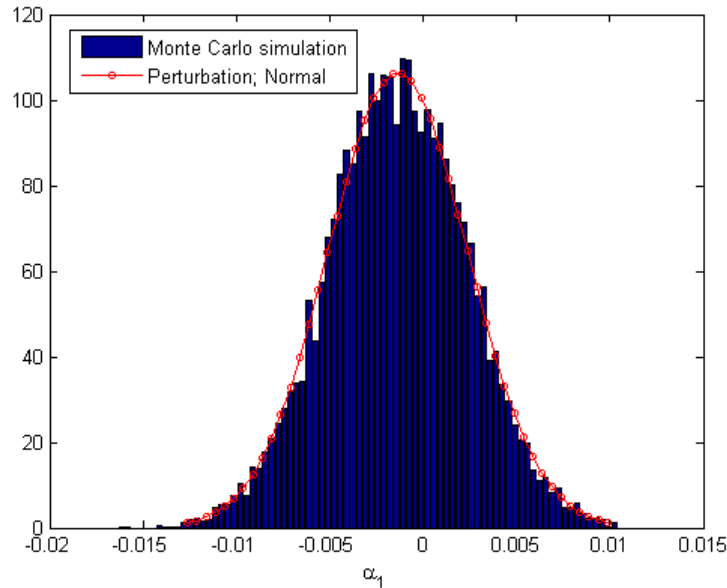
Figure 7.5. Distribution of the real part of the 1st eigenvalue

7.7. Reliability analysis

In general, a reliability analysis is performed for evaluating the robustness of a design. In fact, the reliability analysis quantifies the failure probability of the design. The term "failure" is widely used in engineering for various undesired states of a system. In this example, failure means that one of the system eigenvalues becomes unstable, i.e. the sign of the associated real part turns positive. For brake analysts, it is very important to know what percentage of a brake design will 'fail' either for production variability or due to usage and aging effects. Then, the design modifications which are usually done to reduce brake noises can be carried out for reducing the likelihood of unstable vibration. The failure probability is obtained as:

$$P_{\mathcal{F}} = P\big[\{\alpha_j : \alpha_j > 0\}\big]$$

(7.39)

Among the four modes of the system shown in Figure 7.1, only the first one exceeds the stable region under the influence of the uncertainties. Figure 7.6 shows the distribution of the real part of the first eigenvalue under the influence of uncertainty of all selected variables.
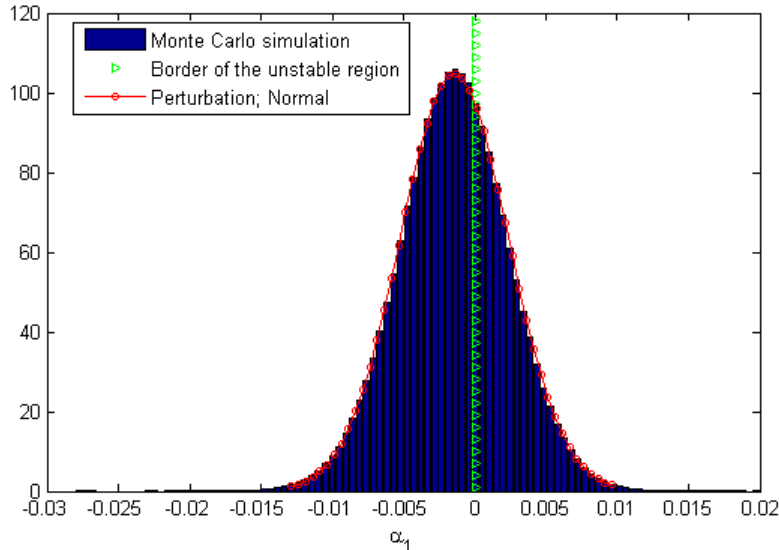
Figure 7.6. Reliability analysis

In Figure 7.6, the green triangles highlight the border of the unstable region. By the use of the results of Monte Carlo simulation, the percentage of failure for the first mode is 35.7. If the output distribution is approximated by Gaussian probability density function, the predicted probability of failure is calculated by

$$P_{\mathcal{F}} = 1 - \Psi \left[\frac{\alpha_j - \xi_{\alpha_j}}{\sigma_{\alpha_j}} \right] \tag{7.40}$$

where $\Psi(z) = \frac{1}{\sqrt{2\pi}} \int_{-\infty}^{z} \exp\left(\frac{-u^2}{2}\right) du$ and $\alpha_j = 0$. Accordingly, the approximated failure probability of the first mode is 35.2 percent. This percentage is calculated by the estimated mean value ξ_{α_j} and standard deviation σ_{α_j} via the perturbation method.

Moreover, one may say that the failure probability is quite large for the system under this study. In fact, the design point is deliberately set slightly below the critical friction coefficient in order to demonstrate how bad a design can be if the variability and uncertainty of the inputs are not considered carefully.

7.8.   Conclusions

The statistics of the complex eigenvalues are studied in this chapter with the application to friction-induced vibration problems. In order to deal with non-proportional damping and the asymmetry of the stiffness matrix, the state-space equations are used. The second-order perturbation method is then extended for incorporating the variability and uncertainty of input variables. A few expressions for calculating the mean value, variance and pseudo-

variance of the complex eigenvalues are derived. The mean value of the eigenvalues is, in fact, a complex-valued number which provides the mean values of the real parts and also the mean value of the imaginary parts. The variance and pseudo-variance of the complex eigenvalues include information of the variance of the real parts, the variance of imaginary parts and the covariance of the real and imaginary parts. The correlation between the real and imaginary parts of the eigenvalues can also be obtained by these statistical measures.

The most important outcome of this study is that the distributions of the real and imaginary parts of the complex eigenvalues can efficiently be approximated without decomposing them into two real-valued numbers (real and imaginary parts). In this way, the results are produced in just one-run, while Monte Carlo simulation requires a large number of samples to find the statistical measures of the outputs.

This study also allows the probability of unstable vibration to be predicted and then provides a very useful tool for design.

8. Surrogate Modelling

The idea behind surrogate modelling is fully explained in this chapter. In order to illustrate how a surrogate model is constructed, a few simple examples are given in this chapter. There are two major steps for constructing a surrogate model: making a sampling plan and training the replacement model. Several careful considerations must be taken for these two steps. These considerations will be fully discussed here.

Note that making a sampling plan is also termed as "Design of Experiment". This term is well-known in different disciplines of science and engineering and is abbreviated to "DOE". However, since in this study "Design and Analysis of Computer Experiment" is abbreviated to "DACE", it is preferred to use the term "sampling plan" in place of "DOE" only to avoid confusion. However, the concept of these two terms is the same.

8.1.   The idea behind surrogate modelling

Most engineering designs nowadays are based on numerical simulations. Such analyses essentially involve a great deal of computational workload which imposes a limit on the number of analyses produced for decision making. On the other hand, analysts must gain an in-depth understanding of the design space in order to come up with an optimum design. To meet this objective, the results of many numerical simulations should be collected, which is not necessarily feasible. For example, in the case of brake squeal, running CEA for the brake shown in chapter 3 takes 12 to 36 hours depending on the computational facilities. Then, imagine that it is aimed to investigate the effects of variability and uncertainty of several parameters on squeal instability. The most straightforward way is to run Monte Carlo simulation. Obviously, a few months must be spent to gain a desirable insight into the problem in this way. Spending such an amount of time would contravene the tight deadlines of industry and would cost car manufacturers significantly.

Alternatively, the use of surrogate (or meta) models can overcome the issue of computational workload. Surrogate modelling can bridge the gaps between the results of a limited number of analyses and capture the major properties of an expensive experiment or numerical simulation. The most common example of surrogate modelling is the use of the least squares fit for predicting the results of an experiment at the points where there is no information. A few tests are done to collect some data points over a desirable range of inputs and then the least squares method provides the best fit to the points. The fitted curve can estimate the outputs with a mathematical function bringing about a significant increase in the speed of producing the results with enough accuracy.

Such an approach can likewise be applied to expensive simulation codes. In fact, the Design and Analysis of Computer Experiments (DACE) has been established on the ground of this notion (Sacks et al., 1989). Designing a computer experiment means approximating the outputs of an expensive code for any desirable input. For this purpose, a sampling plan is firstly made over the design space. Then, these samples are used for estimating the parameters included in the realisation of a regression model and a random process. The replacement model is then able to reproduce the outputs of the expensive code with sufficient accuracy. As it is always beneficial to include the smallest possible number of samples, the estimation of the model parameters is done in an iterative process. The number of observations is increased until the expected accuracy is achieved. Thereafter, the expensive numerical model is replaced with the cheap-to-evaluate surrogate model.

The major steps of constructing a surrogate model, i.e. making a uniform sampling plan and training the predictor, will be explained in the next sections.

8.2.   Sampling plan

In the introduction of surrogate modelling, the importance of sampling plans is emphasized for constructing an accurate replacement model. The reason is mainly due to two aspects of this approach. First of all, the prediction of a desired point which is not a member of the sampling plan is made via interpolation or extrapolation of the sampled points. Therefore, if a desirable point is located far from the sampled points, the accuracy of the approximation will be somewhat lost. This point clarifies why there is an essential need for making a uniform sampling plan over the design space. If some gaps/holes exist in the distributions of the samples over the space, the accuracy of the replacement model will be insufficient.

The second aspect is about the numerical algorithm which creates sampling points. Although a higher number of samples generally lead to a more accurate surrogate model, it is always preferred to keep the number of samples as small as possible. Undoubtedly, the central aim of constructing surrogate models is to reduce the computational cost and time. Therefore, if the number of required samples for covering the design space is so large that making the required observations individually takes a lot of time, there will no longer an advantage to use the replacement models.

In the literature, there are several ways for creating a sampling plan (designing an experiment). In order to understand how these approaches works, the most straightforward technique of sampling is explained here. This method is called "full factorial grid" in the literature.

Imagine that the number of variables in the design domain is k. In other words, the design space is $k-$dimensional. Imagine along each dimension a limited number of points are spread to cover the variation of each parameter. What full factorial grid suggests is for every possible combination of the input variables, a sampling point must be generated in the design space. Therefore, if the number of points along ith dimension is m_i, the total number of required samples will be $n = m_1 \times m_2 \times \cdots \times m_k$. Figure 8.1 shows an example of a full factorial grid in a 3D space. As seen, the number of points along each dimension is 3, 4 and 5, respectively. Therefore, 60 samples are used to cover the design space uniformly.

There are a few points which need particular attention here. Firstly, if the design space consists of several input variables, the number of required samples grows exponentially by the use of full factorial grid. This situation will be exacerbated if a wide range of variations is going to be covered and the output variables behave nonlinearly with respect to the inputs. In such situations, along each dimension several sampling points are required since a small number of points may not represent the outputs behaviour well. As a result, the required number of samples in a multi-dimensional domain (for examples, seven variables with five points along each dimension) will be so big ($5^7 = 78125$ in this example) that it would be

impractical to use this technique of sampling in practice. This fact is known as "curse of dimensionality" in the literature (Forrester et al. 2008).
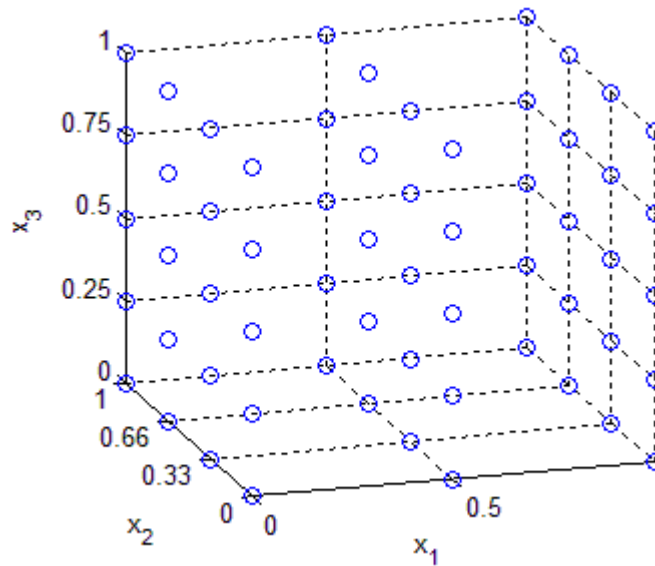
Figure 8.1. An example of full factorial grid sampling plan (Forrester et al. 2008)

The second point is in regard to scaling issues. In the literature, it is always recommended to translate the input variables onto a unit cube (or unit hypercube $[0,1]^k$) in order to avoid the scaling issue. Imagine for the brake under study the variations of disc's Young modulus and the friction coefficient at pads-to-disc interface are needed to be considered. The order of the disc's Young modulus is Giga and the order of friction coefficient is decimals. In order to avoid creating a biased distribution under the influence of the magnitudes of a variable, it is recommended to normalise the variables first and then make a uniform sampling plan over the space. Obviously, the sampling plan can be translated back to the original dimensions at the end of an analysis.

The sampling technique which is widely used in the literature, in particular for DACE, is "Latin hypercube sampling". This technique is usually abbreviated to "LHS". The strong point about LHS is that it can resolve the issue of dimensionality by extending the idea behind "Latin square" to multi-dimensional cases. Figure 8.2 shows an example of Latin square for a 2D space. Imagine for collecting the required observations of a 2D space, only **1**'s of the displayed Latin squared are sampled. Therefore, instead of collecting 16 observations, only four points are sampled. This example, in fact, portrays the difference between the full factorial grid and LHS approaches. The main feature of a Latin square is that no coincidence among the samples is experienced if any of the **1**'s is moved vertically or horizontally along the dimension of the space. This feature can be extended to multi-dimensional cases in order to create a uniform sampling plan with the least possible number of samples.

3	2	4	1
1	4	2	3
4	3	1	2
2	1	3	4

Figure 8.2. An example of Latin square (Forrester et al. 2008)

Now it is aimed to make a sampling plan over the design space shown in Figure 8.1 via the LHS technique. Figure 8.3 shows an example of LHS with 10 sampling points over the space. Each sample is in fact a vector containing three random numbers/values of the design variables in the unit cube. As mentioned earlier, the unit cube can be translated later to the actual ranges of the design parameters. Although the number of samples has decreased significantly from Figure 8.1 to Figure 8.3, the spread of samples is not sufficiently uniform since the samples are mostly located in the centre of the domain.
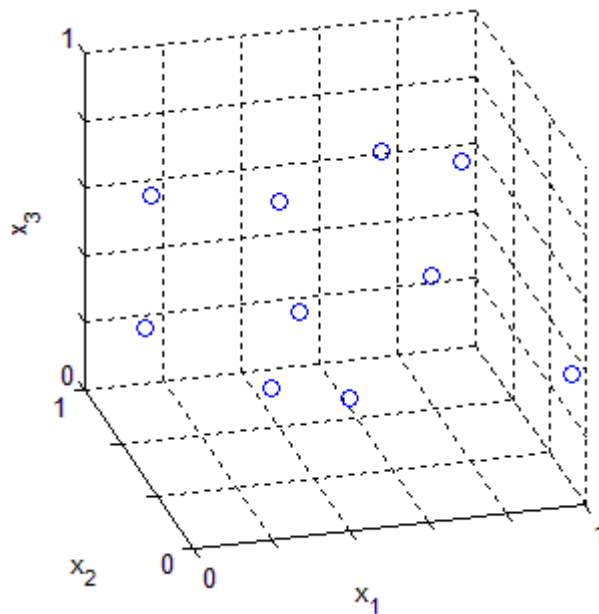
Figure 8.3. An example of LHS for a 3D design space (Forrester et al. 2008)

In order to improve the uniformity of the samples, the "maximin" metric may be employed in the numerical algorithm of LHS. What maximin metric does is to measure the distances among all possible pairs of samples and maximises the distances among the sampling points while the number of points remains as small as possible. The implementation of this algorithm is fully explained in (Forrester et al. 2008). The authors also provided a MATLAB code for making a uniform LHS, which meets maximin metric conditions. The samples which are used for the purpose of this study are generated by this code and termed as "uniform LHS". As a result, the uniformity of the plans are somewhat guaranteed. Figure 8.4 shows the samples spread on the 3D design space with the uniform LHS technique.
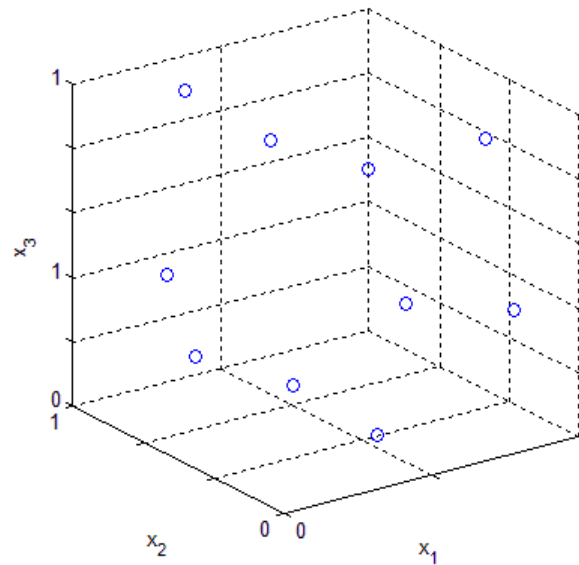
Figure 8.4. An example of uniform LHS for a 3D design space (Forrester et al. 2008)

As seen, the distances among the points are increased and the design space is better covered in comparison with Figure 8.3.

8.3.   Training a predictor

Recently the idea of surrogate modelling has attracted the attention of researchers on the subject of structural dynamics (DiazDelaO and Adhikari, 2010; Kundu et al., 2014). In the literature, a number of methods have been established for constructing a surrogate model, i.e. a mathematical predictor, such as the conventional response surface method (Myers et al. 2009), neural networks (Haykin, 1999), radial basis functions (RBF) of which Kriging is the most well-known one (Jones et al., 1998; Lophaven et al., 2002; Forrester et al., 2008).

Among these methods, Kriging suits multi-dimensional design spaces whose outputs are smooth functions of input variables. As in the current study it is aimed to propose a method to cover variability and uncertainty of several brake design parameters, Kriging is used as the mathematical predictor of squeal instability. Moreover, the results of this study show that squeal instability can be estimated by means of a smooth function. Before applying the Kriging method to the brake squeal problem, the central features of this approach are reviewed here.

Assume that $y = f(\mathbf{x})$ represents the output of a computer simulation or a FE model to a vector of normalized inputs (Figure 8.5). In the case of squeal instability, the response can be either the real parts of the unstable eigenvalues or their squeal indices (damping ratios) corresponding to a set of design parameters. For a k-variable design space, each sample is a vector containing a random value of each design parameter: $\mathbf{x}^{(i)} = (x_1^{(i)}, \cdots, x_k^{(i)})$ and $y^{(i)}$

represents the ith observation. Imagine it is aimed to replace f with a cheap-to-evaluate mathematical model being able to reproduce the responses of the code or FE model.

In order to construct the replacement model, a regression model $F(\boldsymbol{\beta}, \mathbf{x})$ and a random process $\epsilon(\mathbf{x}^{(i)})$ are used to define the realization $\hat{y}$ of the observed data $\mathbf{x}^{(i)}$, i.e.

$$\hat{y}(\mathbf{x}^{(i)}) = F(\boldsymbol{\beta}, \mathbf{x}) + \epsilon(\mathbf{x}^{(i)}) \tag{8.1}$$

where $\boldsymbol{\beta}$ is the vector of the unknown coefficients of the regression model. A linear combination of polynomials of order 0, 1 or 2 is typically considered for the regression model. The coefficients of these polynomials are unknown and must be estimated by the use of the sampled data.
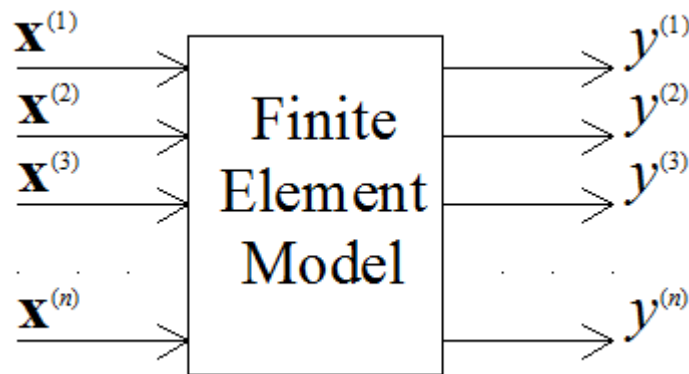
Figure 8.5. Observations needed for training the surrogate model

What plays a vital role in a Kriging predictor is constructing the random process. In the literature, the random process for computer simulations is assumed to be Gaussian. A Gaussian process is the generalised form of a Gaussian probability distribution. Whilst a Gaussian distribution describes the probability of a random variable, a Gaussian process defines the random nature of stochastic functions. At each point in a Gaussian process, there is a normal probability distribution whose mean value is the predicted value of the output and standard deviation is the uncertainty about the prediction. In other words, in this approach the error is normally distributed about the predicted value.

As the mean value is not constant and may change within time, displacement, etc., the probability distribution of the output should not necessarily be Gaussian. Incidentally, the Gaussian process of the brake simulation is not a function of time and only depends on the location of the samples and the distances among them. With this introduction, now it is attempted to derive the equations for the predicted value (the mean value of the Gaussian process) and the error in the predictions.

In order to define a Gaussian process, two pieces of information are essential: the mean value and covariance matrix. The covariance matrix may be defined as:

$$\text{cov}\big[\,\epsilon\big(\mathbf{x}^{(i)}\big),\epsilon(\mathbf{x}^{(j)})\big] = \sigma^2 R\big[\,\epsilon\big(\mathbf{x}^{(i)}\big),\epsilon(\mathbf{x}^{(j)})\big] \tag{8.2}$$

where σ is the standard deviation of the random process and $R\big[\,\epsilon\big(\mathbf{x}^{(i)}\big),\epsilon(\mathbf{x}^{(j)})\big]$ represents the correlation function between the ith and jth samples. A number of correlation functions can be used in place of R, yet Kriging is going to be used in this study. The Kriging correlation function may be expressed as

$$R\big[\,\epsilon\big(\mathbf{x}^{(i)}\big),\epsilon(\mathbf{x}^{(j)})\big] = \exp\left(-\sum_{h=1}^{k}\theta_h\left|x_h^{(i)}-x_h^{(j)}\right|^{p_h}\right) \tag{8.3}$$

where $\left|x_h^{(i)}-x_h^{(j)}\right|$ represents the distance among samples, θ_h shows the activity of a design parameter, and p_h determines the smoothness of the correlation function. It is worth to review these three features of the Kriging correlation function to understand how a mathematical predictor is fitted to a set of samples. Bear in mind that the prediction errors are also a function of the locations of samples and at the location of samples the prediction error is chosen be zero.

First of all, it is important to consider that the correlation function is totally dependent on the absolute distance between the samples. As a result, the correlation will reach to it maximum, i.e. nearly 1, for two samples which are located very close to each other. On the other hand, the correlation will tend to zero if the points are fairly far from each other. The reason behind emphasising the uniformity of the sampling plan can be realised by this term. It will be seen that this correlation function has a vital role in making predictions of untried points. If in a part of the design space, the samples are not uniformly spread, there will be a weak correlation between an untried point and the observed data, and therefore the corresponding predication is not sufficiently accurate.

Parameter θ_h indicates how active a variable is in the computer simulation. Large values of θ_h can be interpreted as high-level of activity while small values of θ_h indicate that variable h can be ignored in the surrogate model. Figure 8.6 shows the influence of θ_h on the correlation function. When θ_h is pretty small (for example, 0.1), even if the samples are located far from each other, the correlation values does not drop quickly. In other words, the output is not very sensitive to the variation of this parameter. One the other hand, a high value of θ_h leads to a rapid decrease in the correlation and this means that more samples for this variable are required to portray its effect sufficiently.

The smoothness of the correlation function is determined by parameter p_h. Typically, the value of this parameter varies from 1 to 2. When p_h approaches 1 and meanwhile the absolute distances between the points are increased, a rapid drop in the value of correlation is experienced (Figure 8.7). However, in the literature, p_h is mostly fixed at 2 in order to have a

smooth drop in the correlation function (Forrester et al. 2008). Likewise, p_h is kept constant at 2 in this study.
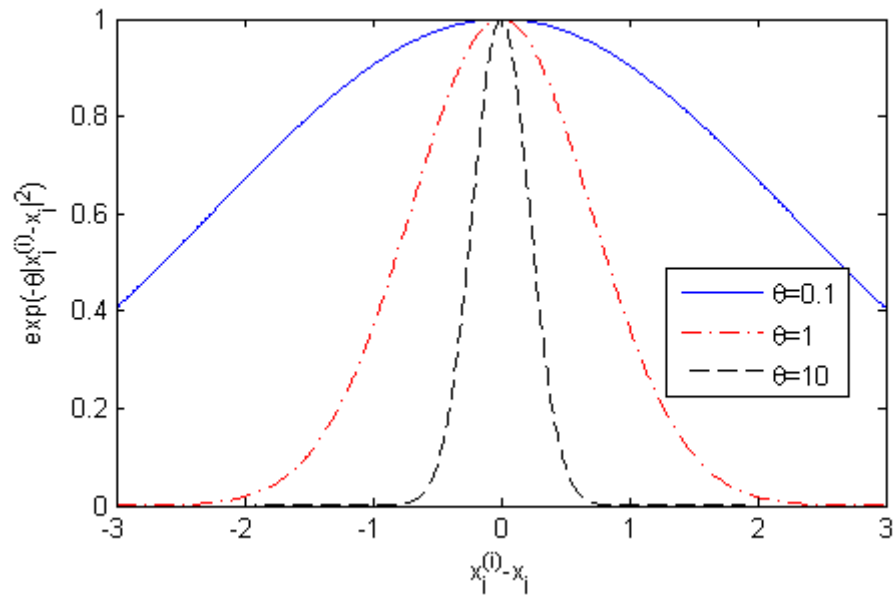
Figure 8.6. Activity of a design parameter (Forrester et al. 2008)
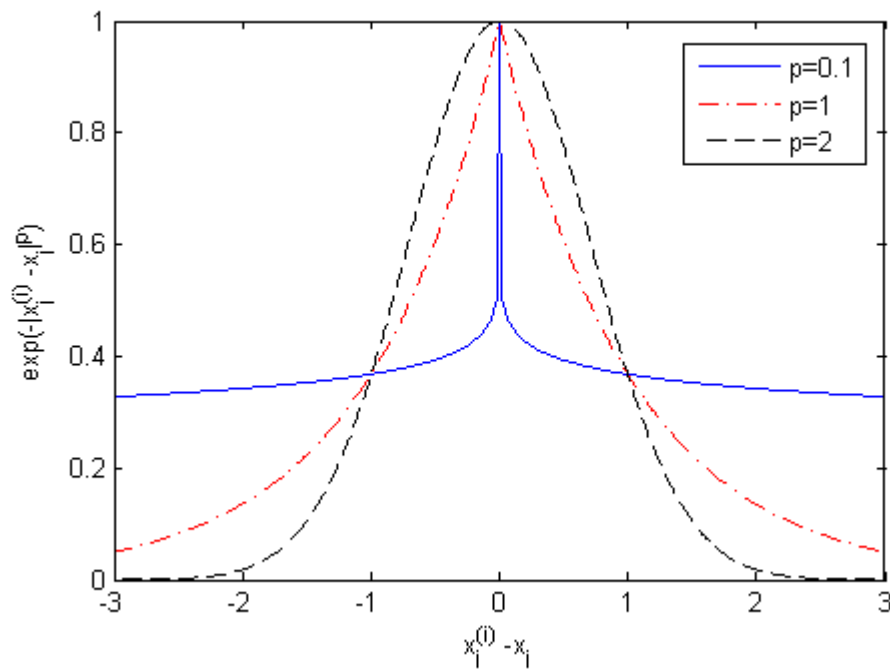
Figure 8.7. Smoothness of the correlation function (Forrester et al. 2008)

Now imagine a number of samples are collected from a design space. It is essential to know how the Kriging correlation function helps make prediction of the output of a desired point in the design space. For this purpose, the "Maximum Likelihood Estimation" (MLE) method is briefly reviewed here.

In the theory of statistics, this method is applied for estimating the mean value and variance of a stochastic process. Imagine for estimating the mean value and variance of squeal instability, the results of millions of simulations are required. However, it is only affordable to collect the results of a few hundreds of simulations due to their computational workload. If it is assumed that the whole dataset, i.e. the results of computer simulations, are generated in a Gaussian process, the mean value and variance of the whole dataset can be estimated by the use of MLE. In other words, this method supposes that the sampled points and their corresponding observations are representative of the whole dataset. According to Figure 8.5, the likelihood of $\mathbf{y} = \{y^{(1)}, y^{(2)}, \dots, y^{(n)}\}^\mathrm{T}$ can be defined by means of the following Probability Density Function (PDF):

$$L\left(y^{(1)}, y^{(2)}, \dots, y^{(n)} \big| \mu, \sigma\right) = \frac{1}{(2\pi\sigma^2)^{n/2}|\mathbf{R}|^2} \exp\left(-\frac{(\mathbf{y} - \mathbf{1}\mu)^\mathrm{T}\mathbf{R}^{-1}(\mathbf{y} - \mathbf{1}\mu)}{2\sigma^2}\right) \tag{8.4}$$

where $\mathbf{R}$ is the n-by-n correlation matrix of the observed data and is formed by means of equation (8.3). μ and σ are the mean value and standard deviation of the Gaussian process, respectively. $\mathbf{1}$ indicates an n-by-1 vector of ones. The values of μ and σ which maximize the above PDF is referred to as the most likely values: $\hat{\mu}$ and $\hat{\sigma}$. In fact, that is the reason why this method is called "maximum likelihood estimation".

The derivatives of equation (8.4) are set to zero to find the most likely values:

$$\hat{\mu} = \frac{\mathbf{1}^\mathrm{T}\mathbf{R}^{-1}\mathbf{y}}{\mathbf{1}^\mathrm{T}\mathbf{R}^{-1}\mathbf{1}}, \hat{\sigma} = \frac{(\mathbf{y} - \mathbf{1}\mu)^\mathrm{T}\mathbf{R}^{-1}(\mathbf{y} - \mathbf{1}\mu)}{n}. \tag{8.5}$$

Substituting the estimated values into equation (8.4) forms *the concentrated likelihood function* (Jones et al., 1998). In the literature, it is common to use the logarithmic form of this function, i.e.

$$\ln(L) \approx -\frac{n}{2}\ln(\hat{\sigma}^2) - \frac{1}{2}ln|\mathbf{R}|. \tag{8.6}$$

Equation (8.6) is dependent on the two sets of unknown parameters: $\boldsymbol{\theta}$ and $\mathbf{p}$ which need to be identified in an optimization process. In (Forrester et al. 2008), a global search method such as Genetic Algorithm (GA) is chosen for finding the optimum values. Due to the fact that the evaluation of this function is not expensive, even GA which is actually an expensive optimisation method can be used to determine the unknown parameters.

Now the estimated values $(\hat{\mu}, \hat{\sigma})$ and the parameters of the correlation function $(\boldsymbol{\theta}, \mathbf{p})$ are employed in making predictions of untried points. Jones et al. (1998) stated that the Kriging correlation function is so powerful that only a constant term $(\hat{\mu})$ can be used in place of the regression model. Accordingly, the prediction of an untried point $\mathbf{x}^*$ is made by the use of $\hat{\mu}$

and a term which is calculated by the correlation between the new point and the observed data. Jones et al. (1998) and Forrester et al. (2008) derived an equation for the predicted value of an untried point:

$$\hat{y}(\mathbf{x}^*) = \hat{\mu} + \mathbf{r}^T \mathbf{R}^{-1}(\mathbf{y} - \mathbf{1}\hat{\mu})$$ (8.7)

where $\mathbf{r}$ is the correlation between the untried point $\mathbf{x}^*$ and the sampled data $\mathbf{x}^{(i)}$:

$$r_i(\mathbf{x}^*) = R\big[\,\epsilon(\mathbf{x}^*), \epsilon(\mathbf{x}^{(i)})\big] \ \text{ where } i = 1,2,\dots,n.$$ (8.8)

This term relates $\hat{y}$ to the absolute distance between the untried point and the sampled data, so the uncertainty about the predicted value must be minor if the new point is sufficiently close to one of the sampled points. On the other hand, there is low confidence about the predicted value of a far-located point. The uncertainty about the predicted values is measured by the "Mean Squared Error" (MSE) which is given in (Jones et al. 1998) and again is dependent on $\mathbf{r}$:

$$\hat{s}^2(\mathbf{x}^*) = \sigma^2 \left[1 - \mathbf{r}^T \mathbf{R}^{-1}\mathbf{r} + \frac{(1 - \mathbf{1}^T \mathbf{R}^{-1}\mathbf{r})^2}{\mathbf{1}^T \mathbf{R}^{-1}\mathbf{r}} \right]$$ (8.9)

It is worth mentioning that the third term in the bracket is often ignored because it is a higher-order small term. The square root of equation (8.9), known as RMSE, is usually used as an index for measuring the accuracy of a surrogate model over the design space. In an iterative process, the number of samples should be increased until RMSE meets a desired criterion for the accuracy of the replacement model. Obviously, when the dimensions of the design space exceed three, it is impossible to visualize the results in one chart. In such cases, it is necessary to employ a validation method which is able to portray the accuracy of the surrogate model. In addition to RMSE, there are some other methods for this purpose. Those methods will be reviewed in the next chapter when the brake surrogate models are going to be constructed.

8.4.   Test functions

In order to illustrate how a surrogate model is constructed, two mathematical test functions are replaced with surrogate predictors in this section. These functions are commonly used in the literature for demonstrating the efficacy of response surface methods. The term "response surface" is often used in place of "mathematical predictor" or "surrogate model" even though

the correlation function is Kriging and the conventional response surface method has not been used. Therefore, this term here means the constructed surrogate model.

The first test function is called Branin:

$$f(x) = \left(x_2 - \frac{5.1}{4\pi^2}x_2 + \frac{5}{\pi}x_1 - 6\right)^2 + 10\left(\left(1 - \frac{1}{8\pi}\right)\cos x_1 + 1\right) + 5x_1 \tag{8.10}$$

where $x_1 = [-5, 10]$ and $x_2 = [0, 15]$. A sampling plan with 20 points is generated by the MATLAB code given in (Forrester et al. 2008):`'bestlh.m'`. For constructing the predictor and calculating RMSE, this reference also provided the MATLAB codes: `ModelInfo.Option='Pred'`, `ModelInfo.Option='RMSE'`. The results are shown in Figure 8.8 and Figure 8.9.
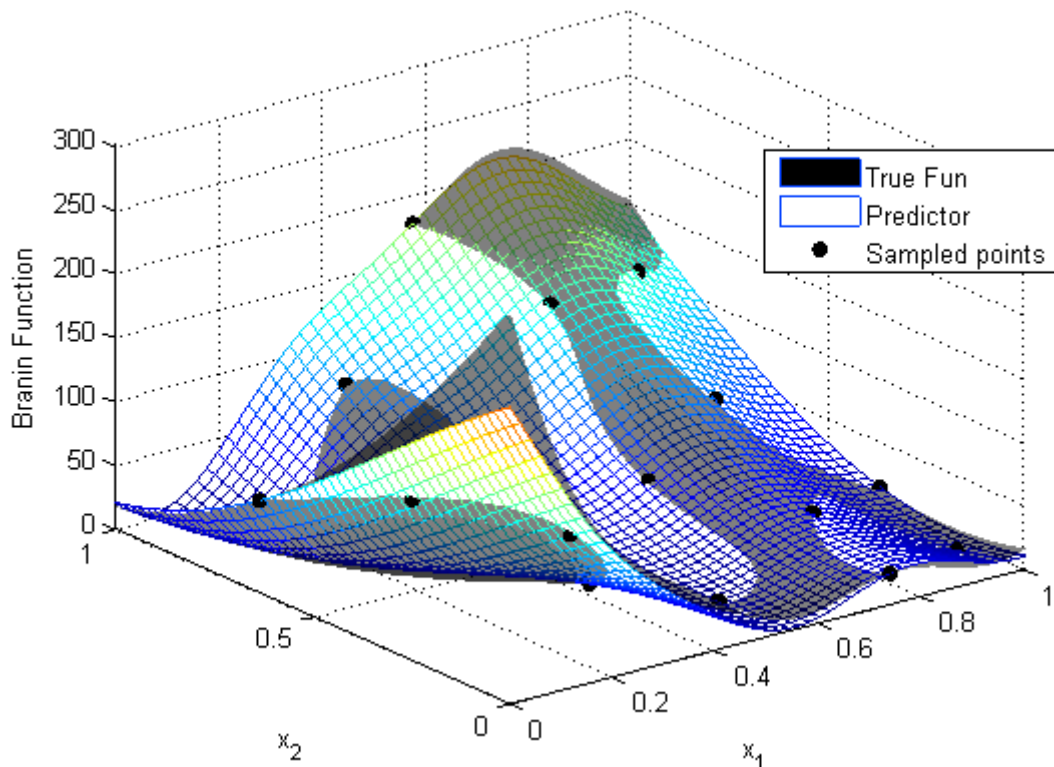
Figure 8.8. Response surface and true Branin function

The black dots in Figure 8.8 show the sampled points. The mesh shows the predictor/response surface and the plain black surface shows the true function. As seen, although the Branin function behaves fairly nonlinear, Kriging method could provide a sufficiently accurate response surface with only 20 samples points. Imagine if the true function were very expensive to evaluate, collecting the results of 20 points for getting an idea about the entire design space would be a very cost-effective method. Bear in mind that

the design space is normalised to the unit cube and therefore x and y axes show the normalised ranges, not the actual ones.

For evaluating the accuracy of the predictor quantitatively, RMSE of the response surface is shown in Figure 8.9. As seen the error of predictions in the centre of the design space is less than 1 percent. There is no doubt that it could be even less if the number of samples were increased. The errors around the corners are fairly large. The reason is due to the spread of samples over the design space. As mentioned earlier, the uniform LHS algorithm measures the distances among the samples and find a plan which maximises the distances while keeping the number of samples as least as possible. Therefore, in order to cover the corner with the uniform LHS, the number of points should be significantly increased. However, it is more efficient to keep the sampling plan as it is and include the corners of the design space deliberately in the plan. This issue will be fully discussed in the next chapter.
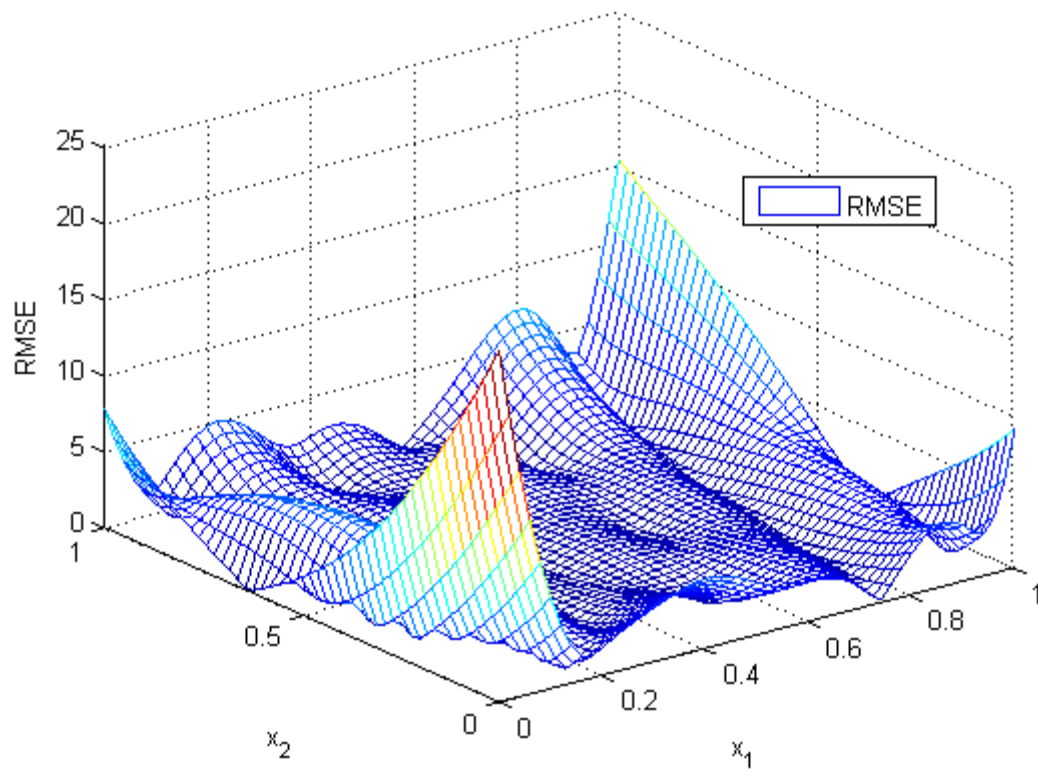
Figure 8.9. RMSE of the replacement model

The second test function is known as Camelback:

$$f(x) = \left(4 - 2.1\, x_1^2 + \frac{x_1^4}{3}\right)x_1^2 + x_1 x_2 + (-4 + 4x_2^2)x_2^2 \tag{8.11}$$

where $x_1 = [-3,3]$ and $x_2 = [-2,2]$. Although in general there is not a rule for determining the number of required samples and it can be different from one case to another, some researchers say ten times the dimensions of the design spaces is a good starting point. As a result, first 20 samples are spread over the design space to see how accurate the constructed predictor will be. Figure 8.10 and Figure 8.11 shows the results of the first attempt with 20 sampled points. Similar to Branin function, the black dots show the samples, the mesh displays the response surface and the black surface shows the true Camelback function.
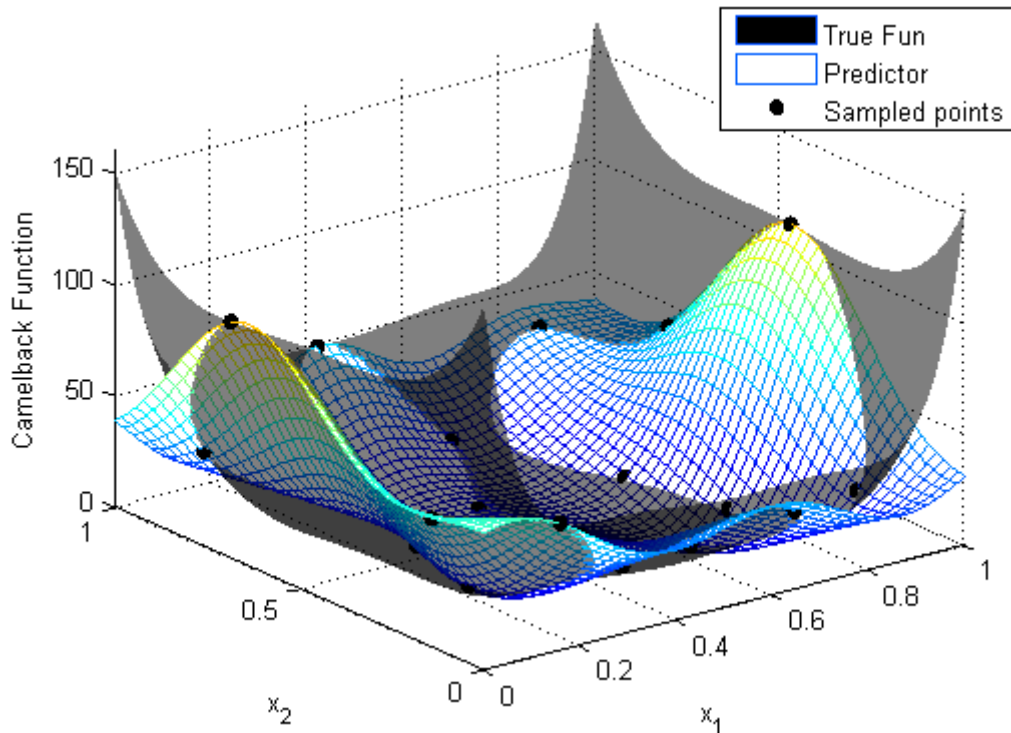
Figure 8.10. Response surface and true Camelback function with 20 sampled points

As seen, in this case the predictor is not working sufficiently accurate due to the particular shape of this function which is completely flat in the middle of the design space. The RMSE of predictions (Figure 8.11) also shows that the error of predictions is quite large not only around the corners but also in the center part of the design space.
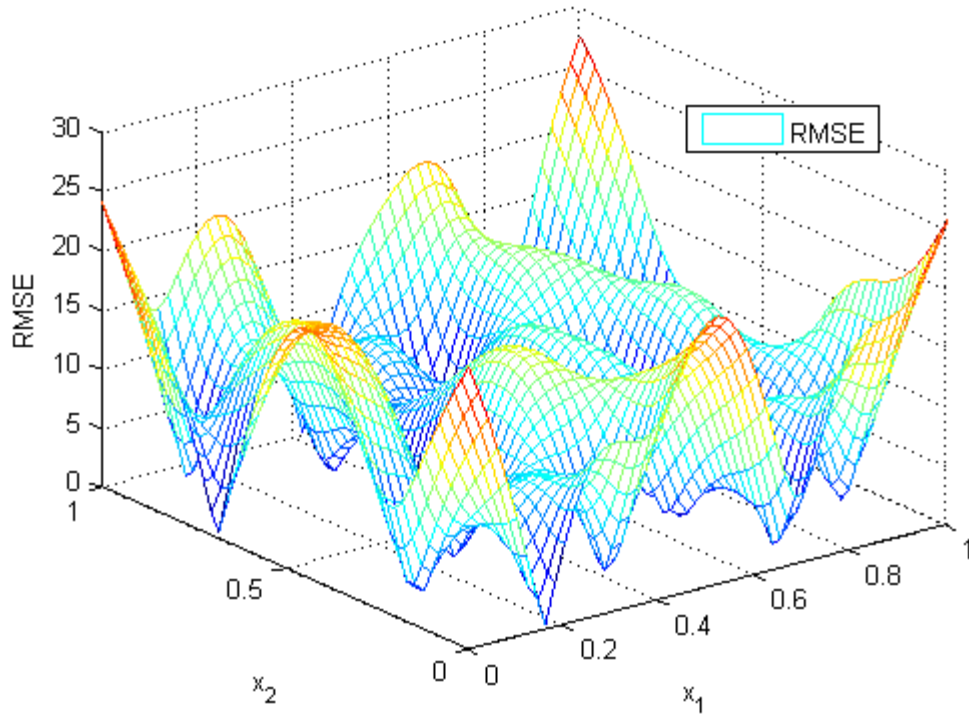
Figure 8.11. RMSE of Camelback predictor with 20 sampled points

Therefore, another attempt is made, but with 50 sampling points this time. The results are shown in Figure 8.11and Figure 8.12. As seen, the true function and predictor are perfectly matched this time. Moreover, looking at the RMSE of predictions reveals that the error is practically zero over the entire design space.
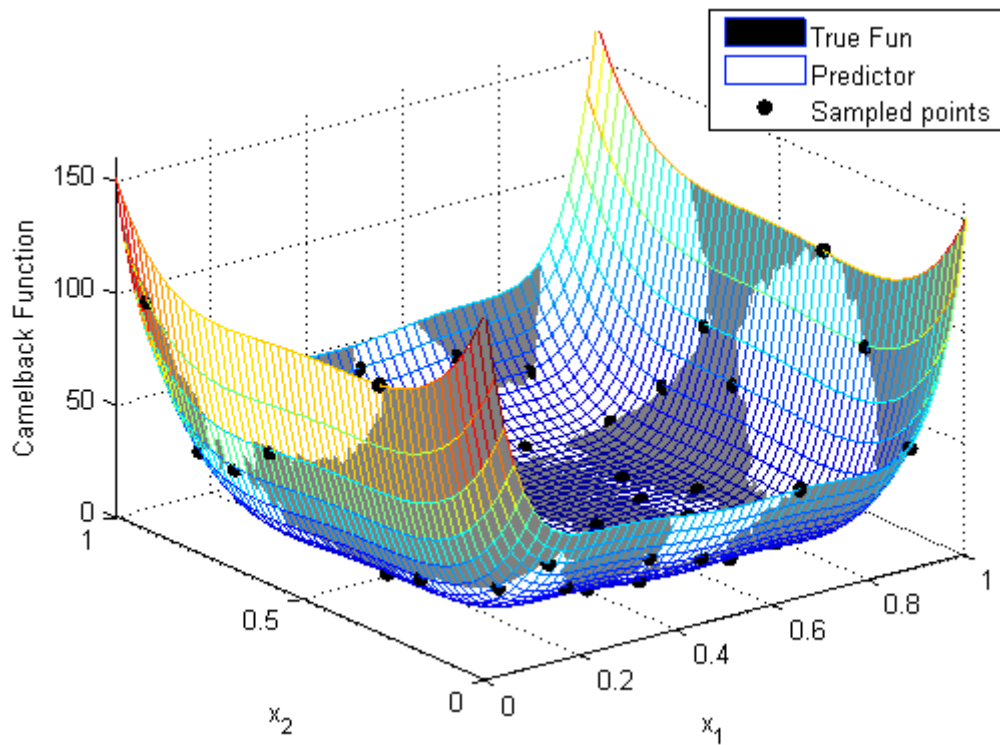
Figure 8.12. Response surface and true Camelback function with 50 sampled points

149
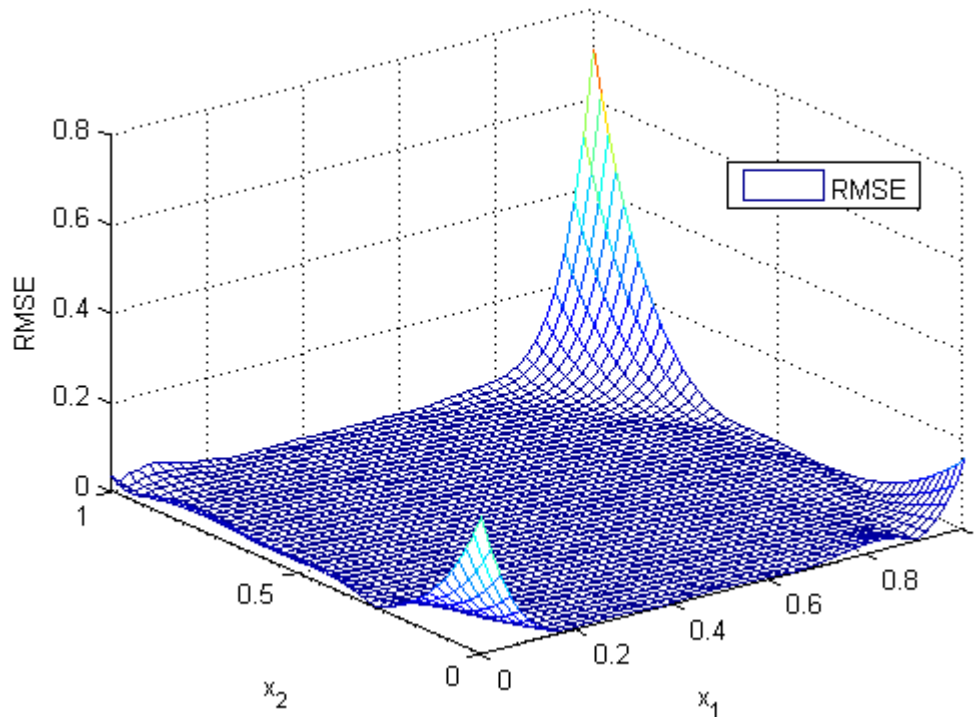
Figure 8.13. RMSE of Camelback predictor with 50 sampled points

8.5.   Conclusions

Constructing a surrogate model relies on two major steps: a uniform sampling plan and training a mathematical predictor. The central features of both steps for making sufficiently accurate predictors have been reviewed in this chapter. The uniform Latin hypercube sampling is able to cover a design space with the least possible number of samples. It can also tackle the issue dimensionality. For constructing a mathematical predictor, a number of methods are available in the literature. Of these methods, Kriging is widely used for many applications due to its efficacy for multi-dimensional cases.

The theory behind Kriging predictor has been reviewed in this chapter and two test functions are used to demonstrate how an accurate predictor must be constructed. The response surfaces of the two test functions unveil the significance of using a validation method like RMSE in the training process. A few other validation methods will be explained and employed for the results of brake surrogate models in the next chapter.

9. Brake Surrogate Models

The theory behind surrogate modelling was reviewed in chapter 8. Now two surrogate models are constructed for the brake squeal problem in order to show how this approach can be useful for uncertainty analysis of brake squeal and structural modification brakes. In the first surrogate model, only two design parameters are included. Therefore, the results can be fully visualised and some important conclusions are drawn.

Then, more design parameters are randomised for the second surrogate model. A few validation methods are explained and implemented on the replacement model in order to make sure the mathematical predictor works accurately. Thereafter, uncertainty analysis is conducted on the model and the probability distribution of the output is obtained. The output distribution can be used for quantifying the probability of failure. Once again, it is worth reminding that the term 'failure' in this study means the likelihood of unstable vibration in a brake model.

9.1.   Advantages of surrogate modelling for brakes

There are three main advantages which can be gained from surrogate modelling of brake systems. First of all, the mathematical predictor can be used for design optimisation of brakes. What commonly brake analysts do is to make some structural modifications on a brake design in order to slightly shift the natural frequencies of brake components and meet the target level for squeal propensity or 'squeal index'. These modifications can be done in a systematic way by using the response surfaces of brake models. These response surfaces provide brake analysts with some trends in which a set of system parameters affect an unstable mode. Then, the analysts can come up with some ideas for the structural modification of brakes.

The second advantage is that uncertainty propagation of design parameters can be mapped onto the output space, i.e. the results of CEA, in a very efficient way. Indeed, this objective forms the central aim of the current study. Although there is no doubt that variability and uncertainty are two inseparable parts of any brake system, they have not properly been considered so far due to the computational time and cost of expensive statistical methods. If the training of the mathematical predictors is done accurately, the uncertainty propagation of system parameters can be done cost-effectively with sufficient accuracy.

The last advantage is reliability analysis and robustness of brakes in terms of squeal propensity. The previous step (uncertainty propagation) provides analysts with a number of probability distributions corresponding to unstable modes. Then, a target level for the squeal propensity can be set in order to find what percentage of brakes will fail due to manufacturing variability or against the environmental effects and usage. The reliability and robustness in this sense can provide car manufacturers with an estimate of warranty costs due to squeal noise. Alternatively, this figure can be used to give suppliers an idea about the quality control of their products. For example, if the manufacturing variability of the first frequency of the disc has 1.5% standard deviation (from its mean value) and the results of reliability analysis shows the design will be robust to 1% standard deviation, the feasibility of manufacturing discs within these limits can be discussed with the suppliers. Based on some reliable information, such limit has not set for the quality control of the components up to this date.

9.2.   Implementation of brake surrogate modelling

The flowchart shown in Figure 9.1 summarises the required steps for surrogate modelling of brake models. In this section, it is attempted to explain each step with an example of the

brake under study. In order to get a better understanding of the current approach, two design parameters are considered in this section. Later on, the results for four-parameter surrogate model are presented.
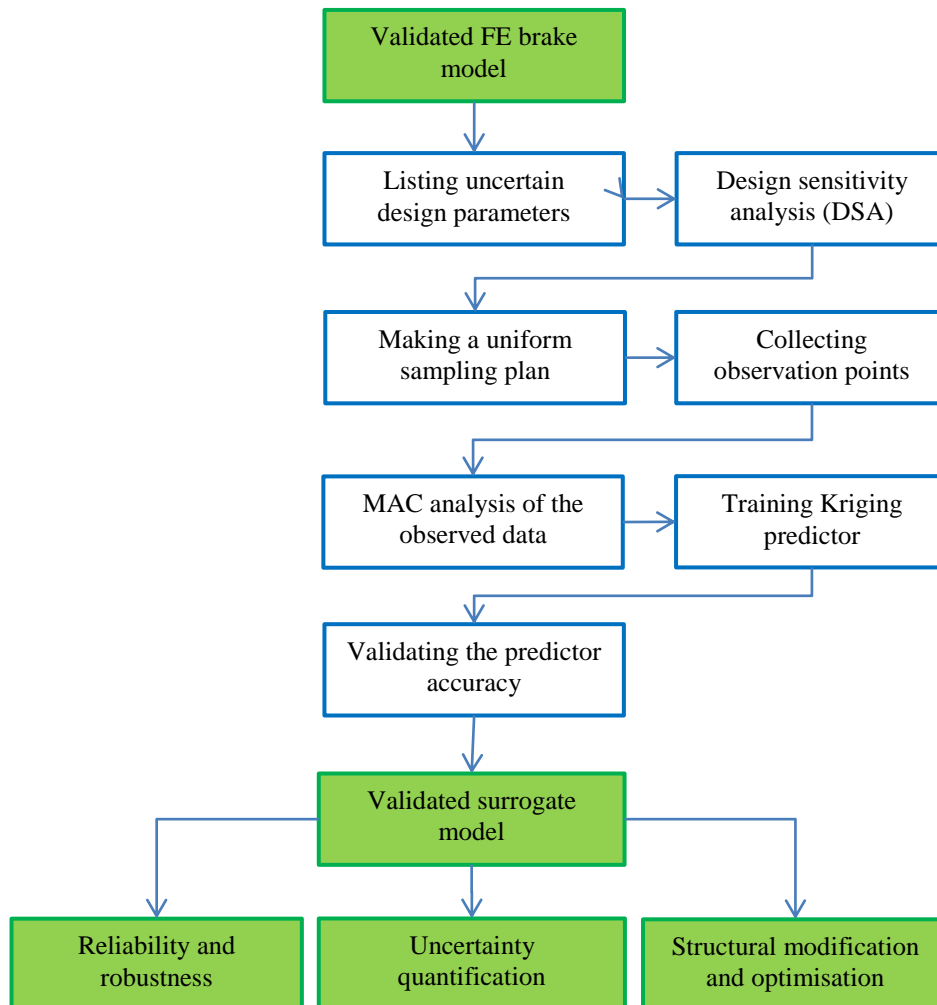
Figure 9.1. The process of brake surrogate modelling

9.2.1.   *Listing uncertain design parameters*

The first step is to provide a list of the design parameters whose values can vary noticeably from those of nominal ones. These variations can be either due to production variability such as material properties or operational condition such as changes in friction coefficient, brake pressure, etc. In general, any parameter for which there is a value in the finite element model can be included in the surrogate model. As in Liverpool University, there was a limited capacity of computational facilities, a fairly short list has been considered in this step. However, it is worthwhile to clarify that there is no limit for the number of uncertain input parameters to be included in this step. If more parameters are included in this step, the level of confidence about the prioritised parameters will be higher. What really helps in this case is brake engineers' experience. Based on their knowledge, five parameters are considered

here for the particular brake under this study: $\{\mu_{\text{pads-to-disc}}, E_{\text{d}}, E_{\text{c}}, E_{\text{t}}, \mu_{\text{abutment}}\}$ where $\mu_{\text{pads-to-disc}}$ represents the friction coefficient at the pads-to-disc contact interfaces. E_{d} and E_{c} denote the disc's and calliper's Young's moduli, E_{t} represents the transverse elastic modulus of the friction material, and μ_{abutment} denotes the friction coefficient at the abutment.

To get an idea of how the variability of the friction material should be randomised, a few modal tests are done on two pads. The updated elastic and shear moduli which bring about a close correlation between the measured and simulated data are shown in Table 9.1. For randomising the friction material properties, according to these results, E_{t} is independently randomised first. Then, in order to avoid getting odd mode shapes, E_{p} (in-plane elastic modulus) and G_{t} (shear modulus) are linked with the randomised value of E_{t} in the way that the ratios between these modulus remain unchanged. Indeed, this is the assumption which is made in this study. Further experimental studies on friction material properties can improve this assumption in the future.

Table 9.1. Pad variability

	1st Bending Freq. (Hz)			1st Torsion Freq. (Hz)			E_{t} (MPa)	E_{p} (MPa)	G_{t} (MPa)
	Test	FE		Test	FE				
Pad 1	1846	1853		2082	2031		552	3170	727
Pad 2	1912	1914		2120	2088		662	3802	872

Once again it is worth reminding that based on Abaqus terminology and notation, E_{t} represents the out-of-plane elastic modulus of a transversely isotropic material, E_{p} denotes the in-plane modulus and G_{t} is the transverse shear modulus.

9.2.2. *Design sensitivity analysis (DSA)*

The design sensitivity analysis (DSA) is extensively applied in structural dynamics, especially model updating. From the mathematical viewpoint, model updating is an optimisation problem which attempts to minimise the discrepancy between experimental and numerical results (for example, mode shapes and frequencies) of a structure. One of the efficient ways of model updating is to find the optimum values based on the sensitivity of outputs to the input parameters (Mottershead et al., 2000). Due to the broad application of model updating in structural dynamics, some software such as MSC Nastran and

Abaqus/Design are able to carry out DSA concerning the resonant frequencies, i.e. imaginary parts of the eigenvalues of the structure.

However, what is significant about squeal instability is the sensitivity of the real part of an unstable eigenvalue to the system parameters. The results of DSA regarding the real parts are useful for the structural modification of brakes to reduce noise and also for constructing the brake surrogate model. Including inactive parameters in the surrogate model increases the computational workload significantly, yet not much information can be gained. As DSA is not available in Abaqus/Standard, the finite difference method is implemented to find the sensitivity of the real part of the unstable eigenvalue with respect to the input parameters. In order to avoid scaling issues, the differences are normalised to the values used in the baseline design (Mottershead et al., 2000). Expression (9.1) shows that the normalised sensitivity of the real part with respect to the input parameters should be calculated:

$$\frac{\left[\alpha_j(q_i + \Delta q_i) - \alpha_j(q_i)\right]/\bar{\alpha}_j}{\Delta q_i/\bar{q}_i} \tag{9.1}$$

where $\bar{q}_j$ represents the value of the ith uncertain parameter and $\bar{\alpha}_j$ indicates the real part of the jth unstable eigenvalue. As mentioned earlier, sensitivity analysis can broadly be conducted on a brake system in order to identify highly active parameters in the model. However, based on brake engineers' experience and knowledge, the number of variables has been restricted to those five ($\mu_{\text{pads-to-disc}}, E_\text{d}, E_\text{c}, E_\text{t}, \mu_{\text{abutment}}$). One consideration is that structural modification of all input variables is not always possible.

One percent variation from the nominal value of each parameter is considered for Δq_i. The results are listed in Table 9.2. At this point, only the absolute values of the derivatives are reported since their magnitudes are important to decide on the sensitive parameters and their signs only show the direction of the gradient.

Table 9.2. The sensitivity of the unstable mode with respect to the parameters of FE model

	Parameter	Nominal values	Normalised sensitivity
1	$\mu_{\text{pads-to-disc}}$	0.50	1.97
2	$E_\text{d}(\text{GPa})$	111.7	8.08
3	$E_\text{c}(\text{GPa})$	70.00	0.67
4	$E_\text{t}(\text{MPa})$	607.1	1.43
5	μ_{abutment}	0.15	0.03

These results reveal that the real part of the unstable eigenvalue is considerably sensitive to disc's Young's modulus. The calliper's Young's modulus, the friction coefficient at the pads-to-disc interface and the transverse modulus of the pad have lower influences, yet they are significant. However, the friction at the abutment has the least effect on this particular mode. Hence, the first four parameters will be used to construct the brake surrogate model and the friction coefficient at the abutment is set aside.

Please note that several studies in the literature concluded that the most effective parameter on squeal instability is the friction coefficient and one may say that our finding is not in agreement with the previous studies. However, two points should be considered here carefully. First of all, the sensitivity analysis has only conducted on a particular unstable mode in this study. In large-scale models, it is often seen that one unstable mode, for example, is very sensitive to the disc's Young's modulus and the other one is sensitive to the friction at abutment. If a number of unstable modes were under study here, most likely the parameter which was active in all unstable modes would be the friction coefficient. Then, the results of DSA would be in consistent with the other studies. Secondly, a number of conclusions in the literature are based on minimal brake models. The results of this study shows that minimal models are very helpful for understanding a phenomenon and the theory behind a problem, but some features of large-scale modes can be very different with those of the minimal ones.

In this study, only one unstable mode of the brake under study is explored via surrogate modelling. Exploring different unstable modes needs a larger number of input variables, larger ranges for the variables, and consequently a larger sampling plan. Due to the limited access to computational facilities in this research, the applicability of surrogate modelling for brake squeal simulation is shown by means of one of the unstable modes in the results. Collecting a larger sampling plan provides enough data points for the other unstable modes and the method can be applied to those modes as well.

9.2.3.   *Making a uniform sampling plan*

In order to train a mathematical predictor of a particular unstable mode, a number of observations are required. These observations are in fact the results of the complex eigenvalue analysis corresponding to different values of the prioritised parameters. The required number of observations is dependent on how many modes are being explored, how many design parameters are being included and how nonlinear an unstable mode is versus the prioritised parameters.

Before looking at the four-parameter surrogate model, a two parameter surrogate model is constructed here in order to better visualise the results. Based on sensitivity analysis of the brake, E_d and μ are the top two sensitive parameters. However, as the effect of friction on this kind of instability is well known (Hoffmann et al. 2002), it is decided to look into the variations of pad's transverse modulus E_t along with E_d in the 2-parameter surrogate model. Once again, it is worth reminding that in this study the variability of the components is represented in the surrogate model via their Young's moduli. Therefore, E_d represents the variability of the disc and E_t denotes the variability of the brake pad in the response surface. The interval in which E_d varies is from 108.349 to 115.051 (mean value 111.7 GPa with 1% standard deviation). E_t varies from 552 to 662 MPa (mean value 607 MPa with 3% standard deviation). Now the uniform LHS is run to generate the required sampling points of the 2D surrogate model. The results are pictured in Figure 9.2.
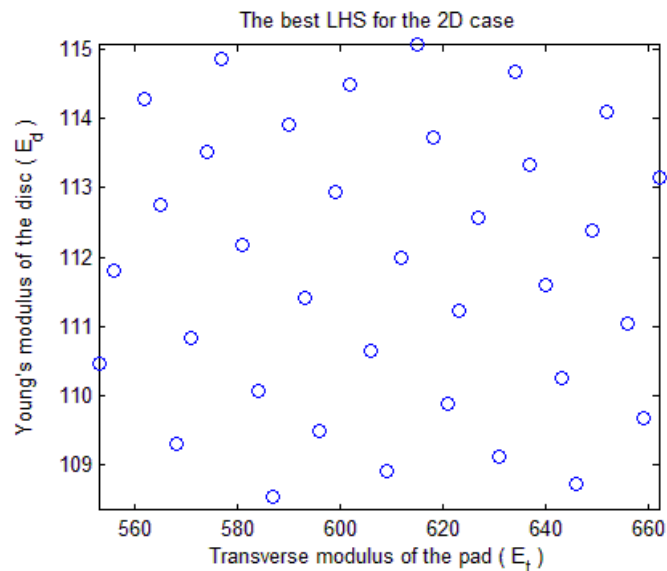
Figure 9.2. The sampling plan for the two-parameter brake surrogate model

In the literature, it is recommended that the design space should be translated onto the unit cube in order to avoid scaling issues. Therefore, a normalised Latin square with 36 points is built first by the uniform LHS; however, they are translated back to the design domain in Figure 9.2 for the convenience of readers. The reason behind choosing 36 points is related to the desired accuracy of the surrogate model. As discussed in chapter 8, in an iterative process, the number of samples should be increased until the expected accuracy of the replacement model is achieved. For this particular example, collecting 36 observations meets the expectation.

9.2.4. Collecting the observation points

Each point in the sampling plan is like a vector containing a random value of each prioritised parameter, in this step E_d and E_t (Figure 9.3). To collect the observation points, Abaqus input files of the brake should be modified according to the randomised values. The input files are then submitted for the complex eigenvalue analysis (CEA). The real parts or the damping ratios of the unstable mode under study are collected for the training purposes.

$$
\left|
\begin{array}{l}
\mathbf{x}^{(1)} = \left\{ E_t^{(1)}, E_d^{(1)} \right\} \xrightarrow{\text{CEA}} y^{(1)} \\
\mathbf{x}^{(2)} = \left\{ E_t^{(2)}, E_d^{(2)} \right\} \xrightarrow{\text{CEA}} y^{(2)} \\
\qquad\qquad \vdots \\
\mathbf{x}^{(n)} = \left\{ E_t^{(n)}, E_d^{(n)} \right\} \xrightarrow{\text{CEA}} y^{(n)}
\end{array}
\right.
$$

Figure 9.3. Collecting the observation points

9.2.5. Training the Kriging predictor

In chapter 8, the theory behind Kriging is fully explained. Also, two mathematical examples are used to demonstrate how a Kriging predictor must be constructed. The reason behind choosing Kriging is due to its efficacy for multi-dimensional cases and also its broad application for computer simulations. In the literature, the capability of Kriging for multi-dimensional cases is appreciated. As far as the output function is a smooth function of the inputs, Kriging function can be used for constructing an accurate replacement model. The results of this research show the real parts/damping ratios of unstable modes of brake models are not very nonlinear or non-smooth function of the inputs. Hence, there is no problem with using Kriging for squeal propensity predictions. Moreover, as this research aims to propose a numerical tool for car manufacturers who intend to look into the effects of variability and uncertainty of several design parameters (at least seven or eight), the method should be of a high capability to deal with multi-dimensional cases. On the ground of these two facts, Kriging has been selected for the purpose of the current study.

The Kriging predictor, i.e. the response surface shown in Figure 9.4, is built by the MATLAB code given in (Forrester et al., 2008): `ModelInfo.Option='Pred'`. As seen, the trend is quite similar to the manner observed for the real part of an unstable mode after bifurcation point. Please note that although the FE brake model is so complicated, the output is not very nonlinear or non-smooth. Therefore, using a surrogate model can quickly produce the output in a few milliseconds and there is no longer a need to wait for Abaqus to produce the results in 12 to 36 hours.
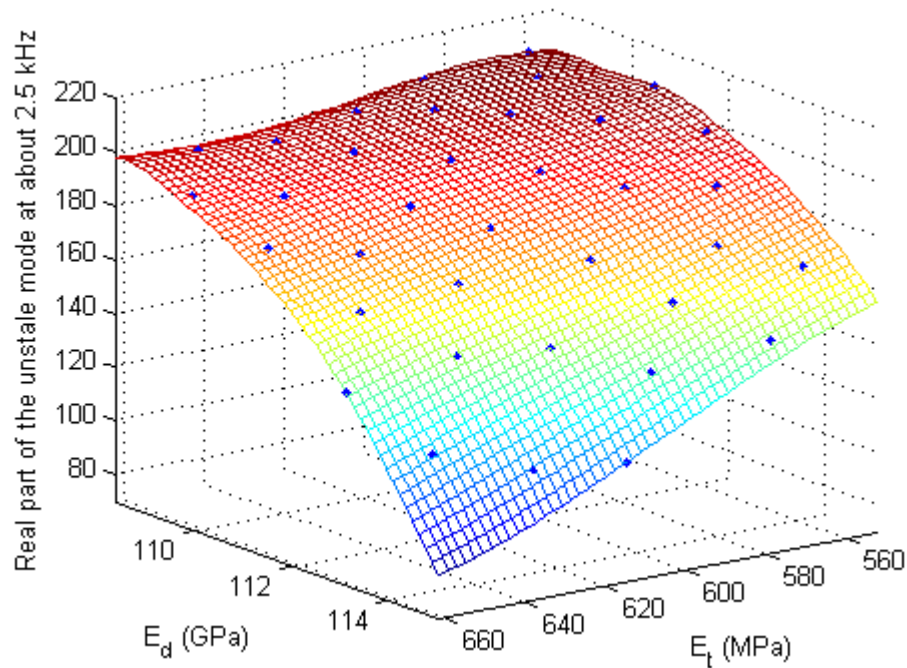
Figure 9.4. Two-parameter brake surrogate model

9.2.6. *Validating the predictor accuracy*

The good point about two-parameter surrogate models is that the root mean squared error (RMSE) of the predicted values can be demonstrated versus the input parameters in one plot. Thus, the accuracy of the response surface can be well assessed. Figure 9.1 shows RMSE of the two-parameter surrogate model over the design space. RMSE is determined by the MATLAB code given in (Forrester et al., 2008): `ModelInfo.Option='RMSE'`.

Figure 9.5 also reveals that the errors on the corner of the design space are considerably larger than the errors in the central part. As discussed in chapter 8, the uniform LHS does not cover the corners of the design space unless the number of sampling points is considerably increased. As a result, RMSE values are fairly large around the corners. However, in the central part of the design space, which is the point of interest here, the errors are practically zero. Since for a 2D case, RMSE can be plotted over the parameter domain, it is not necessary to include the corners in the sampling plan if the central part of the domain is the point of interest. However, for a multi-dimensional case, this study recommends to include the corners in the sampling plan as some indices should be employed to evaluate the errors. Otherwise, although the model may be entirely accurate in the central part of the domain, the errors around the corner can be suppressed in the algorithm to keep by increasing the number of sampling points until the stopping criteria are satisfied. This situation is often not desirable since the sampling process can become very expensive.
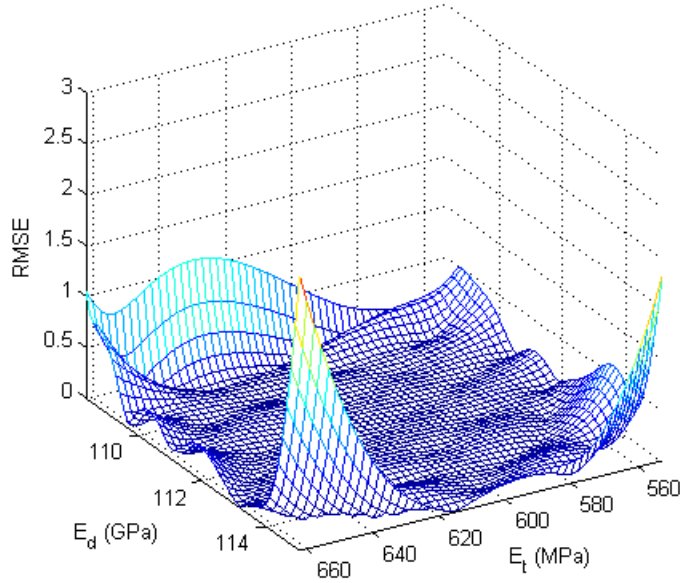
Figure 9.5. RMSE of the predicted values

Figure 9.5 shows the absolute values of RMSE. In order to make a better judgment and determine the percentage of the error, it seems reasonable to normalise RMSE in this way:

$$\delta(\mathbf{x}^*) = \frac{\hat{s}(\mathbf{x}^*)}{\hat{y}(\mathbf{x}^*)} \qquad (9.2)$$

where δ is called 'the coefficient of variation' in this study. In statistics, the coefficient of variation is a dimensionless measure obtained through dividing the standard deviation of a distribution by its mean value. Since in the Kriging model, the errors are normally distributed around the predicted values (Gaussian process), it makes sense to take the same approach for presenting the uncertainties about the predictions. Figure 9.6 shows the coefficient of variation over the design space. A threshold can be set for δ if someone intends to use it as the stopping criterion in the iterative process of surrogate modelling. Based on the accessible computing facilities, the threshold is set to four percent in this study.

Moreover, the CEA results of 15 untried points which are not involved in the sampling plan are produced by the FE model to compare with the predicted results. The actual and predicted values of the unstable mode are listed in Table 9.3.
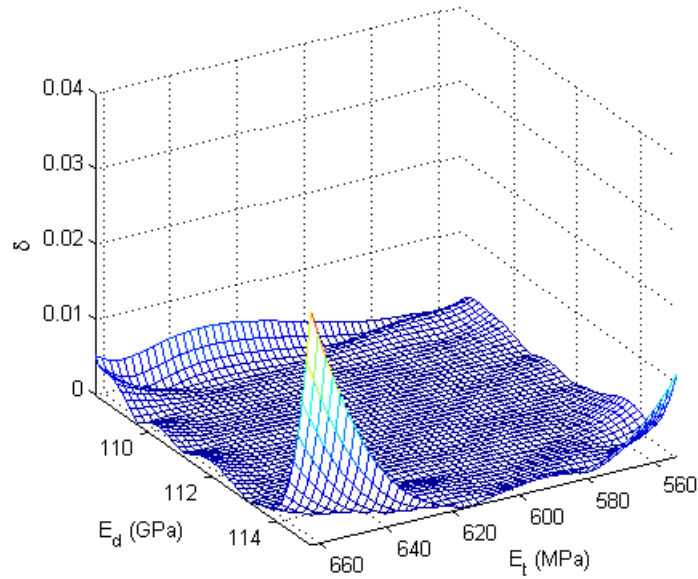
Figure 9.6. The coefficient of variation

The errors in Table 9.3 are practically zero in most cases. These results thus prove the efficacy of the Kriging model in predicting the squeal instability within the simulation model. In order to generalize this conclusion, a surrogate model is built in section 9.4 when the variations of four parameters $\{\mu_{\text{pads-to-disc}}, E_d, E_c, E_t\}$ are taken into consideration.

Table 9.3. Comparing the FE and predicted values of the untried points

No.	E_t (MPa)	E_d (GPa)	FE results	Predicted results	Error (%)
1	607	112.179	179.94	179.96	0.0
2	662	112.657	152.45	152.73	0.2
3	631	108.349	201.10	196.88	2.1
4	592	110.743	197.08	197.30	0.1
5	615	109.785	199.11	199.20	0.0
6	576	108.828	205.68	207.53	0.9
7	646	114.572	110.07	110.71	0.6
8	654	109.306	194.75	195.42	0.3
9	623	113.615	150.05	148.98	0.7
10	566	111.700	195.81	196.29	0.2
11	560	114.094	171.25	170.45	0.5
12	599	115.051	127.06	126.65	0.3
13	584	113.136	174.22	174.25	0.0
14	638	111.221	182.24	182.56	0.2
15	553	110.264	207.40	206.01	0.7

9.3. Structural modification and design optimisation

One of the main advantages of brake surrogate modelling is its applicability for structural modification and design optimisation of brakes. As mentioned in previous chapters, what is common in industry is to structurally modify the brake components so that the likelihood of mode-coupling instability is reduced. Up to now, this job has not been done in a systematic way and mostly done via trial and error techniques. Interestingly, surrogate modelling can pave the way of structural modification and provide brake analysts with some trends within those squeal propensity changes. For demonstrating this advantage of surrogate modelling, the two-parameter response surface of the brake under study is explored here.

Looking at the response surface plotted in Figure 9.4 reveals that in order to reduce the squeal propensity of the particular mode under study, the disc's Young's modulus and pad's transverse modulus should be increased. The real part of the unstable mode with the nominal values of the design parameters was 201. Figure 9.7 now displays the CEA result of a point in the circled area of the response surface. It shows if a brake analyst slightly increases the disc and pad elastic moduli, the real part of the unstable mode drops significantly to 122.
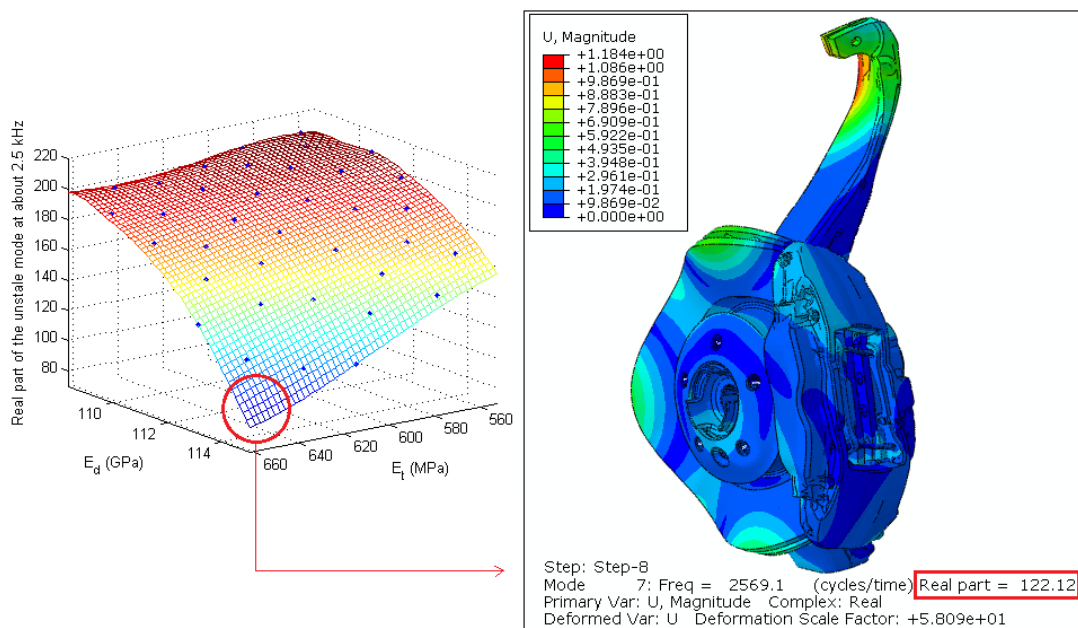
Figure 9.7. Design optimisation via surrogate modelling

Structural modification of brakes is not the central aim of this study. Thus, it is not attempted here to suppress this particular unstable mode or reduce its squeal propensity. However, it is worthwhile to see how the response surface method can facilitate the way of structural modification. Needless to say, finding the optimum values in this way is just a starting point. Since the material properties cannot be changed easily, the geometry of the components should be modified, instead. In order to take the advantages of these results though, the

frequencies of the component can be calculated via the optimum values. Then the structure with nominal values should be structurally modified so that their frequencies match those of determined by the optimum values. Even if it is not feasible to match all frequencies, those which are largely involved in the mode coupling instability can be targeted for this purpose. The implementation of this approach may be followed in the future studies.

9.4.   Uncertainty quantification

Surrogate modelling of brakes provides a cost-effective method of uncertainty quantification. This is the statement which has been frequently repeated from the beginning of this study. Moreover, it has been continuously emphasized that incorporating the effect of variability and uncertainty for designing robust and reliable brakes is inevitable. Now it is time to see how surrogate modelling can help determine the reliability and robustness of a brake design in terms of the likelihood of unstable vibration leading to squeal.

Surrogate modelling replaces the expensive simulation code with a cheap-to-evaluate mathematical predictor. Thereafter, when the validity of the replacement model is confirmed, the predictor is able to reproduce the results of the FE model in a few milliseconds. Obviously, if a higher number of parameters are included in a surrogate model, a greater level of confidence about the reliability and robustness of the design will be achieved. However, it is worth reminding that including inactive parameters increases the computational workload significantly, from which not much information can be gained. Therefore, according to the results of the sensitivity analysis (Table 9.2), the top four sensitive parameters are considered for the uncertainty quantification of the brake under study: $\{\mu_{\mathbf{pads-to-disc}}, E_{\mathbf{d}}, E_{\mathbf{c}}, E_{\mathbf{t}}\}$.

The ranges within which the disc's and pad's Young's moduli vary are reported in section 9.2.3. For the friction coefficient at the pads-to-disc interface, it is assumed the mean value is 0.5 with a standard deviation of 5% (from its mean value). The influence of environmental and operational conditions on the friction coefficient is fairly large, so this is the reason a fairly large variation is considered for this parameter. The calliper is made from aluminium and as mentioned previously the variation of its material properties is not very high. Hence, 1% standard deviation from its mean value (70.0 GPa) is considered for the calliper.

Now another surrogate model must be constructed since the previous one only contains two parameters. A number of attempts have been made to find the right number of sampling points. At the end, a sampling plan with 136 points meets the desired validation criteria.

With the uniform LHS, 120 samples are generated, and then the corners of the design space (2^4) are added to the sampling plan. In total, the CEA results of 136 points are produced by means of the FE model.

In order to make sure that the same unstable mode is being explored, MAC is calculated for the stochastic results. The mode shapes of the sampling points are compared with the one of the baseline design. Those samples bringing about a MAC larger than 90 percent are kept for the training of the predictor. The remainders are discarded from the sampling plan. Therefore, 133 sampling points are employed for the construction of the surrogate model.

For the Kriging predictor, parameters $\boldsymbol{\theta}$ and $\mathbf{p}$ must be identified. Genetic algorithm is used for determining the unknown parameters of the concentrated likelihood function (equation 8.6). The results are $\boldsymbol{\theta} = \{0.1505, 0.6158, -0.875, -0.6715\}^{\mathrm{T}}$ in a logarithmic scale. These results reveal that the disc's Young's modulus undergoes the highest level of activity in the model. The friction coefficient, pad's transverse modulus and calliper's elastic modulus take the second to the fourth places, respectively. These results are sensibly comparable with those of DSA. It is worth noting that these two results should not necessarily be identical since DSA is only carried out at the baseline design point. If it were affordable to run DSA all over the design domain, both DSA and the surrogate model would deliver similar results.

Up to now, a number of validation methods have been explained and implemented on two-parameter surrogate model. However, a new validation technique which has been widely used in the literature is employed in the case of the four-parameter brake surrogate model. This technique is known as "cross-validation method". The reason behind choosing this method is that it is not possible to visualise the entire design space in multi-dimensional cases. Thus, a reliable validation technique must be selected to make sure the constructed surrogate model is sufficiently accurate. The idea behind the cross-validation method is fully explained in (Jones et al., 1998).

In brief, one of the observation points $\mathbf{x}^{(i)}$ is left out when constructing a surrogate model and the remaining points are used to make prediction of $y(\mathbf{x}^{(i)})$. This predication is expressed by $\hat{y}_{-i}$ in which $-i$ indicates the point i is not included in constructing the predictor. If enough information, i.e. observation points, has been collected, excluding one of the points should make very little difference on the estimation of $(\hat{\mu}, \hat{\sigma})$. Otherwise, the number of sampling points is not enough.

To set a criterion for the cross-validation method, "the standardised cross-validated residual" η must be calculated (Jones et al., 1998):

$$\eta\big(\mathbf{x}^{(i)}\big) = \frac{y\big(\mathbf{x}^{(i)}\big) - \hat{y}_{-i}}{\hat{s}_{-i}}. \tag{9.3}$$

The meaning of the standardised cross-validated residual can be better understood by paying attention to the fact that Kriging predictor is indeed a Gaussian process modelling. In other words, at each point/location in the process, the error in the prediction is normally distributed about the predicted value. For the cross-validation procedure, the predicted value is $\hat{y}_{-i}$ and the uncertainty about the prediction, i.e. the standard deviation of the normal distribution, is $\hat{s}_{-i}$. Therefore, in order to be 99.7 % confident that $y(\mathbf{x}^{(i)})$ is placed within $\pm 3\hat{s}_{-i}$, the standardized cross-validated residuals η should not exceed $[-3, 3]$. However, it is not unexpected to observe a few outliers (Jones et al., 1998). The number of outliers will be reduced if the number of sampled points is increased. Figure 9.8 shows the standardized residuals for the four-parameter brake surrogate model. Since 125 out of 133 observations meet the cross-validation criterion, i.e. $\big|\eta\big(\mathbf{x}^{(i)}\big)\big| < 3$, this model is sufficiently accurate for the objectives of this study.
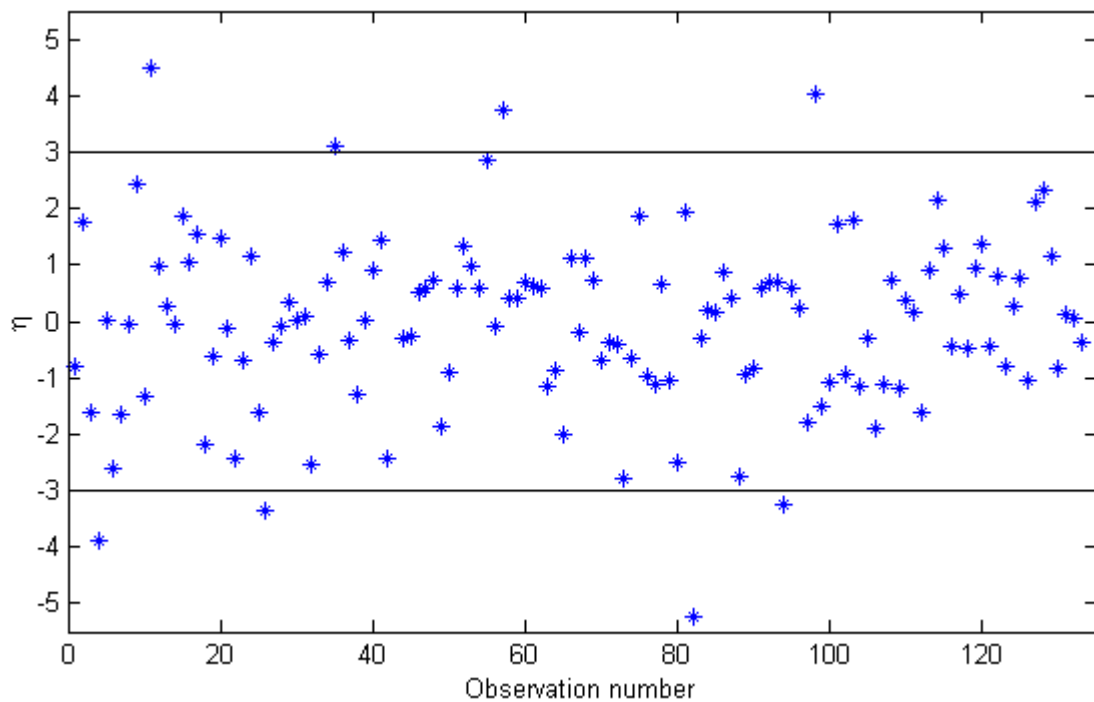
Figure 9.8. The standardised errors of the untried points

In chapter 6, a number of uncertainty analysis techniques are explained. First of all, bear in mind that the brake surrogate model can be used in place of the original FE model in all methods of uncertainty analysis. Regardless of whether a probabilistic or non-probabilistic approach is taken toward the problem, the surrogate model can be taken as the mapping

function. The second important point is that the surrogate model produces the results of a single input in a few milliseconds, so even using the conventional Monte Carlo simulation is not very expensive. As explained in chapter 6, in terms of the statistics of the output, the conventional Monte Carlo simulation (MSC) is more informative than the other methods of uncertainty analysis. Therefore, when it is affordable to run MSC, there is no reason to take the other approaches of uncertainty propagation.

Apart from the method of uncertainty analysis, the probability distribution of the input variables plays a significant role in forming the output profile. Unfortunately, there is no published data for the distributions of the input variables which are used in this study. As discussed before, it is only known that the input distribution of the disc's Young's modulus is Gaussian. Moreover, Sarrouy et al. (2013b) used both uniform and Gaussian distributions for the friction coefficient between the disc and pads. However, no experimental data are used for supporting these assumptions.

In this study, the distributions of all of the input variables are assumed to be truncated Gaussian. In other words, the non-physical values of the input variables have been removed from their domains. The histograms of the input variables are shown in Figure 9.9. It is worth noting that there is no limitation for using any combination of different forms of input distribution in the proposed method. In fact, one of the strongest points of using surrogate modelling and Monte Carlo simulation together is that any form of distributions can be considered for the input variables, and the uncertainty analysis can readily be executed. By the use of a random generator one million vectors of inputs are created. Each vector contains four random values of $\{\mu_{\text{pads-to-disc}}, E_{\text{d}}, E_{\text{c}}, E_{\text{t}}\}$.

The real parts of the eigenvalues of the unstable mode associated with the one-million random inputs are produced in a few minutes by the four-parameter brake surrogate model. Figure 9.10 displays the histogram of the outputs. The dotted line shows the mean value of the distribution. The location of the mean value indicates the output distribution is not Gaussian, and that is expected due to the nonlinear relation of the real part of the unstable mode with the input variables. The mean value of the distribution is 182.1514 and its standard deviation is 21.161.
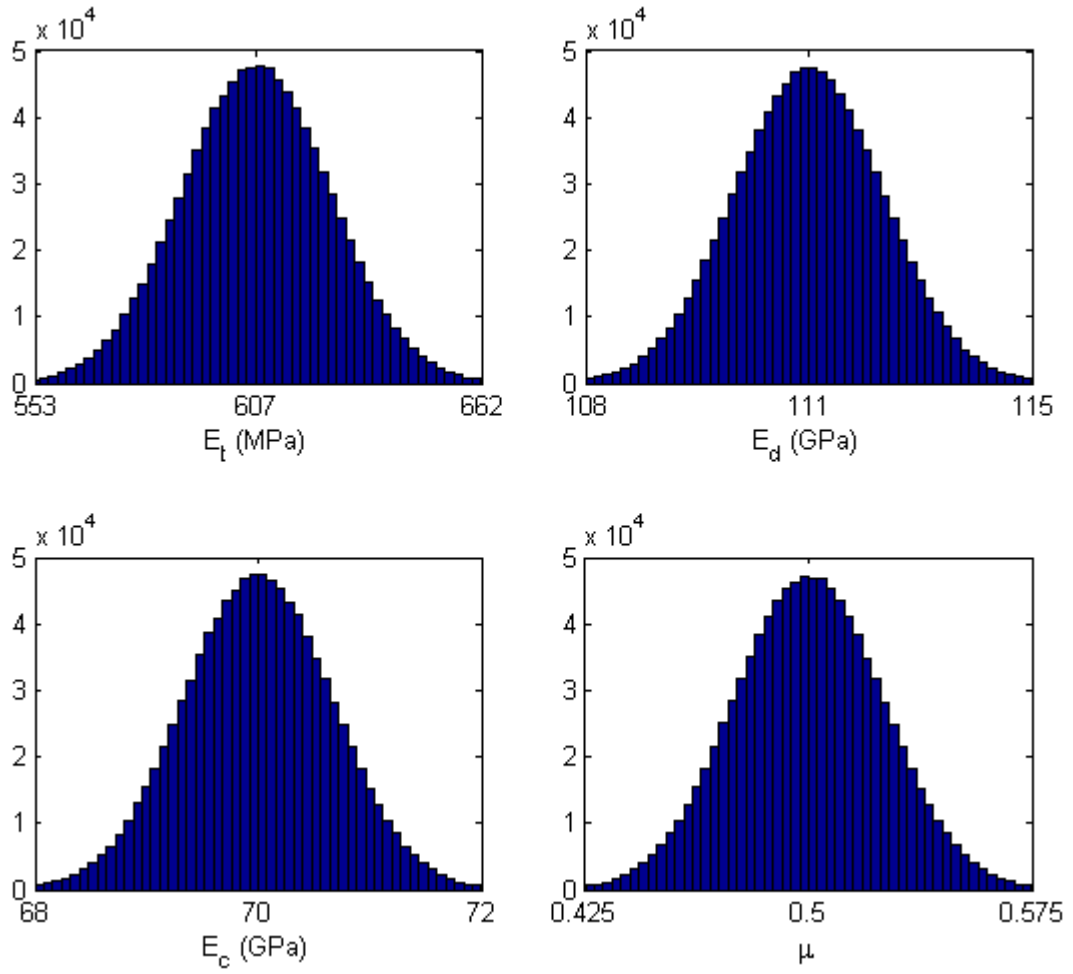
Figure 9.9. Gaussian distributions of the inputs
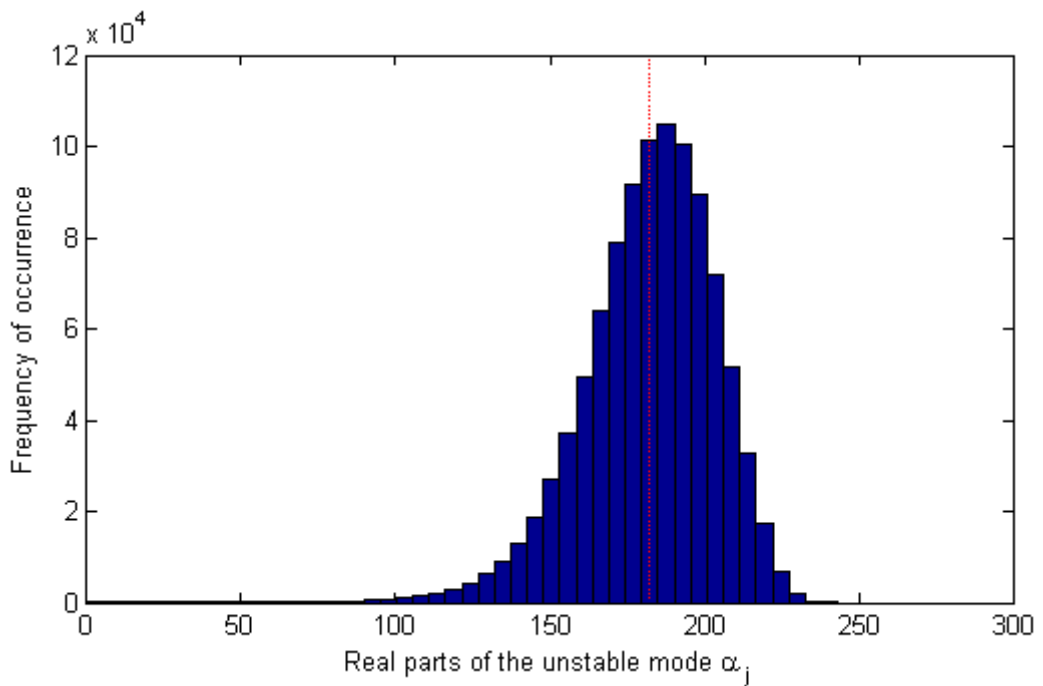
Figure 9.10. The distribution of the output

9.5. Reliability analysis and robustness

Looking back at the first concern about brake systems, the warranty claims are mostly filed due to brake noise, in particular brake squeal. If a practical way is employed to quantify the uncertainty and variability of brake systems, it is possible to figure out what percentage of manufactured brakes will 'fail' in terms of noise either at the end of the production or due to the operational conditions and aging effects. In this sense, squeal noise can be considered a reliability issue in a brake design. The deviation of the material properties from the nominal values, the dissimilarity between assemblies and the imperfection of component geometries can cause the 'failure' at the end of production. However, thermal effects, non-uniform pressure distributions and wear are some examples causing 'failure' during brake operations. Regardless of how these variability and uncertainty of the input variables are characterised in the FE model, the method of quantifying the probability of 'failure' is discussed here.

The constructed surrogate model in this study belongs to a brake design before making structural modifications for reducing noise. In other words, it is very likely for the brake to generate squeal. However, in order to quantify the probability of 'failure', a new surrogate model should be built after the modifications. The probability distribution of the outputs should be produced for the new model and the target level is used to divide the output space into acceptable and unacceptable regions. Then, the probability of failure is evaluated by the probability of the results which exceed the acceptable threshold. The probability of 'failure' can be expressed as

$$p_f = \Pr(\alpha \geq \alpha_{\text{failure}})$$

(9.4)

where α represents the real part of the unstable eigenvalue. Unfortunately, constructing another surrogate model is not affordable within this investigation.

9.6. Multi-output cases

Variability and uncertainty can cause some unstable modes to disappear and some new unstable modes to show up. In such cases, a few surrogate models, typically three or four, must be constructed to investigate all unstable modes of a brake. A single surrogate model cannot completely portray the stochastic nature of all unstable modes. Please note that in this study, the main focus is to establish a methodology instead of solving the squeal problem. The proposed approach remains the same regardless of the form of inputs, the range of inputs, the number of input variables and the number of outputs or unstable modes.

In order to illustrate how the material properties can lead to the generation of a few unstable modes, it is worth focusing on the disc material properties. It is known that cast iron from which discs are usually made can have a fairly large variation in its elastic properties, depending on the carbon content. As in this study, the variability is represented with the Young's moduli of the components, a larger standard deviation for E_d is considered in this section in order to discuss the effect of a large variation in the input variables.

Imagine that the variations of three input parameters ($\mu_{\text{pads-to-disc}}, E_c, E_t$) are kept constant while the mean value and standard deviation of E_d are considered 109.5 GPa and 3.285 GPa, respectively. In other words, E_d varies from 99.64 GPa to 119.35 GPa (with 99.97% probability). However, the constructed surrogate model is only valid from 108.349 GPa and 115.051 GPa (the remainders in the interval of E_d exceed the bounds of the design space in the surrogate models). The histogram of E_d with a larger variation and the range within which the constructed surrogate model is valid are shown in Figure 9.13.

In this case, two-million random values of the input variables are generated. About 800 thousands of samples are discarded as they exceed the range of validity of the constructed surrogate model. The remainders have been used for the purpose of uncertainty propagation. The histogram of the real part of the unstable mode is shown in Figure 9.14. As seen, the mean value of the distribution (the dotted line) is moved to the right in comparison with Figure 9.12 and the profile of the output distribution is slightly different this time. The mean value and standard deviation are now 185.7978 and 26.2885, respectively.
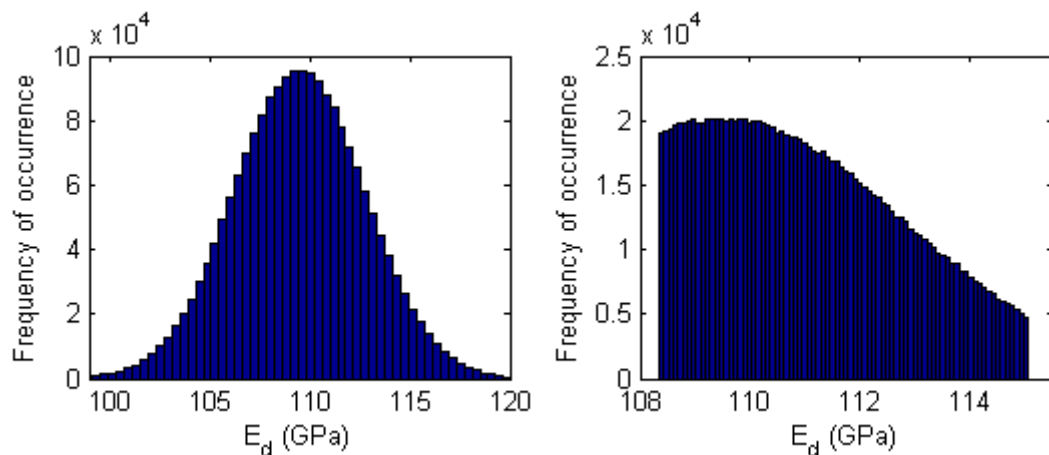
Figure 9.11. A larger variation for disc's Young's modulus: a) the variation of E_d ; b) the range of validity of the surrogate model.
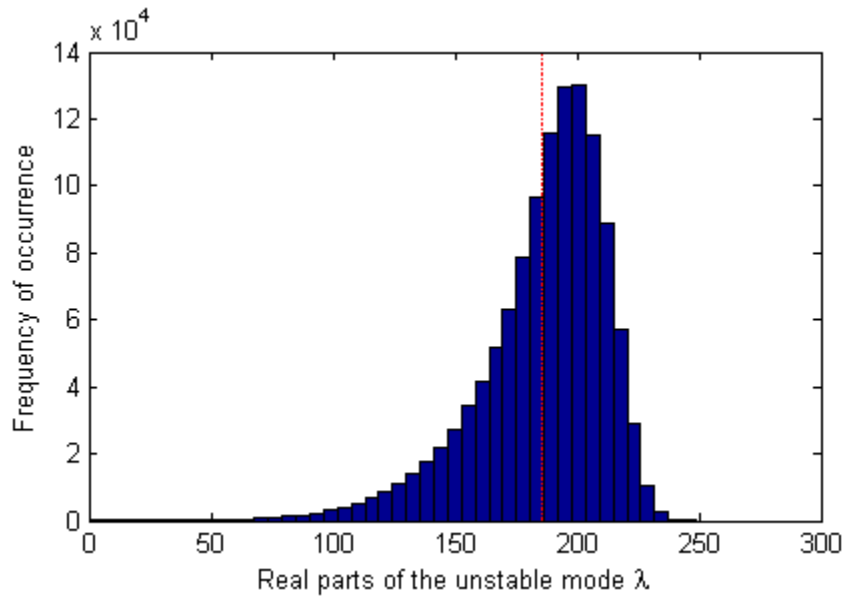
Figure 9.12. Output distribution for the disc with a larger variation of Young's modulus

9.7.   Conclusions

Incorporating the effect of variability and uncertainty is essential to make reliable predictions of squeal instability. Investigating these effects needs a very efficient statistical method by considering the fact that statistical analysis in general relies on the results of deterministic approaches and a single CEA of the brake model takes 12 to 36 hours. To tackle the issue of computational workloads, this study proposes to construct a Kriging surrogate model of brake systems. In other words, the FE model of a brake is replaced with a mathematical predictor being able to reproduce the CEA results of the actual brake model. If the mathematical predictor is trained accurately, the outputs of any desirable input can be produced in a few milliseconds. Thereafter, the surrogate model can be used for three purposes. First, brake analysts can come up with some ideas for structural modifications of brakes. Exploring the surrogate model reveals how the outputs will change versus input variables. Secondly, surrogate modelling paves the way of the uncertainty quantification of squeal instability. Since the real parts of unstable eigenvalues are nonlinear functions of input variables, the most practical way to propagate the uncertainty and variability is Monte Carlo simulation. One the other hand, Monte Carlo simulation is not computationally efficient and cannot be applied to the FE brake model directly. Therefore, the brake surrogate model is used in place of the FE model for the purpose of uncertainty analysis. At last, reliability analysis of the brakes in terms of the likelihood of unstable vibration can also be carried out in this way. Any improvement in the probability of 'failure' will lead to a reduction in the costs caused by warranty claims.

10. Conclusions and Future Works

This chapter summarises the results of the current research and suggests a few topics for future investigations.

10.1. Conclusions

For several decades, a significant effort has been made by researchers in order to discover the cause and effects of brake squeal. Although its root cause is still not fully understood, researchers have established two numerical approaches, i.e. complex eigenvalue analysis and transient analysis, which are able to sufficiently predict squeal propensity. Regardless of the advantages and disadvantages of these two approaches, what has been largely missed in the subject was a practical method for covering the influence of variability and uncertainty in the results. Hence, this study aims to establish a standard practice for brake engineers to incorporate the variations of design variables and parameters in brake squeal simulations.

This study may be divided into two parts for conclusions and discussion: brake squeal problem and uncertainty analysis. In the first part, a full corner brake assembly is studied. The step is to correlate the results of normal mode analysis of brake components with their modal test data. Accordingly, several reasonable assumptions for the nominal values of material properties of brake components and their standard deviation are made. Modal testing on the brake components were done via both LMS test lab and Polytec laser scanning vibrometer. For those brake components having complex geometry like calliper, Polytec laser vibrometer provides very clear deflection shapes being comparable to FE analyses. Moreover, for brake pads, Polytec seems to provide more reliable results although their geometry is not very complex. The non-contact way of measurement via vibrometer helps avoid contact resonances, and therefore acquire more recognisable mode shapes.

Then, the FE model of full brake assembly is validated with experimental data. The complex eigenvalue analysis on the assembly produces unstable mode shapes and frequencies of the brake. In parallel, a number of squeal tests are conducted on the brake test rig via Polytec laser scanning vibrometer. As a dominant unstable mode is observed on the squeal test, whose frequency is very close to the one of the unstable modes predicted by complex eigenvalue analysis, it is believed that the FE model is sufficiently accurate for the purpose of the current study.

In the second part, a comprehensive review on different techniques of uncertainty analysis is conducted. Then, two probabilistic method of uncertainty analysis are selected for the purpose of the current study: 2nd order perturbation method and surrogate modelling. The 2nd order perturbation method is applied on a simplified brake model. In comparison with the conventional probabilistic techniques of uncertainty analysis like Monte Carlo simulation that demand a large number of deterministic analyses, this method approximates the statistical description of complex eigenvalues in one run. However, for large-scale FE models, its implementation is associated with some difficulties.

Therefore, in order to propose a practical method to industry for uncertainty analysis of brake models, the method of surrogate model is studied in this study. The method replaces expensive simulation codes with cheap-to-evaluate mathematical predictors. As a result, even conventional techniques of uncertainty propagation like Monte Carlo can be applied on the replacement model.

The theory behind surrogate modelling is fully reviewed in this study and a few mathematical functions are approximated by this technique. Then, this technique is implemented on the full brake model in two steps. In the first step, in order to visualise the outputs versus all input variables, only two variables are considered for surrogate modelling of squeal instability. When the efficacy of the method is proved in the two dimensional space, it is extended to four design variables. The accuracy of the approximations suggests that Kriging, as one of the mathematical functions which is used for building a predictor, is very effective for the purpose of the current study.

The brake surrogate models are useful for three purposes. First of all, it helps brake engineers to modify a design such that squeal instability is reduced. Structural modification of brakes is a standard practice in industry, which is mostly done by trial-and-error. Surrogate modelling offers a systematic way of doing the modification with massive saving of time and cost.

Secondly, the variations of design variables and also operational variables are efficiently mapped to the results of stability analysis. As mentioned earlier, robust design of brakes in term of the likelihood of unstable vibration leading to noise is one of the main concerns of car manufacturers. Several sources of variability and uncertainty plus the expensive deterministic approaches have hindered industry from considering uncertainty analysis of brakes. Interestingly, the results of the current study show that surrogate modelling overcomes the issue of computational workload and provides a practical way of doing stochastic studies.

Finally, Monte Carlo simulation propagates the variations of input variables and parameters onto the results of stability analysis. Then, instead of a single design point, the scatter of outputs should meet the stability criteria. Accordingly, the reliability and robustness of a brake design in terms of the likelihood of unstable vibration are assessed. The reliability and robustness measure can provide car manufactures with an idea about the cost of warranty claims which may be filed due to brake squeal noise. If the probability of 'failure' for a brake design is significant, brake engineers will be able to revise the design before brakes go into production.

10.2. Future works

Regarding the brake squeal problem, the following aspects need further investigations.

- Damping is one of the factors on which a large number of investigations have been conducted. However, there is not a reliable technique for its measuring and numerical modelling. In particular, in the case of friction material, an extensive study is needed to measure and model damping of transversely isotropic material.

- Friction, contact and wear are the major sources of uncertainty in brakes. Even though a great effort has been made by researchers so far, the physics behind them are not fully understood. Moreover, there is no standard practice in industry to model the nonlinear behaviour of friction and contact. Expensive numerical simulations, on one hand, and the difficultly of measuring these behaviour, on the other hand, are two main reasons that hinder use of nonlinear analysis in industry.

- Characterising friction material properties has been always one of the biggest challenges for car manufacturers. A variety of friction materials are used in brake pads; however, there is no reliable technique to measure their elastic moduli, shear moduli and more importantly Poisson ratios. Although the idea behind this study is that there is no need to have one-hundred percent correlation between tests and finite element models, it does not mean that the nominal value of a parameter and also its range can be defined incorrectly. There are a number of studies in the literature on stochastic model updating. It is vital to conduct such an investigation for friction material properties or brake pads.

- The results of many experimental studies have been proved that thermal effects and humidity play a significant role in triggering brake squeal noise. However, still a practical way for incorporating these effects in brake simulations are needed for large scale finite element models.

Uncertainty analysis of brake squeal instability may be extended in the following routes.

- In this study, the variations of most input variables are made based on some reasonable assumptions. The actual statistical data from component manufacturers/ suppliers are required in order to estimate the likelihood of unstable modes more accurately.

- As complex eigenvalue analysis may underestimate or overestimate the number of unstable modes of a brake system and also as all unstable modes may not lead to squeal noise, feedbacks from the cars in service will help to validate the reliability and robustness measures. Most likely, there is no need for the likelihood of system stability to be 99 percent in order to have quiet brakes in production. The feedbacks may help to set more realistic target levels for these measures.

- In the literature, there are a number of studies focusing on "reliability-based and robust optimisation" of different mechanical systems. Such studies incorporate the effect of variability and uncertainty during design optimisation and there is no need to check the design reliability and robustness at the end of the design stage. On the premise of this study, it is possible to develop a numerical tool for brakes, which incorporates the influence of variability and uncertainty during the structural modification of a brake design. As a result, at the end of the design stages, the brake meets the stability criteria under the variations of design parameters. As a continuation of this study, this tool is being developed in Jaguar Land Rover.

At the end, I believe the completion of PhD is just a start. A reasonable level of knowledge on a subject along with several skills in doing and completing a research topic are learned and achieved during a PhD. Thereof, many other interesting aspects of the subject can be investigated by means of those knowledge and skills.

References

Abaqus documentation, Dassault Systèmes Simulia Corp., Providence, RI, USA.

AbuBakar, A.R. and Ouyang, H. (2006) 'Complex eigenvalue analysis and dynamic transient analysis in predicting disc brake squeal', *International Journal of Vehicle Noise and Vibration* vol. 2, no. 2, pp. 146-155.

AbuBakar, A.R. and Ouyang, H. (2008) 'Wear prediction of friction material and brake squeal using the finite element method', *Wear*, vol. 264, no. 11-12, pp. 1069–1076.

AbuBakar, A.R., Ouyang, H., James, S. and Li, L. (2008) 'Finite element analysis of wear and its effect on squeal generation', *Proceedings of the Institution of Mechanical Engineers, Part D: Journal of Automobile Engineering* vol. 222, no. 7, pp. 1153-1165.

Adhikari, S. and Friswell, M.I. (2001) 'Eigenderivative analysis of asymmetric non-conservative systems', *International Journal for Numerical Methods in Engineering*, vol. 51, no. 6, pp. 709-733.

Adhikari, S. and Friswell, M.I. (2007) 'Random matrix eigenvalue problems in structural dynamics', *International Journal for Numerical Methods in Engineering*, vol. 69,

no. 3, pp. 562-591.

Adhikari, S. and Haddad Khodaparast, H. (2014) 'A spectral approach for fuzzy uncertainty propagation in finite element analysis', *Fuzzy Sets and Systems*, vol. 243, pp. 1-24.

Akay, A. (2002) 'Acoustics of friction', *Journal of the Acoustical Society of America*, vol. 111, no. 4, pp. 1525-1548.

Akay, A., Giannini, O., Massi, F. and Sestieri, A. (2009) 'Disc brake squeal characterization through simplified test rigs', *Mechanical Systems and Signal Processing*, vol. 23, no. 8, pp. 2590–2607.

Allert, B. and Müller, G. (2014) 'Brake-Squeal Simulation: An efficient approach to define countermeasures', *EURODYN 2014*, Porto, Portugal.

Bajer, A., Belsky, V. and Kung, S.-W. (2004) 'The influence of friction-induced damping and nonlinear effects on brake squeal analysis', *SAE Technical paper* 2004-01-2794.

Bergman, F., Eriksson, M. and Jacobson, S. (1999) 'Influence of disc topography on generation of brake squeal', *Wear*, vol. 225-229, pp. 621–628.

Bergman, F., Eriksson, M. and Jacobson, S. (2000) 'The effect of reduced contact area on the occurrence of disc brake squeals for an automotive brake pad', *Proceedings of the Institution of Mechanical Engineers, Part D: Journal of Automobile Engineering*, vol. 214, no. 5, pp. 561-568.

Bryant, D., Fieldhouse, J.D. and Talbot, C. (2011) 'Brake judder − An investigation of the thermo-elastic and thermo-plastic effects during braking', *International Journals of Vehicle Structures and Systems* vol. 3, no. 1, pp. 57-72.

Bryant, D., Solms, F., Fieldhouse, J.D. and Ashraf, N. (2012) 'Investigation of brake pad vibration under dynamic squeal conditions', *Eurobrake2012*, Dresden, Germany.

Butlin, T. and Woodhouse, J. (2009) 'Friction-induced vibration: Should low-order model be believed?', *Journal of Sound and Vibration*, vol. 328 no. 1-2, pp. 92-108.

Butlin, T. and Woodhouse, J. (2010) 'Friction-induced vibration: Quantifying sensitivity and uncertainty', *Journal of Sound and Vibration*, vol. 329, no. 5, pp. 509-526.

Butlin, T. and Woodhouse, J. (2011) ' A systematic experimental study of squeal initiation', *Journal of Sound and Vibration*, vol. 330, no. 21, pp. 5077–5095.

Cantone, F. and Massi, F. (2011) 'A numerical investigation into the squeal instability: Effect of damping', *Mechanical Systems and Signal Processing*, vol. 25, no. 5, pp. 1727–1737.

Chargin, M.L., Dunne, L.W. and Herting, D.N. (1997) 'Nonlinear dynamics of brake squeal', *Finite Elements in Analysis and Design*, vol. 28, no. 1, pp. 69–82.

Chen, S.N., Mottershead. J.E. and Cartmell, M.P. (1994) 'Parametric resonances at subcritical speeds in discs with rotating frictional loads', *Proceedings of the Institution of Mechanical Engineers, Part C: Journal of Mechanical Engineering Science*, vol. 208, no. 6, pp. 417-426.

Chen, F., Abdelhamid, M.K., Blaschke, P. and Swayze, J. (2003) 'On automotive disc brake squeal, part III: Test and evaluation', *SAE Technical paper* 2003-01-1622.

Chen, G.X., Zhou, Z.R., Kapsa, P. and Vincent, L. (2002) 'Effect of surface topography on formation of squeal under reciprocating sliding', *Wear*, vol. 253, no. 3-4, pp. 411–423.

Chen, G.X., Zhou, Z.R., Kapsa, P. and Vincent, L. (2003) 'Experimental investigation into squeal under reciprocating sliding', *Tribology International* vol. 36, no. 12, pp. 961–971.

Chen, G.X., Liu, Q.Y., Jin, X.S. and Zhou, Z.R. (2008) 'Stability analysis of a squealing vibration model with time delay', *Journal of Sound and Vibration* vol. 311, no. 1-2, pp. 516-536.

Coudeyras, N., Sinou, J.-J. and Nacivet, S. (2009a) ' A new treatment for predicting the self-excited vibrations of nonlinear systems with frictional interfaces: The Constrained Harmonic Balance Method, with application to disc brake squeal', *Journal of Sound and Vibration*, vol. 319, no. 3-5, pp. 1175–1199.

Coudeyras, N., Nacivet, S. and Sinou, J.-J. (2009b) 'Periodic and quasi-periodic solutions for multi-instabilities involved in brake squeal', *Journal of Sound and Vibration*, vol. 328, no. 4-5, pp. 520–540.

Culla, A. and Massi, F. (2009) 'Uncertainty model for contact instability prediction', *Journal of the Acoustical Society of America*, vol. 126, no. 3, pp. 1111-1119.

Cunefare, K.A. and Graf, A.J. (2002) 'Experimental active control of automotive disc brake rotor squeal using dither', *Journal of Sound and Vibration*, vol. 250, no. 4, pp. 579–590.

D'Souza, A.F. and Dweib, A.H. (1990) 'Self-excited vibrations induced by dry friction, part 2: Stability and limit-cycle analysis', *Journal of Sound and Vibration* vol. 137, no. 2, pp. 177-190.

Dai, Y. and Lim, T.C. (2008) 'Suppression of brake squeal noise applying finite element

brake and pad model enhanced by spectral-based assurance criteria', *Applied Acoustics*, vol. 69, no. 1-2, pp. 196-214.

Day, A.J., Tirovic, M. and Newcomb, T.P. (1991) 'Thermal effects and pressure distributions in brakes', *Proceedings of the Institution of Mechanical Engineers, Part D: Journal of Automobile Engineering*, vol. 205, no. 3, pp. 199-205.

Day, A.J., Klaps, J. and Ross, C.F. (2012) *Braking of road vehicles 2012*, Inprint and Design Ltd, University of Bradford, UK.

Day, A. (2014) *Braking of Road Vehicles,* Elsevier.

DiazDelaO, F.A. and Adhikari, S. (2010) 'Structural dynamic analysis using Gaussian process emulators', *Engineering Computations*, vol. 27, no. 5, pp. 580-605.

Duffour, P. and Woodhouse J. (2004a) 'Instability of systems with a frictional point contact, part1: Basic modelling', *Journal of Sound and Vibration*, vol. 271 no. 2, pp. 365-390.

Duffour, P. and Woodhouse J. (2004b) 'Instability of systems with a frictional point contact, part2: Model extensions', *Journal of Sound and Vibration*, vol. 271 no. 2, pp. 391-410.

Dweib, A.H. and D'Souza, A.F. (1990) 'Self-excited vibrations induced by dry friction, part 1: Experimental study', *Journal of Sound and Vibration*, vol. 137 no. 2, pp. 163-175.

Eriksson, M., Bergman, F. and Jacobson, S. (1999) 'Surface characterisation of brake pads after running under silent and squealing conditions', *Wear*, vol. 232, no. 2, pp. 163-167.

Ewins, D.J. (2000) *Modal Testing: Theory practice and application,* 2nd edition, Research Studies Press Ltd, Hertfordshire, England.

Festjens, H., Gaël, C., Franck, R., Jean-Luc, D. and Remy L. (2012) 'Effectiveness of multilayer viscoelastic insulators to prevent occurrences of brake squeal: A numerical study', *Applied Acoustics*, vol. 73, no. 11, pp. 1121-1128.

Fieldhouse, J.D. and Newcomb, T.P. (1996) 'Double pulsed holography used to investigate noisy brakes', *Optics and Lasers in Engineering,* vol. 25, no. 6, pp. 455-494.

Fieldhouse, J.D. (2000) 'A study of the interface pressure distribution between pad and rotor, the coefficient of friction and calliper mounting geometry with regard to brake noise', *Brakes 2000: International Conference on Automotive Braking Technologies for the 21st Century*, Wiley.

Fieldhouse, J.D., Ashraf, N. and Talbot, C. (2008) 'The measurement and analysis of the disc/pad interface dynamic centre of pressure and its Influence on brake noise', *SAE Technical paper* 2008-01-0826.

Fieldhouse, J.D., Bryant, D. and Talbot, C. (2011) ' Hot judder - An investigation of the thermo-elastic and thermo-plastic effects during braking', *SAE Technical paper* 2011-01-1575.

Flint, J. and Hultén, J. (2002) 'Lining-deformation-induced modal coupling as squeal generator in a distributed parameter disc brake model', *Journal of Sound and Vibration*, vol. 254, no. 1, pp. 1–21.

Forrester, A., Sóbester, A. and Keane, A. (2008) *Engineering design via surrogate modelling: A practical guide*, Wiley.

Fritz, G., Sinou, J.-J., Duffal, J.-M. and Jézéquel, L. (2007a) 'Effects of damping on brake squeal coalescence patterns – application on a finite element model', *Mechanics Research Communications*, vol. 34, no. 2, pp. 181–190.

Fritz, G., Sinou, J.-J., Duffal, J.-M. and Jézéquel, L. (2007b) 'Investigation of the relationship between damping and mode-coupling patterns in case of brake squeal', *Journal of Sound and Vibration*, vol. 307, no. 3-5, pp. 591–609.

Gauger, U., Hanss, M. and Gaul, L. (2006) 'On the inclusion of uncertain parameters in brake squeal analysis', *Proceeding of the 24th Conference and Exposition on Structural Dynamics, IMACXXIV*, St. Louis, Missouri, USA, 2006.

Ghanem, R.G. and Spanos, P.D. (2003) *Stochastic Finite Elements: A Spectral Approach*, Dover Publications, Mineola, New York.

Giannini, O. and Sestieri, A. (2006) 'Predictive model of squeal noise occurring on a laboratory brake', *Journal of Sound and Vibration*, vol. 296, no. 3, pp. 583–601.

Giannini, O., Akay, A. and Massi, F. (2006) 'Experimental analysis of brake squeal noise on a laboratory brake setup', *Journal of Sound and Vibration*, vol. 292, no. 1-2, pp. 1-20.

Giannini, O. and Massi, F. (2008) 'Characterization of the high-frequency squeal on a laboratory brake setup', *Journal of Sound and Vibration*, vol. 310, no. 1-2, pp. 394–408.

Grange, P., Clair, D., Baillet, L. and Fogli, M. (2009) 'Brake squeal analysis by coupling spectral linearization and modal identification methods', *Mechanical Systems and Signal Processing*, vol. 23, no. 8, pp. 2575–2589.

Guan, D., Su, X. and Zhang, F. (2006) 'Sensitivity analysis of brake squeal tendency to substructures' modal parameters', *Journal of Sound and Vibration*, vol. 291, no. 1-2, pp. 72–80.

Hammerström, L. and Jacobson, S. (2006) 'Surface modification of brake discs to reduce squeal problems', *Wear*, vol. 261, no. 1, pp. 53–57.

Hassan, M.Z., Brooks, P.C. and Barton, D.C. (2009) 'A predictive tool to evaluate disk brake squeal using a fully coupled thermo-mechanical finite element model', *International Journal of Vehicle Design*, vol. 51, no. 1/2, pp. 124 – 142.

Haykin, S.O. (1999) *Neural networks: A comprehensive foundation*, 2nd edition, Prentice Hall.

Hervé, B., Sinou, J.-J., Mahé, H. and Jézéquel, L. (2008) 'Analysis of squeal noise and mode coupling instabilities including damping and gyroscopic effects', *European Journal of Mechanics A/Solids* vol. 27, no. 2, pp. 141–160.

Hervé, B., Sinou, J.-J., Mahé, H. and Jézéquel, L. (2009) 'Extension of the destabilization paradox to limit cycle amplitudes for a nonlinear self-excited system subject to gyroscopic and circulatory actions', *Journal of Sound and Vibration*, vol. 323, no. 3-5, pp. 944–973.

Hetzler, H., Schwarzer, D. and Seemann, W. (2007) 'Analytical investigation of steady-state stability and Hopf-bifurcations occurring in sliding friction oscillators with application to low-frequency disc brake noise', *Communication in Nonlinear Science and Numerical Simulation*, vol. 12, no. 1, pp. 83-99.

Hetzler, H. and Willner, K. (2012) 'On the influence of contact tribology on brake squeal', *Tribology International* vol. 46, no. 1, pp. 237–246.

Hochlenert, D. and Hagedorn, P. (2006) 'Control of disc brake squeal – modelling and experiments', *Structural Control and Health Monitoring*, vol. 13, no. 1, pp. 260-276.

Hochlenert, D., Spelsberg-Korspeter, G. and Hagedorn, P. (2007) 'Friction induced vibrations in moving continua and their application to brake squeal', *Journal of Applied Mechanics*, vol. 74, no. 3, pp. 542-549.

Hochlenert, D. (2009) 'Nonlinear stability analysis of a disk brake model', *Nonlinear Dynamics*, vol. 58, no. 1-2, pp. 63-73.

Hochlenert, D., Spelsberg-Korspeter, G. and Hagedorn, P. (2010) 'A note on safety-relevant vibrations induced by brake squeal', *Journal of Sound and Vibration*, vol. 329, no.

19, pp. 3867–3872.

Hoffmann, N., Fischer, M., Allgaier, R. and Gaul, L. (2002) 'A minimal model for studying properties of the mode-coupling type instability in friction induced oscillations, Mechanics Research Communications', vol. 29, no. 4, pp. 197-205.

Hoffmann, N. and Gaul, L. (2003) 'Effects of damping on mode-coupling instability in friction induced oscillations', *Journal of Applied Mathematics and Mechanics* vol. 83, no. 8, pp. 524-534.

Ibrahim, R.A. (1994) 'Friction-induced vibration, chatter, squeal, and chaos—Part II: Dynamics and modelling', *Applied Mechanics Reviews*, vol. 47, no. 7, pp. 227-253.

Ishii-Dodson, N., Thuesen, J. and Eggleston, D. (2012) 'Analysis of the temperature dependence of different modes of brake squeal noise', *Eurobrake2012*, Dresden, Germany.

Jacobsson, H. (1999) 'Analysis of brake judder by use of amplitude functions', *SAE Technical paper,* 1999-01-1779.

Jacobsson, H. (2003) 'Aspects of Disc Brake Judder', *Proceedings of the Institution of Mechanical Engineers, Part D: Journal of Automobile Engineering*, vol. 217, no. 6, pp. 419-430.

Jang, H., Lee, J.S. and Fash, J.W. (2001) 'Compositional effects of the brake friction material on creep groan phenomena', *Wear*, vol. 251, no. 1-12, pp. 1477–1483.

Johnson, N.L. and Kotz, S. (1969) *Distributions in statistics: Discrete distributions*, John Wiley and Sons Inc.

Johnson, N.L. and Kotz, S. (1970) *Distributions in statistics: Continuous Univariate Distributions-2*, John Wiley and Sons Inc.

Johnson, N.L. and Kotz, S. (1972) *Distributions in statistics: Continuous Multivariate Distributions*, John Wiley and Sons Inc.

Jones, D.R., Schonlau, M. and Welch, W.J. (1998) ' Efficient global optimization of expensive black-box functions ', *Journal of Global Optimization*, vol. 13, no. 4, pp. 455-492.

Jung, S.P., Park, T.W., Chai, J.B. and Chung, W.S. (2011) 'Thermo-mechanical finite element analysis of hot judder phenomenon of a ventilated disc brake system', *International Journal of Precision Engineering and Manufacturing*, vol. 12, no. 5, pp. 821-828.

Júnior, M.T., Gerges, S.N.Y. and Jordan, R. (2008) 'Analysis of brake squeal noise using the

finite element method: A parametric study', *Applied Acoustics*, vol. 69, no. 2, pp. 147–162.

Kang, J. (2009) 'Squeal analysis of gyroscopic disc brake system based on finite element method', *International Journal of Mechanical Sciences*, vol. 51, no. 4, pp. 284–294.

Kang, J., Krousgrill, C.M. and Sadeghi, F. (2009) 'Analytical formulation of mode-coupling instability in disc-pad coupled system', *International Journal of Mechanical Sciences*, vol. 51, no. 1, pp. 52-63.

Kinkaid, N.M., O'Reilly, O.M. and Papadopoulos, P. (2003) 'Automotive disc brake squeal', *Journal of Sound and Vibration*, vol. 267, no. 1, pp. 105-166.

Kinkaid, N.M., O'Reilly, O.M. and Papadopoulos, P. (2005) 'On the transient dynamics of a multi-degree-of-freedom friction oscillator: a new mechanism for disc brake noise', *Journal of Sound and Vibration*, vol. 287, no. 4–5, pp. 901-917.

Kirillov, O.N. (2004) 'Destabilization paradox', *Doklady Physics*, vol. 49, no. 4, pp. 239-245.

Kirillov, O.N. and Seyranian, A.O. (2005) 'The effect of small internal and external damping on the stability of distributed non-conservative systems', *Journal of Applied Mathematics and Mechanics* vol. 69, no. 4, pp. 529-552.

Kruse, S., Zeumer, B., Reuß, P. and Hoffmann, N. (2012) 'Detection of critical instabilities in brake squeal based on nonlinear joint characteristics', *Eurobrake2012*, Dresden, Germany.

Kundu, A., DiazDelaO, F.A., Adhikari, S. and Friswell, M.I. (2014) 'A hybrid spectral and metamodelling approach for the stochastic finite element analysis of structural dynamic systems', *Computer Methods in Applied Mechanics and Engineering*, vol. 270, pp. 201-219.

Kung, S.-W., Stelzer, G., Belsky, V. and Bajer, A. (2003) 'Brake squeal analysis incorporating contact conditions and other nonlinear effects', *SAE Technical paper* 2003-01-3343.

Liles, G. (1989) 'Analysis of disc brake squeal using finite element methods', *SAE Technical paper* 891150.

Lophaven, G., Nielsen, H. and Søndergaard, J. (2002) *DACE: a MATLB Kriging toolbox*, Technical report, Technical University of Denmark, DK-2800 Kgs.

Magnier, V., Brunel, J.F., Bonnay, K. and Dufrénoy, P. (2012) 'Influence of the size of the contact heterogeneities between the disc and the pad on the brake squeal',

Eurobrake2012, Dresden, Germany.

Massi, F., Giannini, O. and Baillet, L. (2006a) 'Brake squeal as dynamic instability: An experimental investigation', *Journal of the Acoustical Society of America*, vol. 120, no. 3, pp. 1388-1398.

Massi, F., Sestieri, A. and Baillet, L. (2006b) 'The effect of modal damping on brake squeal instability', The *Thirteenth International Congress on Sound and Vibration (ICSV13)*, Vienna, Austria.

Massi, F., Baillet, L., Giannini, O. and Sestieri, A. (2007) 'Brake squeal: Linear and nonlinear numerical approaches', *Mechanical Systems and Signal Processing*, vol. 21, no. 6, pp. 2374-2393.

Massi, F., Berthier, Y. and Baillet, L. (2008) 'Contact surface topography and system dynamics of brake squeal', *Wear*, vol. 265, no. 11-12, pp. 1784–1792.

Mills, H.R. (1938) *Brake squeak*, Technical report 9000 B, Institution of Automobile Engineers.

Moens, D. and Vandepitte, D. (2006) 'Recent advances in non-probabilistic approaches for non-deterministic dynamic finite element analysis', *Archives of Computational Methods in Engineering*, vol. 13, no. 3, pp. 389–464.

Möller, B. and Beer, M. (2008) 'Engineering computation under uncertainty – Capabilities of non-traditional models', *Computers and Structures* vol. 86, no. 10, pp. 1024-1041.

Mortelette, L., Brunel, J.F., Boidin, X., Desplanques, Y., Dufrénoy, P. and Smeets, L. (2009) 'Impact of mineral fibres on brake squeal occurrences', *SAE Technical paper* 2009-01-3050.

Mottershead, J.E., Mares, C.M., Friswell, M.I. and James, S. (2000) 'Selection and updating of parameters for an aluminium space-frame model', *Mechanical Systems and Signal processing*, vol. 14, no. 6, pp. 923-944.

Murthy, D.B. and Haftka, R.T. (1988) 'Derivatives of eigenvalues and eigenvectors of a general complex matrix', *International Journal for Numerical Methods in Engineering*, vol. 26, no. 2, pp. 293-311.

Myers, R.H., Montgomery, D.C. and Anderson-Cook, C.M. (2009) *Response surface methodology: Process and product optimisation using designed experiments*, 3rd edition, Willey.

Nayfeh, A.H. (1973) *Perturbation methods*, Wiley, New York.

Nechak, L., Berger, S. and Aubry, E. (2013) 'Non-intrusive generalized polynomial chaos for

the robust stability analysis of uncertain nonlinear dynamic friction systems', *Journal of Sound and Vibration*, vol. 332, no. 5, pp. 1204–1215.

Nishiwaki, M. (1993) 'Generalized theory of brake noise', *Proceedings of the Institution of Mechanical Engineers, Part D: Journal of Automobile Engineering*, vol. 207, no. 3, pp. 195-202.

North, M.R. (1972) *Disc brake squeal- A theoretical model*, Technical report 1972/5, Motor Industry Research Association, Warwickshire, England.

Oberst, S. and Lai, J.C.S. (2011a) 'Chaos in brake squeal noise', *Journal of Sound and Vibration*, vol. 330, no. 5, pp. 955–975.

Oberst, S. and Lai, J.C.S. (2011b) 'Statistical analysis of brake squeal noise', *Journal of Sound and Vibration*, vol. 330, no. 12, pp. 2978–2994.

Oberst, S., Lai, J.C.S. and Marburg, S. (2013) 'Guidelines for numerical vibration and acoustic analysis of disc brake squeal using simple models of brake systems', *Journal of Sound and Vibration*, vol. 332, no. 9, pp. 2284-2299.

Oestreich, M., Hinrichs, N. and Popp, K. (1996) 'Bifurcation and stability analysis for a non-smooth friction oscillator', *Archive of Applied Mechanics*, vol. 66, no. 5, pp. 301-314.

Ostermeyer G.-P., Graf M. (2013) 'Influence of wear on thermoelastic instabilities in automotive brakes', *Wear,* vol. 308, no. 1–2, pp. 113-120.

Ouyang, H., Mottershead, J.E., Brookfield, D.J., James, S. and Cartmell, M.P. (2000) 'A methodology for the determination of dynamic instabilities in a car disc brake', *International Journal of Vehicle Design*, vol. 23, no. 3/4, pp. 241-262.

Ouyang, H., Mottershead, J.E. and Li, W. (2003) 'A moving-load model for disc-brake stability analysis', *Journal of Vibration and Acoustics*, vol. 125, no. 1, pp. 53-58.

Ouyang, H., Gu, Y. and Yang, H. (2004) 'A dynamic model for a disc excited by vertically misaligned, rotating, frictional sliders', *Acta Mechanica Sinica* vol. 20 no. 4, pp. 418-425.

Ouyang, H., Nack, W., Yuan, Y. and Chen, F. (2005) 'Numerical analysis of automotive disc brake squeal: a review', *International Journal of Vehicle Noise and Vibration*, vol. 1, no. 3/4, pp. 207-231.

Ouyang, H., AbuBakar, A.R. and Li, L. (2009) 'A combined analysis of heat conduction, contact pressure and transient vibration of a disk brake', *International Journal of Vehicle Design*, vol. 51, no. 1/2, pp. 190-206.

186

Ouyang, H. (2010) 'Pole assignment of friction-induced vibration for stabilisation through state-feedback control', *Journal of Sound and Vibration*, vol. 329, no. 11, pp. 1985-1991.

Paliwal, M., Mahajan, A., Don, J., Chu, T. and Filip, P. (2005) 'Noise and vibration analysis of a disc–brake system using a stick–slip friction model involving coupling stiffness', *Journal of Sound and Vibration*, vol. 282, no. 3–5, pp. 1273-1284.

Papinniemi, A., Lai, J.C.S., Zhao, J. and Loader, L. (2002) 'Brake squeal: a literature review', *Applied Acoustics*, vol. 63, no. 4, pp. 391–400.

Park, S., Jeong, W. and Park, K. (2012) 'Improvement of Brake Squeal using Shape Optimization based on Frequency Separation', *Eurobrake2012*, Dresden, Germany.

Plaut, R.H. and Huseyin, K. (1973) 'Derivatives of eigenvalues and eigenvectors in non-self-adjoint systems', *AIAA Journal*, vol. 11, no. 2, pp. 250-251.

Popp, K. and Stelter, P. (1990) 'Stick-slip vibrations and chaos', *Philosophical Transactions of the Royal Society of London A*, vol. 332, no. 1624, pp. 89-105.

Puri, M.L. and Ralescu, D.A. (1986) 'Fuzzy Random Variables', *Journal of Mathematical analysis and Application*, vol. 114, pp. 409-422.

Rao, S. (2011) *Mechanical vibrations*, Pearson Education South Asia Pte Ltd.

Rhee, S.K., Tsang, P.H.S. and Wang, Y.S. (1989) 'Friction-induced noise and vibration of disc brakes', *Wear*, vol. 133, no. 1, pp. 39-45.

Ryzhik, B. (2009) 'Friction-induced vibrations of squeal type due to transverse contraction in a flexible disk', *Journal of Sound and Vibration*, vol. 326, no. 3-5, pp. 623–632.

Sacks, J., Welch, W.J., Mitchell, T.J. and Wynn, H.P. (1989) 'Design and analysis of computer experiments', *Statistical Science*, vol. 4, no. 4, pp. 409-423.

Sarrouy, E., Dessombz, O. and Sinou, J.-J. (2013a) 'Stochastic study of a non-linear self-excited system with friction', *European Journal of Mechanics A/Solids*, vol. 40 pp. 1-10.

Sarrouy, E., Dessombz, O. and Sinou, J.-J. (2013b) 'Piecewise polynomial chaos expansion with an application to brake squeal of a linear brake system', *Journal of Sound and Vibration*, vol. 332, no. 3, pp. 577-594.

Schenk, C.A. and Schuëller, G.I. (2005) *Uncertainty Assessment of Large Finite Element Systems*, Springer, Berlin Heidelberg.

Sherif, H.A. (2004) 'Investigation on effect of surface topography of pad/disc assembly on

squeal generation', *Wear*, vol. 257, no. 7-8, pp. 687–695.

Shin, K. Brennan, M.J., Oh, J.-E., Harris, C.J. (2002) 'Analysis of disc brake noise using a two-degree-of freedom model', *Journal of Sound and Vibration,* vol. 254, no. 5, pp. 837-848.

Sinou, J.-J., Thouverez, F. and Jézéquel, L. (2003) 'Analysis of friction and instability by the centre manifold theory for a nonlinear sprag-slip model', *Journal of Sound and Vibration*, vol. 265 no. 3, pp. 527-559.

Sinou, J.-J., Thouverez, F. and Jézéquel, L. (2004) ' Methods to reduce non-linear mechanical systems for instability computation', *Archives of Computational Methods in Engineering*, vol. 11, no. 3, pp. 257-344.

Sinou, J.-J. and Jézéquel, L. (2007) 'Mode coupling instability in friction-induced vibrations and its dependency on system parameters including damping', *European Journal of Mechanics A/Solids* vol. 26, no. 1, pp. 106-122.

Sinou, J.-J. (2010) 'Transient non-linear dynamic analysis of automotive disc brake squeal - On the need to consider both stability and non-linear analysis', *Mechanics Research Communications* vol. 37, no. 1, pp. 96-105.

Sinou, J.-J., Loyer, A., Chiello, O., Mogenier, G., Lorang, X., Cocheteux, F. and Bellaj, S. (2013) 'A global strategy based on experiments and simulations for squeal prediction on industrial railway brakes', *Journal of Sound and Vibration*, vol. 332, no. 20, pp. 5068-5085.

Slavič, J., Bryant, M.D. and Boltežar, M. (2007) 'A new approach to roughness-induced vibrations on a slider ', *Journal of Sound and Vibration*, vol. 306, no. 3-5, pp. 732–750.

Soobbarayen, K., Besset, S. and Sinou, J.-J. (2013) 'Noise and vibration for a self-excited mechanical system with friction', *Applied Acoustics* vol. 74, no. 10, pp. 1191–1204.

Spelsberg-Korspeter, G. (2010) 'Structural optimization for the avoidance of self-excited vibrations based on analytical models', *Journal of Sound and Vibration*, vol. 329, no. 23, pp. 4829–4840.

Spelsberg-Korspeter, G. (2012) 'Eigenvalue optimization against brake squeal: Symmetry, mathematical background and experiments', *Journal of Sound and Vibration*, vol. 331, no. 9, pp. 4259–4268.

Spurr, R.T. (1961) 'A theory of brake squeal', *Proceedings of the Institution of Mechanical*

Engineers: Automobile Division vol. 15, no. 1, pp. 33-52.

Stanbridge, A.B. and Ewins, D.J. (1999) 'Modal testing using a scanning laser doppler vibrometer', *Mechanical Systems and Signal Processing*, vol. 13, no. 2, pp. 255–270.

Tison, T., Heussaff, A., Massa, F., Turpin, I. and Nunes, R.F. (2014) 'Improvement in the predictivity of squeal simulations: Uncertainty and robustness', *Journal of Sound and Vibration*, vol. 333, no. 15, pp. 3394-3412.

Vermot des Roches, G., Balmes, E., Chiello, O. and Lorang, X. (2013) 'Reduced order brake models to study the effect on squeal of pad redesign', *Eurobrake 2013* , Dresden, Germany.

Von Wagner, U. and Hochlenert, D. (2011) 'How do nonlinearities influence brake squeal? ', *SAE Technical paper* 2011-01-2365.

Von Wagner, U., Hochlenert, D. and Hagedorn, P. (2007) 'Minimal models for disk brake squeal', *Journal of Sound and Vibration*, vol. 302, no. 3, pp. 527-539.

Wang, S.K. and Woodhouse, J. (2011) 'The frequency response of dynamic friction: A new view of sliding interfaces', *Journal of the Mechanics and Physics of Solids,* vol. 59, no. 5, pp. 1020-1036.

Woodhouse, J. and Wang, S.K. (2011) 'The frequency response of dynamic friction: Model comparisons', *Journal of the Mechanics and Physics of Solid,* vol. 59, no. 11, pp. 2294-2306.